

RBTH  
1097



THE UNIVERSITY OF  
**SYDNEY**

**RARE BOOKS LIB.**

### **COPYRIGHT AND USE OF THIS THESIS**

This thesis must be used in accordance with the provisions of the Copyright Act 1968.

Reproduction of material protected by copyright may be an infringement of copyright and copyright owners may be entitled to take legal action against persons who infringe their copyright.

Section 51(2) of the Copyright Act permits an authorised officer of a university library or archives to provide a copy (by communication or otherwise) of an unpublished thesis kept in the library or archives, to a person who satisfies the authorised officer that he or she requires the reproduction for the purposes of research or study.

The Copyright Act grants the creator of a work a number of moral rights, specifically the right of attribution, the right against false attribution and the right of integrity.

You may infringe the author's moral rights if you:

- fail to acknowledge the author of this thesis if you quote sections from the work
- attribute this thesis to another author
- subject this thesis to derogatory treatment which may prejudice the author's reputation

For further information contact the University's  
**Director of Copyright Services**

**[sydney.edu.au/copyright](http://sydney.edu.au/copyright)**



THE UNIVERSITY OF  
**SYDNEY**

*Panela Ste* 1/4/2011

This thesis has been accepted for the degree by the  
University of Sydney

# **Quantifying processes of pedogenesis**

**A field study situated in the Werrikimbe National Park in south-eastern Australia**

**Uta Lieselotte Stockmann**

A thesis submitted in fulfilment of the requirements for the degree of Doctor of Philosophy

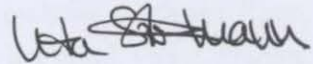
2010  
Faculty of Agriculture, Food and Natural Resources  
The University of Sydney  
New South Wales  
Australia



THE UNIVERSITY OF  
**SYDNEY**

## Statement of originality

The research presented in this thesis has been carried out by me and I have written the text, with the guidance of my supervisors. Where I have used the work of others, due acknowledgment has been made in the text.



Uta Stockmann

## Acknowledgements

Firstly I would like to thank my supervisor, Alex McBratney, and my co-supervisor, Budiman Minasny, for their guidance, support, help and advice throughout the last three and a half years. Their encouragement to tackle such an interesting and challenging project was and continues to be greatly appreciated.

Secondly, a number of people from our research group at The University of Sydney provided valuable support, both professionally and socially. These include: Adrienne Ryan, Balwant Singh, Brendan Malone, Brett Whelan, Craig Lobsey, Damien Field, Grant Tranter, Ichsani Wheeler, Iona Gyorgy, James Quilty, John Bennett, Kanika Singh, Konrad Müller, Marcello Stabile, Markus Gräfe, Pamela Stern and Stephen Cattle. In particular, I would like to thank Michael Short for his tremendous help during the field work of this project and Nathan Odgers for his assistance with the sampling scheme. This is a fairly long list and I have probably forgotten to mention someone, but rest assured, you are not forgotten!

Thank you to The University of Sydney for considering and accepting me for the EIPRS International Postgraduate Student Scholarship that made it possible to study here in Australia.

There are a few people outside of our research group at The University of Sydney who provided valuable help along the way. I would like to thank David Fink and Charles Mifsud who enabled and supervised the work on Terrestrial Cosmogenic Nuclides. I would also like to thank Tim Pietsch and Ken McMillan who enabled and helped me to work on Optically Stimulated Luminescence. Additionally thank you to the Department of Environment & Climate Change of NSW for allowing me permission to undertake sampling at Werrikimbe National Park and for providing spatial information of the study area, and in particular Andrew Marshall for helping to identify a suitable sampling area.

Last but certainly not least, a huge thank you to my family for supporting my decision to conduct this PhD research degree at The University of Sydney in Australia. A special thank you to my big sister, Karola, for falling in love with an Australian because it brought me here, to find my path. Moreover, I would like to thank Karola and Nathan, for their continued support throughout the last three and a half years and for being so happy for me that I was able to study here in this beautiful country. To my grandpa, Prof. Dr. Werner Bergmann, who encouraged me along the way and who is so proud that at least one of his grandchildren is kind of following in his footsteps. To my parents, Mutti und Vati, ich weiss, dass es euch am Anfang schwer gefallen ist, sich für mich zu freuen, weil es bedeutete, dass ihr noch eine Tochter nach Australien 'verloren' habt. Tausend Dank, dass ihr meine Entscheidung letztendlich doch mit Freude unterstützt habt und dass ihr immer für mich da wart, vom 'anderen Ende der Welt'.

## Summary

Despite its fundamental importance for the functioning of ecosystems our knowledge of soil is still limited. In pedology there has been a shift of interest from predicting soil attributes based on empirical quantitative relationships to quantifying pedogenic processes to improve our understanding of pedogenesis. The availability of new sophisticated laboratory techniques has opened up the possibility of addressing the demand of quantifying processes of soil and landscape formation.

Here, the application of *in situ* terrestrial cosmogenic nuclides (TCN) and optically stimulated luminescence (OSL) was studied to parameterise pedogenic processes directly from field data by conducting a field survey in a small subcatchment of Werrikimbe National Park, situated in south-eastern NSW, Australia. The concentration of TCN in soil parent materials was used to investigate processes of soil weathering by deriving *rates of soil production*. Dating individual sand-sized quartz grains with OSL was employed to explore processes of soil mixing by estimating *rates of potential soil turnover*, and also to *estimate the age of soil horizons*.

At Werrikimbe National Park sampling took place in old-growth forest areas along three principal toposequences, located at Spokes Mountain (Ta), Mount Boss (Tb) and Plateau Beech (Te). Three soil profiles along each toposequence were dug to the soil-bedrock or soil-saprolite interface with soil pits varying between 40 and 105 cm in depth. A total of nine soil pits were located at the top, mid-slope and the base of the hillslope. The underlying geology comprised sedimentary and metamorphic rocks of Devonian, Carboniferous and Permian age, consisting of siltstones and fine lithic sandstones.

All soil profiles studied were characterized by horizonation which implied a progressive soil evolution at Werrikimbe over time. Each horizon of the soil profiles was fully analysed in terms of physical and chemical properties including bulk density, particle-size distribution, soil organic carbon content and mineral suite. Topsoils were characterized by stony silty loams to silty clay loams whereas subsoils were characterised by silty loams, silty clay loams and silty clays with a significant amount of stones. For all sampling sites, particle-size distributions showed no clear texture change from A to B horizons. The clay contents increased only gradually with increasing soil depth and ranged from low and moderate (20-40 %) at Spokes Mountain and Mount Boss toposequences to high (>40 %) at the Plateau

Beech toposequence throughout the soil profile. Contents of soil organic carbon were relatively high in the surface horizons (generally exceeding 10 %) and decreased with increasing soil depth to less than 2 %. On all three toposequences, the clay mineral kaolin and the aluminium-oxide gibbsite were dominant. The iron-oxide goethite was also present in each horizon of the nine soil profiles. Chlorite was present in two of the three toposequences. Kaolin, gibbsite and chlorite were all indicators of extensive soil weathering at Werrikimbe.

TCN-derived soil production rates (SPR) varied between 3 and 18 mm kyr<sup>-1</sup>, with maximum soil production occurring between 0 and 50 cm. With a value of 10±4 mm kyr<sup>-1</sup>, the potential average weathering rate ( $P_0$ ) for this warm-temperate to subtropical environment was relatively low. No clear pattern of SPR related to soil depth was observed. However, SPR appeared to be closely related to the terrain attribute profile curvature. This implied that soil erosion and deposition were potentially not in equilibrium on the toposequences sampled. Nevertheless, when applied in a simple model of soil production that incorporated the bulk density of soil and parent materials, the determined average SPR of 10 mm kyr<sup>-1</sup> resulted in soil residence times of up to 80000 years for Werrikimbe, for soil profiles of about 1 m in depth.

SPR determined for Werrikimbe were compared with published SPR from diverse climate regimes and parent materials. The data-set fit well within the range of published TCN-derived SPR. The compilation of TCN-derived SPR showed that values of conversion rates of different parent materials to soil varied, but not over several orders of magnitude as expected. Differences were within one order of magnitude. An average TCN-derived rate of soil production of 47±4 mm kyr<sup>-1</sup> was therefore posited.

Results from OSL analysis confirmed the occurrence of soil mixing in the top 50 cm of soil along the Mount Boss and Plateau Beech toposequences. Soil mixing rates were calculated based on the distribution of ages of individual quartz grains estimated from incremental burial depths. Vertical soil mixing rates of 0.5 mm yr<sup>-1</sup> and 0.2 mm yr<sup>-1</sup> were calculated for the Mount Boss and Plateau Beech toposequences, respectively. The velocity of vertical grain movements appeared to be higher in the top 25 cm of soil compared to 50 cm soil depth. At 1.2 mm yr<sup>-1</sup>, lateral movements of grains were higher at toposequence Mount Boss when compared to toposequence Plateau Beech where rates of 0.01 mm yr<sup>-1</sup> were estimated.

Out of 500 single grains analysed with OSL from each depth increment, a finite age could be estimated for less than 25 %. This proportion of finitely-aged grains to infinitely-aged grains had the tendency to decrease gradually with increasing soil depth. Results also showed that median ages of quartz grains from the topsoils were younger (up to 500 years) than quartz grains from the subsoils. Subsoil quartz grains were characterized by a median age of up to 5000 years. However a few younger grains were found deeper down the profile and older grains near the soil surface. These trends were related to the declining probability of quartz grains buried at depth reaching the soil surface and being set back to zero. The potential for the estimation of one 'true' age for soil horizons was limited, because of the heterogeneous nature of age estimates from individual grains and also due to the fact that a relatively large amount of single grains did not have a natural OSL signal.

The research presented here confirmed that dating methods developed to investigate geomorphologic processes are applicable to deriving rates of pedogenic processes. However, the application of these methods in pedological studies was found to be challenging because of increased uncertainties associated with the determination of SPR or ages of single grains in soil-mantled environments.

## Table of Contents

List of Figures .....	iv
List of Tables .....	viii
Chapter 1 Introduction .....	1
Chapter 2 Quantifying pedogenesis – A literature review .....	5
2.1 Introduction .....	5
2.2 Conceptual models of soil formation – Factors, Processes, Pathways, Energy .....	8
2.3 Soil weathering and production .....	14
2.3.1 Production of soil from parent materials .....	14
2.3.2 Chemical weathering of bedrock to soil .....	20
2.4 Soil mixing – vertical and lateral movements .....	39
2.5 Models of soil formation based on the concept of mass balance .....	52
2.6 Conclusions .....	60
Chapter 3 Study area, sampling design, stable and labile soil properties .....	65
3.1 Materials and Methods .....	65
3.1.1 Characterisation of the study site – Werrikimbe National Park .....	65
3.1.2 Sampling along toposequences, a sampling scheme to investigate pedogenesis quantitatively .....	70
3.1.3 Description of sampled stable and labile soil properties .....	74
3.2 Characterisation of stable and labile soil properties for Werrikimbe National Park .....	78
3.2.1 General description – Toposequences, vegetation, soils .....	78
3.2.2 Bulk density .....	81
3.2.3 Particle size .....	81
3.2.4 Semi-quantitative analysis of clay minerals .....	83
3.2.5 Organic carbon .....	88
3.2.6 Soil acidity (pH) .....	89
3.2.7 Summary .....	91
Chapter 4 <i>In situ</i> Terrestrial Cosmogenic Nuclides .....	93
4.1 Principles of using <i>in situ</i> TCN to investigate pedogenesis .....	93
4.1.1 Principles of TCN production in Earth materials .....	93
4.1.2 Using TCN to estimate rates of erosion or soil production from Earth materials <i>in situ</i> .....	95
4.1.3 A compilation of published TCN-derived SPR .....	99
4.2 Sample preparations for analysis of <i>in situ</i> concentrations of $^{10}\text{Be}$ .....	104
4.3 Data treatment to derive soil production rates from <i>in situ</i> concentrations of $^{10}\text{Be}$ .....	108
4.3.1 Normalization of <i>in situ</i> concentrations of $^{10}\text{Be}$ (using scaling factors) .....	108
4.3.2 Correction of $^{10}\text{Be}$ production for depth below the soil surface and slope .....	109



4.3.3 Quantifying SPR using <i>in situ</i> <sup>10</sup> Be concentrations of soil parent materials .....	110
<b>4.4 Results</b> .....	112
4.4.1 <i>In situ</i> produced concentrations of <sup>10</sup> Be at Werrikimbe National Park .....	112
4.4.2 TCN-derived SPR at Werrikimbe National Park.....	113
<b>4.5 Discussion</b> .....	117
4.5.1 Deriving SPR from soil parent materials <i>in situ</i> .....	117
4.5.2 How does soil form at Werrikimbe National Park?.....	120
4.5.3 Field observations of how soils form over time - based on TCN-derived SPR.....	122
4.5.4 Assumptions on the extent of soil production.....	123
4.5.5 Indications of a similar behaviour of TCN-derived SPR.....	123
4.5.6 Comparison of SPR with soil formation rates derived from other methods.....	127
4.6 Conclusions.....	128
<b>Chapter 5 Optically stimulated luminescence</b> .....	131
<b>5.1 Principles of OSL for investigating pedogenesis</b> .....	131
5.1.1 Mineral grains used for OSL.....	132
5.1.2 Development of the luminescence technique for dating Quaternary sediments.....	133
5.1.3 Applications of OSL to pedogenesis.....	135
5.1.4 Summary .....	138
<b>5.2 Materials and Methods</b> .....	138
5.2.1 Sampling in the field for OSL analysis.....	138
5.2.2 Sample preparations for OSL analysis.....	139
5.2.3 Procedure of OSL on the single grain reader.....	141
<b>5.3 Results and discussion</b> .....	143
5.3.1 Dose rate and gamma spectrometry analysis.....	143
5.3.2 OSL data - Dose estimates.....	146
5.3.2.2 Dose calculations in units of gray .....	149
5.3.2.3 Dose distributions for individual quartz grains.....	151
5.3.3 OSL data - Age estimates .....	162
5.3.3.1 Estimation of one 'true' age from populations of dose distributions.....	162
5.3.3.1 Age distributions for individual quartz grains .....	165
5.3.3.2 Determination of mixing rates from ages of individual quartz grains .....	175
<b>5.4 Conclusions</b> .....	179
<b>5.5 Fallout radionuclides – Caesium-137 (<sup>137</sup>Cs) and excess lead-210 (<sup>210</sup>Pb<sub>ex</sub>)</b> .....	185
5.5.1 Introduction.....	185
5.5.2 Principles of the input of <sup>137</sup> Cs and <sup>210</sup> Pb <sub>ex</sub> to surface soils .....	185
5.5.3 Using <sup>137</sup> Cs and <sup>210</sup> Pb <sub>ex</sub> to investigate short-term processes of pedogenesis.....	187
5.5.4 Results and discussion .....	189
5.5.4.1 Vertical and lateral distribution of <sup>137</sup> Cs and <sup>210</sup> Pb <sub>ex</sub> .....	189
5.5.5 Summary .....	196
<b>Chapter 6 General discussion - Quantifying pedogenesis using sophisticated dating methods – TCN and OSL</b> .....	199
<b>6.1 Modelling 'global' soil production based on the TCN-derived average SPR</b> .....	199
<b>6.2 How did soil form at the undisturbed forested environment of Werrikimbe National Park?</b> .....	208

6.3 Relationship between soil properties with soil forming factors and topography.....	210
6.4 Performance of sophisticated dating methods to investigate pedogenesis.....	212
<b>Chapter 7 Overall conclusions and suggestions for future work .....</b>	<b>215</b>
7.1 Key findings.....	215
7.2 Suggestions for future work .....	217
<b>Bibliography .....</b>	<b>221</b>
<b>Appendix .....</b>	<b>- 1 -</b>

## List of Figures

### Chapter 2

Fig. 2.1. Vertical layering within the critical zone. ....	5
Fig. 2.2. Soil profile evolution as a function of additions, removals, translocations and transformations. ....	10
Fig. 2.3. Gibbs' free energy ( $\Delta G$ ) and entropy (S) for different soils, rocks and minerals. ....	12
Fig. 2.4. Types of mathematical functions commonly used in chronofunctions. ....	16
Fig. 2.5. The rate of soil production versus soil thickness. ....	17
Fig. 2.6. Box-Plot distributions of chemical weathering rates derived from weathering indices (Table 2.1 Part 2). ....	25
Fig. 2.7. Box-Plot distributions of chemical weathering rates derived from field data (Table 2.1 Part 1 and 2). ....	26
Fig. 2.8. A comparison of soil mixing rates and chemical weathering. ....	51
Fig. 2.9. Box-Plot distributions of soil mixing rates from field data. ....	51

### Chapter 3

Fig. 3.1. Location of Werrikimbe National Park, NSW, Australia. ....	66
Fig. 3.2a. Average climatic data for Werrikimbe National Park. ....	67
Fig. 3.2b. Average climatic data for Werrikimbe National Park. ....	68
Fig. 3.3. Tectonic elements of the New England Fold Belt. ....	69
Fig. 3.4. Stream order grid of the study site chosen at Werrikimbe National Park. ....	72
Fig. 3.5. Soil profiles along toposequence Spokes Mountain (Ta). ....	73
Fig. 3.6. Soil profiles along toposequence Mount Boss (Tb). ....	73
Fig. 3.7. Soil profiles along toposequence Plateau Beech (Te). ....	74
Fig. 3.8. Location of derived toposequences and sampling points at Werrikimbe National Park. ....	78
Fig. 3.9. From left: Vegetation at toposequence Spokes Mountain (Ta), Mount Boss (Tb) and Plateau Beech (Te). ....	79
Fig. 3.10. Charcoal inclusions at toposequence Spokes Mountain. ....	80
Fig. 3.11. Results from particle-size analysis for soil profiles sampled along toposequence Spokes Mountain (Ta). ....	81
Fig. 3.12. Results from particle-size analysis for soil profiles sampled along toposequence Mount Boss (Tb). ....	82
Fig. 3.13. Results from particle-size analysis for soil profiles sampled along toposequence Plateau Beech (Te). ....	82
Fig. 3.14. Basal spacings (nm) of clay minerals when subjected to different treatments. ....	83
Fig. 3.15. Diffractograms of clay minerals determined for soil profiles along toposequence Spokes Mountain (Ta). ....	85
Fig. 3.16. Diffractograms of clay minerals determined for soil profiles along toposequence Mount Boss (Tb). ....	86
Fig. 3.17. Diffractograms of clay minerals determined for soil profiles along toposequence Plateau Beech (Te). ....	87
Fig. 3.18. Organic carbon content for soil profiles sampled along toposequence Spokes Mountain (Ta). ....	88
Fig. 3.19. Organic carbon content for soil profiles sampled along toposequence Mount Boss (Tb). ....	89
Fig. 3.20. Organic carbon content for soil profiles sampled along toposequence Spokes Mountain (Te). ....	89
Fig. 3.21. Soil acidity (pH) for soil profiles sampled along toposequence Spokes Mountain (Ta). ....	90
Fig. 3.22. Soil acidity (pH) for soil profiles sampled along toposequence Mount Boss (Tb). ....	90

Fig. 3.23. Soil acidity (pH) for soil profiles sampled along toposequence Plateau Beech (Te).	91
---	----

## Chapter 4

Fig. 4.1. Compilation of TCN-derived SPR (in mm kyr <sup>-1</sup> ) for study sites in Australia and North America.	100
Fig. 4.2. Rates of soil production for field sites from Heimsath et al. (2000; 2001b; 2006) near the Bega Valley in south-eastern Australia.	103
Fig. 4.3. The ANTARES AMS facility at Lucas Heights in Sydney, Australia.	105
Fig. 4.4. Pre-treatment of soil parent materials.	106
Fig. 4.5. Treatment with H <sub>3</sub> PO <sub>4</sub> .	106
Fig. 4.6. Flowchart of <sup>10</sup> Be target preparation.	107
Fig. 4.7. Scaling factor for the rate of production as a function of sampling depth for various surface dip angles.	110
Fig. 4.8. <i>In situ</i> produced concentrations of <sup>10</sup> Be for Werrikimbe National Park.	112
Fig. 4.9. Rates of soil production at Werrikimbe National Park.	113
Fig. 4.10a. Relationship between soil production rate and profile curvature.	114
Fig. 4.10b. Relationship between soil depth and profile curvature.	115
Fig. 4.11. Exponential decline of the annual <sup>10</sup> Be production rate.	117
Fig. 4.12. Simulation of observed uniform distribution of randomized <sup>10</sup> Be concentrations.	118
Fig. 4.13. Simulation of observed exponential distribution of randomized <sup>10</sup> Be concentrations.	119
Fig. 4.14. Simulation of observed exponential distribution of randomized <sup>10</sup> Be concentrations.	119
Fig. 4.15. Simulation of observed exponential distribution of randomized <sup>10</sup> Be concentrations.	119
Fig. 4.16. Soil formation at Werrikimbe National Park, simulated applying a simple soil production model.	121
Fig. 4.17. Soil production rates derived with TCN data, for study sites in Australia and North America.	124
Fig. 4.18a. Average soil production rate, derived with TCN data, for study sites in Australia and North America.	125
Fig. 4.18b. Average soil production rate, derived with TCN data, for study sites in Australia and North America.	126
Fig. 4.19. Probability distribution plots of rates of soil production derived with <i>in situ</i> TCN data and weathering rates of soil derived with other methods.	127

## Chapter 5

Fig. 5.1. A three-zone model for soil-surface disturbances.	137
Fig. 5.2. Proposed effects of pedoturbation on the distribution of dose values, De in Gy, measured with OSL.	137
Fig. 5.3. Sampling in the field for OSL analysis.	139
Fig. 5.4. Flowchart of OSL analysis.	139
Fig. 5.5. Thermoluminescence. Peak from the so-called 110°C trap observed after natural irradiation.	141
Fig. 5.6. Concentrations of measured <sup>238</sup> U (Bq kg <sup>-1</sup> ) plotted against <sup>226</sup> Ra (Bq kg <sup>-1</sup> ).	145
Fig. 5.7. Concentrations of measured <sup>228</sup> Th (Bq kg <sup>-1</sup> ) plotted against <sup>226</sup> Ra (Bq kg <sup>-1</sup> ).	145
Fig. 5.8. Concentrations of measured <sup>210</sup> Pb (Bq kg <sup>-1</sup> ) plotted against <sup>226</sup> Ra (Bq kg <sup>-1</sup> ).	145
Fig. 5.9a. Percentage of grains with an adequate OSL signal, displayed for all soil depths sampled in the six soil profiles.	146

<b>Fig. 5.9b.</b> Percentage of grains with an adequate OSL signal, displayed for all soil depths sampled in the six soil profiles. ....	147
<b>Fig. 5.10.</b> RISØ Luminescence Analyst (Version 3.04b). ....	149
<b>Fig. 5.11.</b> (a) Shine down curve of the natural OSL signal in OSL reader counts per seconds. (b) Growth curve plot of the sensitivity corrected OSL signal ( $L_x/T_x$ ) against the applied dose. ....	150
<b>Fig. 5.12.</b> The use of radial plots for displaying OSL data, exemplified with dose values from soil profile Te38 (1-6 cm depth). ....	152
<b>Fig. 5.13.</b> Radial plots of single-grain dose ( $D_e$ ) estimates in Gy for different depths of the soil profile Tb24 along the toposequence Mount Boss. ....	153
<b>Fig. 5.14.</b> Radial plots of single-grain dose ( $D_e$ ) estimates in Gy for different depths of the soil profile Tb12 along the toposequence Mount Boss. ....	154
<b>Fig. 5.15.</b> Radial plots of single-grain dose ( $D_e$ ) estimates in Gy for different depths of the soil profile Tb6 along the toposequence Mount Boss. ....	155
<b>Fig. 5.16.</b> Radial plots of single-grain dose ( $D_e$ ) estimates in Gy for different depths of the soil profile Te38 along the toposequence Plateau Beech. ....	156
<b>Fig. 5.17.</b> Radial plots of single-grain dose ( $D_e$ ) estimates in Gy for different depths of the soil profile TeM along the toposequence Plateau Beech. ....	157
<b>Fig. 5.18.</b> Radial plots of single-grain dose ( $D_e$ ) estimates in Gy for different depths of the soil profile Te3 along the toposequence Plateau Beech. ....	158
<b>Fig. 5.19a.</b> Dose distributions for soil profiles along toposequence Mount Boss. ....	160
<b>Fig. 5.19b.</b> Dose distributions for soil profiles along toposequence Plateau Beech. ....	161
<b>Fig. 5.20a.</b> Toposequence Mount Boss. Probability distribution plots of depth distributions of individual quartz grain ages. ....	168
<b>Fig. 5.20b.</b> Toposequence Plateau Beech. Probability distribution plots of depth distributions of individual quartz grain ages. ....	169
<b>Fig. 5.21.</b> Burial age distributions determined from single grain OSL data. Age distributions are plotted in form of Box Plots for toposequence Mount Boss (Tb). ....	170
<b>Fig. 5.22.</b> Burial age distributions determined from single grain OSL data. Age distributions are plotted in form of Box Plots for toposequence Plateau Beech (Te). ....	170
<b>Fig. 5.23.</b> Density plot distribution of individual quartz grain ages for soil profile Tb24 along toposequence Mount Boss. ....	171
<b>Fig. 5.24.</b> Density plot distribution of individual quartz grain ages for soil profile Tb12 along toposequence Mount Boss. ....	171
<b>Fig. 5.25.</b> Density plot distribution of individual quartz grain ages for soil profile Tb6 along toposequence Mount Boss. ....	172
<b>Fig. 5.26.</b> Density plot distribution of individual quartz grain ages for soil profile Te38 along toposequence Plateau Beech. ....	172
<b>Fig. 5.27.</b> Density plot distribution of individual quartz grain ages for soil profile TeM along toposequence Plateau Beech. ....	173
<b>Fig. 5.28.</b> Density plot distribution of individual quartz grain ages for soil profile Te3 along toposequence Plateau Beech. ....	173
<b>Fig. 5.29.</b> Histograms of soil mixing rates in $\text{mm yr}^{-1}$ for toposequence Mount Boss. ....	177
<b>Fig. 5.30.</b> Histograms of soil mixing rates in $\text{mm yr}^{-1}$ for toposequence Plateau Beech. ....	177
<b>Fig. 5.31.</b> Soil profiles along toposequence Mount Boss. ....	182
<b>Fig. 5.32.</b> Soil profiles along toposequence Plateau Beech. ....	182
<b>Fig. 5.33.</b> Distribution of soil organic carbon for soil profiles along toposequence Mount Boss and Plateau Beech. ....	183

**Fig. 5.34a.** Vertical distribution of  $^{137}\text{Cs}$  concentrations in the soil profile.....190

**Fig. 5.34b.** Vertical distribution of  $^{137}\text{Cs}$  concentrations in the soil profile.....191

**Fig. 5.35a.** Relationship (linear) between  $^{137}\text{Cs}$  concentrations and soil organic carbon contents in the soil profiles.....192

**Fig. 5.35b.** Relationship (linear) between  $^{137}\text{Cs}$  concentrations and clay contents in the soil profiles. ....192

**Fig. 5.36.** Vertical distribution of  $^{210}\text{Pb}_{\text{ex}}$  concentrations in the soil profile for soil profile T6; located in hill-base position of toposequence Mount Boss.....193

**Fig. 5.37a.** Vertical distribution of  $^{210}\text{Pb}_{\text{ex}}$  concentrations plotted in conjunction with contents of organic carbon in the soil profile for soil profile T6; located in hill-base position of toposequence Mount Boss. ....193

**Fig. 5.37b.** Relationship (linear) between  $^{210}\text{Pb}_{\text{ex}}$  concentrations and soil organic carbon contents. ....194

**Chapter 6**

**Fig. 6.1.** Soil profile development over tens of thousands of years assuming steady-state conditions with no soil gain or loss and constant bulk density of the soil profile, applying the average SPR for semi-arid to tropical environments. ....199

**Fig. 6.2.** Box plots of compiled rates of soil erosion, soil formation and river sediment discharge to the oceans and river sediment retained on the land surface in reservoirs, based on Table 6.1, plotted on the log-scale.....205

## List of Tables

### Chapter 2

Tab. 2.1. Part 1. Chemical weathering rates derived from elemental fluxes (loss and gain) in watersheds and chemical products of the parent materials and weathering products studies. ....	27
Tab. 2.1. Part 2. Chemical weathering rates (CWR) derived <i>in situ</i> in applying weathering indices and TCN-derived total denudation rates for study sites in and outside Australia. ....	30
Tab. 2.1. Part 2, continued. Chemical weathering rates (CWR) derived <i>in situ</i> in applying weathering indices and TCN-derived total denudation rates for study sites in and outside Australia. ....	35
Tab. 2.2. Characteristics of study sites in, and outside, Australia. ....	38
Tab. 2.3. Forms and agents of pedoturbation. ....	39
Tab. 2.4. Soil mixing rates. ....	46
Tab. 2.5. Summary of models of soil formation presented in this literature review (factors, processes, pathways, energy and mass-balance soil formation models). ....	58

### Chapter 3

Tab. 3.1. Location of sampled soil profiles in the field. ....	72
Tab. 3.2a. Physical soil properties. ....	76
Tab. 3.2b. Physical soil properties. ....	76
Tab. 3.2c. Physical soil properties. ....	76
Tab. 3.3a. Chemical soil properties. ....	77
Tab. 3.3b. Chemical soil properties. ....	77
Tab. 3.3c. Chemical soil properties. ....	77

### Chapter 4

Tab. 4.1. A selection of published rates of sediment generation and bedrock lowering/denudation rates determined with TCN ( $^{10}\text{Be}$ , $^{26}\text{Al}$ ). ....	98
Tab. 4.2. TCN-derived SPR for study sites, in and outside, Australia. ....	101
Tab. 4.3. Measurements of terrestrial cosmogenic nuclide concentrations ( $^{10}\text{Be}$ ), Werrikimbe National Park. ....	116
Tab. 4.4. Characteristics of soil formation and soil production rate distributions for the compiled data sets. ....	128

### Chapter 5

Tab. 5.1. Modified single-aliquot regenerative-dose (SAR) protocol. ....	142
Tab. 5.2. Dose rate data calculated from gamma spectrometry data. ....	144
Tab. 5.3. Amount of sensitive and responsive grains out of the total number of grains analysed with OSL. ....	147
Tab. 5.4. Single dose data calculated in applying the Minimum Age Model using an overdispersion of 10 %. ....	164
Tab. 5.5. Soil residence times for equivalent soil depths. ....	176
Tab. 5.6. Calculated average rates of soil mixing for toposequence Mount Boss and Plateau Beech. ....	177

<b>Tab. 5.7.</b> Latitudinal variation of mean bomb-derived strontium-90 inventories at the end of 1983. ....	186
<b>Tab. 5.8.</b> Global variation in the total annual deposition of lead-210. ....	186
<b>Tab. 5.9.</b> Fallout radionuclide data analysed with gamma spectrometry, displayed in conjunction with relevant soil properties. ....	189
<b>Tab. 5.10.</b> Loss/gain of $^{137}\text{Cs}$ and $^{210}\text{Pb}_{\text{ex}}$ in $\text{Bq kg}^{-1}$ along the hillslopes. ....	195
<b>Tab. 5.11.</b> Loss/gain of $^{137}\text{Cs}$ and $^{210}\text{Pb}_{\text{ex}}$ in $\text{Bq m}^{-2}$ along the hillslopes. . .	195

## Chapter 6

<b>Tab. 6.1.</b> Compilation of global rates of river sediment flux, sediment discharge to the oceans, global rates of soil erosion and soil formation (estimates for native vegetation, conservation agriculture and conventional agriculture).....	203
--	-----



“There is nothing in the whole of nature which is more important than or deserves as much attention as the soil. Truly it is the soil which makes the world a friendly environment for mankind. It is the soil which nourishes and provides for the whole of nature; the whole of creation depends on the soil which is the ultimate foundation of our existence.”

*Albert Fallou, 1862*

“The nation that destroys its soil destroys itself!”

*US-President Franklin D. Roosevelt, 1930*

## Chapter 1 Introduction

### *Research Context*

Our knowledge of plant and animal growth and development is far superior to that of the evolution of soil, yet soil plays a fundamental role in natural ecosystems. Soil provides many ecosystem services that are beneficial for humankind (Palm et al., 2007).

To name a few of these important functions, soil holds water from rainfall and irrigation and provides nutrients from organic or mineral sources that are essential for plant growth. Within the soil body, biota decompose organic materials, are responsible for nutrient cycling and also regulate gas fluxes from and to the atmosphere. Furthermore, soil can capture hazardous substances through mineral absorption processes. Soil also acts as purifier for water storages like groundwater, filtering out impurities and contaminants whilst simultaneously adding dissolved minerals (Buchan, 2010).

Despite its fundamental importance for the functioning of ecosystems our knowledge of soil is still limited (Brantley et al., 2007). Ecosystem changes such as change in land use and land management practices can affect the functioning of the soil system, and in turn can have a major impact on the global water and energy balance. Therefore it is important to understand the dynamics of soil systems, particularly given growing evidence that humankind may have accelerated natural soil erosion rates by a factor as large as 30, according to recent publications (Brantley, 2010; Wilkinson and McElroy, 2007).

To understand the complexity of soil we need to explore processes that lead to its formation. Research in pedogenesis has been focused on formalizing soil-forming factors and processes to ultimately model soil formation in the landscape. Early models of pedogenesis described soil formation qualitatively and were mostly limited to a description of soil evolution in the landscape. They led to the development of qualitative models of pedogenesis based on empirical observations and later to quantitative models of pedogenesis based on empirical equations or detailed differential equations derived from fundamental physics.

Early publications attempting to model pedogenesis quantitatively emphasized the importance of collecting field data to be able to mechanistically model soil-formation processes in the landscape (Huggett, 1975; Yaalon, 1975). Kirkby (1977) proposed the first mechanistic soil formation model on the soil profile scale and later Minasny and McBratney (1999, 2001) presented a basic mechanistic model that considered soil formation spatially at the catena scale. This was followed by Salvador-Blanes et al. (2007), who modelled long-term soil profile evolution considering the formation of soil layers. To improve and validate these quantitative

models of pedogenesis field and laboratory work is needed. In order to estimate and verify model parameters it is important to collect real-world data.

The introduction of sophisticated dating methods has made it possible to derive rates for processes of soil formation from field data.

Measurements of *in situ* terrestrial cosmogenic nuclide concentrations from soil parent materials sampled underneath different thicknesses of soil have made it possible to derive soil production rates for different environments. Furthermore, dating of individual quartz grains with optically stimulated luminescence has made it possible to derive the age of soil horizons and potential rates of soil mixing. The determination of soil production rates using terrestrial cosmogenic nuclides and the estimation of rates of soil mixing are a significant breakthrough for the quantification of pedogenesis and have much potential. Further studies are needed and are likely to be profound (Humphreys and Wilkinson, 2007) in terms of enhancing our understanding of soil forming processes and uncovering the history of soil.

*Aims*

- To conduct a field survey in a natural, undisturbed environment to explore the formation of soil profiles.
- To sample soil profiles along a hillslope to better understand soil formation in the landscape.
- To apply a sampling concept ideal for quantifying processes of pedogenesis in the landscape.
- To quantify processes of soil formation in the landscape implementing new dating methods that enable the estimation of rates of pedogenic processes *in situ*.
- And therefore to parameterize pedogenic processes to estimate rates of soil production from parent materials and vertical and lateral movements in the soil profile.
- To use *in situ* terrestrial cosmogenic nuclides to derive rates of soil production from soil parent materials.
- To apply optically stimulated luminescence to derive potential mixing rates of soil and to estimate the age of soil layers in the profile.

This research was funded by the ARC Discovery Project 'How do soils grow?' and the Australian Institute of Nuclear Science and Engineering (Award number AINGRA08133).

## Chapter 2 Quantifying pedogenesis – A literature review

The following literature review will present and discuss various models of pedogenesis. Since comprehensive reviews on models of soil formation have been presented by Hoosbeek and Bryant (1992), Amundson (2004), Schaetzl and Anderson (2005) and Minasny et al. (2008), here, we only summarize the main models and focus on models of soil formation processes such as the weathering of parent materials and soil mixing.

### 2.1 Introduction

Soil is a very complex system composed of a variety of interconnected physical, biological and chemical factors. It exists at the interface of the atmosphere, biosphere, hydrosphere and lithosphere. The interface or zone where soil formation processes take place has become known recently as the *critical zone* (Brantley et al., 2007), where rocks meet life (see Figure 2.1 and Box 2.1). Here, soil weathering, soil mixing and soil erosion processes occur over several time scales, from the colloid ( $\mu\text{m}$ ), grain ( $\text{mm}$ ), soil horizon ( $\text{cm}$ ) and soil profile ( $\text{m}$ ) scales to the landscape ( $\text{km}$ ) and global ( $\text{Mm}$ ) scale.

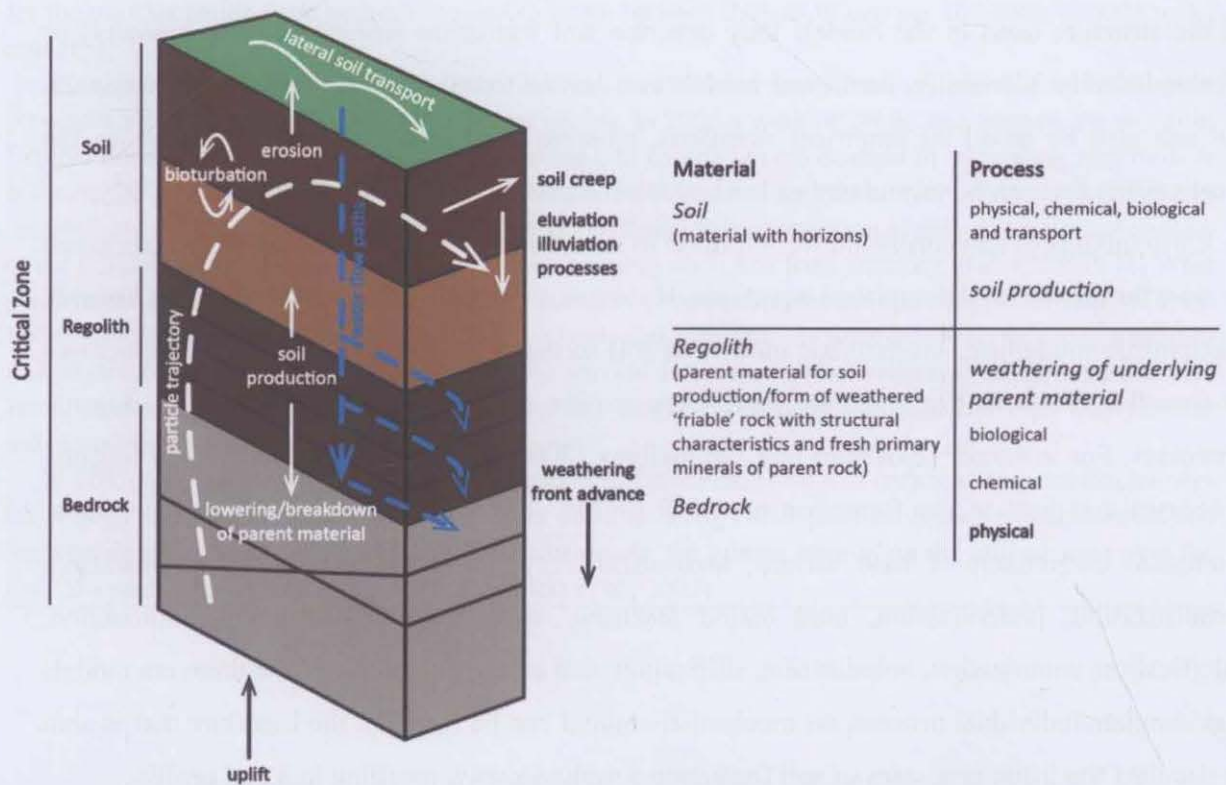


Fig. 2.1. Vertical layering within the critical zone (based on Anderson et al. (2007) and Graham et al. (2010)).

The importance of soil is also reflected in the recent US National Research Council publication “Landscapes on the Edge: New Horizons for Research on Earth’s Surface” (NAS, 2010) that addresses the challenges and opportunities in Earth surface processes. The Earth’s surface is defined as a dynamic interface where physical, chemical, biological, and human processes cause and are affected by forcings in the Earth system.

To understand the complexity of the soil system it is important to investigate soil formation processes quantitatively. Ultimately, quantifying pedogenesis should give answers to questions such as:

- (1) How does soil form?
- (2) At what rate does soil evolve over time? and
- (3) How fast are rates of soil turnover occurring in the soil profile and what influence do they have on pedogenesis?

Over the years, soil scientists have formalised concepts and models of soil formation to improve our knowledge of pedogenesis. Based on the degree of computation these models describe soil formation qualitatively and/or quantitatively. Furthermore, based on the complexity of the structure used in the models they describe soil formation empirically (functionally) or mechanistically. Generally, functional models are limited to a description of pedogenic factors, but can also be based on empirical equations, whereas mechanistic models are based on the mechanisms that can be formulated as mathematical equations (Hoosbeek and Bryant, 1992).

Early models of soil formation were limited to a description of soil evolution in the landscape or were based on simple empirical equations. However, there has been a shift of interest towards mechanistic modelling. Mechanistic models of soil formation implement soil-forming processes to describe soil formation quantitatively. They require a detailed understanding of pedogenic processes. For instance, Bockheim and Gennadiyev (2000) identified a total of 17 soil forming processes that lead to the formation of a soil profile. These processes include argilluviation, biological enrichment of base cations, andisolization, paludization, gleization, melanization, ferrallitization, podzolization, base cation leaching, vertization, cryoturbation, salinization, calcification, solonization, solodization, silification, and anthrosolization. While there are models that simulate individual process, no mechanistic model can be found in the literature that is able to simulate the listed processes of soil formation simultaneously, resulting in a soil profile.

This review will focus on exploring and quantifying the pedogenic processes of the physical and chemical weathering of bedrock, the formation of soil horizons and the rate of soil mixing processes, short-term and long-term.

#### Box 2.1: The Critical Zone

The term critical zone is used quite extensively in recent literature of Earth Sciences. The critical zone is defined as ‘the external terrestrial layer extending from the outer limits of vegetation down to and including the zone of groundwater’, which ‘sustains most terrestrial life on the planet’ (Brantley et al., 2006), (Figure 2.1).

The critical zone is described as the zone where chemical, biological, physical and geological processes are combined to control the development of soils and ecosystems. It is known as a complex mixture of air, water, biota, organic matter and earth materials (Brantley et al., 2007). Within the critical zone, a weathering engine transforms bedrock and biomass into soil, the ‘living skin’ of the Earth (Anderson et al., 2007). The weathering engine is driven by physical and chemical weathering processes that fracture, grind and dissolve the bedrock; and biological ‘weathering’ and turbation processes (Anderson et al., 2007). Within the critical zone, soil acts as an open system that is subject to element gain and losses. Studying this central component of the critical zone is imperative, since knowledge of soils is still limited despite their fundamental importance (Brantley et al., 2007). Rates of soil production and loss, bedrock or outcrop weathering and erosion have been estimated in the literature, but a comparison is often challenging (Brantley et al., 2007). For instance, for undisturbed forested landscapes rates of soil production and soil loss are assumed to be balanced within the critical zone, varying between 7 and 80 mm per 100 years (0.07 and 0.8 mm yr<sup>-1</sup>). In contrast, weathering rates estimated from field data for the transformation from bedrock to regolith range between 0.05 to 10 mm per 100 years (0.0005 to 0.1 mm yr<sup>-1</sup>).

At present, interdisciplinary research is focusing on exploring how chemical, physical and biological processes work together within the weathering engine. In 2006 a working group was formed, the so called Critical Zone Exploration Network ([www.czen.org](http://www.czen.org)), to emphasize the demand in integrating new tools to estimate the processes within the critical zone from field data and therefore to answer process-orientated research questions (Brantley et al., 2006). Questions related to the formation of soil as a major component of the critical zone that need to be explored and answered are (cited from Brantley et al. (2006)): (1) What controls the thickness of the critical zone? Research is focused on how fast and deep weathering of fresh bedrock occurs and what kind of agents are involved, and therefore (2) What controls the rate of chemical and physical weathering? (3) What controls the vertical structure and heterogeneity of the critical zone? Here, research is focused on the mechanisms that ultimately lead to a certain soil type and produce individual soil horizons.

In 2007, volume 3 (Number 5) of the magazine *Elements* explored and reviewed the interdisciplinary knowledge and future research on *The Critical Zone* focusing on its physical and chemical controls and biogeochemical agents and expressing the need to study the human imprint on the critical zone over the past 250 years (Amundson et al., 2007; Anderson et al., 2007).

## 2.2 Conceptual models of soil formation – Factors, Processes, Pathways, Energy

The extent of soil formation is believed to be dependent on local site characteristics. To model the evolution of soil in the landscape, we need to know which factors and processes are important for describing pedogenesis quantitatively. In the following, conceptual models of soil formation are reviewed briefly; they form the basis of mechanistic soil-formation models.

### *Factors*

Dokuchaev is known as the first soil scientist who formulated an equation of soil-forming factors in 1892 (Volobuyev, 1974). The Russian soil scientist linked the formation of soil to environmental factors using a descriptive equation:

$$P = f(K, O, G)B \quad \text{equation (2.1),}$$

where  $P$  is the soil,  $K$  is the climate,  $O$  are the organisms,  $G$  is the ground or parent rock and  $B$  is the time.

In the “Western world” Shaw (1930) can be seen as the first soil scientist, who published an equation that described “potent” soil-forming factors. In his equation he stated that soil ( $S$ ) is formed from parent materials ( $M$ ) by a combination of climatic factors ( $C$ ) and vegetation ( $V$ ) as a function of time ( $T$ ). In addition to these soil forming factors, he also included the processes of erosion and deposition ( $D$ ) to describe soil formation in the landscape:

$$S = M(C+V)^T + D \quad \text{equation (2.2).}$$

Although presented as a mathematical equation, it is only a factorial model, listing the major soil-forming factors. Shaw (1930) emphasised that the influence of these factors in developing soil is not uniform, but rather changes with local conditions.

Shaw’s soil formation equation was discussed in a 2008 issue of ‘Pedometron’ (The Newsletter of the Pedometrics Commission of the IUSS, No. 25, page 25) and it was brought to our attention that Shaw presented his conceptual model at the ‘Second International Congress of Soil Science’ in Leningrad in 1930. Following the presentation, there is a lengthy discussion on Shaw’s model. For instance, a comment was made: “Prof. Romell suggested to Dr. Shaw in order not to hurt the mathematicians feelings to simply put  $S$  equal to a general function of the other symbols”:

$$S = f(M, C, V, T, R) \quad \text{equation (2.3).}$$

However, Shaw did not develop his model any further before he died suddenly in 1939. Furthermore, we learned that Jenny (1941), who published the most referred to and cited model of soil formation, was also a presenter at the Second World Congress of Soil Science and that



Jenny interacted with Shaw in Berkeley (University of California). We also found out that both Shaw and Jenny were aware of Dokuchaev's earlier work on formulating a soil-formation equation. Subsequently, it was hypothesized that Jenny's factors of soil formation equation was developed following the discussions of Shaw's paper in 1930.

Jenny's (1941) state factor model is also called the '*clorpt*' model. It comprises independent variables or state factors that define the state of a soil system. Hence, the state factors are not considered as formers or creators of the soil.

$$S = f(cl, o, r, p, t) \quad \text{equation (2.4),}$$

where *cl* is the climate, *o* are the organisms, *r* is the topography, *p* is the parent material and *t* is the time. The state factors are independent from the soil system and vary in space and time (Amundson and Jenny, 1997).

In its original form the state-factors model was unsolvable. To be solved the indeterminate function *f* needs to be replaced by certain quantitative relationships. Hence, the '*clorpt*' equation has been formalized in quantitative ways based on empirical field observations, where a single factor is defined by keeping the other factors constant (Minasny et al., 2008). Empirical models were developed to describe soil formation in the form of quantitative climofunctions, biofunctions, topofunctions, lithofunctions and chronofunctions, mostly based on numerically intensive statistical methods (McBratney et al., 2003; Yaalon, 1975). Based on the '*clorpt*' model of soil formation McBratney et al. (2003) formulated the '*scorpan*' model, which indeed applies empirical quantitative relationships to predict soil properties from landscape attributes at specific locations in the landscape. The '*scorpan*' model is written as:

$$Sc / Sa = f(s, c, o, r, p, a, n) \quad \text{equation (2.5),}$$

where *Sc* are the soil classes and *Sa* are the soil attributes, *s* is the soil, *c* is the climate, *o* are the organisms, *r* is the topography, *p* is the parent material, *a* is age and *n* is space or the spatial position. The model is used quite extensively in the field of digital soil mapping to predict the recent state of the soil (soil properties), but is not intended for, and can not be applied, for long-term soil formation predictions.

### Processes

One of the first soil scientists who described soil formation as processes instead of factors was Simonson (1959). He considered two processes important for the evolution of soil, i.e. the accumulation of parent materials and the differentiation of soil horizons in the soil profile. Furthermore, he described the evolution of soil types as a function of additions (i.e. organic

matter), removals (i.e. soluble salts), transfers (i.e. humus and sesquioxides) and transformations (i.e. primary minerals into secondary minerals) as demonstrated in Figure 2.2:

$$s = f(\text{addition, removal, translocation, transformation}) \quad \text{equation (2.6).}$$

The soil-forming processes approach by Simonson (1959) can be seen as one of the conceptual frameworks for mechanistic models of soil formation implementing physical laws (Minasny et al., 2008). However, the original work is still a qualitative description.

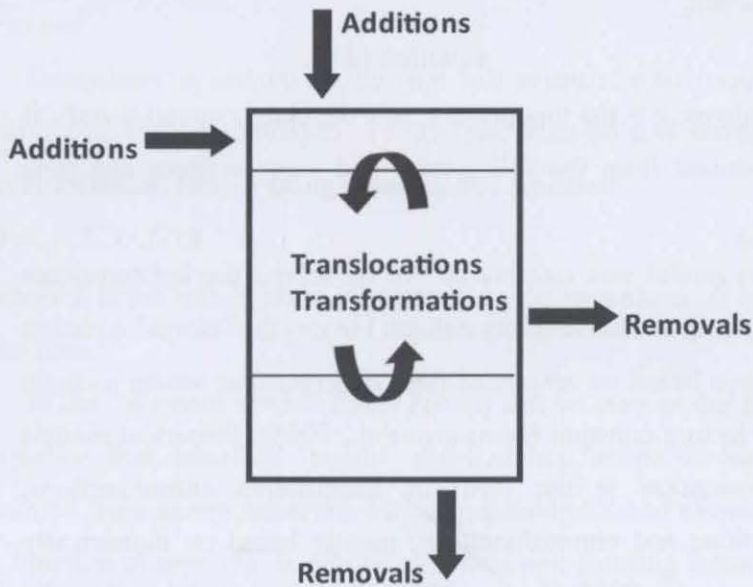


Fig. 2.2. Soil profile evolution as a function of additions, removals, translocations and transformations.

### Pathways

Johnson and Watson-Stegner (1987) introduced the concept of pathway models. They viewed soil evolution as a result of genetic pathways. Their model considers soil as a complex open system with changes in soil thickness and increasing genetic complexities with time. They state that soils ( $S$ ) form progressively ( $P$ ) and regressively ( $R$ ) along interacting pathways:

$$S = f(P, R) \quad \text{equation (2.7),}$$

where  $P$  stands for progressive pedogenic conditions, including processes and factors that promote horizonation, developmental (assimilative) upbuilding and/or subsurface deepening; and  $R$  stands for regressive pedogenic conditions, including processes and factors that promote haploidization, retardant (nonassimilative) upbuilding and/or surface removal. Soil evolves along these progressive and regressive pathways, where some might be dominant over others. This is yet another qualitative description.

### Energy

Models of soil formation based on the concepts of energy describe pedogenic factors and processes implementing the principles of energy or concepts of thermodynamics. The most well known and cited soil scientist addressing this possibility has been Runge (1973). However, in their review Minasny et al. (2008) emphasized the work of Volobuyev from Azerbaijan. Volobuyev published various papers on linking pedogenic processes with laws of energy. The most relevant models for estimating soil formation from energy laws will be included here.

Runge (1973) presented a different type of factorial model, formulating soil evolution based on energy:

$$S = f(o, w, t) \quad \text{equation (2.8),}$$

where  $S$  is the soil,  $o$  is the organic matter production (renewing factor),  $w$  is the amount of water available for leaching (developing vector) and  $t$  is time. Climate and relief are expressed within the vector  $w$ . This energy model relies on gravity as the main source of energy, driving the infiltration of water in the soil, which is responsible for horizonation. The model considers solar energy indirectly in the production process of organic matter. The energy model of Runge (1973) is only useful in a qualitative way, because actual quantitative thermodynamical calculations are not implemented in the model (Hoosbeek and Bryant, 1992).

In an unpublished thesis Regan (1977) studied soil formation through energy processes and created an energy model of soil formation. He based his studies on soils derived from limestone and marine washed sands in Florida, USA. Regan (1977) calculated the total amount of energy needed to form soils by implementing the energy from sunlight; the energy flux from carbon dioxide production by organisms, wind, temperature; the chemical energy of rain; the kinetic energy developed from sloped surfaces; the chemical free energy of phosphorus and the gravitational energy from uplift processes. Running the energy model steady-state conditions of soil formation are reached after only 525 years for soils with sandy parent materials, and after 375 years for soils with calcareous parent materials with a rate of approximately  $5.65 \times 10^3 \text{ kJ m}^{-2} \text{ yr}^{-1}$ . Rates of soil formation with time are obviously underestimated, but nevertheless this model can be seen as a good example for linking the amount of energy needed for soil formation with vegetation and urban growth (Minasny et al., 2008).

The quantification of processes of energy transformation during soil formation was addressed intensively by Volobuyev. For instance, he described the expense of energy in the process of soil formation applicable for all climatic zones as follows (Volobuyev, 1974):

$$Q = Ra = Re^{-1/mK}$$

equation (2.9),

where  $Q$  is the expenditure of energy on soil formation,  $R$  is the energy of solar radiation,  $a$  are the available energy sources,  $K$  is the relative wetness and  $m$  is a factor expressing the participation of biological activity (biota) in energy exchange.

Following on, Volobuyev and Ponomarev (1977) investigated various thermodynamic aspects of soil-forming processes. They calculated Gibbs' free energy ( $\Delta G$ ) and entropy ( $S$ ) for different soil types from individual Gibbs' free energy and entropy values of soil minerals (see Volobuyev and Ponomarev (1977), Table 1, page 6) showing that the thermodynamic characteristics of soil minerals vary significantly for the soil types studied. In addition, they identified two soil groups based on their energy expenditure during mineral formation: (1) one that is characterized by a decrease in Gibbs' free energy and an increase in entropy (2) and one that is characterized by an increase of Gibbs' free energy and a decrease in entropy.

Furthermore, Volobuyev et al. (1980) used these Gibbs' free energy potentials for soils to predict their infiltration or leaching capacity. They showed that the lower the Gibbs' free energy levels of soils, the higher their infiltration capacities. Based on calculations from Volobuyev and Ponomarev (1977) and Volobuyev et al. (1980), Minasny et al. (2008) presented Gibbs' free energy and entropy for different soils, rocks and minerals as shown in Figure 2.3.

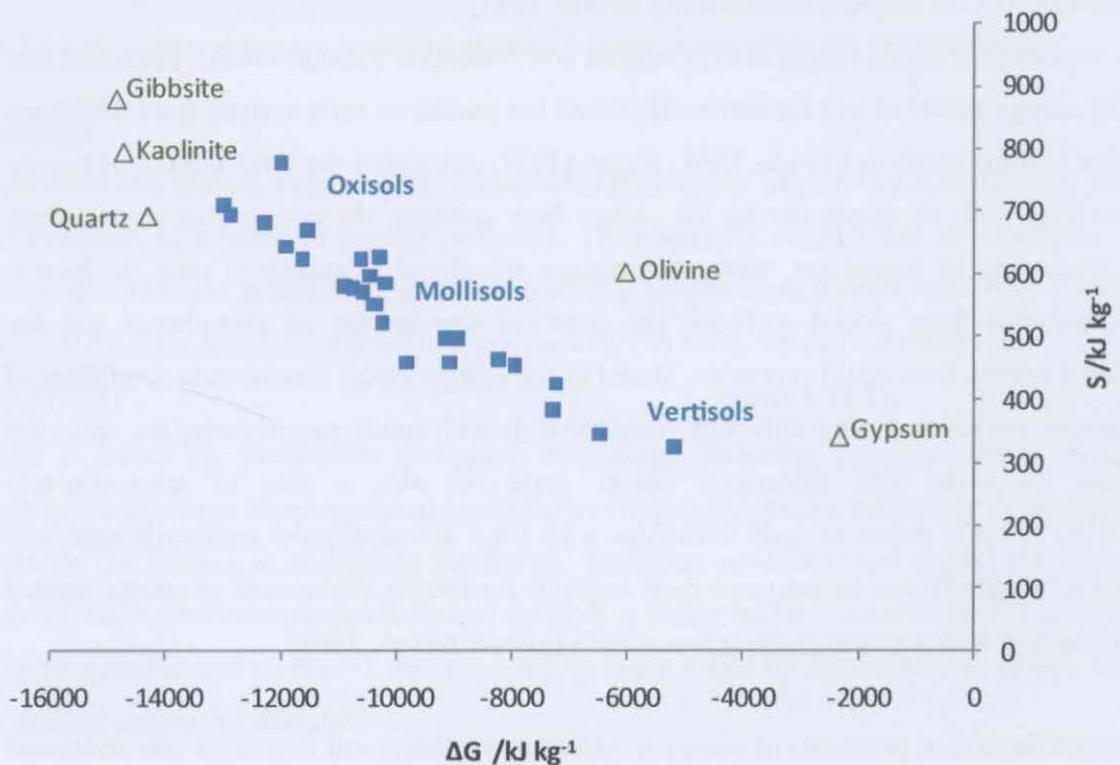


Fig. 2.3. Gibbs' free energy ( $\Delta G$ ) and entropy ( $S$ ) for different soils, rocks and minerals (Graph is based on Minasny et al. (2008)).

Soils enriched with  $\text{SiO}_2$ ,  $\text{Al}_2\text{O}_3$ ,  $\text{Fe}_2\text{O}_3$  and  $\text{CaCO}_3$  and large quantities of residual minerals have low Gibbs' free energy (which is 'lost' during weathering) and high entropy. In the order of higher energy and lower entropy, this is followed by phyllosilicate minerals, carbonates, and soluble salts. A decrease in Gibbs' free energy and an increase in entropy is associated with minerals that have higher intensity of leaching and are more resistant to weathering.

Volobuyev (1984) also formulated an energy model to apply Dokuchaev's equation quantitatively (equation 2.1):

$$Q = R(\pm r) \exp \left[ -\frac{P_c w R 0.67}{m P (\pm p)} \right] \quad \text{equation (2.10),}$$

where  $Q$  is the (annual) expense of energy on soil forming processes,  $R$  is the radiant solar energy,  $P$  is the relative wetness,  $m$  is the biological activity,  $r$  is the radiation balance,  $p$  is the atmospheric precipitation,  $w$  (chemically bound water of mineral soil components) is the rate of mineral transformations in soils and  $P_c$  is water, such as water that is fixed in the mineral, faunal and floral component of soils. Dokuchaev's soil forming factors (equation 2.1) are represented by  $R$  and  $P$  (climate,  $K$ ), by  $m$  (organisms,  $O$ ), by  $P_c$  and  $w$  (parent rock,  $G$ ), and ( $m$ ) by  $p$  and  $r$ .

### Summary

Conceptual models of pedogenesis have been, and are still being developed, for the past 100 years. These include the factorial, processes, pathways and energy models. However, these models are mostly interpreted qualitatively, although some have been applied in a quantitative way, i.e. the factorial model of Jenny that could be solved by applying empirical quantitative relationships to predict soil properties from landscape attributes. These conceptual models can form the basis of mechanistic models.

### 2.3 Soil weathering and production

As described in the previous sections, several processes are responsible for transformations, translocations, additions and removals in the soil system. Ultimately these processes and their associated transformations of energy result in the formation of a particular soil profile. Furthermore, the dynamics of the interacting chemical, physical and biological processes are believed to be induced by different parent materials and climates. The horizonation and differentiation of the soil profile is the result of transformation processes like soil weathering and soil mineralisation, decomposition and humification and aggregate formation as well as translocation processes like eluviation and illuviation.

A common perception in pedology is that pedogenesis is a product of mostly downward moving processes like leaching that lead to the formation of interrelated layers, the A and B horizons (Huggett, 1998). Pedoturbations, the so called soil-mixing processes are seen as processes that are working against horizonation rather than promoting it, because of possible mixing of surface and subsoil materials induced by mixing agents such as soil biota, soil moisture changes and periodic freezing and that are resulting in the subsequent homogenisation of the layers in the soil profile (Huggett, 1998).

The following sections will explore how processes of soil formation are modelled or estimated with field data in the literature.

#### 2.3.1 Production of soil from parent materials

According to NAS (2010): “The breakdown of bedrock – a major factor in Earth surface processes – is among the least understood of the important geological processes.”

The evolution of soil has been explained vastly with the help of chronosequences over time scales of up to millions of years. Traditional theories of soil evolution along chronosequences explain soil development progressively under the influence of environmental factors until soil development is in equilibrium (Huggett, 1998). Accordingly, it is believed that the development of a certain soil type is preset in a certain landscape, i.e. in the German soil classification scheme, on limestone parent materials rendzinas are formed that eventually evolve into brown earths. For instance, chronosequences were created based on conceptual ideas and observations in the field with the help of successional stages of vegetation by placing them in a chronological order, and by exploring soil profiles that developed on surfaces of known age (Schaezel and Anderson, 2005). One discrepancy in formulating chronosequences is the assumption of constant soil-forming factors except time. This is especially unlikely for the soil-forming factors climate

and vegetation cover. New views in evolutionary pedogenesis tried to explain the non-linear behaviour of soil development by assuming that soils evolve through continual formation and destruction, and consequently might progress, regress or stay constant depending on environmental conditions (Huggett, 1998).

Chronosequences can be transformed into chronofunctions by plotting soil and landscape properties against time (or age) using time as the independent variable, based on Jenny's state factor equation (Schaezel and Anderson, 2005):

$$S(\text{Soil}) = f_t(\text{time})cl, o, r, p... \quad \text{equation (2.11).}$$

Furthermore, statistical models can be applied to express chronosequence data (soil and landscape properties) mathematically by fitting curves of soil evolution with time. Schaezel et al. (1994) reviewed types of mathematical functions commonly used in chronofunctions (Figure 2.4).

Demonstrated in Figure 2.4 chronofunctions might be modelled using:

- (1) simple linear behaviour  $Y = a + bt$
- (2) single logarithmic behaviour  $Y = a + b(\log t)$
- (3) exponential behaviour  $Y = a \exp(bt)$
- (4) power functions  $Y = at^b$
- (5) or non-linear-sigmoidal functions  $Y = 1/(a + b \exp(-t))$ .

Linear functions suggest that the soil system evolves at a constant rate through time whereas logarithmic models imply that the soil system is in steady state or will reach a steady state eventually some time in the future. Nonlinear-sigmoidal chronofunctions propose that the soil system evolved along periods of rapid pedogenesis followed by decreasing rates (Schaezel et al., 1994).

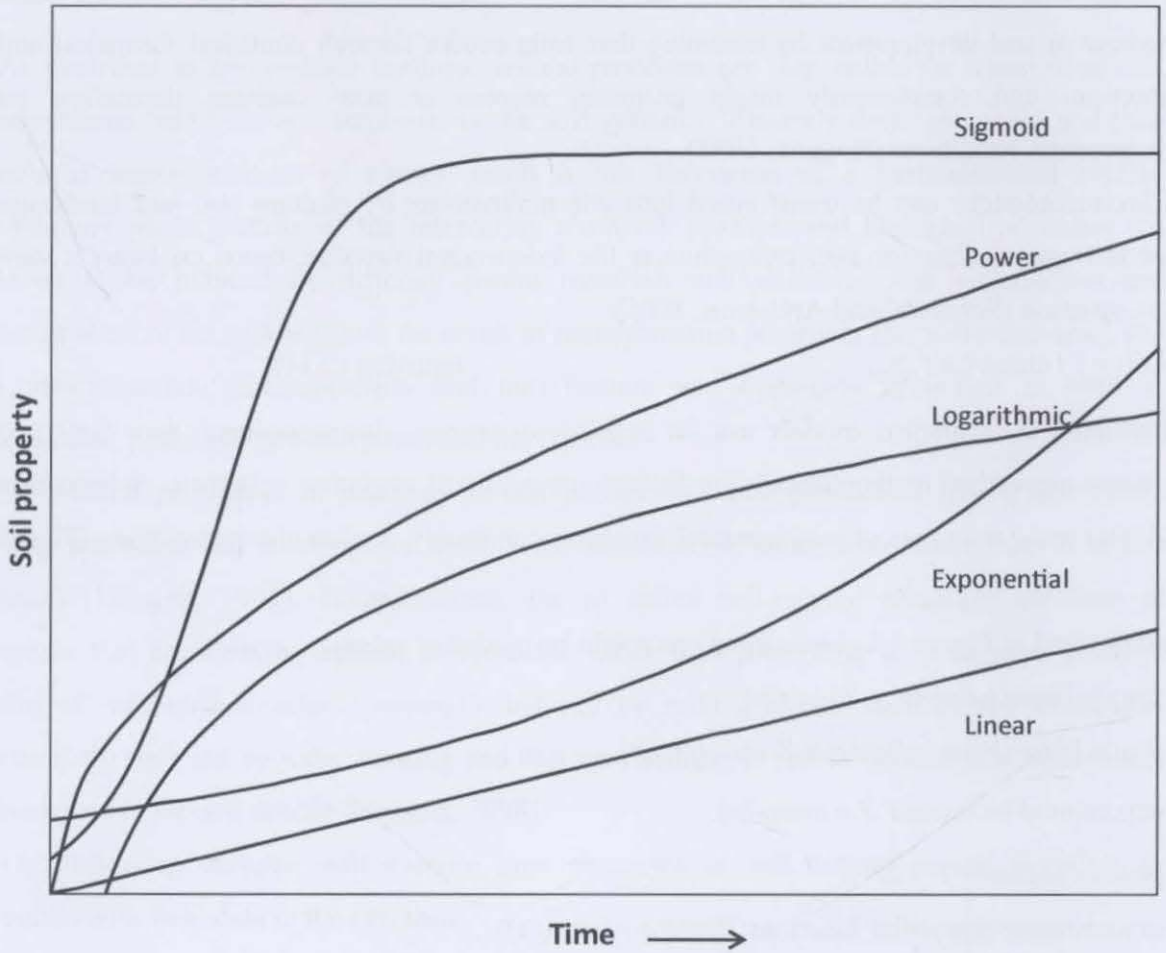


**Fig. 2.4.** Types of mathematical functions commonly used in chronofunctions (adapted from Schaezel et al. (1994)). S-shaped or sigmodial curve, general form of equation:  $Y=1/(a+b\exp(-t))$ ; power functions, general form of equation:  $Y=at^b$ ; logarithmic functions, general form of equation:  $Y=a+b(\log t)$ ; exponential functions, general form of equation:  $Y=a\exp(bt)$ ; simple linear functions, general form of equation:  $Y=a+bt$ .



Following the concepts of chronofunctions, production rates of soil from parent materials (rock) were assumed to decrease with time and were discussed to follow a linear or non-linear function of time (Colman, 1981). However, there are two concepts of soil production that have been discussed much more extensively in the geomorphology literature than in pedology (Figure 2.5).

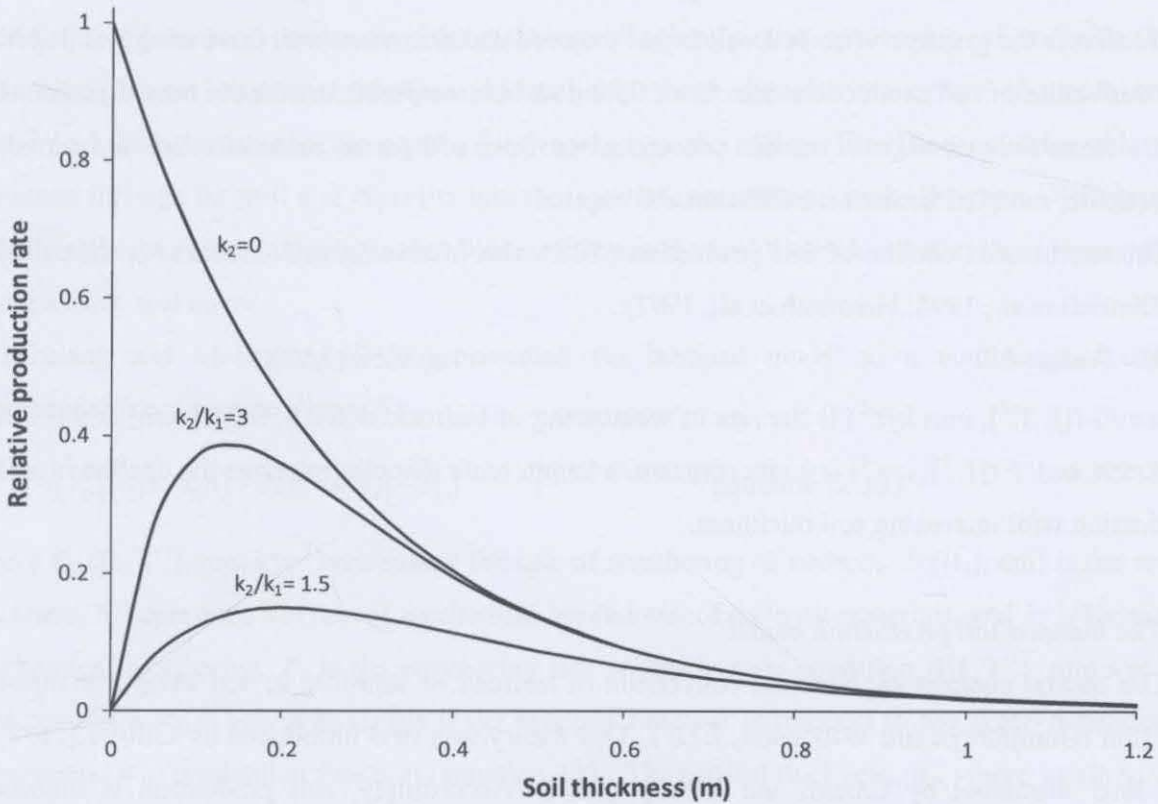


**Fig. 2.5.** The rate of soil production versus soil thickness (based on Minasny and McBratney (2006), based on Furbish and Fagherazzi (2001)). Here, both the exponential and the humped soil production model are presented graphically. Both axes are dimensionless. Soil production is presented graphically depending on different values of the parameter  $k_1$  and  $k_2$  (see equation 2.13 and 2.14). If  $k_2 = 0$  the soil production equals a depth-dependent exponentially decreasing soil production function. If  $k_2/k_1 \geq 0$  soil production shows a ‘humped’ function.

#### (1) *The exponential soil-production model*

This model states that the formation of soil declines exponentially with increasing soil thickness. This theory was discussed conceptually by Ahnert (1977). He assumed that the rate of soil production from hillslopes decreases exponentially with increasing thickness of the overlying soil mantle. The exponential decrease of the rate of soil production with increasing soil thickness is believed to be dependent on the soil temperature and water penetration through the soil profile. The exponential decrease of the temperature range with increasing soil depth is seen as a factor for reduced weathering with increasing depth below the soil surface (Minasny and

McBratney, 1999). Furthermore, the occurrence of moisture related processes like freeze-thaw also decreases exponentially under increasing soil depth.

Heimsath et al. (1997; 1999) verified the exponential decline of soil formation with increasing soil depth with field data from the Tennessee Valley in California, USA, and found field evidence for the theory of exponential decline of soil production with increasing soil depth and parameterized the potential weathering rate of bedrock. According to this research soil production is the greatest when bedrock is just exposed and decreases with increasing soil depth. The derivation of soil production rates from field data became possible with the measurement of *in situ* terrestrial cosmogenic nuclide concentrations from soil parent materials such as bedrock or saprolite, sampled underneath different soil depths.

The exponential decline of soil production (SPR) with increasing soil thickness is described as (Dietrich et al., 1995; Heimsath et al., 1997):

$$\text{SPR} = P_0 \exp(-bh) \quad \text{equation (2.12),}$$

where  $P_0$  ( $[L T^{-1}]$ ,  $\text{mm kyr}^{-1}$ ) is the rate of weathering of bedrock at  $h = 0$ ,  $h$  ( $[L]$ ,  $\text{cm}$ ) is the soil thickness and  $b$  ( $[L^{-1}]$ ,  $\text{cm}^{-1}$ ) is a rate constant, a length scale that characterizes the decline in soil production with increasing soil thickness.

## (2) The humped soil production model

The second concept explains the conversion of bedrock or saprolite to soil using a humped function (Humphreys and Wilkinson, 2007). This theory was first introduced by Gilbert (1877) and later discussed by Carson and Kirkby (1972). Accordingly, soil production is highest underneath a nonzero soil depth. Hence, the weathering of bedrock is greatest underneath an incipient soil depth and slower underneath exposed bedrock or an already thick soil mantle.

The main explanation for the occurrence of a humped model of soil formation is the maximisation of chemical and physical weathering processes under an initial soil depth. The presence of water is discussed as a major factor in this phenomenon by Carson and Kirkby (1972). Water is considered as an important agent for chemical weathering of bedrock or saprolite into soil. Carson and Kirkby (1972) give an example for their reasoning: On an exposed site, like bedrock, water tends to run off, which lowers the rate of chemical weathering. This characteristic also applies for very thin soils where water runs off fast, because of insufficient pore space in the soil to hold the water. In soils with a thick soil cover the circulation of water also tends to be slow, which reduces the rate of weathering. Furthermore, because water tends to run off bare rock, processes of freeze-thaw are also limited underneath shallow or deep soil covers. Granger et al. (2001) proposed that the presence of moisture in an already thin soil cover

seems to be very important for the chemical weathering of granite rock to gneiss, which is relatively resistant to weathering.

Wilkinson and Humphreys (2005) discussed the role of fauna and flora to explain the occurrence of a humped model of soil production. They argue that animals and plants require a moderate soil mantle to promote soil production processes. Yoo et al. (2005) applied this theory when modelling the population of pocket gophers in relation to soil thicknesses. In addition to mesofauna, plant roots make an important contribution to the weathering of saprolite by disturbing the soil-saprolite interface. Most likely those disturbances create channels and therefore access for weathering agents (i.e. water) into the soil profile. Biota are also able to penetrate through the soil and saprolite into the zone of unweathered rock. However, Wilkinson and Humphreys (2005) also argue that biota will reach the soil bedrock interface less frequently under a thick soil cover.

Minasny and McBratney (2006) presented the humped model as a continuous double exponential function (see Figure 5):

$$\frac{\partial e}{\partial t} = -\left(P_0 [\exp(-k_1 h) - \exp(-k_2 h)] + P_a\right) \quad \text{equation (2.13)}$$

where  $P_0$  ( $[L T^{-1}]$ ,  $\text{mm kyr}^{-1}$ ) represents the rate of weathering of bedrock,  $h$  ( $[L]$ ,  $\text{cm}$ ) is the soil thickness,  $k_1$  represents the rate of mechanical breakdown of the rock materials, and  $k_2$  is the rate of chemical weathering,  $P_a$  is the weathering rate at steady-state condition ( $[L T^{-1}]$ ,  $\text{mm kyr}^{-1}$ ) with condition  $k_1 < k_2$ . As  $k_2$  equals 0 the humped function is reduced to the depth-dependent exponential soil production function (equation 11). The critical thickness,  $h_c$ , where weathering is at maximum is given by:

$$h_c = \frac{\ln(k_2 / k_1)}{k_2 - k_1} \quad \text{equation (2.14)}$$

An empirical parameterisation of the humped model from field data is still to be achieved, although Heimsath et al. (2009) assumed a humped form of soil production for a study site at Arnhem Land in Northern Australia for a landscape dominated by outcrops and soil depths no less than 35 cm.

Dietrich et al. (1995) applied the exponential and also the humped model to simulate soil formation in a catchment of the Tennessee Valley in California, USA. With a chosen maximum soil production at 25 cm, the landscape formed is characterised by sharply curved ridges and outcrops. In such an environment with humped soil production, soil depths below the peak of soil production are assumed to be unstable and together with soil erosion this will lead to a

stripping of the soil to bedrock. Consequently, no soil depths that are in equilibrium should be observed in the field for less than the peak in soil production. However, the modelling results of Dietrich et al. (1995) were more consistent with field observations when using an exponential model. Later work by Heimsath et al. (1997) showed that soil formation indeed followed an exponential function at the study site of  $0.077 \text{ mm yr}^{-1}$ .

The parameterisation of weathering rates of parent material to soil derived from *in situ* field data (TCN) will be discussed in more detail in research Chapter 4 (*In situ* Terrestrial Cosmogenic Nuclides). Following Heimsath et al. (1997) a small range of different authors applied the concepts of deriving SPR from TCN data. Soil production rates derived from TCN ranged between  $0.004$  and  $0.4 \text{ mm yr}^{-1}$  (Heimsath et al., 2000, 2001a; Heimsath et al., 2002; Heimsath et al., 2001b; Heimsath et al., 2009; Heimsath et al., 2005; Wilkinson and Humphreys, 2005).

Current research is also focused on finding the conversion rate of bedrock to regolith (Brantley, 2010; Graham et al., 2010). In pedology, bedrock as well as regolith are parent materials for soil production. Different to hard fresh rock, regolith is a form of weathered ‘friable’ rock that still has the structural characteristics and fresh primary minerals of the parent rock and is transformed into soil through physical disruptions. Regolith is already seen as a hospitable substrate, in particular for the soil flora. Published rates of regolith formation for hard granitic rocks are relatively low and range between  $0.004$  to  $0.02 \text{ m yr}^{-1}$  (Dosseto et al., 2008; Graham et al., 2010).

### 2.3.2 Chemical weathering of bedrock to soil

The chemical weathering of bedrock to soil is an important process in forming the soil mantle. Rates of chemical weathering have been estimated from both laboratory and field-based studies applying a variety of investigative methods. However, a time dependent difference between rates in the laboratory and field rates was found (Lasaga et al., 1994). Calculated laboratory rates were much faster when compared to observed field rates by up to five orders of magnitude (Brantley et al., 2007), yet both methods showed a decrease of chemical weathering with time.

In the laboratory, chemical weathering rates mostly depend on the experimental setup like pH, the percolation rate and the weathering state of the silicate minerals, i.e. fresh or partly weathered. For instance, White and Brantley (2003) investigated the long-term dissolution of plagioclase (weathering rate  $R$  in  $\text{mol m}^{-2} \text{ s}^{-1}$ ) extracted from fresh and weathered granite. In one of the longest experimental setups, of over 6 years, they determined parabolically decreasing

weathering rates of  $7.0 \times 10^{-14} \text{ mol m}^{-2} \text{ s}^{-1}$  for fresh Panola Granite, and found significantly less chemical weathering rates of  $2.1 \times 10^{-15} \text{ mol m}^{-2} \text{ s}^{-1}$  for partially weathered Panola Granite, which reached steady-state in only 2 months. After extrapolating decreasing weathering rates of fresh plagioclase with time, they concluded it would take several thousand years of reaction to replicate the rate of the naturally weathered plagioclase under identical experimental conditions.

Chemical fluxes in a watershed can be determined using the solute discharge flux  $Q_{i,dis}$  for a chemical species  $i$  based on a mass-balance approach:

$$Q_{i,dis} = C_{i,dis} \frac{V}{At} \quad \text{equation (2.15),}$$

where  $C_{i,dis}$  is the chemical concentration of a chemical species  $i$ ,  $V$  is the fluid mass,  $A$  is the geographic area of the watershed and  $t$  is time (White and Blum, 1995).

In watershed studies, chemical weathering kinetics of silicate (temperature dependence of dissolution rate) are often modelled empirically with the help of the Arrhenius equation, which describes the dependence of chemical weathering rates on the temperature ( $W_X$ ) in natural systems (White and Blum, 1995):

$$W_X = A \exp [-(\Delta E_X/RT)] \quad \text{equation (2.16),}$$

where  $A$  is an empirical constant that incorporates the effects of surface area and surface reactivity,  $\Delta E_X$  is the activation energy for the weathering reaction that releases element  $X$  ( $\text{kJ mol}^{-1}$ ),  $R$  is the universal gas constant ( $\text{J K}^{-1} \text{ mol}^{-1}$ ), and  $T$  is the absolute temperature in Kelvin ( $^{\circ}\text{K}$ ). Based on silicon-dioxide ( $\text{SiO}_2$ ) and sodium ( $\text{Na}$ ) fluxes, activation energies for chemical weathering were calculated to be 59.4 and 62.5  $\text{kJ mol}^{-1}$ , respectively.

A range of chemical weathering rates estimated from field data (usually expressed by  $\text{M L}^{-2} \text{ T}^{-1}$ ) can be found in the literature, a selection is presented in Table 2.1, Part 1 and Part 2. Part 1 summarizes chemical weathering rates based on elemental fluxes (loss and gain) in watersheds, and the chemical composition of the parent materials and weathering products studied. For instance, Colman and Dethier (1986) summarized rates of chemical weathering with time based on catchment mass-loss from solutes, varying between  $0.003 \text{ mm yr}^{-1}$  and  $0.04 \text{ mm yr}^{-1}$  for different climates and parent materials (Dethier, 1986; Pačes, 1986; Pavich, 1986; Velbel, 1986).

In another study Alexander (1988) calculated rates of chemical weathering based on mass-balance equations for 18 watersheds with noncarbonate lithologies. The predicted rates of about  $0.0017$  to  $0.16 \text{ mm yr}^{-1}$  were mostly dependent on the volume of runoff water and the soil to rock ratio, i.e. the mass of soil/mass of bedrock weathered to produce that amount of soil.

Summarizing Table 2.1 Part 1, we can see that rates of chemical weathering vary between  $0.00017 \text{ mm yr}^{-1}$  calculated for a tropical environment by Owens and Watson (1979) and  $0.473 \text{ mm yr}^{-1}$  calculated for a humid-tropical environment by Wakatsuki and Rasyidin (1992). However, the majority of compiled chemical weathering rates from these watershed studies ranged between approximately  $0.01$  to  $0.1 \text{ mm yr}^{-1}$ . A pattern of chemical weathering rates being grouped by study areas with similar climate regimes and parent materials was not readily discernible in the data.

In the current literature, various studies are now focusing on calculating chemical weathering rates of bedrock *in situ* to investigate soil formation processes. Calculated rates are presented in Table 2.1, Part 2, with Table 2.2 listing the main characteristics of the environments studied. The so-called weathering indices are used to estimate the extent of chemical weathering based on mass balance calculations or the ratio between the chemistry of fresh parent rock to that of weathered rock or soil (Taylor and Eggleton, 2001). Generally, the rock to soil ratio of an immobile, slowly weatherable mineral is used to estimate rates of chemical weathering based on its loss and gain. In most of the studies, zircon (Zr) is used.

#### *Definitions*

##### Total denudation rate

The term total denudation rate refers to the combined rate of chemical and physical weathering of rock to soil.

In publications of Riebe et al. (2003, 2004a, b), Green et al. (2006), Yoo et al. (2007) and Burke et al. (2009; 2007) total rates of denudation or weathering were substituted with rates of soil production derived with TCN. To estimate the extent of chemical weathering, determined chemical weathering rates (weathering indices) were subtracted from rates of soil production (TCN).

In the publication of Dixon et al. (2009), however, total denudation rates were calculated by combining determined chemical weathering rates (weathering indices) and rates of soil production (TCN). TCN-derived soil production rates were therefore substituted with rates of physical weathering.

Riebe et al. (2003, 2004a, b) calculated *in situ* rates of chemical weathering using weathering indices in conjunction with soil production rates derived from *in situ* cosmogenic nuclides. Soil production rates were substituted with total denudation rates to estimate the degree of chemical

weathering. The conservation of mass equation for the chemical weathering rate as a fraction of the total denudation (weathering) rate is written as:

$$W = D (1 - [Zr]_{\text{rock}}/[Zr]_{\text{soil}}) \quad \text{equation (2.17),}$$

where  $W$  is the chemical weathering flux in  $[M L^{-2} T^{-1}]$  or  $[L T^{-1}]$ ,  $D$  is the total denudation rate, and  $[Zr]_{\text{rock}}$  and  $[Zr]_{\text{soil}}$  are the concentrations in rock and soil of Zr.

Riebe et al. (2003, 2004a, b) estimated chemical weathering to vary between as low as  $0.0041 \text{ mm yr}^{-1}$  and as high as  $0.14 \text{ mm yr}^{-1}$ . At the study site in Rio Icacos, Puerto Rico (Riebe et al., 2003), results showed that chemical weathering accounted for 58 and 68 % of the total loss by chemical and physical weathering. On average  $0.021 \text{ mm yr}^{-1}$  were accounted for by chemical weathering of saprolite and  $0.054 \text{ mm yr}^{-1}$  were attributed to combined chemical weathering and physical soil weathering. Results from the study site at the Santa Rosa Mountains in Nevada (Riebe et al., 2004b) showed that chemical weathering rates decreased with increasing altitude from  $0.02$  to  $0 \text{ mm yr}^{-1}$ , suggesting a trend of dominance of physical erosion with increasing altitude. Sparsely vegetated, high-altitude crystalline terrain in particular seemed to be characterized by very slow silicate weathering rates. For 42 different study sites with granitic parent materials located in diverse climate regimes, the data analysis suggested that chemical weathering rates increased proportionally with supply rates of fresh material, i.e. 'supply-limited' weathering (Riebe et al., 2004a).

In the majority of the following studies conceptual ideas of Riebe et al. (2003, 2004a, b) have been employed. Green et al. (2006) conducted a study in the Bega Valley in south-eastern Australia to quantify chemical weathering along a hillslope, implementing soil production rates of the area as analysed by Heimsath et al. (2000). They calculated that mass loss by chemical weathering accounted for 35 % to 55 % of the total mass loss from the hillslope.

Results from Burke et al. (2007) indicated a decrease of chemical weathering of saprolite with increasing overlying soil thickness. At the study site Point Reyes in California, USA, chemical weathering accounted for 13 to 51 % of total denudation rates. Assumptions were made that spatial variation in chemical weathering is controlled by the topography of the study sites. Accordingly, weathering rates decreased with slope across the divergent ridge and increased with upslope contributing area in the convergent swale. Results also showed that measurements of saprolite abrasion pH were closely related to weathering indices, assuming that the intensity of chemical weathering decreased linearly with an increase in saprolite pH from 4.7 to 7.

Yoo et al. (2007) combined geochemical mass balance with sediment transport to predict rates of soil chemical weathering and transport on hillslopes. This research was conducted at a site in the south-eastern highlands (Frogs Hollow) in south-eastern Australia. Results showed losses of

soil chemical weathering rates of  $0.029 \text{ mm yr}^{-1}$  on the ridge and consequently gains of  $0.029 \text{ mm yr}^{-1}$  at the lowest slope positions. Additionally, Yoo et al. (2007) investigated soil residence times by linking soil transport and topography. Results indicated residence times for soil of 4 kyr on the ridge to 0.9 kyr at the base of the hillslope.

Burke et al. (2009) compared the extent of chemical weathering for field sites in the lowlands and highlands around the area of the Bega Valley in south-eastern Australia and found indications for lower rates of chemical weathering for the highland (47 %) compared to the lowland sites (57 %). Dixon et al. (2009) applied a similar approach for the Sierra Nevada Mountains in California, USA. Results implied that chemical weathering of saprolite to soil peaked at mid elevations compared to high and low elevation sites and that physical erosion rates increased with both saprolite weathering rates and intensity. In contrast to previous publications, total denudation rates were calculated as the sum of total chemical weathering and soil production rates.

### *Summary*

- Soil mantled landscapes are believed to be the result of two main concepts of soil formation: (1) the exponential soil production model and (2) the humped soil production model.
- The exponential decline of soil production with increasing soil thickness was verified with field data *in situ*. Calculated rates of weathering of parent material are as low as  $0.004$  and as high  $0.4 \text{ mm yr}^{-1}$ .
- The humped model was used to explain soil formation conceptually for some landscapes, but an empirical parameterisation is still to be achieved from field data.
- Laboratory derived chemical weathering rates of rocks or minerals are generally more rapid than rates estimated from field data.
- Minimum rates of chemical weathering derived from field data are as low as  $0.01 \text{ mm yr}^{-1}$  with maximum rates of about  $0.5 \text{ mm yr}^{-1}$ .
- The majority of chemical weathering rates estimated from catchment based mass loss of elements range between  $0.01$  to  $0.1 \text{ mm yr}^{-1}$  with mean values of about  $0.060 \text{ mm yr}^{-1}$ .
- Rates of chemical weathering derived with so called weathering indices vary from  $0$  to  $0.144 \text{ mm yr}^{-1}$  with mean values of about  $0.022 \text{ mm yr}^{-1}$  and were relatively similar to chemical weathering rates estimated from catchment based methods (Figure 2.6 and 2.7), although rates derived with weathering indices were generally lower.



- Rates of total denudation were estimated for all chemical weathering studies based on weathering indices using terrestrial cosmogenic nuclides. Generally, calculated rates of chemical weathering were lower than rates of physical weathering.
- Both datasets on chemical weathering rates (Table 2.1 Part 1 and Part 2) showed no distinct pattern of weathering rates being dependent on different climates and parent materials of the sites studied.

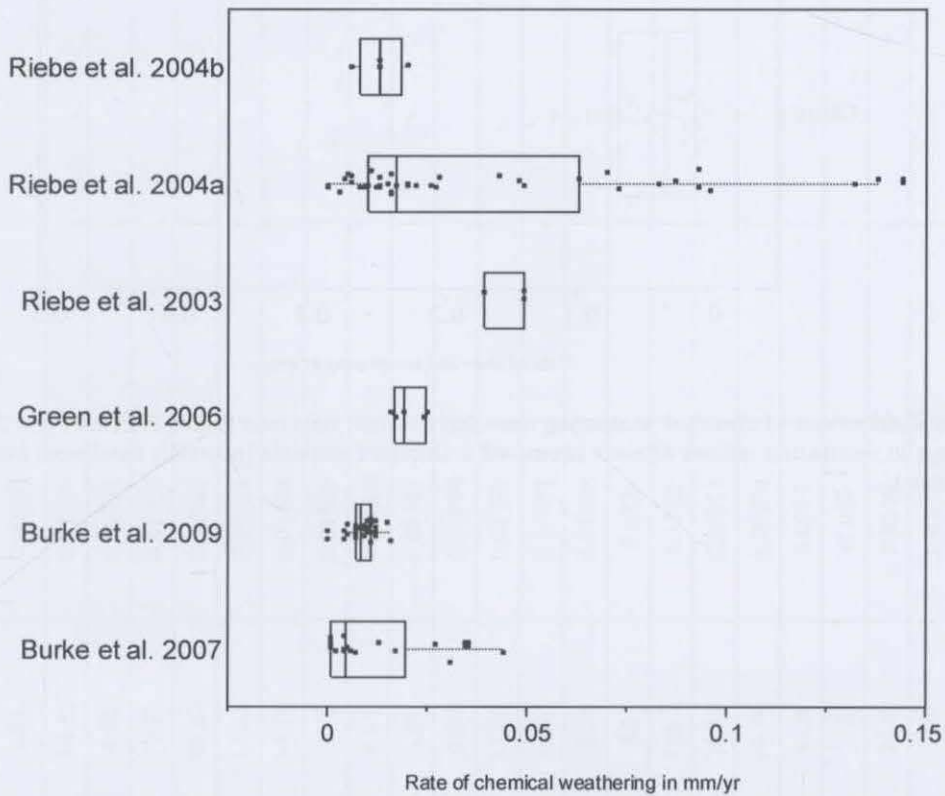


**Fig. 2.6.** Box-Plot distributions of chemical weathering rates derived from weathering indices (Table 2.1 Part 2). Graph shows the range in the datasets derived from *in situ* field data using weathering indices; the line in the middle of the box refers to the median of the distribution.

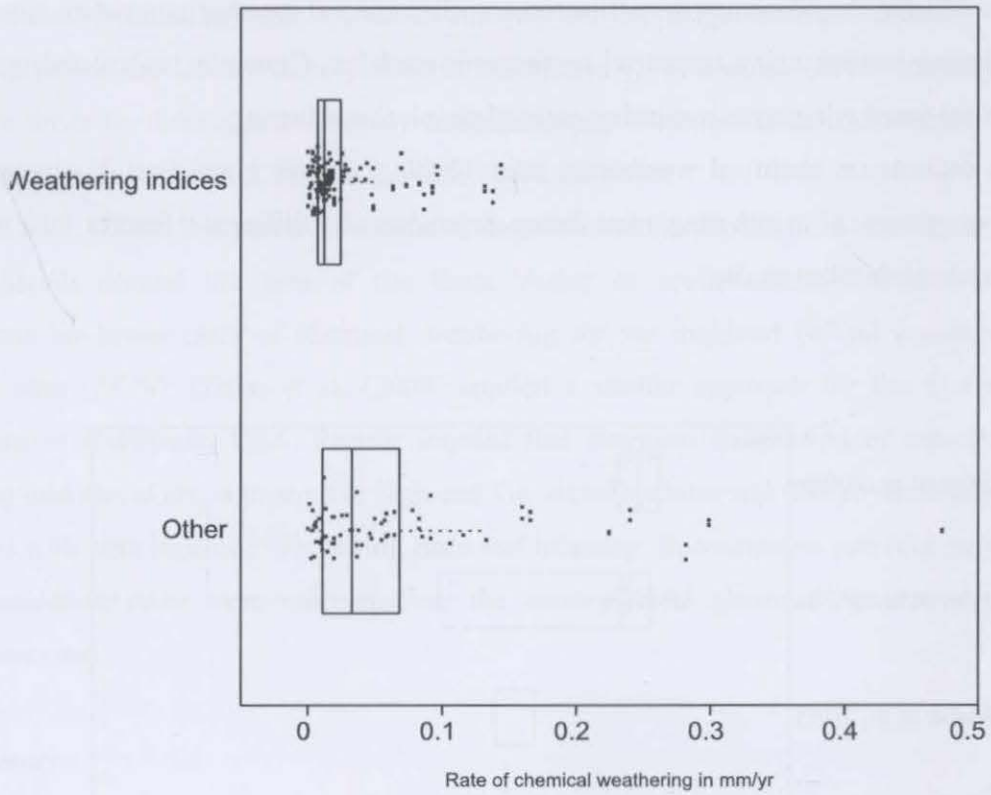


**Fig. 2.7.** Box-Plot distributions of chemical weathering rates derived from field data (Table 2.1 Part 1 and 2). Graph demonstrates range in weathering indices datasets compared to different methods (generally catchment based mass balance from solutes).

**Tab. 2.1.** Part 1. Chemical weathering rates derived from elemental fluxes (loss and gain) in watersheds and chemical products of the parent materials and weathering products studies

Reference	ID	Rate (mm kyr <sup>-1</sup> )	Rate (mm yr <sup>-1</sup> )	Elevation (m)	Climate	Geology
Alexander, 1985	Maryland	5.81	0.00581			
	California	10.79	0.01079			
	California	4.98	0.00498			
	Maryland	19.92	0.01992			
	Wales	40.67	0.04067			
	Wales	13.28	0.01328			
	British Columbia	54.78	0.05478			
	Luxembourg	19.92	0.01992			
	Hong Kong	6.64	0.00664			
	Hong Kong	5.81	0.00581			
	Hong Kong	9.96	0.00996			
	England	11.62	0.01162			
	England	14.94	0.01494			
	Virginia	18.26	0.01826			
	Virginia	83	0.083			
	Java	116.2	0.1162			
	England	38.18	0.03818			
	Idaho	64.74	0.06474			
	Wyoming	91.3	0.0913			
	Wyoming	166	0.166			
	New Mexico	24.9	0.0249			
	New Mexico	49.8	0.0498			
	New Mexico	240.7	0.2407			
	Hawaii	83	0.083			
	Mexico	91.3	0.0913			
	Mexico	298.8	0.2988			
	Papua	282.2	0.2822			

Reference	ID	Rate (mm kyr <sup>-1</sup> )	Rate (mm yr <sup>-1</sup> )	Elevation (m)	Climate	Geology
	Wyoming	132.8	0.1328			
	Colorado	58.1	0.0581			
Alexander, 1988	CA	11	0.011	220		Adamellite
	CH, BC, Can.	60	0.06	185		Till/quartz diorite
	CS, BC, Can.	78	0.078	945		Till/quartz diorite
	England	55	0.055	232		Granite
	France	106	0.106	152		Gneiss
	Idaho	65	0.065	478		Adamellite
	Luxemburg	46	0.046	90		Metashale
	Maryland	37	0.037	280		Greenstone (metabas.)
	Minnesota	20	0.02	98		Till/gabbro
	Maryland	5.8	0.0058	67		Schist
	Maryland	20	0.02	70		Serpentinite
	N. Hamp.	29	0.029	300		Till/gneiss
	Scotland	160	0.16	542		Till/granite
	V1, Victoria	33	0.033	144		Dacite
	V2, Victoria	57	0.057	203		Dacite
	Wash.	85	0.085	1150		Till/quartz diorite
	WF, Wales	26	0.026	105		Till/wacke
	WP, Wales	19	0.019	90		Till/wacke
	ZJ, Zimbabwe	18	0.018	160		Adamellite
	ZR, Zimbabwe	1.7	0.0017	60		Adamellite
Cleaves, 1993	Baltimore, Maryland	9.1	0.0091		Warm temperate	Plagioclase-muscovite-quartz
Dethier, 1986	Pacific Northwest	3	0.003		Cold temperate	Sedimentary and metamorphic
Edmond et al., 1995	Guayana Shield, South America	10	0.01			Granite
Owens and Watson, 1979	Rhodesia-Juliasdale	4.4	0.0044	1900	Tropical	Granite
	Rhodesia-Rusape	0.17	0.00017	1600	Tropical	Granite

Reference	ID	Rate (mm kyr <sup>-1</sup> )	Rate (mm yr <sup>-1</sup> )	Elevation (m)	Climate	Geology
Paces, 1986	Bohemian Maffif, X-0	8.9	0.0089	724	Warm temperate	Biotitic gneiss with muscovite, sillimanite, quartzites
	X-8	14	0.014	744	Warm temperate	Biotitic gneiss with muscovite, sillimanite, quartzites
	X-7	32	0.032	635	Warm temperate	Biotitic gneiss with muscovite, sillimanite, quartzites
Pavich, 1986	Virginia Piedmont	4	0.004	250	Cool temperate	Occoquan Granite
Pavich, 1989	Appalachian Piedmont	20	0.02			Metamorphic rocks
	Appalachian Piedmont	4	0.004			Metamorphic rocks
Ruxton, 1968	Papua New Guinea	58	0.058		Humid tropical	Volcanic material
Velbel, 1986	Watershed 27, Coweeta	37	0.037		Warm temperate	Garnet, plagioclase
	Southern Blue Ridge	37	0.037		Cold temperate	Gneiss
Wakatsuki & Rasyidin, 1992	Hubbard Brook	47	0.047		Cold temperate	
	Iu, granitic	224	0.224		Humid subtropical	
	Iu, basic pyroclastic	473	0.473		Humid subtropical	

**Tab. 2.1.** Part 2. Chemical weathering rates (CWR) derived *in situ* in applying weathering indices and TCN-derived total denudation rates for study sites in and outside Australia (rates of  $\text{t km}^{-2} \text{yr}^{-1}$  were converted to  $\text{mm yr}^{-1}$  in assuming a bulk density of soil of  $1200 \text{ kg m}^{-3}$ ).

Reference	ID	Soil depth (cm)	CWR (published rate)	CWR ( $\text{mm yr}^{-1}$ )	Total denudation rate (published rate)	Total denudation rate ( $\text{mm yr}^{-1}$ )
Burke et al., 2007 <sup>1)</sup>	Pit 6	15	35 m Myr <sup>-1</sup>	0.035	59 m Myr <sup>-1</sup>	0.059
	Pit 20	15	44 m Myr <sup>-1</sup>	0.044	59 m Myr <sup>-1</sup>	0.059
	Pit 9	29	13 m Myr <sup>-1</sup>	0.013	58 m Myr <sup>-1</sup>	0.058
	Pit 7	40	31 m Myr <sup>-1</sup>	0.031	50 m Myr <sup>-1</sup>	0.050
	Pit 17	40	6 m Myr <sup>-1</sup>	0.006	50 m Myr <sup>-1</sup>	0.050
	Pit 19	40	17 m Myr <sup>-1</sup>	0.017	50 m Myr <sup>-1</sup>	0.050
	Pit 5	48	27 m Myr <sup>-1</sup>	0.027	50 m Myr <sup>-1</sup>	0.050
	Pit 16	55	5 m Myr <sup>-1</sup>	0.005	36 m Myr <sup>-1</sup>	0.036
	Pit 8	60	4 m Myr <sup>-1</sup>	0.004	36 m Myr <sup>-1</sup>	0.036
	Pit 15	70	2 m Myr <sup>-1</sup>	0.002	18 m Myr <sup>-1</sup>	0.018
	Pit 25	70	4 m Myr <sup>-1</sup>	0.004	18 m Myr <sup>-1</sup>	0.018
	Pit 26	70	4 m Myr <sup>-1</sup>	0.004	18 m Myr <sup>-1</sup>	0.018
	Pit 14	75	1 m Myr <sup>-1</sup>	0.001	18 m Myr <sup>-1</sup>	0.018
	Pit 10	80	7 m Myr <sup>-1</sup>	0.007	28 m Myr <sup>-1</sup>	0.028
	Pit 1	90	1 m Myr <sup>-1</sup>	0.001	14 m Myr <sup>-1</sup>	0.014
	Pit 24	100	1 m Myr <sup>-1</sup>	0.001	11 m Myr <sup>-1</sup>	0.011
	Pit 12	120	1 m Myr <sup>-1</sup>	0.001	11 m Myr <sup>-1</sup>	0.011
Pit 21	120	1 m Myr <sup>-1</sup>	0.001	11 m Myr <sup>-1</sup>	0.011	
Burke et al., 2009 <sup>2)</sup>	FH 1	52	3.9±1.2 m Myr <sup>-1</sup>	0.004	18.7±1.0 m Myr <sup>-1</sup>	0.019
	FH2	50	11.7±0.6 m Myr <sup>-1</sup>	0.012	19.5±1.0 m Myr <sup>-1</sup>	0.020
	FH3	55	8.5±0.7 m Myr <sup>-1</sup>	0.009	17.6±1.0 m Myr <sup>-1</sup>	0.018
	FH4	65	7.3±0.5 m Myr <sup>-1</sup>	0.007	14.4±1.0 m Myr <sup>-1</sup>	0.014
	FH5	40	15.2±0.7 m Myr <sup>-1</sup>	0.015	23.8±2.2 m Myr <sup>-1</sup>	0.024
	FH6	104	3.5±0.2 m Myr <sup>-1</sup>	0.004	6.6±1.0 m Myr <sup>-1</sup>	0.007
	FH7	58	8.6±0.6 m Myr <sup>-1</sup>	0.009	16.6±1.0 m Myr <sup>-1</sup>	0.017
	FH8	65	6.9±0.6 m Myr <sup>-1</sup>	0.007	14.4±1.0 m Myr <sup>-1</sup>	0.014

Reference	ID	Soil depth (cm)	CWR (published rate)	CWR (mm yr <sup>-1</sup> )	Total denudation rate (published rate)	Total denudation rate (mm yr <sup>-1</sup> )
	FH9	48	9.5±0.8 m Myr <sup>-1</sup>	0.010	20.3±1.2 m Myr <sup>-1</sup>	0.020
	FH10	55	0.0 m Myr <sup>-1</sup>	0	17.6±1.0 m Myr <sup>-1</sup>	0.018
	FH-B1	50 (96)	5.0±1.1 m Myr <sup>-1</sup>	0.005	17.6±1.0 m Myr <sup>-1</sup>	0.018
	FH-B2	30 (100)	11.0±1.41 m Myr <sup>-1</sup>	0.011	27.4±4.5 m Myr <sup>-1</sup>	0.027
	FH-B3	70 (120)	5.0±0.5 m Myr <sup>-1</sup>	0.005	11.4±1.0 m Myr <sup>-1</sup>	0.011
	FH-B4	70 (120)	7.0±0.4 m Myr <sup>-1</sup>	0.007	11.4±1.0 m Myr <sup>-1</sup>	0.011
	FH-B5	25 (60)	11.0±0.7 m Myr <sup>-1</sup>	0.011	30.6±4.5 m Myr <sup>-1</sup>	0.031
	FH-2MP	35	7.8±1.5 m Myr <sup>-1</sup>	0.008	24.5±5.0 m Myr <sup>-1</sup>	0.025
	Highland mean (from above)	55	8.1±0.8 m Myr <sup>-1</sup>	0.008	19.7±1.7 m Myr <sup>-1</sup>	0.020
	NR0	65	7.6±0.5 m Myr <sup>-1</sup>	0.008	14.4±3.0 m Myr <sup>-1</sup>	0.014
	NR1	75	6.9±0.4 m Myr <sup>-1</sup>	0.007	11.8±2.0 m Myr <sup>-1</sup>	0.012
	NR2	72	7.2±0.2 m Myr <sup>-1</sup>	0.007	12.6±2.0 m Myr <sup>-1</sup>	0.013
	NR3	72	9.5±0.4 m Myr <sup>-1</sup>	0.010	12.6±2.0 m Myr <sup>-1</sup>	0.013
	NR4	49	12.0±0.6 m Myr <sup>-1</sup>	0.012	19.9±4.0 m Myr <sup>-1</sup>	0.020
	NR5	30	15.6±1.0 m Myr <sup>-1</sup>	0.016	29.1±5.0 m Myr <sup>-1</sup>	0.029
	NR6	58	9.7±0.5 m Myr <sup>-1</sup>	0.010	16.6±2.0 m Myr <sup>-1</sup>	0.017
	NR7	75	6.7±0.4 m Myr <sup>-1</sup>	0.007	11.8±1.0 m Myr <sup>-1</sup>	0.012
	NR-A1	60	7.2±0.6 m Myr <sup>-1</sup>	0.007	14.2±1.0 m Myr <sup>-1</sup>	0.014
	NR2-MP	50	11.2±0.5 m Myr <sup>-1</sup>	0.011	17.6±2.0 m Myr <sup>-1</sup>	0.018
	SN-B1	50	11.1±0.6 m Myr <sup>-1</sup>	0.011	19.5±2.0 m Myr <sup>-1</sup>	0.020
	SN-B1B	65	6.6±0.6 m Myr <sup>-1</sup>	0.007	14.4±1.0 m Myr <sup>-1</sup>	0.014
	SN-B3	40	12.2±0.9 m Myr <sup>-1</sup>	0.012	23.8±2.0 m Myr <sup>-1</sup>	0.024
	SN-B4	40	8.8±0.0 m Myr <sup>-1</sup>	0.009	23.8±2.0 m Myr <sup>-1</sup>	0.024
	SN-B5	55	8.8±0.7 m Myr <sup>-1</sup>	0.009	17.6±1.0 m Myr <sup>-1</sup>	0.018
	SN-B6	60	11.8±0.3 m Myr <sup>-1</sup>	0.012	16.0±1.0 m Myr <sup>-1</sup>	0.016
	H2B1	70	3.5±0.4 m Myr <sup>-1</sup>	0.004	7.2±1.0 m Myr <sup>-1</sup>	0.007
	H2B2	60	6.5±0.6 m Myr <sup>-1</sup>	0.007	16.0±1.0 m Myr <sup>-1</sup>	0.016

Reference	ID	Soil depth (cm)	CWR (published rate)	CWR (mm yr <sup>-1</sup> )	Total denudation rate (published rate)	Total denudation rate (mm yr <sup>-1</sup> )
	Lowland mean (from above)	58	9.1±0.5 t km <sup>-2</sup> yr <sup>-1</sup>	0.009	16.6±2.0 t km <sup>-2</sup> yr <sup>-1</sup>	0.017
Green et al., 2006	Transport distance 0 m	N.A.	20.0±1.2 t km <sup>-2</sup> yr <sup>-1</sup>	0.017		
	Transport distance 3-15 m	N.A.	28.6±1.0 t km <sup>-2</sup> yr <sup>-1</sup>	0.024		
	Transport distance 15-30 m	N.A.	29.4±1.6 t km <sup>-2</sup> yr <sup>-1</sup>	0.025		
	Transport distance 30-45 m	N.A.	23.0±1.3 t km <sup>-2</sup> yr <sup>-1</sup>	0.019		
	Transport distance >45 m	N.A.	19.3±2.1 t km <sup>-2</sup> yr <sup>-1</sup>	0.016		
Riebe et al., 2003 <sup>3)</sup>	RIS1	50-150	47±11 t km <sup>-2</sup> yr <sup>-1</sup>	0.039	79±18 t km <sup>-2</sup> yr <sup>-1</sup>	0.066
	RIS2	50-150	59±14 t km <sup>-2</sup> yr <sup>-1</sup>	0.049	101±23 t km <sup>-2</sup> yr <sup>-1</sup>	0.084
	RIS3	50-150	59±13 t km <sup>-2</sup> yr <sup>-1</sup>	0.049	97±2 t km <sup>-2</sup> yr <sup>-1</sup>	0.081
	Average soil samples (above)		56±13 t km <sup>-2</sup> yr <sup>-1</sup>	0.047	90±21 t km <sup>-2</sup> yr <sup>-1</sup>	0.075
Riebe et al., 2004a	Rio Icacos, Puerto Rico					
	RI-1		51±10 t km <sup>-2</sup> yr <sup>-1</sup>	0.043	87±15 t km <sup>-2</sup> yr <sup>-1</sup>	0.073
	RI-4		59±9 t km <sup>-2</sup> yr <sup>-1</sup>	0.049	97±14 t km <sup>-2</sup> yr <sup>-1</sup>	0.081
	McNaab Track, New Zealand					
	MT-3		88±17 t km <sup>-2</sup> yr <sup>-1</sup>	0.073	195±31 t km <sup>-2</sup> yr <sup>-1</sup>	0.163
	MT-4		115±25 t km <sup>-2</sup> yr <sup>-1</sup>	0.096	235±45 t km <sup>-2</sup> yr <sup>-1</sup>	0.196
	MT-5		58±10 t km <sup>-2</sup> yr <sup>-1</sup>	0.048	131±20 t km <sup>-2</sup> yr <sup>-1</sup>	0.109
	Chiapas Highlands, Mexico					
	SS		34±6 t km <sup>-2</sup> yr <sup>-1</sup>	0.028	122±14 t km <sup>-2</sup> yr <sup>-1</sup>	0.102
	Jalisco Highlands, Mexico					
	ST-1		166±42 t km <sup>-2</sup> yr <sup>-1</sup>	0.138	556±71 t km <sup>-2</sup> yr <sup>-1</sup>	0.463
	ST-3		84±14 t km <sup>-2</sup> yr <sup>-1</sup>	0.070	212±22 t km <sup>-2</sup> yr <sup>-1</sup>	0.177
	ST-4		158±69 t km <sup>-2</sup> yr <sup>-1</sup>	0.132	622±72 t km <sup>-2</sup> yr <sup>-1</sup>	0.518
	ST-5		173±44 t km <sup>-2</sup> yr <sup>-1</sup>	0.144	549±59 t km <sup>-2</sup> yr <sup>-1</sup>	0.458
	Panola Mtn., GA, USA					
	PM		10±2 t km <sup>-2</sup> yr <sup>-1</sup>	0.008	23±3 t km <sup>-2</sup> yr <sup>-1</sup>	0.019
	Jalisco Lowlands, Mexico					



Reference	ID	Soil depth (cm)	CWR (published rate)	CWR (mm yr <sup>-1</sup> )	Total denudation rate (published rate)	Total denudation rate (mm yr <sup>-1</sup> )
	RT-1		112±25 t km <sup>-2</sup> yr <sup>-1</sup>	0.093	462±50 t km <sup>-2</sup> yr <sup>-1</sup>	0.385
	RT-2		104±22 t km <sup>-2</sup> yr <sup>-1</sup>	0.087	399±46 t km <sup>-2</sup> yr <sup>-1</sup>	0.333
	Santa Rosa Mtn., NY, USA					
	SR-1		7±3 t km <sup>-2</sup> yr <sup>-1</sup>	0.006	106±11 t km <sup>-2</sup> yr <sup>-1</sup>	0.088
	SR-3		0±3 t km <sup>-2</sup> yr <sup>-1</sup>	0	132±14 t km <sup>-2</sup> yr <sup>-1</sup>	0.110
	SR-4		15±4 t km <sup>-2</sup> yr <sup>-1</sup>	0.013	144±15 t km <sup>-2</sup> yr <sup>-1</sup>	0.120
	SR-6		16±4 t km <sup>-2</sup> yr <sup>-1</sup>	0.013	104±11 t km <sup>-2</sup> yr <sup>-1</sup>	0.087
	SR-7		24±7 t km <sup>-2</sup> yr <sup>-1</sup>	0.020	117±12 t km <sup>-2</sup> yr <sup>-1</sup>	0.098
	SR-10		-2±6 t km <sup>-2</sup> yr <sup>-1</sup>	-0.002	117±12 t km <sup>-2</sup> yr <sup>-1</sup>	0.098
	Sonora Desert, Mexico					
	CE-3		31±11 t km <sup>-2</sup> yr <sup>-1</sup>	0.026	194±32 t km <sup>-2</sup> yr <sup>-1</sup>	0.162
	JC-1		34±13 t km <sup>-2</sup> yr <sup>-1</sup>	0.028	191±20 t km <sup>-2</sup> yr <sup>-1</sup>	0.159
	Fall River, Sierra Nevada, USA					
	FR-2		99±30 t km <sup>-2</sup> yr <sup>-1</sup>	0.083	485±92 t km <sup>-2</sup> yr <sup>-1</sup>	0.404
	FR-5		75±16 t km <sup>-2</sup> yr <sup>-1</sup>	0.063	384±54 t km <sup>-2</sup> yr <sup>-1</sup>	0.320
	FR-6		19±7 t km <sup>-2</sup> yr <sup>-1</sup>	0.016	104±25 t km <sup>-2</sup> yr <sup>-1</sup>	0.087
	FR-8		7±1 t km <sup>-2</sup> yr <sup>-1</sup>	0.006	40±4 t km <sup>-2</sup> yr <sup>-1</sup>	0.033
	Antelope Lake, Sierra Nevada, USA					
	AL-4		15±4 t km <sup>-2</sup> yr <sup>-1</sup>	0.013	72±8 t km <sup>-2</sup> yr <sup>-1</sup>	0.060
	AL-5		19±20 t km <sup>-2</sup> yr <sup>-1</sup>	0.016	86±11 t km <sup>-2</sup> yr <sup>-1</sup>	0.072
	AL-9		26±13 t km <sup>-2</sup> yr <sup>-1</sup>	0.022	119±12 t km <sup>-2</sup> yr <sup>-1</sup>	0.099
	AL-10		12±3 t km <sup>-2</sup> yr <sup>-1</sup>	0.010	91±8 t km <sup>-2</sup> yr <sup>-1</sup>	0.076
	Adams Peak, Sierra Nevada, USA					
	AP-3		24±3 t km <sup>-2</sup> yr <sup>-1</sup>	0.020	140±13 t km <sup>-2</sup> yr <sup>-1</sup>	0.117
	AP-4		6±4 t km <sup>-2</sup> yr <sup>-1</sup>	0.005	100±9 t km <sup>-2</sup> yr <sup>-1</sup>	0.083
	AP-5		20±9 t km <sup>-2</sup> yr <sup>-1</sup>	0.017	162±15 t km <sup>-2</sup> yr <sup>-1</sup>	0.135
	AP-11		14±6 t km <sup>-2</sup> yr <sup>-1</sup>	0.012	93±12 t km <sup>-2</sup> yr <sup>-1</sup>	0.078

Reference	ID	Soil depth (cm)	CWR (published rate)	CWR (mm yr <sup>-1</sup> )	Total denudation rate (published rate)	Total denudation rate (mm yr <sup>-1</sup> )
	AP-13		18±6 t km <sup>-2</sup> yr <sup>-1</sup>	0.015	124±12 t km <sup>-2</sup> yr <sup>-1</sup>	0.103
	Fort Sage, Sierra Nevada, USA					
	A1		5±4 t km <sup>-2</sup> yr <sup>-1</sup>	0.004	83±7 t km <sup>-2</sup> yr <sup>-1</sup>	0.069
	A2(s)		13±4 t km <sup>-2</sup> yr <sup>-1</sup>	0.011	63±17 t km <sup>-2</sup> yr <sup>-1</sup>	0.053
	A3(s)		32±12 t km <sup>-2</sup> yr <sup>-1</sup>	0.027	173±43 t km <sup>-2</sup> yr <sup>-1</sup>	0.144
	A4(s)		111±43 t km <sup>-2</sup> yr <sup>-1</sup>	0.093	755±263 t km <sup>-2</sup> yr <sup>-1</sup>	0.629
	Sunday Peak, Sierra Nevada, USA					
	SP-1		19±5 t km <sup>-2</sup> yr <sup>-1</sup>	0.016	129±12 t km <sup>-2</sup> yr <sup>-1</sup>	0.108
	SP-3		3±7 t km <sup>-2</sup> yr <sup>-1</sup>	0.003	93±11 t km <sup>-2</sup> yr <sup>-1</sup>	0.078
	SP-8		11±5 t km <sup>-2</sup> yr <sup>-1</sup>	0.009	86±12 t km <sup>-2</sup> yr <sup>-1</sup>	0.072
	Nichols Peak, Sierra Nevada, USA					
	NP-1		16±7 t km <sup>-2</sup> yr <sup>-1</sup>	0.013	127±12	0.106
Riebe et al., 2004b <sup>4)</sup>	SR-10 (top of transect)					
	SR-3		-2±6 t km <sup>-2</sup> yr <sup>-1</sup>	0	117±12 t km <sup>-2</sup> yr <sup>-1</sup>	0.098
	SR-1		0±3 t km <sup>-2</sup> yr <sup>-1</sup>	0	132±14 t km <sup>-2</sup> yr <sup>-1</sup>	0.110
	SR-1		7±3 t km <sup>-2</sup> yr <sup>-1</sup>	0.006	106±11 t km <sup>-2</sup> yr <sup>-1</sup>	0.088
	SR-4		15±5 t km <sup>-2</sup> yr <sup>-1</sup>	0.013	144±15 t km <sup>-2</sup> yr <sup>-1</sup>	0.120
	SR-6		16±5 t km <sup>-2</sup> yr <sup>-1</sup>	0.013	104±11 t km <sup>-2</sup> yr <sup>-1</sup>	0.087
	SR-7 (base of transect)					
			24±7 t km <sup>-2</sup> yr <sup>-1</sup>	0.020	117±12 t km <sup>-2</sup> yr <sup>-1</sup>	0.098

**Tab. 2.1.** Part 2, continued. Chemical weathering rates (CWR) derived *in situ* in applying weathering indices and TCN-derived total denudation rates for study sites in and outside Australia (rates of  $t\ km^{-2}\ yr^{-1}$  were converted to  $mm\ yr^{-1}$  in assuming a bulk density of soil of  $1200\ kg\ m^{-3}$ ).

Reference	ID	Soil depth (cm)	CWR <sub>soil</sub> ( $t\ km^{-2}\ yr^{-1}$ )	CWR <sub>saprolite</sub> ( $t\ km^{-2}\ yr^{-1}$ )	CWR <sub>total</sub> ( $t\ km^{-2}\ yr^{-1}$ )	Erosion rate ( $t\ km^{-2}\ yr^{-1}$ )	Total denudation rate ( $t\ km^{-2}\ yr^{-1}$ )	
Dixon et al., 2009 <sup>5)</sup>	LD-0	6	0	75.4	75.4	66.2	141.5	
	LD-1	25	0	104.8	104.8	126.4	231.2	
	LD-2	27	24.4	34.4	58.7	80.5	139.3	
	LD-3	40	34.9	3.8	38.6	34.3	73	
	LD-4	45	38.5	27.5	66.1	54.8	120.8	
	LD-5	53	22.7	19.7	42.4	37.1	79.5	
	LD-6	75	5.5	53.4	58.9	45.7	104.6	
	Mean			18.0±6.1	45.6±13.2	63.6±8.4	63.6±12.1	127.1±20.1
	WB-0	53	13	39.5	52.5	57.5	110	
	WB-1	64	10.9	40.7	51.7	54.2	105.8	
	WB-2	70	0	43.1	43.1	34.2	77.4	
	WB-3	110	31.3	0	31.3	34.8	66.1	
	WB-4	75	5.1	25.4	30.6	35.1	65.6	
	WB-5	75	21.2	15.9	37.1	27.5	64.6	
	WB-6	60	11.4	6.4	17.8	23.6	41.4	
	WB-7	90	28.3	35.1	63.4	43.2	106.5	
	WB-8	80	5.7	18	23.7	34.3	57.9	
	Mean			14.1±3.6	24.9±5.3	39.0±5.0	38.3±3.8	77.3±8.2
BM-2006-1	BM-2006-1	107	0	87	87	89.5	176.5	
	BM-2006-2	29	25.2	66.5	91.7	103.3	195.1	
	BM-2006-3	102	17.4	98.1	115.5	131.1	246.6	
	BM-2006-4	127	31.3	53.9	85.1	86.2	171.3	
	Mean			24.4±7.9	69.0±10.6	93.4±5.6	104.4±8.1	197.8±13.3
PC-1	PC-1	80	4.2	158	162.2	131.8	294	
	PC-2	110	13.2	67.6	80.8	59.4	140.2	
	PC-2006-1	107	0	124.1	124.1	82	206.1	
	PC-2006-2	91	0	131.3	131.3	92.3	223.6	

Reference	ID	Soil depth (cm)	$CWR_{soil}$ ( $t\ km^{-2}\ yr^{-1}$ )	$CWR_{saprolite}$ ( $t\ km^{-2}\ yr^{-1}$ )	$CWR_{total}$ ( $t\ km^{-2}\ yr^{-1}$ )	Erosion rate ( $t\ km^{-2}\ yr^{-1}$ )	Total denudation rate ( $t\ km^{-2}\ yr^{-1}$ )
	PC-2006-3	61	0	172.6	172.6	122.7	295.4
	PC-2006-4	71	21.2	76.1	97.3	63.2	160.4
	Mean		6.4±4.0	121.6±19.0	128.1±15.9	91.9±13.4	220.0±29.2
	KR-1	33	N.A.	4.8	N.A.	N.A.	36
	KR-2	25	N.A.	0	N.A.	N.A.	77.4
	KR-2006-1	64	6.5	17.7	24.3	52.1	76.4
	KR-2006-3	64	5.4	16.7	22.1	41.2	63.3
	Mean		6.0±0.5	9.8±4.4	23.2±1.1	46.7±5.4	63.3±9.6
Reference	ID	Soil depth (cm)	$CWR_{soil}$ ( $mm\ yr^{-1}$ )	$CWR_{saprolite}$ ( $mm\ yr^{-1}$ )	$CWR_{total}$ ( $mm\ yr^{-1}$ )	Erosion rate ( $mm\ yr^{-1}$ )	Total denudation rate ( $mm\ yr^{-1}$ )
Dixon et al., 2009 <sup>5)</sup>	LD-0	6	0	0.034	0.034	0.03	0.064
	LD-1	25	0	0.048	0.048	0.057	0.105
	LD-2	27	0.02	0.016	0.036	0.037	0.073
	LD-3	40	0.029	0.002	0.031	0.016	0.046
	LD-4	45	0.032	0.013	0.045	0.025	0.069
	LD-5	53	0.019	0.009	0.028	0.017	0.045
	LD-6	75	0.005	0.024	0.029	0.021	0.05
	WB-0	53	0.011	0.018	0.029	0.026	0.055
	WB-1	64	0.009	0.019	0.028	0.025	0.052
	WB-2	70	N.A.	0.02	0.02	0.016	0.035
	WB-3	110	0.026	0	0.026	0.016	0.042
	WB-4	75	0.004	0.012	0.016	0.016	0.032
	WB-5	75	0.018	0.007	0.025	0.013	0.037
	WB-6	60	0.01	0.003	0.012	0.011	0.023
	WB-7	90	0.024	0.016	0.04	0.02	0.059
	WB-8	80	0.005	0.008	0.013	0.016	0.029

Reference	ID	Soil depth (cm)	CWR <sub>soil</sub> (mm yr <sup>-1</sup> )	CWR <sub>saprolite</sub> (mm yr <sup>-1</sup> )	CWR <sub>total</sub> (mm yr <sup>-1</sup> )	Erosion rate (mm yr <sup>-1</sup> )	Total denudation rate (mm yr <sup>-1</sup> )
	BM-2006-1	107	0	0.04	0.04	0.041	0.08
	BM-2006-2	29	0.021	0.03	0.051	0.047	0.098
	BM-2006-3	102	0.015	0.045	0.059	0.06	0.119
	BM-2006-4	127	0.026	0.025	0.051	0.039	0.09
	PC-1	80	0.004	0.072	0.075	0.06	0.135
	PC-2	110	0.011	0.031	0.042	0.027	0.069
	PC-2006-1	107	0	0.056	0.056	0.037	0.094
	PC-2006-2	91	0	0.06	0.06	0.042	0.102
	PC-2006-3	61	0	0.078	0.078	0.056	0.134
	PC-2006-4	71	0.018	0.035	0.052	0.029	0.081
	KR-1	33	N.A.	0.002	N.A.	N.A.	N.A.
	KR-2	25	N.A.	N.A.	N.A.	N.A.	N.A.
	KR-2006-1	64	0.005	0.008	0.013	0.024	0.037
	KR-2006-3	64	0.005	0.008	0.012	0.019	0.031

<sup>1)</sup>Total denudation rates taken from Heimsath et al. (2005)

<sup>2)</sup>Total denudation rates were taken from Heimsath et al. (2006)

<sup>3)</sup>Riebe et al. (2003) used amalgamated soil samples to determine chemical weathering rates and total denudation rates

<sup>4)</sup>Riebe et al. (2004b) used amalgamated soil samples and parent material (49 soil samples, 28 samples of parent material) to determine chemical weathering rates and total denudation rates

<sup>5)</sup>Erosion rates equal rates of soil production, here total denudation rates are calculated as the sum of total chemical weathering and erosion rates

**Tab. 2.2.** Characteristics of study sites in, and outside, Australia.

<b>Study sites in Australia</b>				
<b>Reference</b>	<b>Study site</b>	<b>Elevation</b>	<b>Climate</b>	<b>Geology</b>
Green et al., 2006	Bega Valley, NSW	200 m	Warm-temperate Rainfall 910 mm yr <sup>-1</sup>	Granite and granodiorite of the Bega Batholith
Burke et al., 2009	Snug (lowland), Brown Mountain (escarpment crest), NSW	200 m 1000 m	Warm-temperate Rainfall 870 mm yr <sup>-1</sup> Rainfall 690 mm yr <sup>-1</sup>	Ordovician metasediments and Devonian granites
<b>Study sites outside Australia</b>				
<b>Reference</b>	<b>Study site</b>	<b>Elevation</b>	<b>Climate</b>	<b>Geology</b>
Dixon et al., 2009	Sierra Nevada Mountains, California, USA	1186 to 29991 m	Mixed-conifer to subalpine Rainfall 330-1200 mm yr <sup>-1</sup>	Granitic rocks
Burke et al., 2007	Point Reyes, California, USA	150 m	Mediterranean Rainfall 800 mm yr <sup>-1</sup>	Granitic rocks (quartz diorite, granodiorite)
Riebe et al., 2003	Rio Icacos, Puerto Rico	700 m	Tropical Rainfall 4200 mm yr <sup>-1</sup>	Quartz diorite
Riebe et al., 2004a	42 different study sites		Mean annual temperatures: 2 to 25°C Mean annual rainfall: 220 to 4200 mm yr <sup>-1</sup>	Granite
Riebe et al., 2004b	Santa Rosa Mountains, Nevada, USA, Transect	2090 to 2750 m	Mean annual temperatures and rainfall from 3.6°C, 650 mm yr <sup>-1</sup> (base) to -0.4°C, 850 mm yr <sup>-1</sup> (top)	Granodiorite

## 2.4 Soil mixing – vertical and lateral movements

Soil mixing processes ultimately result in the detachment, transport, sorting and deposition of material within the soil mantle and on its surface (Paton et al., 1995). Consequently, these pedoturbations initialise vertical and lateral movements in the soil mantle.

Various forms and agents of pedoturbation can be seen in Table 2.3. Here, soil creep is characterized as mainly induced by gravity-related mass movements (graviturbation). However, creep is also caused by bioturbation via processes like burrowing and the growth and decay of roots which is followed by the refilling of generated holes from the upslope side. In Table 2.3 pedoturbation caused by water is restricted to rain splash and movement of water down the profile, excluding overland lateral transport processes and deposition by water, i.e. rill or gully soil erosion caused by water. The most relevant pedoturbations for pedogenic studies are soil creep and bioturbation, as well as eluviation and illuviation processes that transport soil particles due to the movement of water down the soil profile.

**Tab. 2.3.** Forms and agents of pedoturbation (based on Schaetzel and Anderson (2005)).

<i>Form of Pedoturbation</i>	<i>Soil mixing agents</i>
Aeroturbation	Gas, air, wind
Anthroturbation	Humans
Aquaturbation	Water (rain splash, eluviation/illuviation processes)
Argilliturbation	Shrinking and swelling of clays
Cryoturbation	Freeze-thaw activity, ice crystals
Crystallurbation	Crystals, such as ice and various salts
Faunalturbation (Bioturbation)	Animals, including insects
Floralturbation (Bioturbation)	Plants
Graviturbation	Mass movements, such as creep
Impacturbation	Extraterrestrial impacts such as comets and meteorites, and human-generated impacts, i.e. artillery shells and bombs
Seismiturbation	Earthquakes

Table 2.4 summarizes various rates of pedoturbation that are found in the literature by the mixing agents involved. Some rates of pedoturbation were excluded, because of their specific nature and these are discussed in the text only. Listed rates of pedoturbation were mainly based on observed pedoturbation processes in the field such as ants moving soil particles or litter, or by examining and interpreting the products of such processes (Schaetzel and Anderson, 2005). Most estimates were therefore based on more or less short-term observations rather than estimating long-term mixing rates from dating soil particles *in situ*. We can see that rates of pedoturbation vary extensively in their rapidity and that ants, termites and earthworms are one of the major agents causing pedoturbations.

**Box 2.2: The Macquarie School of ‘bioturbation’**

Research from ‘Macquarie University’ in Sydney, Australia, identifies bioturbation processes as one of the key components of pedogenesis. Based predominantly on observations in Australia, Paton, Humphreys and Mitchell (1995) published ‘A New Global View on Soils’, describing pedogenesis as depending predominantly on bioturbation, slope processes and the landscape studied, and introducing an alternative view on the genesis of soils in pedology. Geoff Humphreys was credited with first using the term “bioturbation” in pedology by Don Johnson (the term and concept of bioturbation is originally from ichnology and oceanography describing the displacement and mixing of sediment particles and solutes by benthic fauna or flora).

Paton et al. (1995) proposed that the formation of texture contrast soil resulted from interacting slope and pedogenic processes with bioturbation processes being the main drivers in forming the clay rich subsoil horizon. They argued that the downward movement of clay via lessivage has been overemphasised and in fact plays a minor role in forming duplex soil profiles in landscapes. Therefore, rather than transporting fine materials down the profile via leaching processes, clay and silt-sized materials are moved down the soil profile or downslope by biological agents resulting in an accumulation of coarser materials on the top of the profile. Consequently, the authors put more emphasis on lateral rather than vertical movements in the soil profile. It was noted that especially the deeply weathered so called duplex soils in tropical Australia would have formed under the proposed circumstances. Furthermore, they used these processes to explain the formation of basal stone layers occurring below the so called biomantle; the zone that is produced largely by bioturbation in the soil profile (Johnson, 1990). Stones that are too large for the bioturbating agents to be transported to the soil surface will accumulate below the burrowing depths of the soil fauna.

Following on, Wilkinson and Humphreys (2005) concluded that rates of bioturbation are significantly faster than rates of soil production. They hypothesized that soil mixing rates exceed soil production rates by up to 3 orders of magnitude for study sites in south-eastern Australia, and based their argument on soil mixing rates by faunal agents of about 0.429 to 10.6 mm yr<sup>-1</sup> and soil production rates of about 0.013 to 0.061 mm yr<sup>-1</sup>. In 2009 Wilkinson et al. (2009) reviewed estimates of bioturbation that were extrapolated from short-term observations, mostly recorded by researchers from their school. In this context, the importance of biogenic agents in pedogenic studies was again emphasized. Bioturbation rates for earthworms were reported to be as high as 10-50 t ha<sup>-1</sup> yr<sup>-1</sup> (0.833-4.167 mm yr<sup>-1</sup>) with some reaching 100 t ha<sup>-1</sup> yr<sup>-1</sup> (8.33 mm yr<sup>-1</sup>). Ants, termites and vertebrates recorded comparable rates of approximately 1-5 t ha<sup>-1</sup> yr<sup>-1</sup> (0.083-0.417 mm yr<sup>-1</sup>); for ants rates of about 5-10 t ha<sup>-1</sup> yr<sup>-1</sup> (0.417-0.833 mm yr<sup>-1</sup>) were also noted.

Wilkinson et al. (2009) acknowledged the role of Charles Darwin in emphasising the effect of biota on soil. Darwin can be seen as one of the first scientists who observed and recorded mixing of plant and mineral matter in soil by earthworm activities. He proposed a mixing rate of 0.244 cm<sup>2</sup> yr<sup>-1</sup> for temperate maritime environments. Furthermore, Darwin made an inference that around 26,886 earthworms live in an acre (4046 m<sup>2</sup>) of pasture soil and that each earthworm would ingest 20 ounces of soil each year (560 g yr<sup>-1</sup>, which translates to a total amount of 15 t of soil annually) (Source: ‘Pedometron’, The Newsletter of the Pedometrics Commission of the IUSS, No. 20, page 14).

Following research initiated by Humphreys, who died unexpectedly in 2007, Wilkinson is continuing his legacy at ‘The Macquarie School’, investigating the importance of biological mixing of soils and its implications for pedogenesis.



**Box 2.3: The term ‘bioturbation’ in pedology**

At the 19<sup>th</sup> World Congress of Soil Science in Brisbane, Australia (1-6 August 2010), we learned that the term ‘bioturbation’ was introduced to pedology by Winfried E. Blum and Robert Ganssen in 1972 in their publication about ‘Soil-forming processes of the Earth’ for the journal ‘Die Erde’, at least to the German speaking ‘soil scientist’ (Blum and Ganssen, 1972). Blum and Ganssen (1972) used the term “bioturbation” for explaining ‘horizon blurring’ processes by burrowing animals like earthworms, insects or small mammals who habituate the soil environment. They noted that bioturbation processes by termites in tropical and sub-tropical environments resulted in a complete mixing of soil horizons of up to 3 m of depth, destroying pedogenic structures most likely formed by leaching.

*Bioturbation*

The influence of plants and animals on soil formation was not recognised profoundly in early publications of soil science. For instance, Jenny (1941) did not examine the role of animals as part of the o-(organisms)-factor, “because of lack of sufficient observational data...”. Furthermore, Carson and Kirkby (1972) nominated faunal and floral mixing agents as being of secondary or minor importance in causing soil creep. Carson and Kirkby (1972) defined processes of soil creep (only) as diffusion processes or mass movements in the soil profile, mostly caused by re-working of the soil surface, because of soil moisture and temperature changes such as frost cycling and resulting from the steady application of downhill shear stress. Nevertheless, they acknowledged possible rates of soil creep produced by soil fauna and flora in addition to those resulting from mass movements. On the other hand Paton et al. (1995) argued that bioturbation processes play a major role in forming a soil profile (see Box 2.2 ‘The Macquarie School of ‘bioturbation’).

In the current literature there is still debate about how much influence bioturbation actually has on soil transport or soil mixing processes and therefore pedogenesis, and if bioturbation results in net downslope movement or not (Amundson, 2004; Wilkinson et al., 2009). Biological activity in soils mostly depends on the soil structure including porosity, texture and stone content; water content; the roots that hold the soil together; and available nutrients. Often the A-horizon or topsoil is the part of the soil profile where most bioturbation processes take place and therefore would be equivalent to the so called biomantle (Amundson, 2004).

It is believed that bioturbation processes are able to either promote the development of horizons (*horizonation*) in texture contrast soils or impede soil horizonation altogether (*haplodization*) through the homogenisation of the topsoil and the subsoil as well as material transport between the subsoil and the topsoil. Furthermore, it is also believed that bioturbation processes can be responsible for the formation of stone layers, generally occurring at the interface between the A and B horizons (Lobry de Bruyn and Conacher, 1990; Muller-Lemans

and van Dorp, 1996; Paton et al., 1995; Wilkinson et al., 2009). Particularly small mammals like gophers are thought to cause the creation of a stone layer in some areas of the soil profile (Gabet et al., 2003). However it was also suggested that termites could be partly responsible for their creation, because of selective transfer of certain fine soil particle sizes, clay and silt, to the surface (Lobry de Bruyn and Conacher, 1990).

#### *Bioturbation – a) Faunaturbation*

Agents that predominantly cause faunaturbation are earthworms, ants, termites, gophers, wombats, ground squirrels and mice (Muller-Lemans and van Dorp, 1996). Hole (1981) classified those agents into two groups, exopedonic (outside the soil) and endopedonic (inside the soil) agents. He also listed 12 soil fauna related activities that take place within a soil body: mounding, mixing, forming voids, back-filling voids, forming and destroying peds; regulating soil erosion, movement of water and air, plant litter, nutrient cycling, biota and producing special constituents. In the following rates of soil turnover by faunal agents are going to be discussed. Most of the discussed rates are presented in Table 2.4.

Hole (1981) summarized that Arctic ground squirrels and pocket gophers are able to excavate up to 1.5 mm of soil each year, that birds are able to turnover the complete litter layer of a subtropical rainforest floor in Australia in only 3 weeks and that earthworms required only up to 300 years for forming an ochric epipedon by mixing of the topsoil (A2) and the litter layer (O).

Samedov and Nadirov (1990) concluded that biota, especially earthworms and woodlice can increase soil productivity significantly. Earthworms and woodlice promoted the neutralization of acid (pH 3.4-5.5) decay products and their alkalisation (to pH 6.8-8.6) due to digestion of the soil and plant residues. They also influenced the total chemical composition of the soil, changing Gibbs' free energy of soil ( $-\Delta G$ ) from -231 to -237 or to -254 kcal 100 g<sup>-1</sup>. Furthermore, Samedov and Nadirov (1990) also hypothesized that earthworms and woodlice might participate in the formation of secondary soil minerals with low lattice energies.

Different to Hole (1981), Muller-Lemans and van Dorp (1996) reported that it took less than 20 years for earthworms to turnover the topsoil of European grasslands, which resulted in intensive and more or less homogeneous mixing of the topsoil. For earthworm activities transport rates of around 2 kg m<sup>-2</sup> yr<sup>-1</sup> (equivalent to 1.6 mm yr<sup>-1</sup>) of dry matter from deep soil to top soil are listed.

In Amundson (2004) turnover rates of soil by earthworms were cited to be of around 3 years for the upper 10 cm of a Canadian prairie soil and around 700 years for the upper 50 cm of a soil

in England, resulting in a homogenization of the upper soil profile. Furthermore, mixing rates of 360 years for the upper 75 cm of soil were reported for ground squirrels in California.

Buchan (2010) noted that earthworms are able to digest approximately 90 t of soil per ha each year (equivalent to  $7.5 \text{ mm yr}^{-1}$ ). Comparing the listed studies, we can conclude that earthworms seem to play a very active role in inter-mixing the layers in the soil profile.

Gabet et al. (2003) reviewed rates of bioturbation caused by earthworms (between  $0.54$  to  $10 \text{ mm yr}^{-1}$ ), ants (between  $0.005$  to  $1.8 \text{ mm yr}^{-1}$ ) and termites (between  $0.013$  to  $0.41 \text{ mm yr}^{-1}$ ). They summarized that earthworms are able to excavate tunnels up to 5 mm thick in the soil that either collapse or promote the formation of macropores. The latter would increase the soil porosity by 3 to 10 times. Different to earthworms they suggested that ants are able to generate relatively deep burrows into the soil. However, ants were classified as selective burrowers who base their burrowing activity on the grain-size of the soil, accordingly being absent in most very fine-grained soils. Gabet et al. (2003) also noted that vertebrates usually dig burrows of up to 25 cm in diameter down to 30 cm below the soil surface with dens reaching depths of up to 1 m. However, the role of vertebrates in reaching and breaking up the parent material and therefore promoting soil formation was assumed to be minor.

Yoo et al. (2005; 2007) proposed that an increasing number of fauna participate in soil mixing as soil thickens, especially larger organisms like wombats who were observed to preferentially habituate the base of hillslopes. Naturally, thicker soils are a more preferable habitat for vertebrates, because of increased plant productivity, soil moisture and space for burrowing and nesting. At a study site in the Tennessee Valley in California with known soil production rates (Heimsath et al., 1999; McKean et al., 1993), Yoo et al. (2005) investigated and modelled pocket gopher activities in relation to sediment transport and soil thickness. Modelling results suggested that pocket gophers spend only about 9 kJ of energy annually on producing downslope transport of soil, which is equivalent to 1 % of the total energy expenditure on burrowing. However, it was presumed that most of the energy is used for shearing, mixing and elevating. Yoo et al. (2005) estimated gopher induced gross sediment flux to be  $50 \text{ cm}^2 \text{ yr}^{-1}$  to  $140 \text{ cm}^2 \text{ yr}^{-1}$ , which relates to soil turnover rates of only 40 to 100 years for the first 50 cm of soil of an area of  $1 \text{ m}^2$ .

#### *Bioturbation – b) Floraturbation*

Processes that initiate floraturbation are plant growth and decay and also tree throw.

Gabet et al. (2003) reviewed the impact of plants on soil mixing rates. They reported that the axial (up to 1.45 MPa) and radial (up to 0.91 MPa) pressure caused by root growth is sufficient enough to break up bedrock and therefore contribute to physical weathering, and would also be

substantial enough to push up a column of approximately 100 m thick soil. It was also presented that plant roots are able to enter soft rock matrixes through small cracks, promoting the breakdown of the rock. After their decay plant roots leave behind macropores that become important preferential pathways for subsurface water flows. Furthermore, they stated that tree throw results in uprooting and consequently in the excavation of soil, leaving a pit behind which is prone to be refilled. Thus, tree throw is another agent that can promote the homogenisation of the surface or subsurface soil. Gabet et al. (2003) also discussed a publication of Gill and Jackson (2000) who reported increased turnover rates for roots with increasing temperature and therefore implied that sediment flux by root growth and decay could increase with increasing global temperatures.

Tonneijck and Jongmans (2008) investigated the vertical distribution of organic matter in volcanic ash soils in Ecuador. They implemented a semi-quantitative micromorphological analysis of soil faunal pedofeatures and high-resolution radiocarbon dating. Results implied that bioturbation was highly responsible for the vertical distribution of soil organic matter, with illuviation and roots playing a minor role in transporting soil organic matter in soils. However, the authors assumed that vertical transport of soil organic matter via leaching plays an insignificant role in volcanic ash soils, because of large metal to soil organic matter ratios which limited the mobility of soil organic matter. Here, bioturbation did not result in the homogenization of the topsoil and subsoil, but in a gradual increase of organic carbon in the soil profile. This was explained by the presence of endogeic species, who tend to move soil horizontally (Anderson, 1988), and transport material over short vertical distances only. Movement over short vertical distances was also explained by the occurrence of upwards directed shifting of bioturbation in response to soil thickening due to soil organic matter accumulation.

### *Soil creep*

Soil creep defines the slow mass wasting process of soil on a slope, under the influence of gravity (Source: Glossary of Soil Science terms, Soil Science Society of America).

Saunders and Young (1983) listed various rates of soil creep in  $\text{mm yr}^{-1}$ , referring to the downslope movement of soil particles near the soil surface. The highest rates were recorded for temperate climates predominantly affecting soil movement in the surface soils down to the first 25 cm with rates of about  $0.5\text{-}2 \text{ mm yr}^{-1}$  for the temperate maritime zone and generally higher rates for the temperate continental zone of about  $2\text{-}10 \text{ mm yr}^{-1}$ . For tropical environments rates of approximately  $4\text{-}5 \text{ mm yr}^{-1}$  were listed. Recorded rates of solifluction, a process often difficult

to separate from soil creep, were recorded to be as low as  $1 \text{ mm yr}^{-1}$  and as high as  $300 \text{ mm yr}^{-1}$  for polar and montane climate zones with most rates clustered around  $10\text{-}100 \text{ mm yr}^{-1}$ . It was also stated that the majority of rates of solifluction affected soil movement down to  $50 \text{ cm}$  of depth.

Heimsath et al. (2002) used optically stimulated luminescence to investigate process of soil creep at a study site with known soil production in the Bega Valley in south-eastern Australia. They defined soil creep caused by burrowing agents (e.g. worms, ants, moles) and tree throw as the main factor for creeping soil. With the help of OSL, they determined when soil grains had last visited the soil surface and measured vertical soil mixing rates of  $0.1\text{-}0.4 \text{ mm yr}^{-1}$ . Results indicated that the amount of grains that have visited the surface decreased with increasing soil thickness. Heimsath et al. (2002) used a Monte Carlo simulation to demonstrate particle transport. Results of the simulation assumed that soil creep involved independent movement of mineral grains throughout the soil body and that the grains were reburied or eroded by overland flow upon reaching the soil surface.

Kaste et al. (2007) calculated diffusion-like mixing rates of  $0.1$  to  $0.2 \text{ mm yr}^{-1}$  for the Bega Valley in south-eastern Australia using fallout radionuclides ( $^7\text{Be}$  and  $^{210}\text{Pb}$ ). These mixing rates are comparable to mixing rates of quartz grains of  $0.1\text{-}0.4 \text{ mm yr}^{-1}$  calculated by Heimsath et al. (2002).

### *Rainsplash*

Lobry de Bruyn and Conacher (1990) cited annual erosion rates caused by rainsplash of  $0.25 \text{ mm yr}^{-1}$ .

Tab. 2.4. Soil mixing rates.

Reference	Location	Soil mixing rate (published rates)	Soil mixing rate (mm yr <sup>-1</sup> )	Soil mass moved to surface (mm yr <sup>-1</sup> )	Moving agent
<i>Source: modified after Lobry de Bruyn and Conacher, 1990</i>					
Williams, 1968	Northern Australia				Termites
Lee and Wood, 1971a	Northern Australia	470 g m <sup>-2</sup> yr <sup>-1</sup>	0.39	5.4	Termites
Holt et al., 1980	Northern Australia			0.083	Termites
Spain and McIvor, 1988	Northern Australia			0.917-2.17	Termites
Nye 1955	West Africa	1.25 t ha <sup>-1</sup> yr <sup>-1</sup>	0.104		Termites
Maldague 1964	Africa			1.47	Termites
Lepage 1972, 1973	Africa			2	Termites
Lepage, 1974	Africa	0.67-0.90 t ha <sup>-1</sup> yr <sup>-1</sup>	0.056-0.075		Termites
Nel and Malan, 1974	Africa	0.35 t ha <sup>-1</sup> yr <sup>-1</sup>	0.029		Termites
Pomeroy, 1976	Africa				Termites
Wood and Sands, 1978	Africa	0.3 t ha <sup>-1</sup> yr <sup>-1</sup>	0.025		Termites
Aloni et al., 1983	Africa	4.0 t ha <sup>-1</sup> yr <sup>-1</sup>	0.333		Termites
Akamigbo, 1984	Africa			0.308	Termites
Bagine, 1984	Africa	1.06 t ha <sup>-1</sup> yr <sup>-1</sup>	0.088		Termites
Lepage, 1984	Africa				Termites
Gupta et al., 1981	India	15.9 g m <sup>-2</sup> day <sup>-1</sup>	4.8		Termites
Salick et al., 1983	South America	0.02 and 0.78 t ha <sup>-1</sup> yr <sup>-1</sup>	0.002-0.065		Termites
Aloni and Soyer, 1987	Africa	3 t ha <sup>-1</sup> yr <sup>-1</sup>	0.25	0.25	Termites
Nutting et al., 1987	North America	0.07 and 0.56 t ha <sup>-1</sup> yr <sup>-1</sup>	0.006 and 0.047		Termites
Greenslade, 1974	South Australia	400 cm <sup>3</sup> ha <sup>-1</sup> yr <sup>-1</sup>			Ants
Humphreys, 1981	Eastern Australia	8.41 t ha <sup>-1</sup> yr <sup>-1</sup>	0.701		Ants
Briese, 1982	South-eastern Australia	0.35-0.42 t ha <sup>-1</sup> yr <sup>-1</sup>	0.029 and 0.035		Ants
	Eastern Australia	<0.05 t ha <sup>-1</sup> yr <sup>-1</sup>	<0.004		Ants

Reference	Location	Soil mixing rate (published rates)	Soil mixing rate (mm yr <sup>-1</sup> )	Soil mass moved to surface (mm yr <sup>-1</sup> )	Moving agent
Talbot, 1953	Michigan America			0.07	Ants
Lyford, 1963	America	0.6 t ha <sup>-1</sup> yr <sup>-1</sup>	0.05		Ants
Salem and Hole, 1968	Wisconsin America	11.36 t ha <sup>-1</sup> yr <sup>-1</sup>	0.947	20	Ants
Rogers, 1972	America			0.0002-0.0006	Ants
Wiken et al., 1976	America	11.36 t ha <sup>-1</sup> yr <sup>-1</sup>	0.947		Ants
Levan and Stone, 1983	Wisconsin America			0.133	Ants
Waloff and Blackith, 1962	England	8.24 t ha <sup>-1</sup> yr <sup>-1</sup>	0.687		Ants
Sudd, 1969	England			40-400 mg nest <sup>-1</sup> day <sup>-1</sup>	Ants
Bucher and Zuccardi, 1967	Argentina	11 t ha <sup>-1</sup> yr <sup>-1</sup>	0.917	0.007	Ants
Lobry de Bruyn and Conacher, 1990	N/A	3 t ha <sup>-1</sup> yr <sup>-1</sup>	0.25		Soil erosion by rainsplash
<i>Source: listed publications</i>					
Carson and Kirkby, 1972	N/A	0.003 cm <sup>2</sup> yr <sup>-1</sup>			Wedging by grass roots
Carson and Kirkby, 1972	N/A	0.10 cm <sup>2</sup> yr <sup>-1</sup>			Rabbits, burrowing and refilling
Carson and Kirkby, 1972	N/A	0.25 cm <sup>2</sup> yr <sup>-1</sup>			Worms, distribution of surface casts
Carson and Kirkby, 1972	N/A	0.15 cm <sup>2</sup> yr <sup>-1</sup>			Worms, burrowing and refilling
Muller-Lemans, 1996	Europe		1.7	1.67	Earthworms
Gabet et al., 2003	N/A	5.4 x 10 <sup>-4</sup> to 0.01 m yr <sup>-1</sup>	0.54 to 10		Earthworms
Amundson, 2004 (cited from Darwin)		0.02 cm <sup>2</sup> yr <sup>-1</sup>			Earthworms
Buchan, 2010	N/A	90 t ha <sup>-1</sup> yr <sup>-1</sup>	7.5		Earthworms (digestion)
Wilkinson et al., 2009	Various	10-100 t ha <sup>-1</sup> yr <sup>-1</sup>	0.833-8.33		Earthworms

Reference	Location	Soil mixing rate (published rates)	Soil mixing rate (mm yr <sup>-1</sup> )	Soil mass moved to surface (mm yr <sup>-1</sup> )	Moving agent
Gabet et al., 2003	N/A	$1.3 \times 10^{-5}$ to $4.1 \times 10^{-4}$ m yr <sup>-1</sup>	0.013 to 0.41		Termites
Paton et al., 1995	N/A	1-5 kg m <sup>-2</sup> yr <sup>-1</sup>	0.833-4.167		Ants, termites, earthworms
Wilkinson and Humphreys, 2005	South-eastern Australia		10.6		Earthworms and ants
Wilkinson and Humphreys, 2005	South-eastern Australia		0.428 to 0.714		Ants, termites and cicades
Wilkinson et al., 2009	Various	1-5 t ha <sup>-1</sup> yr <sup>-1</sup>	0.083-0.417		Ants, termites, vertebrates
Yoo et al., 2005	N/A	50 to 140 cm <sup>2</sup> yr <sup>-1</sup>			Pocket gopher (simulation model)
Hole, 1981	Arctic climates	18 t ha <sup>-1</sup> yr <sup>-1</sup>	1.5		Ground squirrel
Heimsath et al., 2002	South-eastern Australia	10 to 40 cm kyr <sup>-1</sup>	0.1 to 0.4		Soil creep
Kaste et al., 2007	South-eastern Australia	10 to 20 cm kyr <sup>-1</sup>	0.1 to 0.2		Diffusion-like mixing rates
Saunders and Young, 1983	Temperate maritime climates		0.5-2		Soil creep
Saunders and Young, 1983	Temperate continental climates		2-10		Soil creep
Saunders and Young, 1983	Tropical climates		4-5		Soil creep
Saunders and Young, 1983	Polar and montane climates		1-300 10-100		Solifluction

Note: Soil mixing rates recorded in mass per area per year were converted to mm yr<sup>-1</sup> in assuming a soil bulk density of 1200 kg m<sup>-3</sup> in the conversion processes.



*Modelling pedoturbation*

In their review, Gabet et al. (2003) provided quantitative models of bioturbation and sediment transport. They formulated a general slope-dependent model to determine the horizontal volumetric flux of sediment ( $q_{sx}$ ) caused by root growth and decay.

$$q_{sx} = \frac{(xr\tau)}{(\rho_r)} \quad \text{equation (2.18),}$$

where  $x$  (in m) is the net horizontal displacement of soil,  $r$  (in  $\text{kg m}^{-2}$ ) is the root mass per unit area,  $\tau$  (per  $\text{year}^{-1}$ ) is the root turnover rate, and  $\rho_r$  (in  $\text{kg m}^{-3}$ ) is the density of root material. They then calculated values for sediment flux by root growth and decay for three different types of vegetation with  $2.1 \times 10^{-4} \text{ m}^2 \text{ yr}^{-1}$  for temperate grasslands,  $6.8 \times 10^{-4} \text{ m}^2 \text{ yr}^{-1}$  for sclerophyllous shrubs and  $8.8 \times 10^{-4} \text{ m}^2 \text{ yr}^{-1}$  for temperate forests.

Gabet et al. (2003) also quantified the horizontal alteration of soil along a hillslope caused by tree throw applying the following equations:

$$q_s = \frac{\text{vol}}{\text{event}} \times \frac{\text{distance}}{\text{event}} \times \frac{\text{events}}{\text{area}} \times \frac{\text{events}}{\text{time}} \quad \text{equation (2.19),}$$

$$x_n = \overline{x_d} - \overline{x_u} = \frac{2}{\pi}(W + D) \sin\theta \quad \text{equation (2.20),}$$

Where  $q_s$  is the horizontal sediment flux,  $x_n$  is the long-term net horizontal transport distance,  $x_d$  the horizontal distance of displacement of the root plate centroid caused by trees that were falling directly downslope,  $x_u$  the horizontal distance of displacement of the root plate centroid caused by trees that were falling directly uphill,  $W$  the width of the root plate and  $D$  the depth of the excavated pit.

Gabet et al. (2003) calculated horizontal sediment flux ( $q_s$ ) of  $8 \times 10^{-4} \text{ m}^2 \text{ yr}^{-1}$  on a  $10^\circ$  slope by substituting equation 19 with equation 18 for an excavated pit width of 4 m, a pit depth of 0.7 m, a mound volume of  $4 \text{ m}^3$  and an uprooting rate of 4 trees  $\text{ha}^{-1} \text{ yr}^{-1}$  (with  $q_{sx}$  equal to  $4.8 \times 10^{-3} \text{ m}^2 \text{ yr}^{-1} \sin\theta$ ).

Salvador-Blanes et al. (2007) considered bioturbation processes and the redistribution of soil particles in their model of soil profile evolution. In considering the addition and removal of soil particles to or from the soil profile and also their translocation within the soil profile the process of horizonation was implemented in the model. Soil mixing was modelled by incorporating parameterized bioturbation processes resulting from earthworm, ant and termite activity (assumed surface casting of  $1\text{-}5 \text{ kg m}^{-2} \text{ yr}^{-1}$ , cited from Paton et al. (1995)). Due to a lack of parameterisation, illuviation and eluviation processes were not taken into account. However,

running the model resulted in stone layers in the soil profile, which was attributed to high mixing velocities because of bioturbation.

### Summary

Soil mixing rates by faunal agents reported in the literature are relatively fast compared to discussed rates of chemical and physical weathering (Figure 2.8):

- Lobry de Bruyn and Conacher (1990) published soil mixing rates from ants and termites ranging between approximately 0.002 and 0.950 mm of soil turnover each year (Table 2.4). Soil mixing rates from ants and termites taken from the selection of other published data ranged from 0.002 to 1.8 mm yr<sup>-1</sup>. However, soil turnover rates by ants and termites seem to be of similar orders of magnitude for the compared studies (Figure 2.9).
- Similar to ants and termites, most soil mixing rates caused by earthworms fell into the range of about 0.5 to 4 mm of soil turnover each year, although much higher rates of 7.5 and 10.6 mm yr<sup>-1</sup> were also recorded. Higher rates of soil alterations by earthworms may occur because unlike ants and termites earthworms also ingest the soil material, in addition to moving soil particles by mounding and burrowing. Furthermore, turnover rates of the whole topsoil by earthworms were as fast as 300 to 700 years and resulted in a homogenisation of the soil material.
- Soil turnover rates recorded for vertebrates range from 0.08 to 1.5 mm yr<sup>-1</sup> and are very similar to mixing rates recorded for ants, termites and earthworms.
- *In situ* measured rates of soil creep predominantly caused by burrowing agents and tree throw are much lower than reported assumed turnover rates by ants, termites and earthworms. These rates, calculated by applying sophisticated laboratory methods to investigate pedogenic processes *in situ*, ranged between 0.1 and 0.4 mm of soil turnover each year. However, rates of soil creep determined using other methods were either very similar to mixing rates from ants, termites and earthworms with 0.5 to 5 mm yr<sup>-1</sup>, or exceed these rates by far, i.e. 10-300 mm yr<sup>-1</sup> for polar and montane environments.
- Comparing published rates of soil turnover with chemical weathering rates (Fig. 2.8) demonstrated that the range in turnover rates of soil by mixing agents exceeded the range of chemical weathering rates significantly.

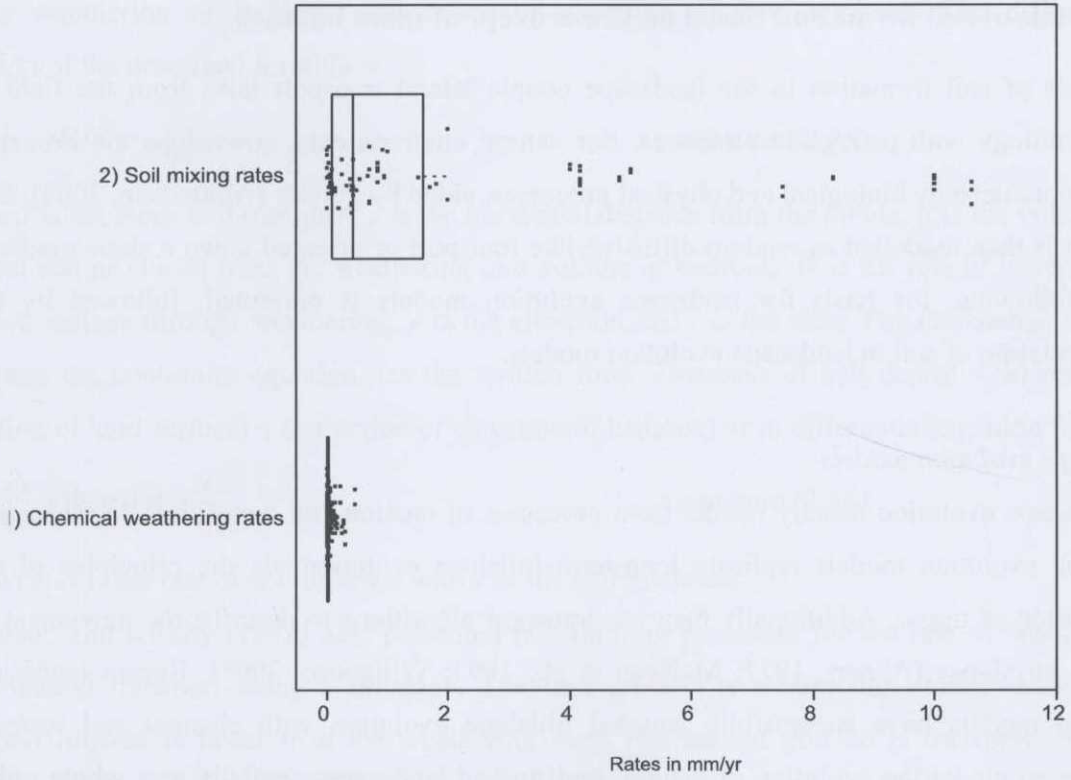


Fig. 2.8. A comparison of soil mixing rates and chemical weathering.

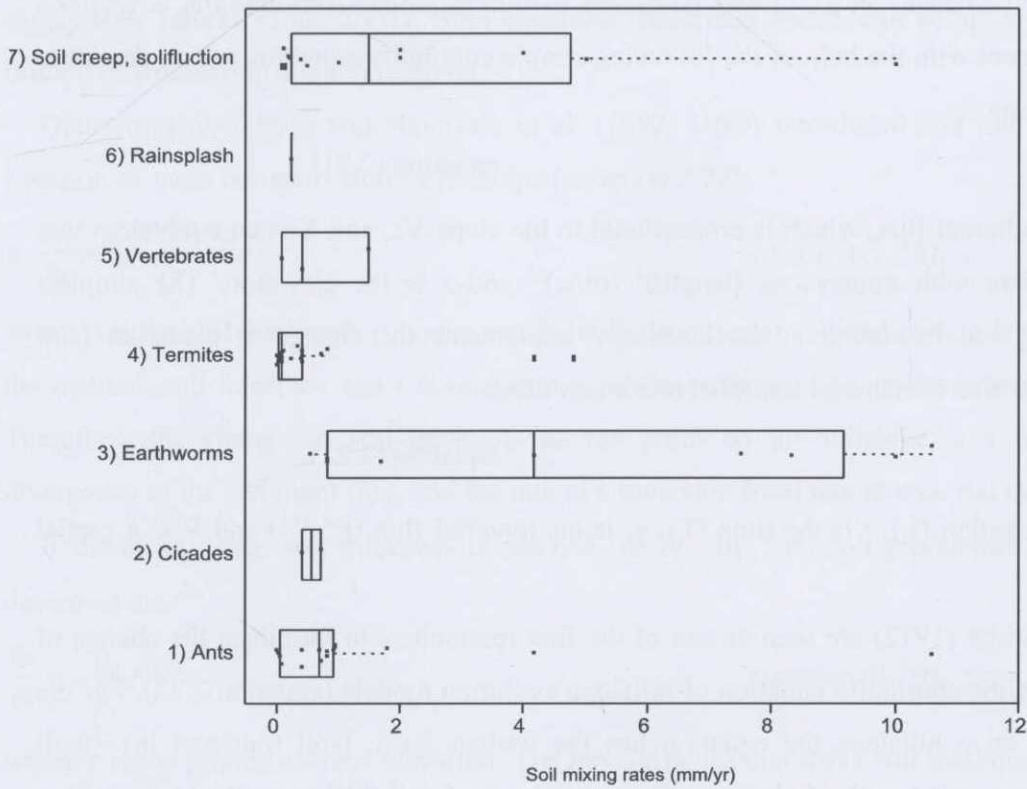


Fig. 2.9. Box-Plot distributions of soil mixing rates from field data (presented in Table 2.4). Values of soil mixing rates in  $\text{mm yr}^{-1}$  are plotted separately for discussed soil mixing agents.

## 2.5 Models of soil formation based on the concept of mass balance

Models of soil formation in the landscape couple lateral transport laws from the field of geomorphology with pedogenic processes. For natural environments, downslope movement is generally induced by biological and physical processes, aided by gravity (Amundson, 2004). Soil transport is then modelled as random diffusive-like transport or oriented down a slope gradient. In the following, the basis for landscape evolution models is presented, followed by the implementation of soil in landscape evolution models.

### *Landscape evolution models*

Landscape evolution usually results from processes of erosion and deposition. In particular, landscape evolution models replicate long-term hillslope evolution via the principles of the conservation of mass. Additionally they use transport algorithms to describe the movement of material on slopes (Ahnert, 1977; McKean et al., 1993; Willgoose, 2005). Recent landscape evolution models have successfully coupled hillslope evolution with channel and tectonic processes to model the evolution of natural, undisturbed landscapes spatially as a whole rather than restricted solely to hillslope development (Willgoose, 2005).

As described in Minasny et al. (2008) landscape evolution models simulate the downslope transport of sediment with the help of the following simple continuity equation, which describes diffusive-like transport:

$$q_s = -K\nabla z \quad \text{equation (2.21),}$$

where  $q_s$  is the sediment flux, which is proportional to the slope  $\nabla z$ , and  $K$  is an equivalent to a diffusion coefficient with dimensions  $(\text{length})^2 (\text{time})^{-1}$  and  $z$  is the elevation. The simplest model simulating soil formation in the landscape implements the change in elevation (soil thickness) as a function of material transport (sediment flux):

$$\frac{\partial z}{\partial t} = -\nabla q_s \quad \text{equation (2.22),}$$

where  $z$  is the elevation (L),  $t$  is the time (T),  $q_s$  is the material flux ( $L^3 T^{-1}$ ) and  $\nabla$  is a partial derivative vector.

Carson and Kirkby (1972) are seen as one of the first researchers to introduce the change of soil thickness into the continuity equation of hillslope evolution models (equation 2.22). For the transport of soil on a hillslope the equation has the written form: (soil transport in) – (soil transport out over a unit length of slope profile) – (increase of soil thickness due to expansion

during weathering of bedrock) = (decrease of elevation of land surface). The differential equation of the described formula is:

$$\frac{\partial S}{\partial x} - (\mu - 1)W = -\frac{\partial y}{\partial t} \quad \text{equation (2.23),}$$

where  $S$  is the mean soil transport,  $x$  is the horizontal distance from the divide,  $\mu$  is the volume of mineral soil produced from the weathering unit volume of bedrock,  $W$  is the rate of lowering of bedrock surface through weathering,  $y$  is the elevation and  $t$  is the time. For the change in soil thickness the continuity equation has the written form: (Increase of soil depth) = (Increase of elevation of land surface) + (reduction of elevation of bedrock) or in differential equation form:

$$\frac{\partial z}{\partial t} = \frac{\partial y}{\partial t} + W = \mu W - \frac{\partial S}{\partial x} \quad \text{equation (2.24),}$$

where  $\partial z/\partial t$  is the rate of soil increase with  $z$  as the soil thickness.

Carson and Kirkby (1972) also presented two limiting processes for the rate of weathering and material transport along a hillslope. The first process is weathering limited; hence the transport process is faster than the weathering rate. The second process is transport limited; hence the rate of weathering is faster than the transport process. If the weathering rate (soil production) and the transport rate (erosion) equal each other, then the soil depth is at a local steady state (Burke et al., 2007). Both equations, described above, can be applied to transport-limited or weathering-limited removal.

Dietrich et al. (1995) and Heimsath et al. (1997; 1999) introduced soil into the continuity equation of mass transport along a hillslope (equation 2.22):

$$\rho_s \frac{\partial h}{\partial t} = -\rho_r \frac{\partial e}{\partial t} - \nabla q_s \quad \text{equation (2.25),}$$

where  $h$  is the soil thickness,  $\rho_s$  and  $\rho_r$  are the bulk densities of soil and rock,  $e$  is the elevation of the bedrock-soil interface and  $t$  is time and  $q_s$  is the sediment flux in the horizontal direction. Therefore, the change in soil thickness at any point on the hillslope is a function of the divergence of the sediment flux, and the rate of conversion from parent material to soil.

If the steady-state soil thickness is reached ( $\partial h/\partial t = 0$ ), then soil production ( $\partial e/\partial t$ ) can be described as:

$$\frac{\partial e}{\partial t} = -\frac{\rho_s}{\rho_r} K \nabla^2 z \quad \text{equation (2.26),}$$

where  $z$  is the ground surface elevation. The key variables that drive soil thickness on hillslopes are assumed to be the slope curvature, the transport coefficient, the soil production rate and time (Amundson, 2004).

### *Modelling soil formation in the landscape*

In 1975 Yaalon discussed conceptual models of pedogenesis and raised the question, can soil-forming functions like Jenny's (1941) be solved? Yaalon (1975) expressed the need for collecting field data to model soil formation mechanistically. Therefore, he stated that the future of modelling soil formation relies on replacing statistically based models with physically more significant mathematical models.

Yaalon (1975) emphasized the importance of implementing spatial differentiation (catenation), the relief factor (catenary slope), material fluxes on a given pedomorphic surface (vertical and lateral) and different parent materials and time steps in modelling soil formation. Within the proposed model, he considered vegetation as the dependent variable of the ecosystem, varying with soil properties.

Huggett (1975) proposed the first mechanistic model of soil formation in the landscape. His publication can be seen as the first application of landscape evolution modelling in soil science. Huggett (1975) introduced the concept of a homomorphic model to simulate the soil system on the catena scale over millennial time scales. A homomorphic modelling approach groups "...several components..." of the soil system "...to form one single element in the model...".

More importantly, he suggested simulating soil formation in a three-dimensional soil profile. He also proposed to simulate soil in form of layers more or less organized parallel to the parent material. For instance, within the soil profile the rate of weathering should decrease with depth, whereas the bulk density should increase. Huggett (1975) stated that in terms of landscape evolution contours that concave downslope should lead to convergent flowlines and convex contours should lead to divergent flowlines and that flow should tend to converge in hollows and diverge over spurs. All 'thalweg' and valley basins should join in one complex network, based on 1<sup>st</sup> and 2<sup>nd</sup> order stream lines.

Kirkby (1977, 1985) presented the first comprehensive mechanistic model of soil profile development in interaction with a hillslope model based on mass-balance, which can be seen as a valuable basis for quantitative soil profile modelling or even soil catena modelling. To predict the development of soils over time quantitatively, the mass balance model estimates the water flow through the soil and the uptake of nutrients from the soil. The soil profile development model consists of three parts, the weathering profile, the inorganic profile and the organic profile.

Kirkby's soil profile model is based on the accumulated amount of 'soil deficit',  $w$ , which represents the amount of parent rock converted into a soil mantle:

$$w = \int(-\infty, z = 0)(1 - P) dz \quad \text{equation (2.27),}$$

where  $P$  is the proportion of bedrock remaining in the soil profile (unweathered rock) and  $z$  is the depth below the soil surface.  $P =$  unweathered parent material, takes values between zero and one.

The mass balance model for the accumulated soil layer of the soil profile is:

$$\frac{\partial w}{\partial t} = \frac{\partial}{\partial x} \left[ J - S \frac{(1 - P_s)}{P_s} \right] \quad \text{equation (2.28),}$$

where  $P_s$  are the properties remaining in the part of the soil profile where mechanical erosion occurs (mostly at the surface),  $x$  is the distance from the divide,  $t$  is the time,  $S$  is the mechanical sediment transport measured in the  $x$  direction and  $J$  is the chemical sediment transport.

Within the model inorganic minerals are treated as mixtures of elementary oxides, which dissolve independently to create ions (Gibbs' free energy to calculate equilibrium reactions). In the model the soil organic matter material experiences production, accumulation, vertical mixing and decomposition. Mixing rates of organic matter act as a diffusion process; transporting organic material from areas of high to those of low concentration. At the surface accumulated organic matter is transferred downwards through vertical mixing in balance with an upward mixing of inorganic material. The most important product of decomposition of organic matter is  $\text{CO}_2$ . Within the model produced  $\text{CO}_2$  release is simulated with diffusion processes, mainly gaseous diffusion. The soil pH is calculated as a result of this  $\text{CO}_2$  distribution.

Kirkby (1985) enhanced his soil profile model by also simulating the processes of percolation, equilibrium solution, leaching of solutes, ionic diffusion, organic mixing, leaf fall, organic decomposition and mechanical denudation. Each process leads to second-order linear partial differential equations.

Minasny and McBratney (1999, 2001) introduced a basic mechanistic quantitative soil formation model based on the conceptual ideas of Huggett (1975) and Heimsath et al. (1997). Their soil formation model considers soil formation spatially at the catena scale and is written for predicting regolith depth and soil formation at the landscape scale over millennial time scales, simulating soil formation over tens of thousands of years. The continuity equation of the model is based on the assumption that the change of soil thickness over time depend (1) on the production of soil from the weathering of parent material and (2) on the transport of soil through natural surface erosion. The rate of weathering and the erosive diffusivity are the main parameters used in the soil formation model. The weathering of bedrock was characterized as an exponential decline with increasing soil cover thickness based on equation 2.12 applying

concepts from Dietrich et al. (1995) and Heimsath et al. (1997). It was assumed that the weathering rate of bedrock to soil,  $P_0$ , is mainly controlled by the climate whereas the empirical constant,  $b$ , is believed to depend on the thermal properties of the rock or soil. The transport rate of materials was defined similar to Darcy's law for water transport in soils whereas the movement of materials within the landscape was expressed in terms of diffusive transport. The erosive diffusivity of the soil material was assumed to be controlled by factors of soil erosion, soil physical properties, and climate. Running the soil formation model over millennial timescales showed that the initial soil production rate is high and that it slows down exponentially until it reaches steady state at around 40,000 years, applying a value for  $P_0$  of  $0.19 \text{ mm yr}^{-1}$ .

Based on the soil-formation model of Minasny and McBratney (2001), Salvador-Blanes et al. (2007) improved the modelling of *in situ* long-term soil profile evolution by implementing particle size transformation, horizonation (layers of regolith formed from bedrock with each time step) and bioturbation processes. Horizonation was introduced in the model by taking into account the translocation of particles within the soil profile. However, due to the influence of bioturbation processes, running this model resulted in the formation of stone layers in the soil profile. Running the model also showed that after 10,000 years a soil profile of about 1.25 m is formed, and that this profile lacked any horizonation. After a simulation time of 20,000 to 80,000 years the thickness of the soil profile increased to 1.80 m and by that time period a total of three horizons were developed in the soil profile.

The soil-formation models discussed predict soil profile development *in situ* or along a hillslope starting from parent materials and ending with the formation of soil being in equilibrium, which was simulated over tens of thousands of years and modelling steps of 100 to 1000 years.

In the following soil-formation models, the evolution of soil is not simulated as starting from *in situ* bedrock. The presence of soil is assumed already and processes that lead to the formation of the soil profiles studied are simulated. Generally, these models predict soil in yearly time steps up to 1000 years. They are not designed to simulate soil profile development from parent rock over millennial time scales, but to model processes in soil.

Sommer et al. (2008) presented a soil-landscape genesis model that simulated the evolution of a hummocky agricultural landscape with a time-split modelling approach. Fallout radionuclide data implied regressive processes of pedogenesis during the last 50 years for the studied landscape. For the progressive period, soil formation was therefore modelled by simulating



pedogenic processes such as decarbonisation and carbonisation, silicate weathering and clay translocation and their quantification by a spatially-distributed, coupled water flow and solute transport model. For the modelling of the regressive period a modified version of the dynamic, physically based EROSION-3D model was used, which allows the spatially-distributed modelling of soil erosion and soil deposition. In their modelling approach Sommer et al. (2008) coupled geological-historical information with spatially-distributed pedogenic processes and their recent changes to better simulate the current development of the landscape studied.

Finke and Hutson (2008) introduced a model to simulate formation of calcareous soils formed on loess (15,000 BP to present). Model simulations were based on Jenny's factors of soil formation (Jenny, 1941) using the LEACHC model. Additional soil-forming processes were implemented to describe the effect of the soil fauna and flora on various soil properties, assuming an annual rate of bioturbation of  $30 \text{ t ha}^{-1}$  ( $2.5 \text{ mm yr}^{-1}$ ). Running the model showed that it takes about 1297 years to decarbonise 1 m of loess parent material. Results also showed a clear effect of bioturbation on soil formation, reducing the decarbonisation of the topsoil and affecting clay migration processes.

### *Summary*

The models of soil formation reviewed coupled lateral transport laws from modelling hillslope formation in the landscape with pedologic processes. These models simulate soil formation in a quantitative-mechanistic sense based on mass-balance.

However, some model soil formation over millennial time scales starting from parent materials and ending with the formation of soil being in equilibrium whilst others simulated soil processes that lead to the formation of a certain soil type over centennial time scales, already assuming the presence of the soil body.

An overview of all models presented and discussed in this literature review is given in Table 2.5. In Table 2.5 models of pedogenesis are summarized according to the concepts applied in the model listed.

**Tab. 2.5.** Summary of models of soil formation presented in this literature review (factors, processes, pathways, energy and mass-balance soil formation models). Models are grouped based on the concepts used and the type of the model (based on Minasny et al. (2008)).

Model concept	Model description	Model type	Reference
<i>Factorial</i>			
Soil-forming factors	$S = f(c,l,o,r,p,t)$	Qualitative (empirical)	Dokuchaev, 1892; Shaw, 1930; Jenny, 1941
	$S = f(s,c,o,r,p,a,n)$ ; $S = f(\text{time})c,l,o,r,p...$	Qualitative empirical	McBratney et al., 2003; Chronofunctions
Soil-forming processes	$S = f(\text{addition, removal, translocation, transformation})$	Qualitative	Simonson, 1959
Soil evolution along pathways	$S = f(\text{Progressively, Regressively})$	Qualitative	Johnson and Watson-Stegner, 1989
<i>Energy</i>			
Soil energy model	$S = f(o,w,t)$	Qualitative	Runge, 1973
Soil energy model	Soil formation is modelled through quantifying processes of energy, i.e. radiation, kinetic energy...	Mechanistic	Regan, 1977
Soil energy model	Soil formation modelled via energy expenditure	Quantitative-empirical-mechanistic	Volobuyev, 1974
Soil energy model	Thermodynamic aspects in soil-forming processes, i.e. Gibbs' free energy and entropy of soil minerals	Quantitative-empirical-mechanistic	Volobuyev and Ponomarev, 1977
<i>Mass-balance</i>			
Soil weathering: Soil production function	$SPR = P_0 \exp(-bh)$ verified with field data	Quantitative-mechanistic	Heimsath et al., 1997
Soil weathering: The 'hump' function	$\frac{\partial e}{\partial t} = - (P_0 [\exp(-k_1 h) - \exp(-k_2 h)] + P_a)$	Quantitative-mechanistic	Dietrich et al., 1995; Furbish and Fagherazzi, 2001; Minasny and McBratney 2006
Soil weathering: Coupling chemical-physical weathering	$W = D (1 - [Zr]_{\text{rock}}/[Zr]_{\text{soil}})$	Quantitative-mechanistic	Riebe et al., 2003, 2004a, 2004b; Burke et al., 2007; 2009; Green et al., 2006; Yoo et al., 2007

Model concept	Model description	Model type	Reference
<i>Mass-Balance</i>			
Pedoturbations: Soil creep	Monte Carlo simulation of independent movement of soil grains in soil profile	Quantitative-mechanistic	Heimsath et al., 2002
Soil landscape model	Catena scale, 3 dimensional, homomorphic; lateral and vertical fluxes of material	Quantitative-mechanistic	Huggett, 1975
Soil landscape model	Soil formation over millennial time scales, Coupling weathering, diffusive transport and erosive diffusivity, fluxes simulated within the system	Quantitative-mechanistic	Minasny and McBratney, 1999, 2001; Dietrich et al., 1995; Heimsath et al., 1999
Soil profile model	Soil profile formation in interaction with hillslope processes, fluxes simulated within the soil system	Quantitative-mechanistic	Kirkby, 1977; 1985
Soil profile model	Soil profile evolution over millennial time scales, implementing horizonation and bioturbation, fluxes simulated within the system	Quantitative-mechanistic	Salvador-Blanes et al., 2007
Soil process model	Soil landscape evolution via simulating soil forming processes over centennial time scales, i.e. silicate weathering, soil erosion...		Sommer et al., 2008; Finke and Hutson, 2008

## 2.6 Conclusions

In pedology most studies have focused on the prediction of soil properties from landscape attributes at specific sites based on empirical quantitative relationships (McBratney et al., 2003). However, to understand and improve knowledge of pedogenesis, a mechanistic model that can simulate the development of soil under various conditions or scenarios needs to be formalised. This growing movement in pedology has directed the focus towards mechanistic modelling of soil formation. From this literature review we have learned that in order to verify mechanistic models of soil formation, it is essential to quantify pedogenic processes with field data.

By reviewing research related to this topic, it can be concluded that processes of pedogenesis have been estimated from field data, particularly rates of soil weathering and rates of soil mixing. However, we also learned that the majority of these estimates were based on watershed studies or observational data and that it is necessary to further investigate soil formation processes *in situ* to develop models of soil formation further and to be able to model better soil evolution.

Colman and Dethier (1986) discussed that the largest constraint in estimating weathering rates (chemical and/or physical) from field studies is the lack of independent age estimates of the weathered materials studied. In recent years sophisticated laboratory techniques have become available that can be used to quantify such processes of soil formation *in situ*.

*In situ* terrestrial cosmogenic nuclides (TCN) and optically stimulated luminescence (OSL) are such tools to investigate pedogenesis quantitatively via numerical dating. Both techniques have been used widely in the fields of geology and geomorphology until they became accessible for pedology related studies. TCN and OSL can now be applied to investigate long-term processes of pedogenesis on millennial time scales; and OSL can also be used to investigate short-term processes of pedogenesis on a time scale of a few hundred years.

The concentration of TCN in soil parent materials can be used to investigate processes of soil weathering *in situ* by deriving *rates of soil production*. Dating individual sand-sized quartz grains with OSL can be applied to explore processes of soil mixing by estimating *rates of potential soil turnover*, and also to estimate the 'age' of soil horizons.

The following paragraphs will answer and reflect on the questions about pedogenesis that have been formulated in the introduction to this literature review:

### (1) *How does soil form?*

We know that soil forms via a combination of interrelated physical, chemical and biological processes.

Traditional concepts in pedology explain soil formation progressively depending on environmental factors and processes along a sequence of preset soil types with soil formation eventually reaching equilibrium.

Furthermore, soil profile evolution is described as a product of mostly downward moving processes that led to the formation of interrelated layers or horizons. Alternately soil profile evolution is described as depending predominantly on a combination of bioturbation and slope processes.

Chronofunctions have been applied to explain soil formation along linear and non-linear functions, i.e. exponential, polynomial or sigmoidal behaviour.

However, we learned that the formation of soil from parent materials was predominantly explained by two concepts: (1) the exponential soil production model and (2) the humped soil production model. More recently, sophisticated laboratory methods have made it possible to verify and parameterize the concept of exponential decline of soil formation with increasing soil thickness, using field data over millennial time scales. Soil production following a humped model with maximised soil production at an intermediate soil depth was assumed for some field sites, but a parameterization of this function is still lacking. Evidence for the humped concept comes from observing high rates of chemical and physical weathering under initial soil cover in the field.

(2) *At what rate does soil evolve?*

We learned that rates of soil formation are initially fast and decrease with time.

We also learned that field data have confirmed the concept of exponential decline of weathering of parent materials to soil with increasing soil thickness *in situ* (TCN-derived). Estimated rates of soil production from field data were as low as  $0.004 \text{ mm yr}^{-1}$  and as high as  $0.4 \text{ mm yr}^{-1}$ .

Modelling soil formation mechanistically over millennial time scales by implementing an exponential soil production model with relatively high rates of weathering of bedrock to soil of  $0.19 \text{ mm yr}^{-1}$  resulted in steady-state after around 40 000 years.

Results from studies comparing the rate of chemical and physical weathering *in situ* showed that chemical weathering rates were generally lower, accounting for less than 50 % of the total weathering rate. Mean rates of chemical weathering were about  $0.022 \text{ mm yr}^{-1}$  with a maximum rate of  $0.14 \text{ mm yr}^{-1}$ .

(3) *How fast are rates of soil turnover occurring in the soil profile, and what influence do they have on pedogenesis?*

We learned that mixing rates of soil were much faster than rates of soil production from parent materials. Mixing rates as high as  $10.6 \text{ mm yr}^{-1}$  were recorded and we learned that it was assumed that rates of bioturbation exceed soil production rates by up to 3 orders of magnitude. Particularly earthworms seemed to play a very active role in turbating the soil profile.

It can be concluded that in most of the reviewed pedoturbation studies, especially bioturbations impeded the horizonation of a soil profile by homogenising the soil material. However, bioturbation processes promoting the formation of horizons in the soil profile were also proposed.

Determining rates of soil mixing *in situ* by dating individual soil particles (OSL, fallout radionuclides) resulted in rates of soil turnover of about  $0.2 \text{ mm yr}^{-1}$ . These rates were lower than those estimated from observational field studies, where soil turnover was generally more than  $0.5 \text{ mm yr}^{-1}$ , for a variety of mixing agents.

Implementing relatively high rates of soil turnover of up to about  $4 \text{ mm yr}^{-1}$  in mechanistic models of soil formation resulted in the formation of stone layers in the soil profile. Does this result implicate that high rates of bioturbation are questionable?

However, within this literature review it became apparent that work on quantifying soil-forming processes *in situ* to verify and improve mechanistic models of soil formation is still minimal and therefore vital (Bockheim and Gennadiyev, 2009; Pelletier and Rasmussen, 2009). The application of *in situ* TCN and OSL to parameterise pedogenic processes will be the focus of the research Chapters 4 and 5.

Ultimately, a soil model should be able to simulate the formation and generation of the 3 unique aspects of: soil horizons, soil aggregates and processes of soil colloids (see Box 2.4).

**Box 2.4: What defines soil science?**

Jock Churchman (2010) from the University of Adelaide identified three aspects that are unique to the discipline of soil science, these aspects distinguish soil science among scientific disciplines generally. These are:

- (1) the formation and properties of soil horizons,
- (2) the occurrence and properties of aggregates in soil, and
- (3) the occurrence and behaviour of soil colloids.

He added that the possibility that these aspects could be reduced to other sciences is dismissed because they can be explained more usefully at a larger size scale or by a more complex context than those belonging to more basic sciences such as physics or chemistry. The three unique aspects are considered to comprise a research tradition for soil science, which, due to their ultimate irreducibility, is constituted as a special science. These unique aspects cross sub-discipline boundaries so that both soil science and soils should be considered holistically rather than via the separate sub-disciplines through which they have often been studied in the past.

Parts of this literature review will be published in the scientific Journal 'Advances in Agronomy': Stockmann, U., Minasny, B., McBratney, A. (2011): Quantifying processes of pedogenesis. In: *Advances in Agronomy* **113**, to be published.

Faint, illegible text at the top of the page, possibly a header or introductory paragraph.

Second block of faint, illegible text.

Third block of faint, illegible text.

Fourth block of faint, illegible text.

Fifth block of faint, illegible text.

Faint text at the bottom of the page, possibly a footer or concluding paragraph.



## Chapter 3 Study area, sampling design, stable and labile soil properties

This chapter provides a characterisation of the study site, a description of the sampling scheme and a description of the materials and methods used in this study. Section 3.1.1 characterises the study area in terms of climate, geology and soils, followed by a description of the sampling scheme used in this study (section 3.1.2). In section 3.1.3 materials and methods used to analyse stable and labile soil parameters in the laboratory are described. Section 3.2 discusses stable and labile soil properties at the Werrikimbe National Park study site.

### 3.1 Materials and Methods

In this research, the selection of the study site was a very important consideration. Some fundamental criteria needed to be considered in choosing a study site appropriate for conducting research on quantifying processes of pedogenesis on millennial time scales over tens of thousands of years.

- (1) It was necessary to find an uncultivated, natural study site that was still accessible for sampling to take place. Such a site with no disturbance by human activities was crucial in investigating the *in situ* formation of soil. Therefore, we selected the location in one of the National Parks of New South Wales, in Australia with permission from the NSW Department of Environment & Climate Change.
- (2) The chosen study site needed to have significant relief in order to investigate soil profile formation along a hillslope.
- (3) The underlying parent materials needed to contain the mineral quartz in relative abundance. Quartz was required for sophisticated dating techniques to quantify the processes of pedogenesis.

#### 3.1.1 Characterisation of the study site – Werrikimbe National Park

The field survey was conducted in a subcatchment of Werrikimbe National Park with an area of approximately 100 km<sup>2</sup>.

With a total area of 33,292 ha, Werrikimbe National Park is situated along the Great Escarpment in north-eastern New South Wales, about 60 km west of the coastal town of Port Macquarie (refer to Figure 3.1). This rainforest mountain park is located about 1100 m above sea level with Mount Banda Banda (1258 m) and Spokes Mountain (1230 m) the highest points in the area. Werrikimbe National Park is one of the first high country rainforest parks that was reserved as a National Park in NSW, after being declared 'wilderness' in 1975. In 1986

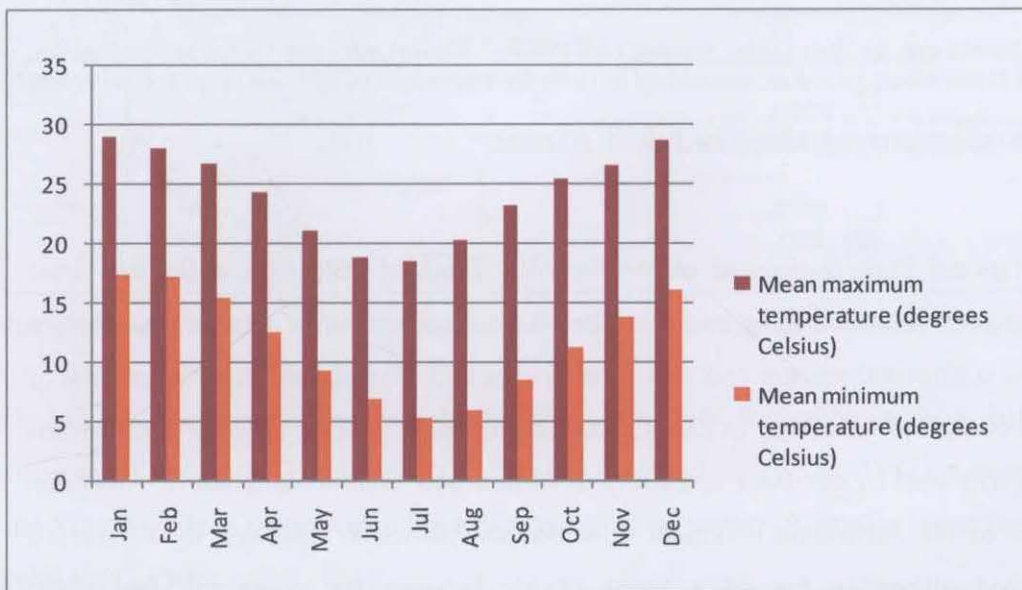
Werrikimbe National Park became part of the ‘Gondwana Rainforests of Australia’ and was classified as a World Heritage site. Since then the National Park has been part of the Central Eastern Rainforest Reserves of Australia (CERRA), with areas of old growth wet and dry sclerophyll forests, and cool temperate, warm temperate and sub-tropical rainforests (Hunter, 2004).



Fig. 3.1. Location of Werrikimbe National Park, NSW, Australia.

### Climate

Werrikimbe National Park lies in the warm-temperate to sub-tropical climatic zone. The closest weather station recording the daily temperature and rainfall values is situated at Yarras, Mount Seaview. Mean daily maximum temperatures range from 27 to 29°C in summer and 18 to 20°C in winter. Mean daily minimum temperatures range from 16 to 17°C in summer and 5 to 7°C in winter. Very hot conditions can be experienced in the summer due to hot and dry north-westerly winds from central Australia, with the highest daily temperature recorded to date of 42°C in January 1994. During the winter months south-westerly fronts can cause very cold conditions and even the occasional snowfall in the Banda Banda Mountains with the lowest temperature recorded to date of -5.1°C in July 1970.



**Fig. 3.2a.** Average climatic data for Werrikimbe National Park (Source: Weather station at Yarras, Mount Seaview, Australian Bureau of Meteorology, recording commenced in 1949, therefore mean temperatures were calculated using data from 1949 to 2010).

([http://www.bom.gov.au/climate/averages/tables/cw\\_060085\\_All.shtml](http://www.bom.gov.au/climate/averages/tables/cw_060085_All.shtml))

The broader area of Werrikimbe National Park usually experiences a seasonally dry spring and a wet period during autumn, with an average number of 163 rain days per year. Mean monthly rainfall ranges from 174 to 242 mm in summer to 61 to 108 mm in winter. The higher regions of the Banda Banda Mountains are characterised through a relatively humid climate with an annual rainfall of up to 2136 mm (Atkinson, 1999).

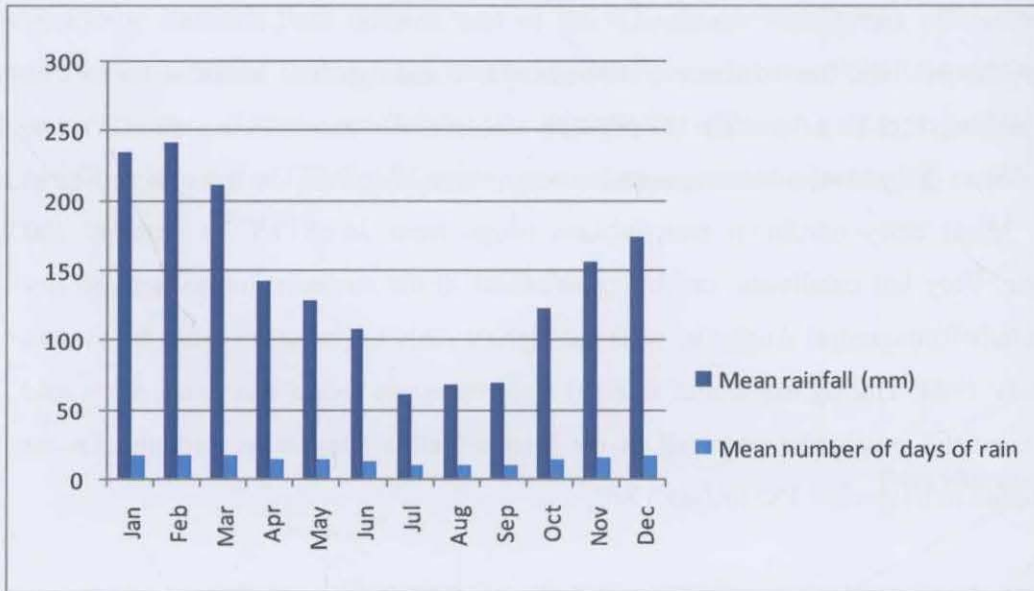


**Fig. 3.2b.** Average climatic data for Werrikimbe National Park (Source: Weather station at Yarras, Mount Seaview, Australian Bureau of Meteorology, recording commenced in 1949, therefore mean rainfall was calculated using data from 1949 to 2010).

([http://www.bom.gov.au/climate/averages/tables/cw\\_060085\\_All.shtml](http://www.bom.gov.au/climate/averages/tables/cw_060085_All.shtml))

### *Geology*

Werrikimbe National Park is situated within the New England Fold Belt along the Great Escarpment of eastern Australia (Figure 3.3). The Great Escarpment is part of the eastern Australian passive continental margin and was formed about 85 Myr ago during the creation of the new coastline of eastern Australia. In Late Cretaceous to Early Tertiary time the Tasman Sea opened by rifting followed by sea-floor spreading to form a new continental shelf of Australia. This eastern edge of the Australian continent downwarped eastwards followed by a reversed flow of rivers, and ultimately formed a Great Divide between the coast and the inland sedimentary basins (Murray Basin and the Great Artesian Basin). Since their creation the Great Divide shifted by volcanism, scarp retreat and river capture. With the development of an easterly drainage system, valleys coalesced to form the Great Escarpment facing the Tasman Sea (Branagan and Packham, 2000; Weissel and Seidl, 1997).

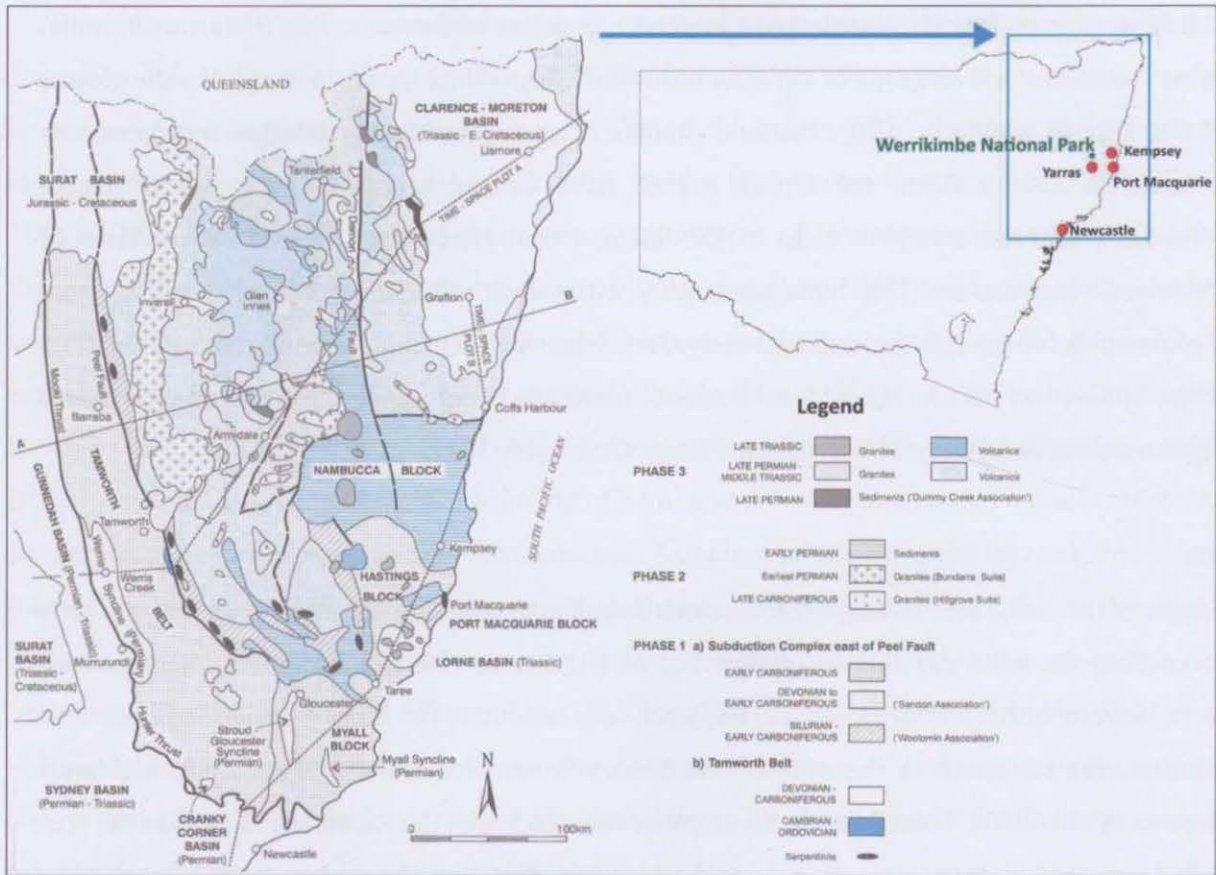


Fig. 3.3. Tectonic elements of the New England Fold Belt (after Branagan and Packham (2000)).

The Great Escarpment has retreated inland since its formation with a believed average escarpment retreat of  $2 \text{ km Myr}^{-1}$  ( $2 \text{ mm yr}^{-1}$ ) (Weissel and Seidl, 1997). Cenozoic volcanism and Miocene faults complicated the topography of the eastern Australian coastline (Ollier, 1995; Seidl et al., 1996).

The formation of the Great Escarpment separates a plateau with relatively low apparent erosion rates from a coastal belt with higher denudation rates (Seidl et al., 1996). Based on a mass balance approach the volume per unit length material eroded seaward from the escarpment was estimated to be  $41 \text{ to } 68 \text{ km}^2$  (Seidl et al., 1996).

For the main part, Werrikimbe National Park is underlain by sedimentary and metasedimentary rocks of Devonian and Carboniferous ages. Igneous rocks of Permian to Tertiary age can also be found at some sites of the park.

The area comprises of Carboniferous and Permian rocks of the Hastings Block, whose deformation occurred in the Upper Permian age. The Hastings Block (Figure 3.3) contains two major sedimentary successions, an upward succession of Devonian to Lower Carboniferous distal turbidites and middle Carboniferous marine to continental facies originated from a dacitic

or basaltic source. Werrikimbe National Park also consists of a narrow belt of Lower Permian marine limestone, and outcrops of Permian ultra-basic serpentine, Upper Permian Gundle granite and the Triassic porphyry, adamellite and rhyolite component. These geological intrusions can be found at Mount Boss, the Upper Forbes river catchment and Mount Banda Banda. Sedimentary and metamorphic rocks of Devonian, Carboniferous and Permian age consist of mudstones, siltstones and fine lithic sandstones with minor calcareous sediments and channel conglomerates. These late Devonian to early Carboniferous Boonanghi Beds occur in the Banda Banda Mountains. Lithic sandstones contain quartz, feldspar and volcanic grains whereas conglomerates contain devitrified volcanic clasts (Atkinson, 1999; Corkery, 1993).

### *Soils*

Soils of the study area belong to moderately deep Krasnozems, moderately deep Red or Grey-Brown Podzolic soils and shallow yellow Earths (Atkinson, 1999). Werrikimbe National Park has no recent history of glaciations. Research showed that The Last Glacial Maximum in Australia was restricted to the area of the Snowy Mountains and the Tasmanian highlands (Barrows et al., 2000). Therefore, the assumption was made that the formation of soils in the area studied occurred at least more than 10,000 years ago (this time frame corresponds to the last glacial period).

Soil evolution in the area is related to the formation and subsequent erosion of the Great Escarpment. Erosion of the Great Escarpment has been estimated to be in the orders of 20 mm per 1000 years. It is also postulated that continuous erosion processes of the Great Escarpment impeded the preservation of old landforms and subsequently 'very old' soils (see McKenzie et al. 2004).

#### **3.1.2 Sampling along toposequences, a sampling scheme to investigate pedogenesis quantitatively**

At Werrikimbe National Park, sampling sites were chosen in areas with minimal disturbance by human activities. The land management history of the park was consulted with the help of spatial data from the Department of Environment & Climate Change and in personal communication with the park ranger Andrew Marshall. Prior to the field survey areas of undisturbed old growth forest with no known history of intensive logging were identified. The sampling took place within three sites of Werrikimbe National Park: Spokes Mountain, Plateau Beech and Mount Boss. All three sites belonged to one subcatchment with an area of approximately 100 km<sup>2</sup>.

The decision was made to sample along three principal toposequences to better understand the formation of a soil profile along a hillslope (Amundson, 2004). The proposed sampling scheme is optimal for investigating soil-landscape evolution (Huggett, 1975), because soils situated along a toposequence are related to each other by the topography they are found in (Milne, 1935). The location of toposequences in the subcatchment of Werrikimbe National Park was determined by using a sampling scheme devised by Odgers et al. (2008). This sampling scheme was designed especially for quantitative soil-landscape modelling combining the concepts of catenas, random sampling and stream order (after Strahler (1957)). A so called  $k$ th order toposequence, located in a streamshed of the order  $k$ , was derived from a digital elevation model (DEM), selected along a path uphill to the top of a hill and downhill to a stream or valley bottom, starting from a random seed point in the landscape. Sampling points along the toposequences can then be determined via equal distance or equal distance in elevation. In this thesis, the equal distance was chosen to determine sampling points along the three toposequences at Spokes Mountain, Plateau Beech and Mount Boss. The location of the soil profiles in the field was obtained using GPS equipment. However, the conceptual scheme of locating sampling points had its limitations in the field, because of occasional low GPS signal reception which was caused by sporadically dense crown cover of the forest trees.

The model of Odgers et al. (2008) required a digital elevation model and a stream order grid of the study area (Figure 3.4). The digital elevation model with a resolution of  $25 \times 25$  m (Datum: MGA56) was obtained from the Department of Lands, whereas the stream order grid was created using the software ARCGIS (ESRI) and TAS (Lindsay, 2008). The created stream order grid was verified using spatial data provided by the Department of Environment and Climate Change. For the site at Spokes Mountain a third order (toposequence 'Ta'), for the site at Mount Boss a second order (toposequence 'Tb') and for the site at Plateau Beech a first order (toposequence 'Te') toposequence was chosen. Three soil profiles along each toposequence were dug to the soil-bedrock or soil-saprolite interface with soil pits varying between 50 and 105 cm in depth. A total of nine soil pits were located at the top, midslope and the base of the hillslope (Table 3.1 and Figure 3.4 to 3.7). Table 3.1 displays the location of the nine soil pits (characterized by latitude and longitude coordinates; elevation and slope data, obtained in the field).

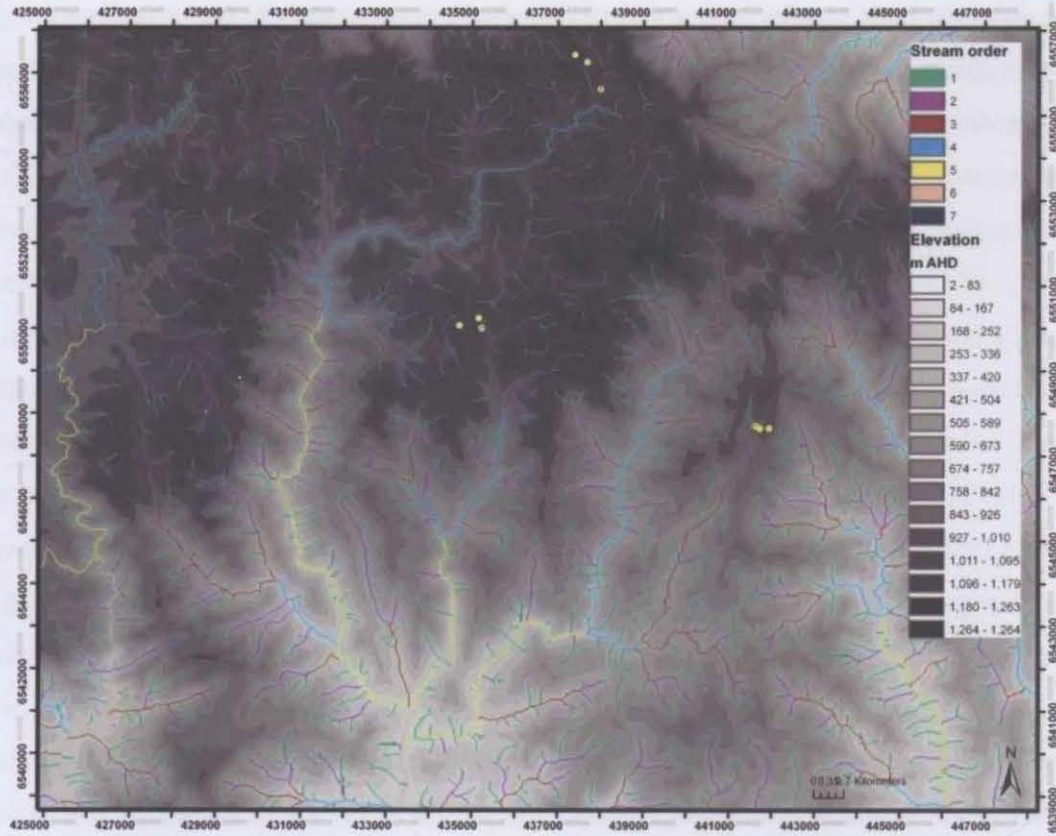


Fig. 3.4. Stream order grid of the study site chosen at Werrikimbe National Park. Sampling points along toposequences are highlighted in yellow. The graph shows that all toposequences belong to one catchment.

Tab. 3.1. Location of sampled soil profiles in the field.

Soil Profile	Position	Lat	Long	Elevation	Slope [degrees]
<b>Toposequence Spokes Mountain (Ta)</b>					
Ta16	hilltop	-31.124	152.343	1145	1
Ta12	mid-hill	-31.126	152.346	1104	20
Ta2	hill-base	-31.132	152.349	1024	22
<b>Toposequence Mount Boss (Tb)</b>					
Tb24	hilltop	-31.204	152.390	979	1
Tb12	mid-hill	-31.204	152.388	931	15
Tb6	hill-base	-31.204	152.387	902	9
<b>Toposequence Plateau Beech (Te)</b>					
Te38	hilltop	-31.182	152.315	1092	1
TeM	mid-hill	-31.180	152.319	1065	12
Te3	hill-base	-31.182	152.320	1008	2

Soil samples for the analysis of stable and labile soil properties were taken using two sampling concepts: sampling according to the layers (horizons) of the soil profile and sampling along intervals of equal soil depths (0-5 cm, 5-10 cm, 10-20 cm, 20-30 cm and 40-50 cm). For the sampling scheme per soil horizon, samples were taken in the top, middle and bottom



centimetres of each horizon in order to obtain soil material representative of the entire soil horizon depth.

The combination of these two vertical sampling schemes was chosen for optimal description and comparison of stable and labile soil properties along the toposequences sampled.



**Fig. 3.5.** Soil profiles along toposequence Spokes Mountain (Ta). From the left: Soil profile Ta16, soil profile Ta12 and soil profile Ta2.



**Fig. 3.6.** Soil profiles along toposequence Mount Boss (Tb). From the left: Soil profile Tb24, soil profile Tb12 and soil profile Tb6.



**Fig. 3.7.** Soil profiles along toposequence Plateau Beech (Te). From the left: Soil profile Te38, soil profile TeM and soil profile Te3.

### 3.1.3 Description of sampled stable and labile soil properties

For investigating soil profile evolution predominantly stable soil properties are important. However, labile soil properties were also analysed to fully describe the state of the nine soil profiles at the time of sampling.

The soil samples were analysed for their physical (wetness, bulk density, particle size distribution) and chemical properties (pH, electrical conductivity, content of organic carbon). The clay fraction of the soils was analysed further for soil minerals (mineralogy suite) using X-ray diffraction (XRD) spectroscopy.

#### *Bulk density*

Soil cores of 7.5 cm in diameter and 6 cm in height were taken from each layer of the nine soil profiles to determine the bulk density of the soils (Grossman and Reinsch, 2002). Soil samples were weighed in field-condition and also in oven-dry (105 °C) condition to determine the bulk density of the soil following equation (1):

$$\text{soil bulk density } (\rho_b) = \frac{m_{\text{fine earth}}}{V_{\text{sample}} - V_{\text{coarse fraction}}} \quad \text{equation (3.1)}$$

The soil core samples were also used to determine the water content of the soil in field condition (gravimetric and volumetric).

### *Particle Size Analysis*

The percentages of clay, silt, fine sand and coarse sand of the sampled soil material were analysed in the laboratory using the hydrometer method (Glendon and Dani, 2002). Prior to the analysis, organic matter was removed from the sub-samples applying several treatments of hydrogen peroxide ( $H_2O_2$ ). Soil texture grades were then determined by plotting the particle size data into a texture triangle.

### *Soil minerals*

The mineralogy of the soils was determined by X-ray diffraction (XRD) spectroscopy using a wavelength of 0.178897 nm (Cobalt alpha). For XRD analysis clay samples were prepared as a random powder mount as well as an oriented sample mount (Moore and Reynolds, 1989). Oriented sample mounts in the form of corundum tiles were analysed after applying the following treatments:

- air-dry  $K^+$ -saturated or  $Mg^{2+}$ -saturated tiles;
- 3 different heat treatments of  $K^+$ -saturated tiles (heated to 100°C, 300°C and 550°C)
- additional saturation with glycerol of  $Mg^{2+}$ -saturated tiles

Random powder samples were used to identify aluminium and iron oxides whereas oriented sample mounts were used for the identification of clay minerals (Brindley and Brown, 1980).

### *pH*

The pH of the soil samples was measured in water and also in a 0.01 M  $CaCl_2$  solution using a pH meter and a composition of 5 g of soil to 25 ml of deionised water or  $CaCl_2$  solution (Rayment and Higginson, 1992).

### *Electrical conductivity*

The electrical conductivity of the soil samples (in units of  $mS\ m^{-1}$ ) was determined in a solution of water with a composition of 5 g of soil to 25 ml of deionised water using a EC meter (Rayment and Higginson, 1992).

### *Organic carbon*

The organic carbon content of the soil was analysed using the 'Elementar Vario MAX CNS' macro elemental analyser (Elementar Analysensysteme GmbH, Hanau, Germany). Prior to measurement samples were cleared of root material and ground to less than 53  $\mu m$ . Subsamples of 750 mg each were analysed for their organic carbon content on the 'Elementar Vario MAX

CNS'. This instrument measures the carbon content of soil via a high temperature combustion method.

**Tab. 3.2a.** Physical soil properties.

<b>Toposequence Ta – Spokes Mountain, location: Ta2 base of hill, Ta12 mid-hill, Ta16 hilltop</b>							
<b>Horizon</b>	<b>depth [cm]</b>	<b>Bulk density [g cm<sup>-3</sup>]</b>	<b>Clay [%] &lt;2 µm</b>	<b>Silt [%] 2-20 µm</b>	<b>fSand [%] 20-200 µm</b>	<b>cSand [%] 200-2000 µm</b>	<b>Texture</b>
Profile Ta16 A1	0-5	1.0	25	31	19	25	SiL
Profile Ta16 B21	5-32	1.1	26	32	19	23	SiL
Profile Ta16 B22	32-55	1.2	32	29	17	22	SiCL
Profile Ta12 A11	0-5	0.8	25	29	16	30	SiL
Profile Ta12 A12	5-25	1.0	24	33	15	28	SiL
Profile Ta12 B21	25-39	1.4	24	34	15	27	SiL
Profile Ta12 B22	39-59	1.4	28	34	13	25	SiCL
Profile Ta2 A1	0-15	1.4	19	26	23	32	SiL
Profile Ta2 B21	15-40	1.3	16	26	22	36	SiL
Profile Ta2 B22	40-50	1.5	20	28	20	32	SiL

**Tab. 3.2b.** Physical soil properties.

<b>Toposequence Tb – Mount Boss, location: Tb6 base of hill, Tb12 mid-hill, Tb24 hilltop</b>							
<b>Horizon</b>	<b>depth [cm]</b>	<b>Bulk density [g cm<sup>-3</sup>]</b>	<b>Clay [%] &lt;2 µm</b>	<b>Silt [%] 2-20 µm</b>	<b>fSand [%] 20-200 µm</b>	<b>cSand [%] 200-2000 µm</b>	<b>Texture</b>
Profile Tb24 A11	0-5	0.9	43	33	12	12	SiC
Profile Tb24 A12	5-35	0.9	45	32	12	11	SiC
Profile Tb24 B2	35-55	1.1	45	29	12	14	SiC
Profile Tb24 BC	55-100	1.4	41	29	15	15	SiC
Profile Tb12 A1	0-10	0.6	34	36	16	14	SiCL
Profile Tb12 B1	10-40	0.7	38	35	14	13	SiCL
Profile Tb12 BC	40-90	1.4	34	34	19	13	SiCL
Profile Tb6 A1	0-10	0.2	26	34	19	21	SiL
Profile Tb6 B2	10-40	0.6	25	36	19	20	SiL
Profile Tb6 BC	40-62	0.6	25	42	18	15	SiL

**Tab. 3.2c.** Physical soil properties.

<b>Toposequence Te – Plateau Beech, location: Te3 base of hill, TeM mid-hill, Te38 hilltop</b>							
<b>Horizon</b>	<b>depth [cm]</b>	<b>Bulk density [g cm<sup>-3</sup>]</b>	<b>Clay [%] &lt;2 µm</b>	<b>Silt [%] 2-20 µm</b>	<b>fSand [%] 20-200 µm</b>	<b>cSand [%] 200-2000 µm</b>	<b>Texture</b>
Profile Te38 A1	0-20	1.1	49	25	9	17	SiC
Profile Te38 B21	20-40	1.4	51	25	9	15	SiC
Profile Te38 B22	40-70	1.4	55	18	11	16	SiC
Profile Te38 B3	70-88	1.5	31	35	13	21	SiCL
Profile TeM A1	0-14	1.0	46	28	9	17	SiC
Profile TeM B2	14-38	1.2	48	27	10	15	SiC
Profile TeM B3	38-68	1.3	50	27	10	13	SiC
Profile Te3 A1	0-10	0.7	46	27	10	17	SiC
Profile Te3 B21	10-37	1.0	48	26	10	16	SiC
Profile Te3 B22	37-78	1.1	53	24	10	13	SiC
Profile Te3 B23	78-103	1.1	53	24	9	14	SiC

Tab. 3.3a. Chemical soil properties.

Toposequence Ta – Spokes Mountain, location: Ta2 base of hill, Ta12 mid-hill, Ta16 hilltop						
Horizon	depth [cm]	Organic Carbon [%]	pH [H <sub>2</sub> O]	pH [CaCl <sub>2</sub> ]	EC [dS/m]	Texture
Profile Ta16 A1	0-5	9.82	4.99	3.90	0.054	SiL
Profile Ta16 B21	5-32	6.60	5.08	4.13	0.031	SiL
Profile Ta16 B22	32-55	3.45	5.16	4.18	0.020	SiCL
Profile Ta12 A11	0-5	14.91	4.21	3.30	0.148	SiL
Profile Ta12 A12	5-25	5.29	4.74	3.91	0.053	SiL
Profile Ta12 B21	25-39	5.06	4.92	3.96	0.039	SiL
Profile Ta12 B22	39-59	3.33	4.87	4.01	0.029	SiCL
Profile Ta2 A1	0-15	9.15	5.06	3.96	0.063	SiL
Profile Ta2 B21	15-40	7.23	5.52	4.11	0.031	SiL
Profile Ta2 B22	40-50	2.98	5.59	4.12	0.013	SiL

Tab. 3.3b. Chemical soil properties.

Toposequence Tb – Mount Boss, location: Tb6 base of hill, Tb12 mid-hill, Tb24 hilltop						
Horizon	depth [cm]	Organic Carbon [%]	pH [H <sub>2</sub> O]	pH [CaCl <sub>2</sub> ]	EC [dS/m]	Texture
Profile Tb24 A11	0-5	14.22	5.22	4.29	0.126	SiC
Profile Tb24 A12	5-35	9.95	5.03	4.25	0.088	SiC
Profile Tb24 B2	35-55	6.36	4.96	4.32	0.048	SiC
Profile Tb24 BC	55-100	2.50	5.24	4.43	0.022	SiC
Profile Tb12 A1	0-10	15.81	5.08	3.95	0.106	SiCL
Profile Tb12 B1	10-40	13.77	4.78	4.12	0.070	SiCL
Profile Tb12 BC	40-90	1.14	5.34	4.47	0.014	SiCL
Profile Tb6 A1	0-10	37.53	5.34	4.38	0.126	SiL
Profile Tb6 B2	10-40	28.61	4.97	4.26	0.122	SiL
Profile Tb6 BC	40-62	22.41	4.93	4.44	0.079	SiL

Tab. 3.3c. Chemical soil properties.

Toposequence Te – Plateau Beech, location: Te3 base of hill, TeM mid-hill, Te38 hilltop						
Horizon	depth [cm]	Organic Carbon [%]	pH [H <sub>2</sub> O]	pH [CaCl <sub>2</sub> ]	EC [dS/m]	Texture
Profile Te38 A1	0-20	5.85	5.23	4.06	0.045	SiC
Profile Te38 B21	20-40	1.95	5.11	4.13	0.015	SiC
Profile Te38 B22	40-70	1.34	5.07	4.11	0.012	SiC
Profile Te38 B3	70-88	0.75	5.07	4.14	0.010	SiCL
Profile TeM A1	0-14	6.48	5.06	3.97	0.060	SiC
Profile TeM B2	14-38	2.66	5.03	4.12	0.025	SiC
Profile TeM B3	38-68	1.61	5.15	4.16	0.013	SiC
Profile Te3 A1	0-10	9.48	4.91	4.00	0.061	SiC
Profile Te3 B21	10-37	4.63	4.97	4.10	0.033	SiC
Profile Te3 B22	37-78	1.99	5.09	4.15	0.011	SiC
Profile Te3 B23	78-103	1.59	5.07	4.21	0.012	SiC

### 3.2 Characterisation of stable and labile soil properties for Werrikimbe National Park

Relevant physical and chemical soil properties are shown in Table 3.2a to 3.3c and will be explained in summary. Detailed descriptions of soil profiles can be found in the appendix.

#### 3.2.1 General description – Toposequences, vegetation, soils

##### *Toposequences*

Figure 3.8 gives an overview of the location of the three toposequences sampled within this study area. As shown in Figure 3.7 toposequence Ta was located at Spokes Mountain, toposequence Tb was located at Mount Boss and toposequence Te was located at Plateau Beech. Each toposequence was approximately 1 km long and the sample sites were located at the top of the hill, mid-hill and the base of the hillslope.

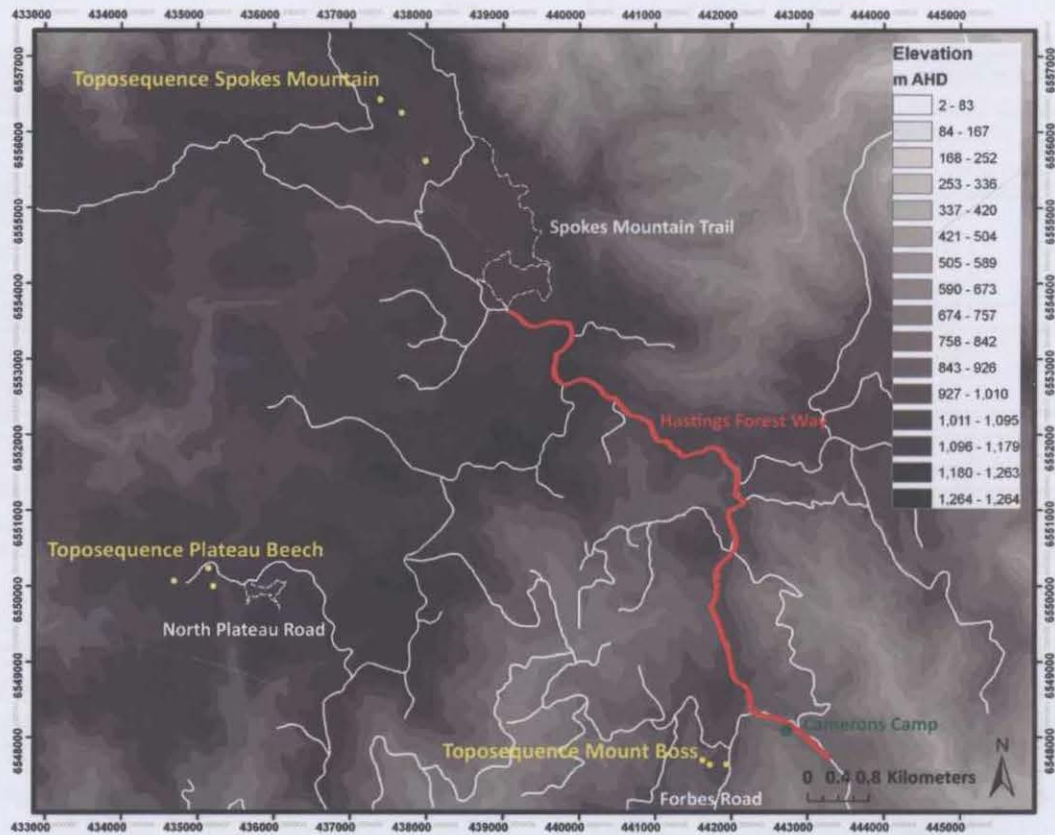


Fig. 3.8. Location of derived toposequences and sampling points at Werrikimbe National Park.

##### *Vegetation*

The vegetation at Plateau Beech consisted of cool temperate rainforest, whereas the vegetation at Mount Boss and Spokes Mountain consisted of sclerophyll forest with wet

sclerophyll forest at Mount Boss and dry sclerophyll forest at Spokes Mountain. The sclerophyll forests had a significant understory.



Fig. 3.9. From left: Vegetation at toposequence Spokes Mountain (Ta), Mount Boss (Tb) and Plateau Beech (Te).

Tree throws were observed in the upper slope area at Plateau Beech and outcrops were observed in the landscape at Spokes Mountain.

### Soils

Soil types belonged to the soil group of Kandosols and Dermosols under the Australian soil classification system (Isbell et al., 1997), or Acrisols, Luvisols and Lixisols under FAO-Unesco World Reference Base. Soils at Spokes Mountain belonged to Black and Grey Kandosols whereas soils at Plateau Beech belonged to Red and Brown Dermosols and at Mount Boss to Brown Dermosols.

Kandosols are classified as strongly weathered earths with minor changes in soil texture and are often believed to be relict soils. The B horizon of Kandosols is weakly structured with a lack of a clear or abrupt textural horizon (Isbell et al., 1997; McKenzie et al., 2004).

Dermosols also lack a clear or abrupt textural B horizon, but have moderately to strongly structured B2 horizons. They are common in high rainfall coastal zones along the great escarpment of Australia and preserved under native forest vegetation (rainforest, eucalyptus). Most Dermosols contain about 50 % of rock fragments in the B horizon. Together with small ped sizes (5-10 mm) the identification of more than weak structural B horizons is sometimes challenging resulting in classification of these soils as Mellic Kandosols (Isbell et al., 1997; McKenzie et al., 2004). The latter soil characteristics were common for the soils studied.

The depth of the soil pits ranged from 50 cm to 105 cm for all toposequences with a general increase of soil depth from the hilltop to the base of the hillslope. At Spokes Mountain the range in soil thicknesses were different compared to toposequences at Mount Boss and Plateau Beech. Spokes Mountain soil profiles were approximately 50 cm thick, whereas soil profiles at Mount Boss and Plateau Beech were much deeper at approximately 65 and 105 cm, respectively. Soil profiles Tb24 and Tb12 were characterised by a gradual boundary to the parent in the BC layer, starting from 45 cm soil depth for Tb24 and 60 cm soil depth for Tb12.

The forest floor was covered with a 3 cm thick layer of decomposed plant litter at all study sites. For each soil profile, a dark brown A-horizon between 5 and 35 cm thick was observed. The soil profile 'Tb24' from the Mount Boss toposequence and the soil profile 'Ta12' from the Spokes Mountain toposequence also had a slightly lighter darkish brown lower surface layer or A12 of approximately 20 cm thickness. All A-horizons contained a considerable amount of roots (10-50 %). Charcoal resulting from former burning events in the park was present in all surface layers from soil profiles along the toposequence at Mount Boss, and was also found in surface layers at Spokes Mountain (Figure 3.10).



**Fig. 3.10.** Charcoal inclusions at toposequence Spokes Mountain, exemplified for layer 3 of soil profile Ta16 (hilltop position). Inclusions are circled.

Subsoils were characterized through a moderately deep B2-horizon, occasionally overlain by an upper subsoil B1-horizon and underlain by a lower subsoil BC-horizon. At Mount Boss and Plateau Beech a dark reddish brown to reddish brown B-horizon was observed in each profile, whilst a dark yellowish to yellowish brown B-horizon was observed on the Spokes Mountain toposequence. Roots were found down to the soil-saprolite or soil-bedrock interface with a frequency of 2-10 %, decreasing down the profile to less than 2 %.

The upper parts of the topsoils were relatively strongly bioturbated with weak to moderate consistence, whereas subsoils were weak to moderately bioturbated with moderate to strong



consistence. Burrowing agents like earthworms, spiders, grubs and ants were observed during sampling for all toposequences. Small mammals that might have been present in the area are the Hastings River Mouse, the Yellow-bellied Glider as well as the Spotted-tailed Quoll.

### 3.2.2 Bulk density

The bulk densities of the loamy and clayey soils ranged from low to moderate, with a few very low values for the toposequence at Mount Boss (Hazelton and Murphy, 2007). Topsoils were characterized with low bulk densities of 1.0 to 1.3 g cm<sup>-3</sup>, whereas subsoils were characterized through moderate bulk densities of 1.3 to 1.5 g cm<sup>-3</sup>.

### 3.2.3 Particle Size

The topsoils were characterized by stony silty loams or silty clay loams with a moderate amount of stones. The subsoils were characterized by silty loams, silty clay loams to silty clays with a significant amount of stones. Soil profiles along toposequence Spokes Mountain were characterized by a low clay content (> 25 %) whereas soil profiles along toposequence Mount Boss were characterized by a low to moderate clay content (> 20 %, < 40 %). The clay content ranged from moderate to high (> 40 %) throughout the soil profiles at toposequence Plateau Beech. All soil layers contained a considerable amount of silt (15 to 40 %), which was inherited from the sedimentary parent material.

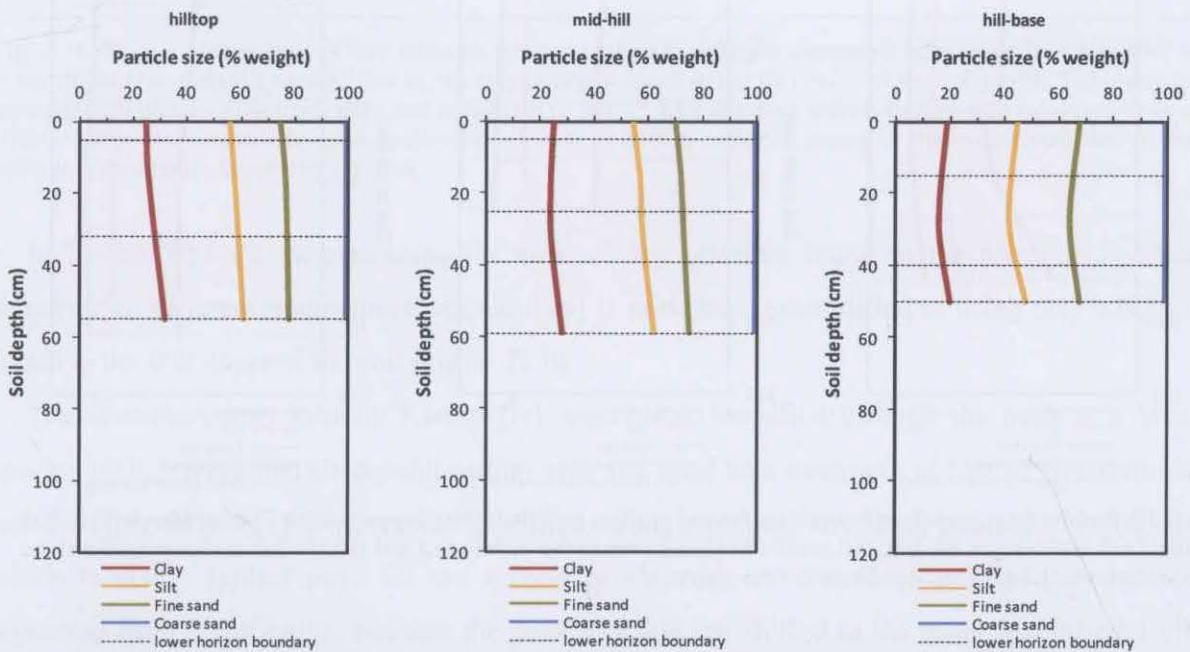


**Fig. 3.11.** Results from particle-size analysis for soil profiles sampled along toposequence Spokes Mountain (Ta). Soil profile Ta16 is shown on the left, soil profile Ta12 is shown in the middle and soil profile Ta2 is shown on the right. The lower horizon boundary is indicated in the graphs.

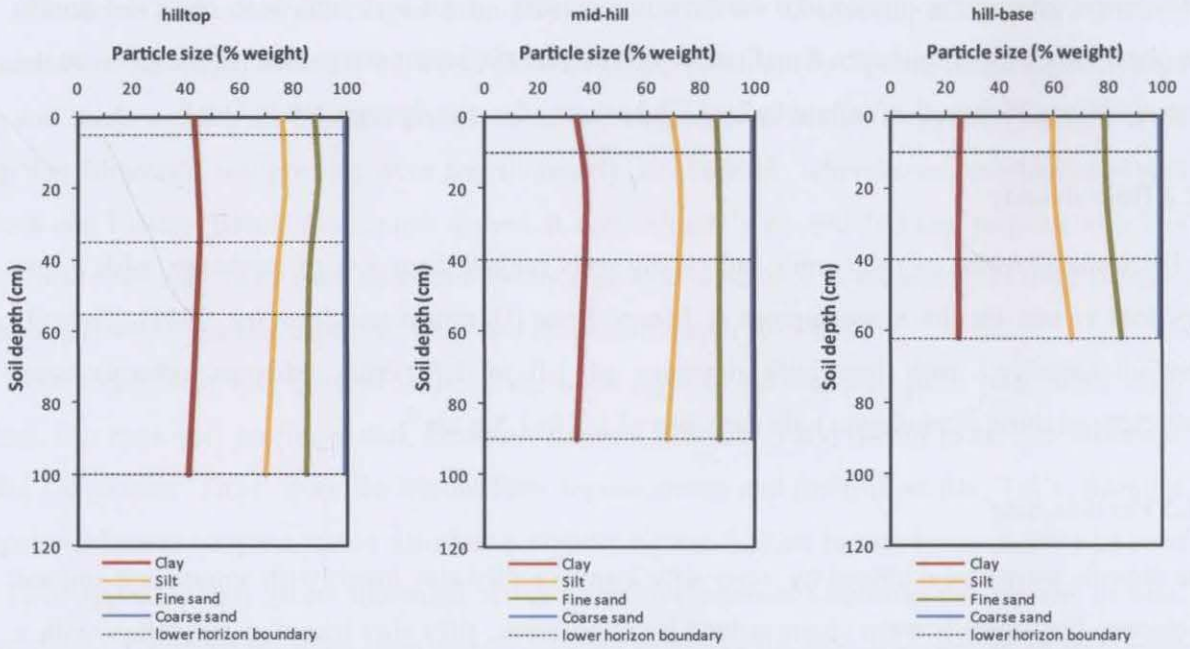


**Fig. 3.12.** Results from particle-size analysis for soil profiles sampled along toposquence Mount Boss (Tb). Soil profile Tb24 is shown on the left, soil profile Tb12 is shown in the middle and soil profile Tb6 is shown on the right. The lower horizon boundary is indicated in the graphs.

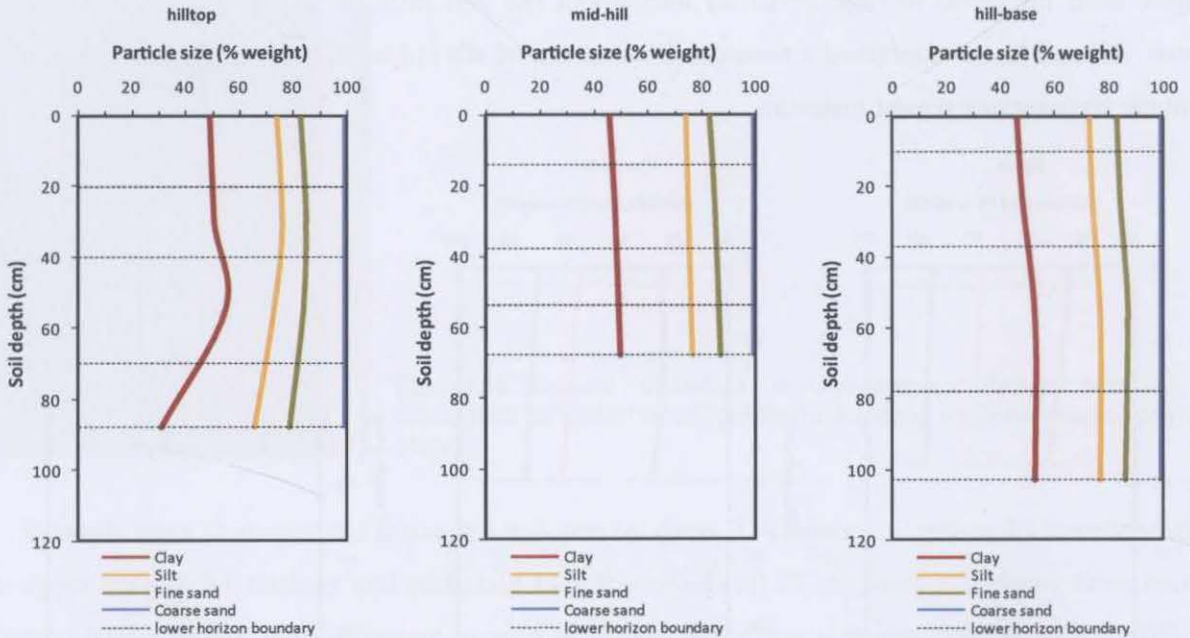


**Fig. 3.13.** Results from particle-size analysis for soil profiles sampled along toposquence Plateau Beech (Te). Soil profile Te38 is shown on the left, soil profile TeM is shown in the middle and soil profile Te3 is shown on the right. The lower horizon boundary is indicated in the graphs.

### 3.2.4 Semi-quantitative analysis of clay minerals

Soil minerals were identified by prominent peaks at different basal spacings (d-spacing in nm) on the diffractograms analysed with X-ray diffraction. Each mineral can be identified through its association with an expected or known peak at various basal spacings, which can be altered under applied treatments on ceramic tiles saturated with clay suspensions.

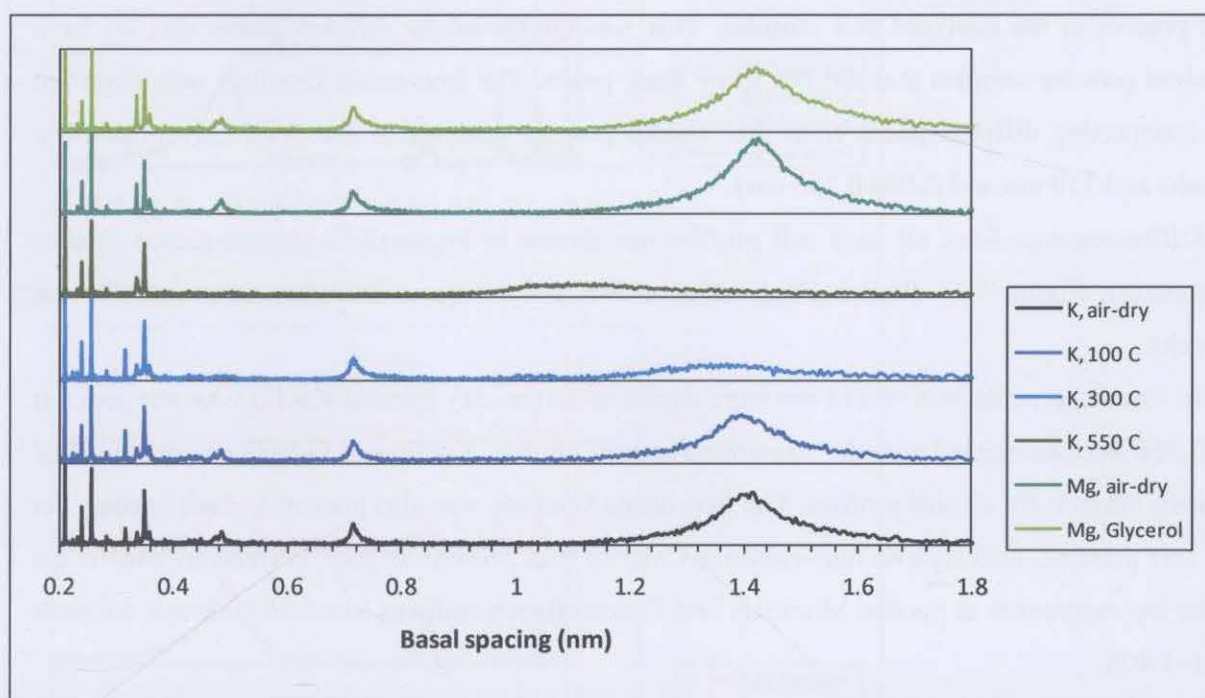


**Fig. 3.14.** Basal spacings (nm) of clay minerals when subjected to different treatments (clay saturated tiles) prior to X-ray diffraction analysis; exemplified by the clay minerals found in the B21-layer of the soil profile Ta2 along the toposequence Spokes Mountain. Clay and potassium ( $2 \text{ mol l}^{-1}$  KCl solution) saturated tiles were subjected to three different heat treatments. Clay and magnesium ( $2 \text{ mol l}^{-1}$   $\text{MgCl}_2$  solution) saturated tiles were subjected to one additional treatment of applying glycerol.

In Figure 3.14 the basal spacing (in nm) of clay minerals found in the forest soils when subjected to different treatments (ceramic tiles) is presented, exemplified in using clay minerals found in the B21-layer of the soil profile Te38.

The secondary clay mineral Kaolin (1:1 layer) was identified through the peak at a basal spacing of 0.718 nm and its decomposition after the third heat treatment at 550 °C. Interlayered non-swelling Chlorite (2:2 layer) was identified through the peak at a basal spacing of 1.408 nm, which is also a typical peak for the secondary clay mineral Vermiculite. Chlorite could be separated from Vermiculite, because the peak at 1.408 nm shifted to the basal spacing of 1.00-1.45 nm after the second heat treatment (300 °C) and then shifted to the basal spacing of around 1.00 nm after the third heat treatment (550 °C). If Vermiculite, a 2:1 secondary clay mineral,

was present in the clay suspensions all peaks would have shifted to a basal spacing of 1.00 nm after each heat treatment. The presence of Vermiculite was not expected in the extensively weathered forest soils. The aluminium-oxide Gibbsite was identified through its main peak at a basal spacing of 0.356 nm.

The prominent peaks at 0.25 nm belong to the mineral corundum. However, this is a discrepancy or artefact as corundum is the main material used to make the ceramic tiles and is not present in the analysed soil samples. This was confirmed by diffractograms derived from random powder samples that did not show these peaks. The iron-oxide Goethite was identified by interpreting diffractograms from the random powder analysis of the dried clay suspension (peaks at 0.150 nm and 0.198-0.200 nm).

Diffractograms from all nine soil profiles are shown in Figure 3.15 (toposequence Spokes Mountain), Figure 3.16 (toposequence Mount Boss) and Figure 3.17 (toposequence Plateau Beech).

In summary, peaks at  $d=0.718$  nm were attributed to the clay mineral Kaolin whereas peaks at  $d=0.356$  were associated with the aluminium-oxide Gibbsite. Kaolin and Gibbsite were identified in each horizon for all soil profiles. The iron-oxide Goethite was also present in each horizon for all soil profiles. Interlayered non-swelling Chlorite was present in each horizon in two of the three toposequences at Spokes Mountain and Plateau Beech and was identified through the peak at  $d=1.408$ .

The type of clay mineral in the soil is often representative of the degree of *in situ* weathering the soil has experienced. From the results of the semi-quantitative analysis of clay minerals the soils appear to be highly weathered. Kaolin, Gibbsite and Chlorite are all indicators of extensive soil weathering, with Chlorite being an indicator of highly weathered soils in relatively humid environments (Schaetzel and Anderson, 2005).

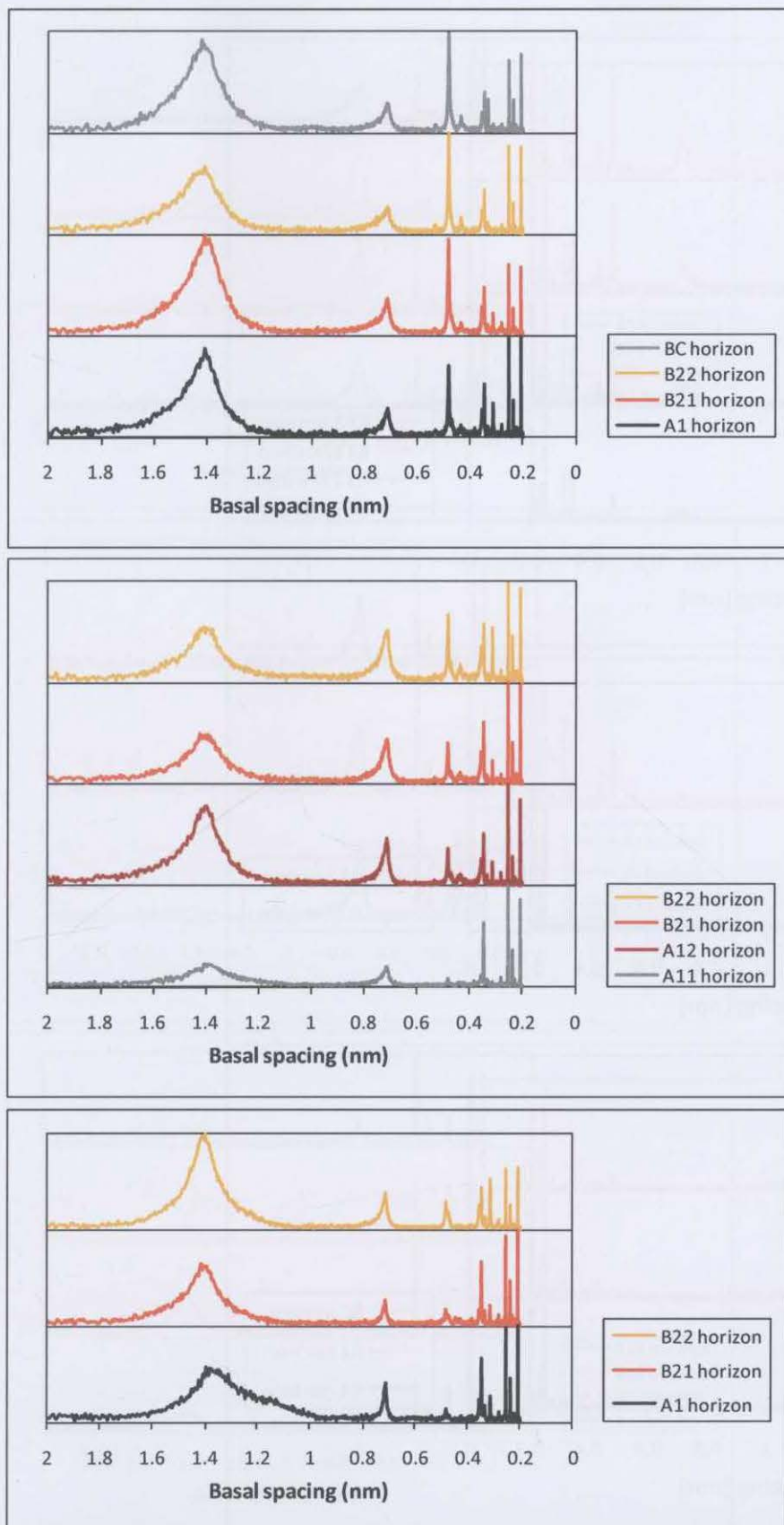


**Fig. 3.15.** Diffractograms of clay minerals determined for soil profiles along toposequence Spokes Mountain (Ta). Diffractograms are presented for each soil profile, from the hilltop (Ta16), mid-hill (Ta12) to the base of the hill (Ta2). They are displayed for each layer of the soil profiles.

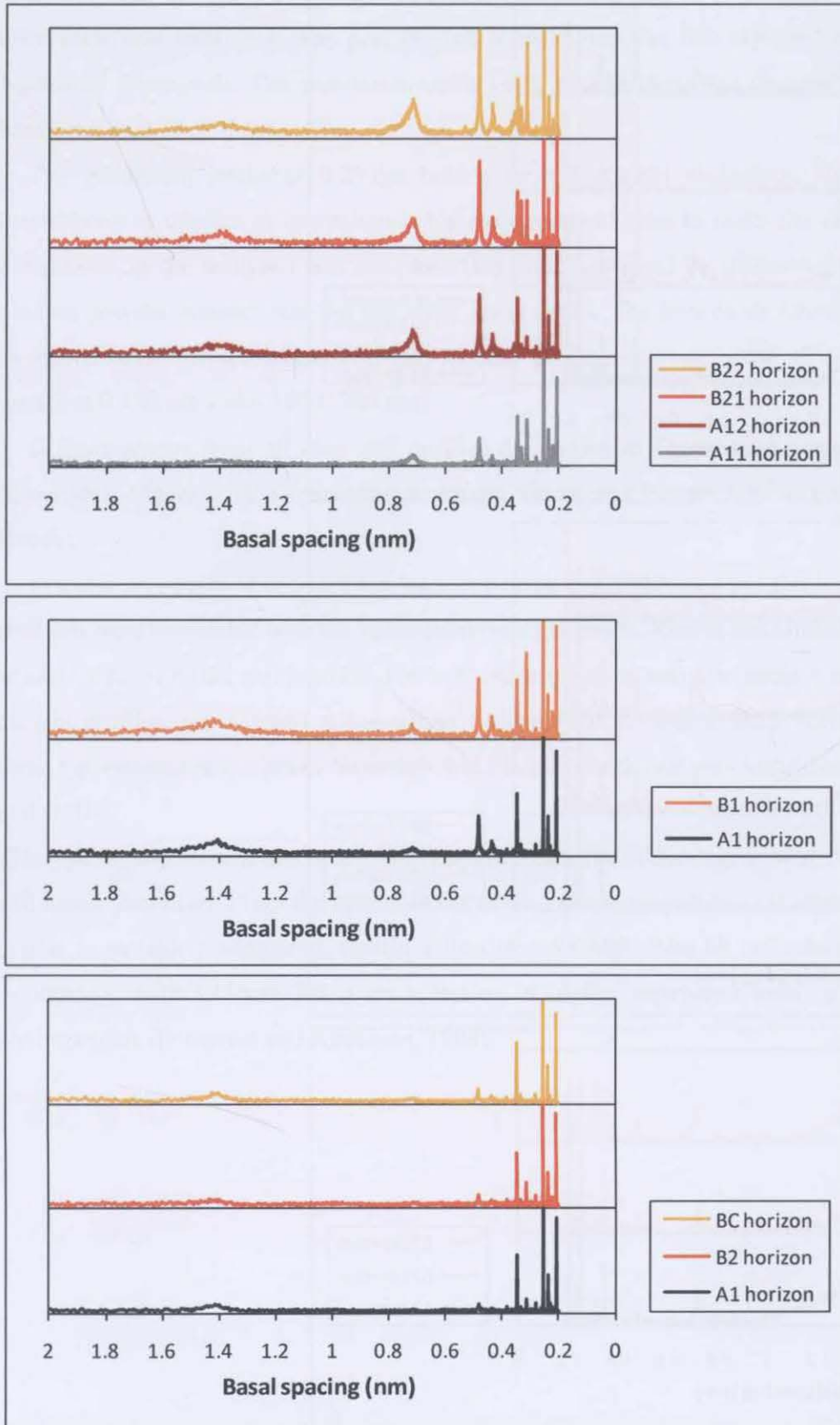


**Fig. 3.16.** Diffractograms of clay minerals determined for soil profiles along toposequence Mount Boss (Tb). Diffractograms are presented for each soil profile, from the hilltop (Tb24), mid-hill (Tb12) to the base of the hill (Tb6). They are displayed for each layer of the soil profiles.

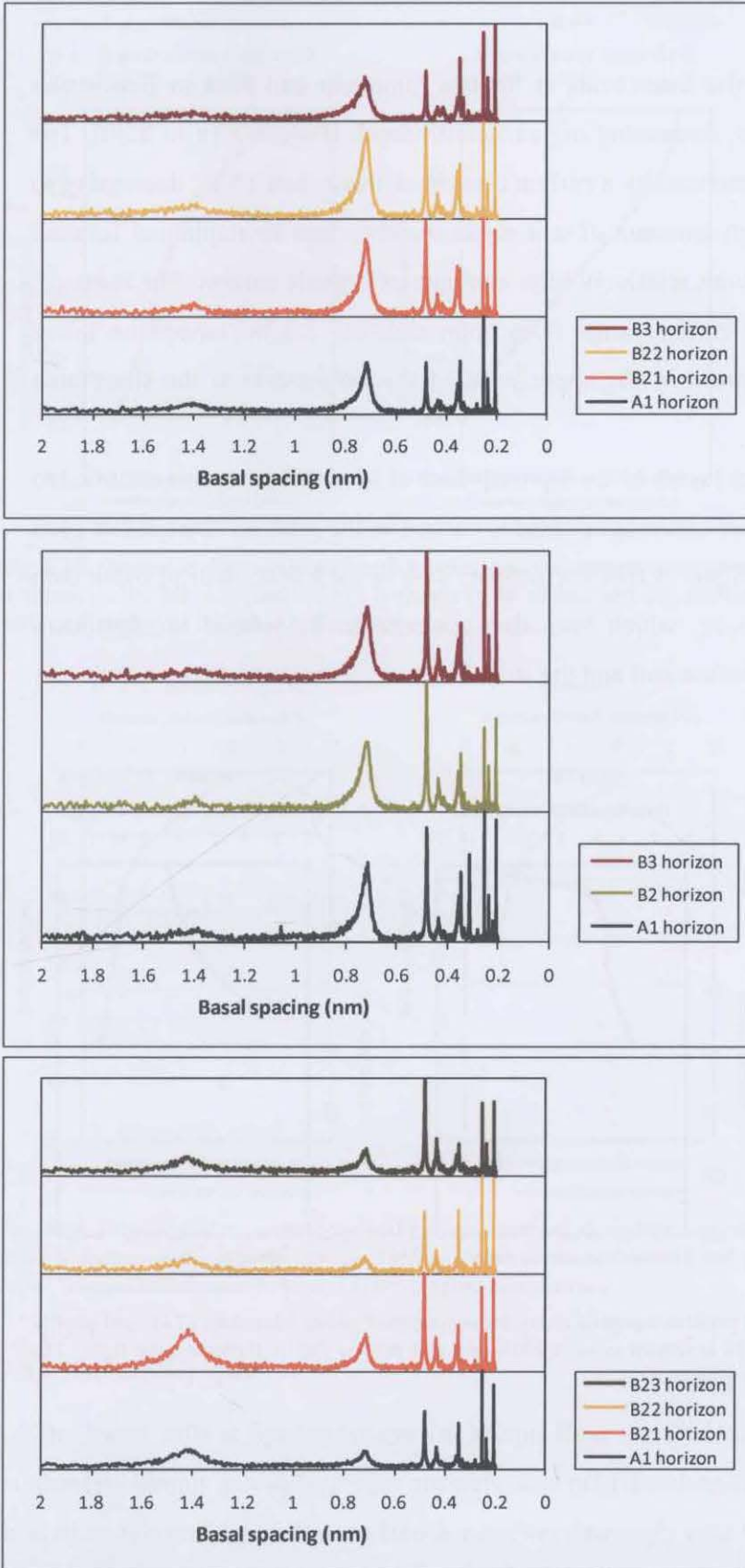


**Fig. 3.17.** Diffractograms of clay minerals determined for soil profiles along toposquence Plateau Beech (Te). Diffractograms are presented for each soil profile, from the hilltop (Te38), mid-hill (TeM) to the base of the hill (Te3). They are displayed for each layer of the soil profiles.

### 3.2.5 Organic Carbon

The organic carbon content of the forest soils at Spokes Mountain and Plateau Beech was approximately 10 % in the topsoils, decreasing to 1-3 % with depth (Figure 3.18 to 3.20). The topsoils at Mount Boss were characterized by a carbon content of more than 15 %, decreasing to 1 % with depth. The relatively high amounts of soil organic carbon can be explained because forest soils are usually associated with relatively high amounts of organic carbon. For instance, predicted contents of soil organic carbon range from approximately 3.3 % (topsoil on lower slopes) to approximately 11 % (topsoil in the upper parts of the catchment) in the study area (Johnston et al., 2003).

Charcoal was found in all surface layers of the toposequence at Mount Boss and is assumed to be the reason for significantly higher contents of organic carbon in the topsoil of the forest soils along this toposequence (refer to Figure 3.19). For profile 'Tb6' a carbon content of more than 20 % was obtained for each horizon, which was also assumed to be related to significant amounts of charcoal found in the surface soil and the subsoil.

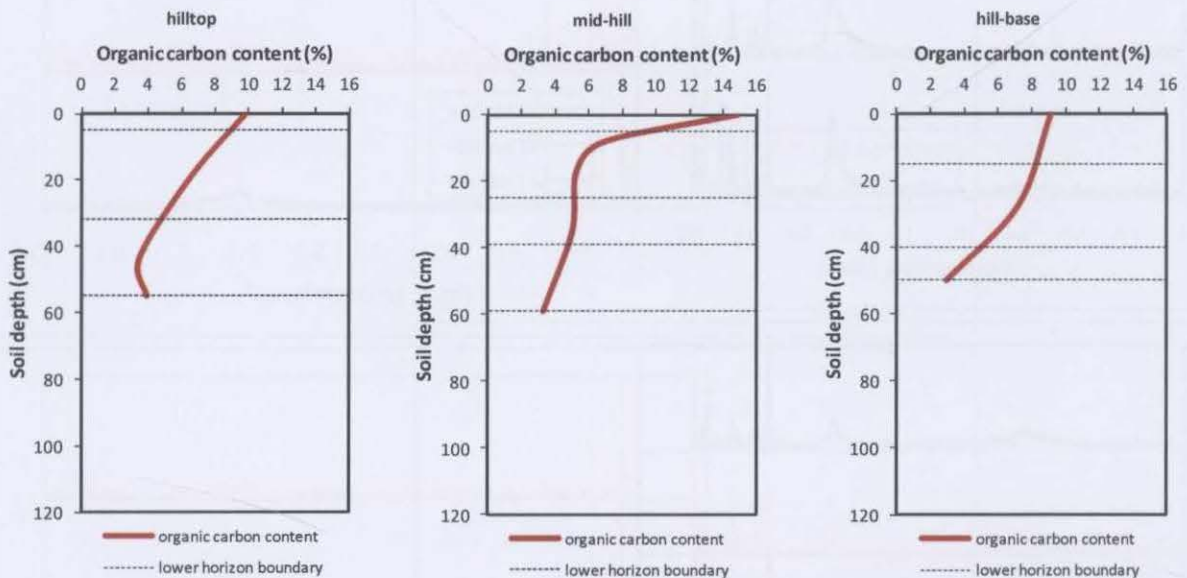


**Fig. 3.18.** Organic carbon content for soil profiles sampled along toposequence Spokes Mountain (Ta). Soil profile Ta16 is shown on the left, soil profile Ta12 is shown in the middle and soil profile Ta2 is shown on the right. The lower horizon boundary is indicated in the graphs.



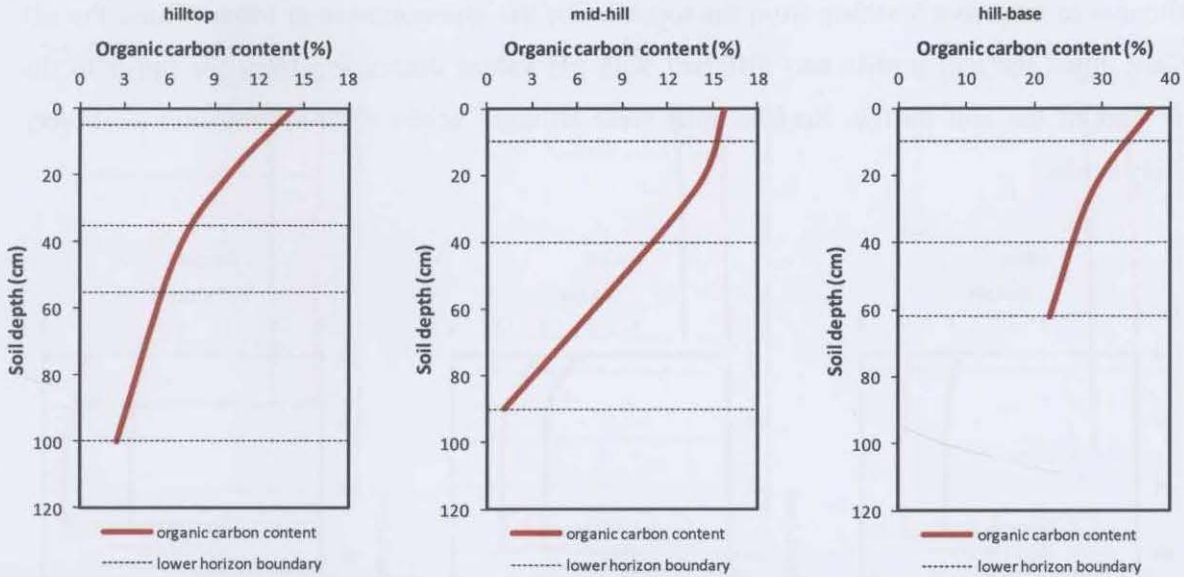


Fig. 3.19. Organic carbon content for soil profiles sampled along toposequence Mount Boss (Tb). Soil profile Tb24 is shown on the left, soil profile Tb12 is shown in the middle and soil profile Tb6 is shown on the right. The lower horizon boundary is indicated in the graphs.

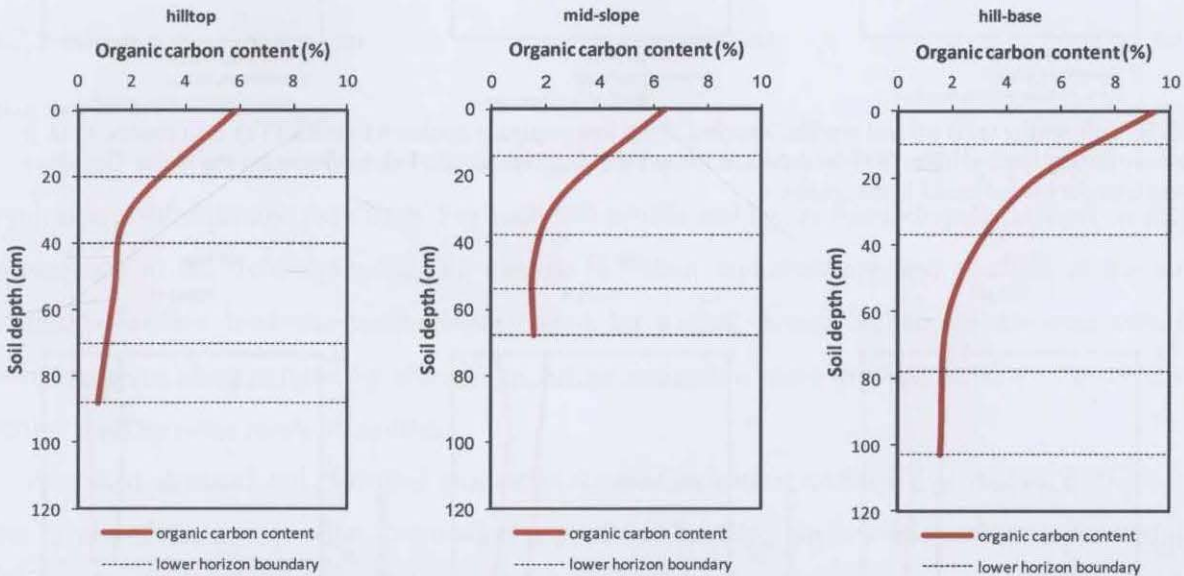
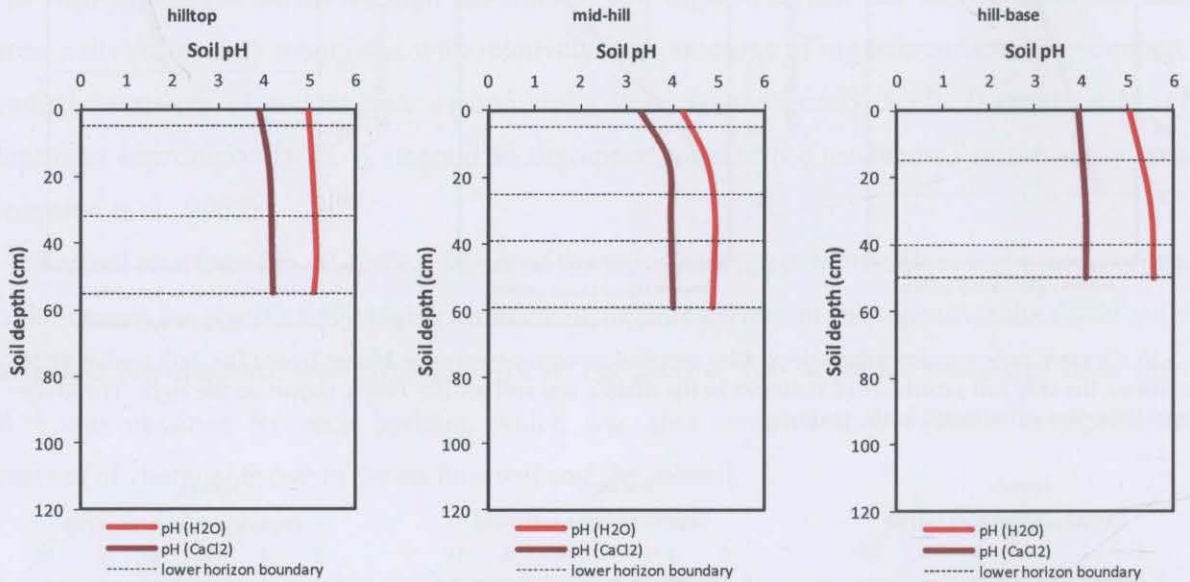


Fig. 3.20. Organic carbon content for soil profiles sampled along toposequence Spokes Mountain (Te). Soil profile Te38 is shown on the left, soil profile TeM is shown in the middle and soil profile Te3 is shown on the right. The lower horizon boundary is indicated in the graphs.

### 3.2.6 Soil acidity (pH)

The forest soils at Spokes Mountain, Mount Boss and Plateau Beech were characterized by a moderately strong, strongly to very strongly acid pH (Hazelton and Murphy, 2007). Surface soils at Spokes Mountain and Plateau Beech were very strongly acid whereas subsoils were classified as strongly acid soils. The difference in pH values between the surface soil and the subsoil followed a natural gradient where pH values increase from the upper to the lower part of the soil

profile due to intensive leaching from the topsoil. For the toposequence at Mount Boss, the pH gradient down the soil profile was different with pH values decreasing from the upper to the lower part of the soil profile. Surface soils were strongly acidic whereas subsoils were very strongly acidic.



**Fig. 3.21.** Soil acidity (pH) for soil profiles sampled along toposequence Spokes Mountain (Ta). Soil profile Ta16 is shown on the left, soil profile Ta12 is shown in the middle and soil profile Ta2 is shown on the right. The lower horizon boundary is indicated in the graphs.

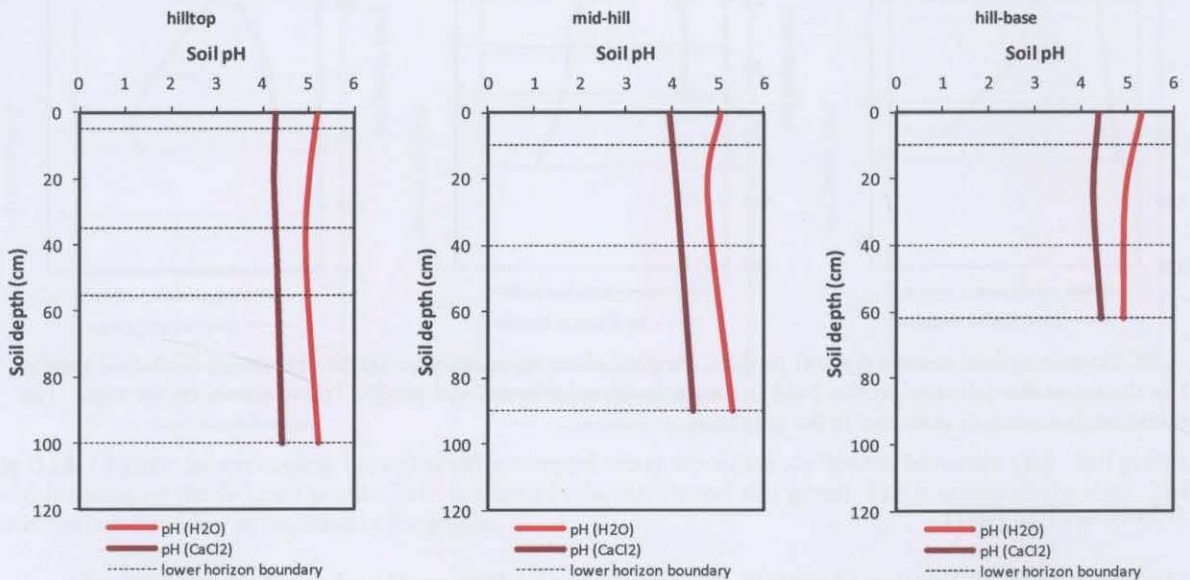


**Fig. 3.22.** Soil acidity (pH) for soil profiles sampled along toposequence Mount Boss (Tb). Soil profile Tb24 is shown on the left, soil profile Tb12 is shown in the middle and soil profile Tb6 is shown on the right. The lower horizon boundary is indicated in the graphs.

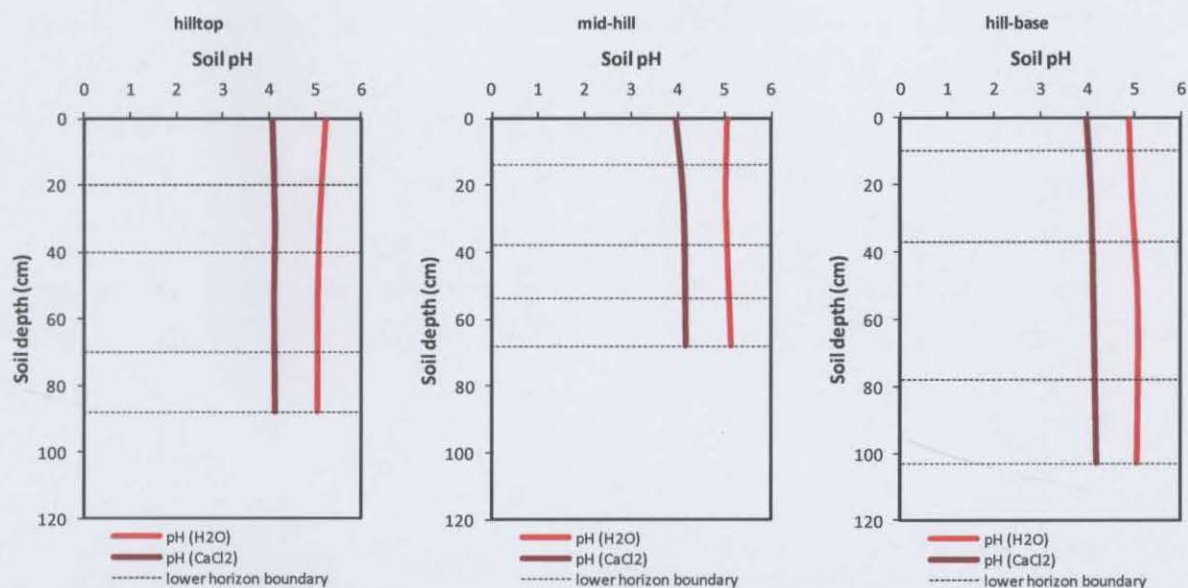


Fig. 3.23. Soil acidity (pH) for soil profiles sampled along toposquence Plateau Beech (Te). Soil profile Te38 is shown on the left, soil profile TeM is shown in the middle and soil profile Te3 is shown on the right. The lower horizon boundary is indicated in the graphs.

### 3.2.7 Summary

#### *Soil horizons*

All soil profiles studied were characterized by horizonation which implies progressed soil evolution at Werrikimbe over time. For each soil profile soil layers were identified based on their appearance in the field depending on change in colour and structure and strength of the soil material. Surface horizons were characterized by a dark brown colour palette and subsoil horizons were characterized by changes in colour towards a more greyish, yellowish or reddish brown and the occurrence of mottles.

Analysed physical and chemical properties showed an almost uniform distribution throughout the layers of the soil profiles. Particularly, particle-size distributions showed no clear texture change from A to B horizons for any of the soil profiles studied. Clay contents increased only gradually with increasing soil depth. Soil pH was generally less acidic for A horizons and increased down the soil profile, whereas contents of soil organic carbon were relatively high in the surface horizons and decreased with increasing soil depth to less than 2%. In particular, the surface soils of toposquence Spokes Mountain and Plateau Beech were characterized by about 10% of soil organic carbon, whereas contents of soil organic carbon at toposquence Mount Boss exceeded 15% in the surface soils. The soil profile in hill-base position of toposquence Mount Boss was characterized by the highest amount of soil organic carbon throughout the soil profile, with amounts of approximately 40% in the surface soil. The increased amounts of soil

organic carbon along toposquence Mount Boss reflected the occurrence of charcoal, remaining from former burning events.

Acidic soil pH is the product of leaching of exchangeable cations from soil; a process that can be accelerated in environments with high rainfall like Werrikimbe National Park and that is not unusual for forest soils with high amounts of soil organic carbon. Various acids are formed during the decomposition of this organic material. High soil organic carbon contents result from the abundance of litter available for decomposition at the forest soils and are also connected to the presence of charcoal in most soil profiles due to former burning events.

### *Pedogenesis*

Based on the glacial history of Werrikimbe, it can be assumed that soils formed long before Holocene times. Reflecting back on results from the semi-quantitative analysis of clay minerals, soils appeared to be highly weathered. The identified clay minerals Kaolin, Gibbsite and Chlorite are all indicators of extensive soil weathering.

## Chapter 4 *In situ* Terrestrial Cosmogenic Nuclides

Sophisticated laboratory techniques that can be used to quantify processes of soil formation *in situ* over tens of thousands of years have become available. In this chapter, *in situ* terrestrial cosmogenic nuclides will be applied to derive the rate of soil production for the study sites chosen, in Werrikimbe National Park, and subsequently to investigate the processes of weathering of parent materials to soil. Calculated rates of soil production will also be explored and discussed in relation to other publications.

### 4.1 Principles of using *in situ* TCN to investigate pedogenesis

Recently, terrestrial cosmogenic radionuclides (TCN) have become an important tool to determine the rates of soil production. Prior to the application of TCN in Earth sciences, meteoric cosmogenic nuclides (MCN) were applied to investigate the evolution of Earth materials. MCN are produced in the atmosphere, reaching the Earth's surface via precipitation. Their production flux is up to 1000 times larger than the production rate of *in situ* radionuclides. However, the distribution of atmospheric production rates of meteoric  $^{10}\text{Be}$  is not well constrained (von Blanckenburg, 2006).

#### 4.1.1 Principles of TCN production in Earth materials

TCN are produced *in situ* via the interaction of secondary cosmic rays with Earth materials. Secondary cosmic rays consist of charged particles, mainly protons, neutrons and muons that perform a nuclear reaction with the atoms of the target material and ultimately produce cosmogenic nuclides via spallation and negative muon capture. TCN accumulate preferentially in certain target materials over time. Their production in atoms  $\text{g-mineral}^{-1} \text{ year}^{-1}$  occurs in the uppermost metres of the Earth's surface and decreases exponentially with depth (Bierman and Nichols, 2004). Subsequently, concentrations of TCN reflect the near surface residence time of Earth materials and high concentrations of TCN in Earth materials imply longer exposure to cosmic rays.

The production rate of TCN in Earth materials is dependent on the characteristics of the site studied, such as altitude, latitude, rock chemistry and density, geometry, shielding by slope and sediment or soil overburden as well as the flux of cosmic rays (Gosse and Phillips, 2001). Beryllium-10 ( $^{10}\text{Be}$ ) has mainly been used for quantifying landscape evolution in TCN research. This is due to the relatively well known production rate of  $^{10}\text{Be}$  at sea level and high latitude

(>60°) (Gosse and Phillips, 2001) and its non-existence in rocks prior to its emergence into the cosmic ray field (von Blanckenburg, 2006). The annual production rate of  $^{10}\text{Be}$  was measured using quartz grains, sampled from glacially polished rocks with no shielding and of known age in the Sierra Nevada Mountain ranges by Nishiizumi et al. (1989). The production rate of  $^{10}\text{Be}$  was estimated as an average rate of  $6.03 \text{ atoms g}^{-1} \text{ yr}^{-1}$ . Stone (2000) revised the calculated production rates to  $5.1 \pm 0.3 \text{ atoms g}^{-1} \text{ yr}^{-1}$  for  $^{10}\text{Be}$  at sea level and high latitude after incorporating recent knowledge about nuclide and muon capture production.

#### *Definitions*

**Muon, slow negative:** Nuclear particles of short lifetime ( $1 \times 10^{-6} \text{ s}$  at rest) and a mass 207 times that of an electron. The probability of their capture by atoms is low; hence the production rate of cosmogenic nuclides by slow negative muons is low. Once a muon is captured by the shell of an atom, it can react with the nucleus to produce a cosmogenic nuclide. The attenuation depth is a few metres.

**Muons, fast:** Fast muons are both negative and positive muons of high (GeV) energy which, when slowed down, emit  $\gamma$ -rays that cause photo-disintegration reactions in nuclei, thereby leading to the release of neutrons of sufficient energy to produce cosmogenic nuclides by spallation. Their attenuation length is of the order of a few  $10^1 \text{ m}$ . Muonic production dominates at depths  $> 3 \text{ m}$ .

**Nucleons:** Secondary cosmic rays consisting mainly of neutrons and protons whose flux rapidly attenuates when interacting with solids.

**Production rate:** Rate at which cosmogenic nuclides are produced in a given mass of chemically defined target material in a given time (units:  $\text{atoms g-mineral}^{-1} \text{ yr}^{-1}$ ).

**Spallation:** Nuclear reaction in which a nucleon of several MeV energy interacts with a target nucleus to release clusters of protons and neutrons, resulting in the production of a different nuclide without fission of the nucleus and without necessarily capturing the incoming nucleon.

(source: after von Blanckenburg (2006))

$^{10}\text{Be}$  is an ideal agent for TCN dating, because it is almost non-existent in rocks prior to cosmic ray exposure due to its radioactive nature. It is produced via the nuclear spallation of oxygen ( $\text{O}_2$ ) and silica ( $\text{SiO}_2$ ) in the mineral lattice of quartz (Bierman and Nichols, 2004) and essentially immobile after its production in surface materials (Brown et al., 2003). The mineral quartz is therefore an excellent target mineral for TCN studies:

- (1) It is abundant in silicate rocks and sediments.
- (2) It is resistant to weathering and will therefore preserve accumulated  $^{10}\text{Be}$  in its crystal structure.
- (3) And it has a simple stoichiometric target chemistry that is of advantage for isolating  $^{10}\text{Be}$  in the laboratory.

All of the above characteristics of quartz result in uniform *in situ* production rates of  $^{10}\text{Be}$  within its crystal structure (von Blanckenburg, 2006). In TCN research  $^{10}\text{Be}$  is often used in conjunction with Aluminium-26 ( $^{26}\text{Al}$ ).  $^{26}\text{Al}$  is also produced in the mineral quartz via nuclear spallation. However, in this research only  $^{10}\text{Be}$  was measured, because of its relatively well known production rate, and also due to the higher analytical precision of measuring  $^{10}\text{Be}$  with AMS.

#### 4.1.2 Using TCN to estimate rates of erosion or soil production from Earth materials *in situ*

In the following a brief review on the origins and applications of using TCN to investigate the formation of landscapes is presented. The application of TCN to quantify the evolution of landscapes became possible 20 years ago with the development of Accelerator Mass Spectrometry (AMS) in the late 1980s (Elmore and Phillips, 1987). With AMS  $^{10}\text{Be}$  concentrations as low as  $10^6$  atoms g-mineral<sup>-1</sup> can be detected.

##### Definitions

Accelerator Mass Spectrometer (AMS): Mass-sensitive analysing system that accelerates ions to MeV energy. This technique is necessary to measure the extremely small number of rare cosmogenic nuclide relative to a stable reference isotope that is present in known amounts in the target sample material (i.e.  $^{10}\text{Be}/^9\text{Be}$ ).

##### Terms often used in publications on terrestrial cosmogenic nuclides:

Denudation rate: The total rate of removal of mass from, and in depths near the Earth's surface. It is the combined effect of physical (erosion rate) and chemical (weathering rate) processes. Since cosmogenic nuclides accumulate as material moves towards the surface by removal of material above, they always measure the total rate (erosion and weathering), and hence the denudation rate.

Erosion rate: The rate of lowering of the Earth's surface due to mechanical processes. In the literature, it is a common inaccuracy to call cosmogenic nuclide-derived denudation rates 'erosion rates' or even 'sediment generation rates'. This terminological simplification is a valid approximation only in areas in which the weathering rate is negligible when compared to the (physical) erosion rate.

Weathering rate: Partial dissolution of bedrock by surficial fluids, and removal of soluble ions in solution. The weathering rate is included in cosmogenic nuclide-derived denudation rates.

(source: after von Blanckenburg (2006))

Soil production rates: Based on conceptual ideas of calculations of 'erosion rates' (Nishiizumi et al., 1991). They are defined as the rate of conversion of bedrock to soil, predominantly affected by the mechanical disruption or physical weathering of bedrock (Heimsath et al., 1999).

A paper by Lal (1991) introduced the prospect of applying *in situ* concentrations of TCN for determining the age of landscapes and quantifying various geomorphic processes. Since then, TCN have been widely used in the field of geomorphology to investigate the rate of landscape formation (Bierman and Nichols, 2004; von Blanckenburg, 2006). TCN were applied to date fault scraps, fluvial and coastal terraces, alluvial fans, lava flows, glacial retreats and moraines to name a few. Furthermore, TCN were used to estimate rates of outcrop erosion and rates of sediment generation. These studies have also been conducted with a geomorphologic background, providing information about the total rate of landscape denudation or sediment generation from bare rock surfaces in the landscape, situated in a range of climatic regimes (i.e. polar, temperate, arid).

A compiled list of erosion rates and sediment generation rates presented here (Table 4.1), is a revised and updated version of Bierman (1994) and Bierman and Nichols (2004). Bierman (1994) summarized erosion rates derived from TCN for different rock materials (granite, limestone, sandstone) and concluded that rates ranged from 0.002 to 0.03 mm yr<sup>-1</sup> for continental to maritime climates. Here, erosion rates refer to total rates of denudation (see box definitions).

Later, Bierman and Nichols (2004) reviewed and compared outcrop erosion rates from different settings identifying trends within erosion rates in relation to different climatic patterns. Granitic surface rocks in humid regions of Australia appeared to be eroding faster (0.006 mm yr<sup>-1</sup>) than those in arid regions (0.0003 mm yr<sup>-1</sup>) (Bierman and Caffee, 2002). Nevertheless, overall measured erosion rates were relatively low. Bierman and Nichols (2004) hypothesized that low erosion rates estimated from exposed rock surfaces (and consequently very high nuclide activities) could be the result of the combination of base-level stability (of drainage basins), arid microclimate and the lack of jointing in rock surfaces. However, erosion rates of quartz-rich outcrops in Namibia showed no relation to mean annual precipitation (Bierman and Nichols, 2004). Additionally, no climatic pattern could be detected for basin-scale erosion rates in the Sierra Nevada, USA that ranged from 0.009-0.083 mm yr<sup>-1</sup> (Riebe et al., 2001). Very low erosion rates of less than 0.0003 mm yr<sup>-1</sup> were estimated from ice core data in Antarctica (Bierman, 1994). Studies conducted in arid regions resulted in the assumption that weathering of bedrock beneath a colluvial sediment cover supplied more sediment to basins when compared to erosion of exposed bedrock alone. In addition, TCN concentrations from outcrop samples were generally higher than concentrations measured from other materials. This lead to the conclusion that outcrops are the most stable elements in landscape evolution and that they are eroding relatively slowly (Bierman and Nichols, 2004).



For humid regions like the Llano Uplift in Texas it was found that outcrops ( $0.03 \text{ mm yr}^{-1}$ ) were eroding more slowly than the drainage basin as a whole (Bierman and Nichols, 2004). On the other hand, for the semi-arid environment of the Rio Puerco Basin in New Mexico, Bierman et al. (2005) determined a relatively high erosion rates of  $0.1 \text{ mm yr}^{-1}$ . High erosion rates were explained by conditions of easily erodible lithologies, sparse vegetation and monsoon dominated rainfall. Summarizing rates of outcrop erosion in Table 4.1, there appears to be no significant pattern of erosion rates velocities being dependent on different climate regimes, with most outcrop erosion rates ranging between  $0.001$  and  $0.08 \text{ mm yr}^{-1}$ .

One of the first applications of cosmogenic nuclides related to soil science is the paper by McKean et al. (1993). Rather than TCN the authors used MCN concentrations of  $^{10}\text{Be}$  in soil materials to quantify the rates of soil weathering. They calculated an average rate of soil formation of  $0.0026 \pm 0.0007 \text{ mm yr}^{-1}$ . However, the method of using MCN to estimate rates of soil weathering did not advance.

**Tab. 4.1.** A selection of published rates of sediment generation and bedrock lowering/denudation rates determined with TCN ( $^{10}\text{Be}$ ,  $^{26}\text{Al}$ ).

Reference	Landscape	Climate	Sediment generation rate	Sediment generation rate ( $\text{mm yr}^{-1}$ )	Outcrop erosion rate	Outcrop erosion rate ( $\text{mm yr}^{-1}$ )
Clapp et al., 2000	Nahal Yael, Israel	Arid	$74 \pm 16 \text{ t km}^{-2} \text{ yr}^{-1}$ (long-term)	0.062		
Clapp et al., 2002	New Mexico	Arid	$275 \pm 65 \text{ g m}^{-2} \text{ yr}^{-1}$ Bedrock erosion: $102 \pm 24 \text{ m Myr}^{-1}$	0.23 0.1		
Clapp et al., 2002	Yuma Wash, Arizona	Arid	$81 \pm 5 \text{ g m}^{-2} \text{ yr}^{-1}$	0.068	$30 \pm 2 \text{ m Myr}^{-1}$	0.030
Bierman, 1994		Continental to maritime			$2\text{-}30 \text{ m Myr}^{-1}$	0.002-0.030
Bierman and Caffee, 2002	Northern Territory, Australia	Arid to humid			$0.3\text{-}5.7 \text{ m Myr}^{-1}$	0.0003-0.006
Bierman et al., 1999	Baffin Island, Wisconsin				$1.1 \text{ m Myr}^{-1}$	0.001
Bierman et al., 2005	Rio Puerco Basin	Semi-arid			$100 \text{ m Myr}^{-1}$	0.1
Bierman, 1994	Antarctica	Polar				0.0003
Nishiizumi et al., 1991	Antarctica	Polar			$0.1\text{-}15 \text{ m Myr}^{-1}$	0.001-0.015
Cockburn et al., 2000	SW African Margin				$20 \text{ m Myr}^{-1}$	0.02
Cockburn et al., 1999	Namib desert, Namibia	Arid			$5.7 \text{ m Myr}^{-1}$	0.006
Colgan et al., 2002	South central Wisconsin					0.01-0.25
Granger et al., 2001	Diamond Mountains, California	Arid			$15\text{-}60 \text{ mm kyr}^{-1}$	0.015-0.060
Nichols et al., 2005	Chemehuevi Mountain piedmont, Mojave desert	Arid			$10\text{-}21 \text{ mm kyr}^{-1}$	0.010-0.021
Nichols et al., 2006	Alabama Hills, California	Arid			$1.4\text{-}20 \text{ m Myr}^{-1}$	0.0014-0.020
Riebe et al., 2001	Sierra Nevada, USA				$9\text{-}83 \text{ mm kyr}^{-1}$	0.009-0.083
Stroeven et al., 2002	Parkajoki, Sweden				$1.6 \text{ m Myr}^{-1}$	0.002

The paper by Lal (1991) also initiated the application of TCN in pedological studies. Heimsath et al. (1997) used the concepts discussed in Lal (1991) to establish the use of TCN to derive soil production rates (SPR). Soil production rates were defined as the rate of conversion of bedrock to soil, predominantly affected by the mechanical disruption or physical weathering of bedrock. The publication of Heimsath et al. (1997) on applying TCN in soil production studies, verified the conceptual framework of exponential decrease of soil formation with increasing soil thickness (Ahnert, 1977) with field data from the Tennessee Valley in California, USA. Hence, quantifying the rate of soil production *in situ* from parent materials became a possibility. Since then Heimsath et al. (2000, 2001a; 2006; 1997; 1999; 2001b; 2009; 2005) and also a small number of different authors have derived soil production rates using cosmogenic nuclides. Wilkinson et al. (2005b) investigated the rate of soil production from parent materials at a study site in south-eastern Australia. Small et al. (1999) applied the concept of deriving soil production rates to study rates of regolith production from bedrock in an alpine environment in Wisconsin, USA and found that regolith production was almost twice as fast under a 90 cm thick regolith mantle as on bare rock surfaces.

As discussed in section 2.4.2 of the literature review, Riebe et al. (2003, 2004a, b) applied the method of calculating soil production rates proposed by Heimsath et al. (1997) to investigate the extent of chemical weathering during soil formation for various climate regimes. Here, total production rates of soil varied between 0.02 and 0.63 mm yr<sup>-1</sup>. Dixon et al. (2009) also derived rates of soil production to study the influence of chemical weathering on total denudation rates. Here, soil production rates were assumed to be equivalent to physical rates of soil production only. They ranged between 0.012 and 0.075 mm yr<sup>-1</sup>. Soil production rates published by Riebe et al. (2003, 2004a, b) and Dixon et al. (2009) are given in Table 2.1 Part 2.

#### 4.1.3 A compilation of published TCN-derived SPR

Here, published TCN-derived soil production rates from different environmental settings are reviewed further to discuss conceptual models of soil production and their verification with field data. Therefore, only studies are compiled that investigated how soil formed over time (Heimsath et al., 2000, 2001a; Heimsath et al., 2006; Heimsath et al., 1997; Heimsath et al., 1999; Heimsath et al., 2001b; Heimsath et al., 2009; Heimsath et al., 2005; Wilkinson et al., 2005b). As presented in the literature review, two concepts of soil production have been discussed in relation to TCN-derived SPR. One concept explains soil production using a depth-dependent exponential function (Ahnert, 1977) where the formation of soil declines exponentially with increasing soil thickness. The second concept explains soil production using a humped function (Gilbert, 1877), where the

production of soil from parent materials is abundant underneath an incipient soil cover and less prominent on exposed parent materials or an already thick soil mantle.

A compilation of soil production rates from different parent materials, climatic zones and continents, including the tectonically quiet Australia, and the tectonically active North America are presented in Table 4.2. As shown, the estimated rates of soil formation ranged between 0.004 and 0.4 mm yr<sup>-1</sup>. All of the SPR's listed in Table 4.2 are derived from parent materials below soil of certain thickness as well as from outcrops to provide reference values for soil production at zero depth. The relationship between average SPR's and soil depth for each of these study sites are presented in Figure 4.1 and will be further discussed with reference to the site location.

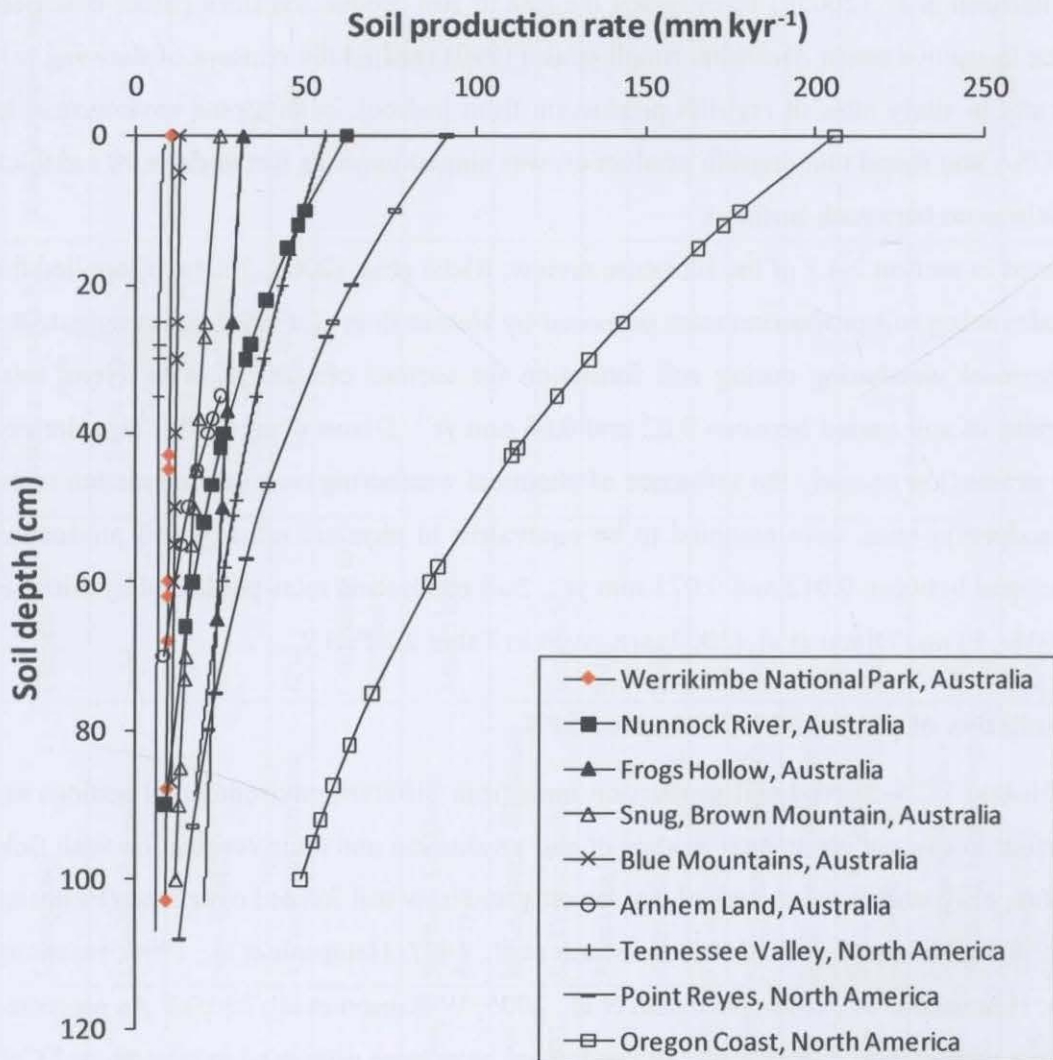


**Fig. 4.1.** Compilation of TCN-derived SPR (in mm kyr<sup>-1</sup>) for study sites in Australia and North America. SPR are plotted conventionally as in pedology, demonstrating the behaviour of a parameter down the soil profile. Calculations are made with SPR as the dependent variable. Here, the best fit for SPR ( $P_0$ ) is plotted individually for all data sets. It is shown that SPR follow an exponential decline with increasing soil thickness.

Tab. 4.2. TCN-derived SPR for study sites, in and outside, Australia.

Study sites in Australia						
Reference	Study site	Elevation	Climate	Geology	$P_0$ (mm kyr <sup>-1</sup> ) <sup>*</sup>	$b^{**}$
This study	Werrikimbe National Park, NSW	1100 m	Warm-temperate to sub-tropical Rainfall 2000 mm yr <sup>-1</sup>	Devonian, Carboniferous Permian sedimentary and metamorphic rocks	10 ±4	0.125±0.617
Heimsath et al., 2000	Bega Valley, NSW	200 m	Warm-temperate Rainfall 910 mm yr <sup>-1</sup>	Granite and granodiorite of the Bega Batholith	62±6	2.180±0.354
Heimsath et al., 2001a	Southeastern highlands, Frogs Hollow, NSW	900 m	Semi-arid Rainfall 550-750 mm yr <sup>-1</sup>	Ordovician metasediments and Devonian granites	31±11	0.419±1.034
Heimsath et al., 2006	Snug (lowland), Brown Mountain (escarpment crest), NSW	200 m	Warm-temperate Rainfall 870 mm yr <sup>-1</sup> Rainfall 690 mm yr <sup>-1</sup>	Ordovician metasediments and Devonian granites	21±12 29±6	0.511±1.080
Heimsath et al., 2009	Arnhem Land, Tin Camp Creek, NT	150 m	Tropical Seasonal rainfall (Oct. to Apr.) 1400 mm yr <sup>-1</sup>	Sandstone	75±24	3.194±0.724
Wilkinson et al., 2005	Southeastern highlands, Blue Mountains, NSW	1100 m	Warm-temperate Rainfall 900-1000 mm yr <sup>-1</sup>	Triassic sandstone	13±1	0.215±0.268
Study sites in North America						
Dixon et al., 2009	Sierra Nevada Mountains, California, USA	1186 to 2991 m	Mixed-Conifer to subalpine Rainfall 330-1200 mm yr <sup>-1</sup>	Granitic rocks		
Heimsath et al., 1997; 1999	Tennessee valley, California, USA	200 m	Semi-arid Rainfall 760 mm yr <sup>-1</sup>	Greenstone, greywacke, sandstone and chert (Jurassic-Cretaceous Franciscan assemblage)	56±11	1.305±0.825
Heimsath et al., 2001b	Oregon coast range, USA	300 m	Humid-temperate Rainfall 2000 mm yr <sup>-1</sup>	Eocene turbidite sandstone and siltstone (Tye/Flourney Formation)	268± 25	0.030±0.020
Heimsath et al., 2005	Point Reyes, California, USA	150 m	Mediterranean Rainfall 800 mm yr <sup>-1</sup>	Granitic rocks (quartz diorite, granodiorite)	91±6	1.817±0.266

<sup>\*</sup> $P_0$  is the potential physical and chemical weathering rate of parent materials at depth  $h=0$  (mm kyr<sup>-1</sup>); <sup>\*\*</sup> $b$  is the rate constant (mm<sup>-1</sup>)

### Australia: a tectonically quiet continent

The majority of publications that used TCN-derived soil production rates were located across two different climatic zones in Australia (presented in Table 4.2). Field studies were conducted on soil-mantled hillslopes in the warm-temperate climate of southeastern Australia (Heimsath, 2006; Heimsath et al., 2000, 2001a; Heimsath et al., 2006; Wilkinson et al., 2005b) and the monsoonal tropical climate of northern Australia (Heimsath et al., 2009).

Studies by Heimsath et al. (2000, 2001a; 2006) were situated along transects of the Great Escarpment of south-eastern Australia incorporating sites in the coastal lowlands, at the base of the escarpment and in the highland areas (900 m). These field studies confirmed that along the passive margin of south-eastern Australia, erosion rates decrease from the escarpment base to the escarpment crest (Heimsath et al., 2006; Seidl et al., 1996) and soil production rates decrease exponentially with increasing soil thickness at all study sites. In the studied environments soil production appeared to be influenced by burrowing animals and soil creep (Heimsath et al., 2002). Potential weathering rates of the granitic parent materials at the lowland site of Snug and the escarpment base site of Nunnock River were characterized by  $P_0$  values of  $21 \pm 12 \text{ mm kyr}^{-1}$  and  $61 \pm 6 \text{ mm kyr}^{-1}$ , whereas the highland sites of Frogs Hollow and Brown Mountain were defined by  $P_0$  values of  $31 \pm 11 \text{ mm kyr}^{-1}$  and  $29 \pm 6 \text{ mm kyr}^{-1}$ . Comparing derived SPR for the lowland and highland sites showed no apparent variations of SPR in orders of magnitude (Figure 4.2).

Wilkinson et al. (2005a) explored production of shallow soils over sandstone parent materials in the Blue Mountains, a study site also located in the southeastern Australian highlands. With a  $P_0$  value of  $13 \pm 1 \text{ mm kyr}^{-1}$ , potential weathering rates of sandstone were lower than at sites near the Bega Valley. At the Blue Mountain site, soil formation seemed to depend on a finite depth of soil with a peak in soil production of  $18 \text{ mm kyr}^{-1}$  at 10 cm of soil cover. Therefore, it was assumed that soil production potentially followed a humped function (Gilbert, 1877) in this soil-mantled, bedrock dominated environment.

At the study site of Heimsath et al. (2009) in tropical northern Australia, Arnhem Land, soil production was suggested to follow a humped soil production function because of observed maximum SPR under an intermediate soil thickness. Furthermore, the soil landscape was characterized by outcrops and soil thicknesses greater than the maximum in soil production. Soil thickness less than the peak in soil production could not be observed. These characteristic are all indicators for a landscape potentially derived from humped soil production (Dietrich et al., 1995).

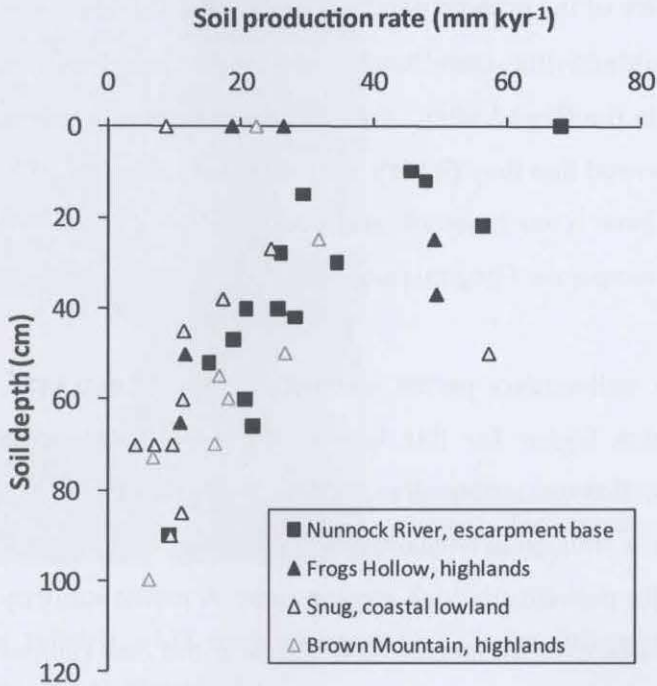


Fig. 4.2. Rates of soil production for field sites from Heimsath et al. (2000; 2001b; 2006) near the Bega Valley in south-eastern Australia. SPR for lowland and highland sites are very similar, they do not vary much in orders of magnitude.

In Arnhem Land, soil production was greatest underneath 35 cm of soil with a value of  $20 \text{ mm kyr}^{-1}$ . However, soil production clearly followed an exponential decline with increasing soil thickness with a  $P_0$  value of  $75 \pm 23 \text{ mm kyr}^{-1}$ , if only samples from sedimentary parent materials were considered. Soil production in Arnhem Land was influenced by tree throw resulting from cyclonic activities and by bushfires. The tropical climate of Arnhem Land is significantly different to the climates of field sites located in the southeastern Australian highlands, but nevertheless soil production occurred in similar ways (Heimsath et al., 2009).

Soil production rates of the Australian landscapes are compared with rates from study sites outside Australia.

#### North America: a tectonically active continent

In North America, TCN-derived SPR were estimated for three different climatic zones (Table 4.2). Heimsath et al. (1997; 1999; 2001b; 2005) conducted field studies in the semi-arid and the Mediterranean climate of California, USA, and the humid-temperate climate of Oregon, USA. For all field sites exponentially decreasing soil production rates with increasing soil thickness were found. At the field site in the Tennessee Valley, California, the potential weathering rate of the sedimentary parent material was characterized by a  $P_0$  value of  $56 \pm 11 \text{ mm kyr}^{-1}$ , and at Point

Reyes, California, the potential weathering rate of the granitic parent material ( $P_0$ ) had a value of  $91 \pm 5 \text{ mm kyr}^{-1}$ . At both of these sites, biogenic activities contributed to the production of soil; an observation that is similar to the field sites in the Bega Valley, Australia. Comparing  $P_0$  values calculated for the study sites in California showed that they fit very well within the range of SPR determined for Australian environments. There is no order of magnitude difference between these rates. The data set from the humid-temperate Oregon coast range, however, does not display the same range of SPR values.

With a potential weathering rate of the sedimentary parent material of  $268 \pm 25 \text{ mm kyr}^{-1}$ , TCN-derived soil production rates are much higher for this humid-temperate environment compared to the previously presented SPR. But one order of magnitude higher SPR are not necessarily unusual. The Oregon coast range is situated in a tectonically very active environment where landslides and periodic fires account for periodically high erosion rates. A recent study by DiBiase et al. (2010) investigated erosion rates over millennial time scales in the San Gabriel Mountains, California, tectonically a very similar environment to the Oregon Coast range. The San Gabriel Mountains are also located in a highly tectonically active area and have experienced high erosion rates over the years ( $35\text{-}1100 \text{ mm kyr}^{-1}$ ). Potentially, SPR would also be one order of magnitude higher in this environment.

The compiled TCN-derived SPR data will be used further to investigate the effect of geographical variations (climate, parent materials, and tectonic settings) on the production of soil from parent materials. In addition, a comparison of TCN-derived SPR with soil formation rates derived by other methods will be included. This will be addressed and discussed in relation to the SPR data from Werrikimbe National Park.

#### 4.2 Sample preparations for analysis of *in situ* concentrations of $^{10}\text{Be}$

TCN preparations and TCN laboratory analysis were carried out in collaboration with Dr David Fink and Dr Charles Mifsud at the Australian National Tandem for Applied RESearch, Accelerator Mass Spectrometry (ANTARES AMS) facility at The Australian Nuclear Science and Technology Organisation (ANSTO) at Lucas Heights in Sydney, Australia (see Figure 4.3), following procedures described in Child et al. (2000) and Fink and Smith (2007). This research was funded by the Australian Institute of Nuclear Science and Engineering (Award No. AINGRA08133).





**Fig. 4.3.** The ANTARES AMS facility at Lucas Heights in Sydney, Australia. Photograph shows the 10MV tandem accelerator (Source: ANSTO Sydney).

For reliable AMS measurements of  $^{10}\text{Be}$  the following needs to be achieved in the laboratory (Child et al., 2000):

- The final target material that is analysed on the accelerator must be free of contamination by elements such as iron (Fe), calcium (Ca), titanium (Ti) and in particular boron ( $^{10}\text{B}$ ), which is an isobaric interference for  $^{10}\text{Be}$  (both isotopes have the same mass) and must be kept to concentrations lower than 1 ppm.
- The quartz must be cleaned of atmospheric  $^{10}\text{Be}$ .
- The final target sample must be transformed into a suitable form for AMS analysis such as Berylliumoxide ( $\text{BeO}$ ).

As described in Chapter 3, in the field, soil pits were dug to the soil-parent material interface. Samples of soil parent material were then collected from the soil-bedrock/-saprolite interface for TCN analysis. The collected samples of approximately 1500 g of soil parent material were crushed to less than 2 cm using a jaw crusher, ground with the help of a disc pulveriser and sieved to less than 500  $\mu\text{m}$ . (Figure 4.4) A minimum of 500 to 600 g of the 212 to 500  $\mu\text{m}$  fraction was used for further treatment in the laboratory.

To the 212-500  $\mu\text{m}$  fraction, a chemical pre-treatment was applied to separate the target mineral quartz from external contaminations in the sample (minerals other than quartz, such as feldspar). The sample was subjected to repeated cycles of washes with water to remove silty materials. To completely eliminate 'silty precipitations', this was followed by repeated acid washings with hydrochloric acid (HCl) and nitric acid ( $\text{HNO}_3$ ) (3:1 ratio), followed by washings

with a 50 % sodium hydroxide (NaOH) solution for neutralisation and to disperse external contaminants.



**Fig. 4.4.** Pre-treatment of soil parent materials. The photo on the left hand side shows a jaw crusher to crush rock samples to less than 2 cm and the photo on the right hand side shows a disc pulveriser to ground the 2 cm fraction to less than 500  $\mu\text{m}$  (Source: ANSTO Sydney).

Prior to the treatment of quartz minerals with hydrofluoric acid (HF) to etch away the outside of the quartz rind and to ensure complete elimination of feldspars, the samples were treated with phosphoric acid ( $\text{H}_3\text{PO}_4$ ) and NaOH. This involved heating the samples up to 6 times in  $\text{H}_3\text{PO}_4$  solution to 250°C until they formed a white gel (caused by external contaminations), demonstrated in Figure 4.5, several washes with water to remove contaminants and heating of the washed samples in NaOH solution for neutralisation and to disperse external contaminants.



**Fig. 4.5.** Treatment with  $\text{H}_3\text{PO}_4$ . The photo on the left hand side shows the point of white gel-formation resulting from external contaminants in the sample (Source: ANSTO Sydney).

The chemical pre-treatment resulted in approximately 30 to 90 g of purified quartz. The cleaned quartz crystals were then dissolved in HF at low heat (around 60°C). The resulting digestant was fumed off at 150°C with 5 ml of perchloric acid to remove dissolved silica and fluorides.

To extract  $^{10}\text{Be}$  and separate the isotope from unwanted elements and any possible isobars and non *in situ* cosmogenic isotopes (atmospheric  $^{10}\text{Be}$ ), further laboratory treatments were applied. This involved spiking the sample with the Be-carrier (around 0.3 mg), which had a known concentration of  $^9\text{Be}$ , and performing extraction chemistry, ion chromatography, pH-specific precipitation and oxidization to BeO, the suitable form of Be for AMS analysis (see flowchart, Figure 4.6). BeO was then loaded onto cathodes for analysis on the accelerator. In addition, also Niobium (Nb) powder was added to the cathode, because it improves the ion source operation during AMS analysis. As described earlier, AMS is a very mass-sensitive, precise technique, that detects concentrations of radioisotope atoms as low as  $10^6$  per g of quartz for  $^{10}\text{Be}$ .

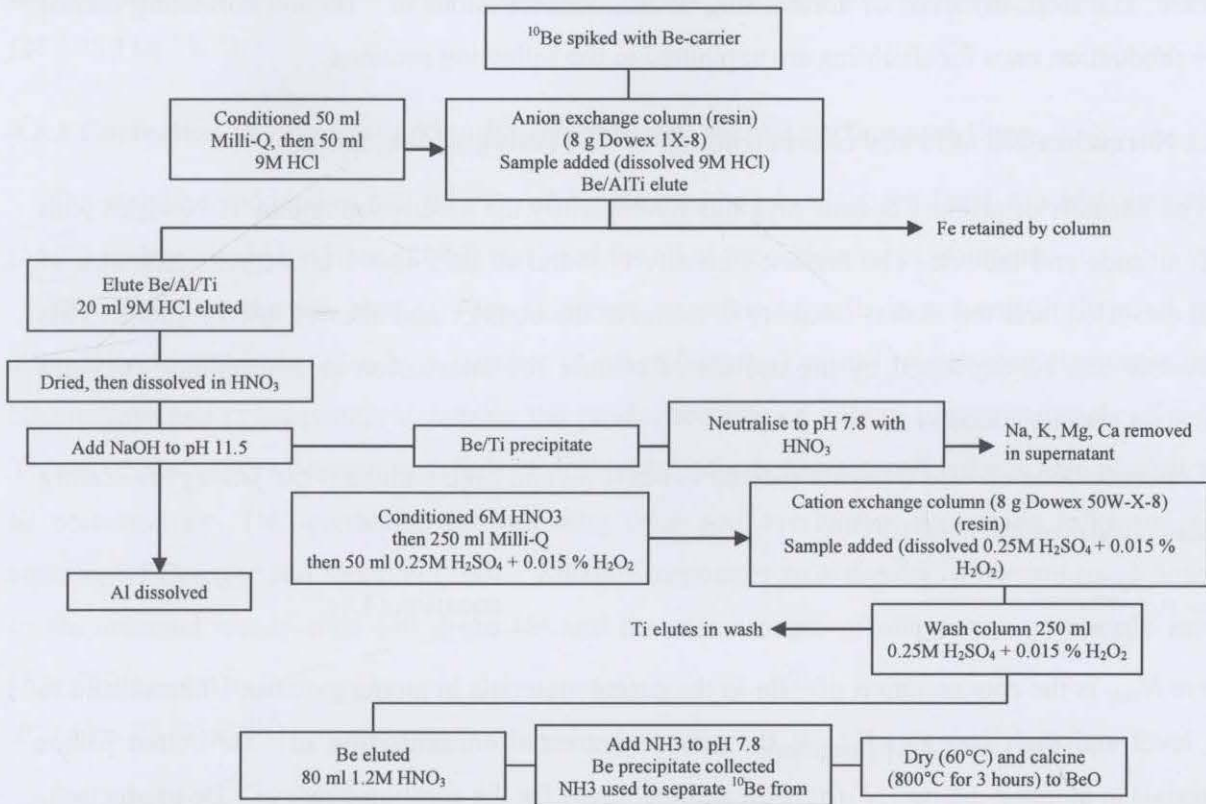


Fig. 4.6. Flowchart of  $^{10}\text{Be}$  target preparation using  $\text{H}_2\text{SO}_4 + \text{H}_2\text{O}_2$  reagent to remove Ti and NaOH at pH 11.5 to separate Al (after Child et al. (2000)).

AMS measured the ratio of  $^{10}\text{Be}$  to  $^9\text{Be}$  in the prepared sample with a detection limit of  $5 \times 10^{-15}$ . The ratio was then converted to concentrations of  $^{10}\text{Be}$  in atoms per gram-quartz.

Converting  $^9\text{Be}/^{10}\text{Be}$  isotope ratios to concentrations of  $^{10}\text{Be}$  in atoms g-quartz $^{-1}$  involved (Balco, 2006):

- (1) the measured  $^{10}\text{Be}/^9\text{Be}$  isotope ratio and its standard error
- (2) the mass of Be added with the Be carrier in the chemical processing and its uncertainty
- (3) the mass of the quartz sample itself and
- (4) the typical number of atoms of  $^{10}\text{Be}$  in a laboratory processed blank plus its uncertainty.

All  $^{10}\text{Be}$  results were normalized using the NIST SRM 4325 standards.

### 4.3 Data treatment to derive soil production rates from *in situ* concentrations of $^{10}\text{Be}$

Prior to data analysis and interpretation, the calculated concentrations of  $^{10}\text{Be}$  were corrected for altitude and latitude to enable the comparison with results from other locations. Furthermore, annual production rates of  $^{10}\text{Be}$  were corrected for shielding, slope and depth below the soil surface. The steps involved of normalising *in situ* concentrations of  $^{10}\text{Be}$  and correcting annual  $^{10}\text{Be}$  production rates for shielding are explained in the following sections.

#### 4.3.1 Normalization of *in situ* concentrations of $^{10}\text{Be}$ (using scaling factors)

The intensity of primary cosmic rays and subsequently the production rate of TCN varies with both altitude and latitude. The highest intensity is found at sites above 60 degrees and sites of high elevation, and the lowest intensity is found at the equator and sites of low elevation. This behaviour can be explained by the decline of cosmic ray attenuation as atmospheric pressure decreases (Stone, 2000).

Concentrations of  $^{10}\text{Be}$  were normalized to sea level and high latitude ( $>60^\circ$ ) using the scaling factors published by Stone (2000).

$$N_{corr} = \frac{N_{raw}}{F_\lambda(p)} \quad \text{equation (4.1),}$$

where  $N_{corr}$  is the concentration of  $^{10}\text{Be}$  in the parent materials in atoms g-quartz $^{-1}$ , normalized to sea level and high latitude,  $N_{raw}$  is the raw or untreated concentration of  $^{10}\text{Be}$  of the parent materials in atoms g-quartz $^{-1}$ ,  $F_\lambda(p)$  is the scaling factor for the combined rate of  $^{10}\text{Be}$  production.

$$F_\lambda(p) = f_{sp} S_\lambda(p) + (1 - f_{sp}) M_\lambda(p) \quad \text{equation (4.2),}$$

where  $S_\lambda(p)$  is the rate of  $^{10}\text{Be}$  production by spallation as a function of pressure  $p$  at sea level and high latitude; and  $f_{sp}$  is the fraction of spallogenic production at the surface at sea level (0.978 for  $^{10}\text{Be}$ ).

$$S_{\lambda}(p) = a + b \exp[-p/150] + cp + dp^2 + ep^3 \quad \text{equation (4.3),}$$

where  $a$ ,  $b$ ,  $c$ ,  $d$  and  $e$  are scaling coefficients taken from Table 1 in Stone (2000).

$$M_{\lambda}(p) = M_{\lambda 1013.25} \exp[(1013.25 - p)/242] \quad \text{equation (4.4),}$$

where  $M_{\lambda}(p)$  is the rate of  $^{10}\text{Be}$  production by muon capture as a function of pressure  $p$  at sea level and high latitude; and  $M_{\lambda 1013.25}$  is a scaling coefficient taken from Table 1 in Stone (2000).

The long-term average atmospheric pressure  $p$  at the sampling site was calculated following Dunai (2000):

$$p = p_0 \left( 1 - \frac{\beta_0 H}{T_0} \right)^{\frac{g_0}{R_d \beta_0}} \quad \text{equation (4.5),}$$

where  $p_0$  is the pressure at sea level (1013.25 hPa),  $\beta_0$  the temperature decrease with elevation ( $6.5 \text{ mK m}^{-1}$ ),  $H$  is the altitude in meters,  $T_0$  the temperature at sea level in Kelvin (288.15 K),  $g_0$  the standard level value of the acceleration due to gravity ( $9.80665 \text{ m s}^{-2}$ ) and  $R_d$  the gas constant ( $287.05 \text{ J kg}^{-1} \text{ K}^{-1}$ ).

#### 4.3.2 Correction of $^{10}\text{Be}$ production for depth below the soil surface and slope

The standard production rate of  $^{10}\text{Be}$  of  $5.1 \pm 0.3 \text{ atoms g}^{-1} \text{ yr}^{-1}$  at sea level and high latitude ( $>60^\circ$ ) as determined by Stone (2000) was used for all of the following calculations.

The annual production rate of  $^{10}\text{Be}$  in parent materials of soils is not only influenced by altitude and latitude but also by a number of other factors. The soil overburden attenuates the cosmic rays and consequently decreases the production rate of  $^{10}\text{Be}$  in parent materials of soil. Therefore, sampling of parent materials at different depths below the soil surface also needed to be corrected for. This correction for shielding from soil overburden was made following an equation of Granger and Muzikar (2001), which incorporates bulk density of the soil ( $\rho_{\text{soil}}$ ) down to the assumed steady-state soil depth ( $h$ ) and the mean length of attenuation of cosmic rays ( $\Lambda = 150/\rho_{\text{soil}} \text{ cm}$ ).

$$P_{\text{Be}}(h) = P_{\text{Be}}(0) e^{-h/\Lambda} \quad \text{equation (4.6),}$$

where  $P_{\text{Be}}(h)$  is the depth corrected production rate of  $^{10}\text{Be}$  and  $P_{\text{Be}}(0)$  is the production rate of  $^{10}\text{Be}$  at sea level and high latitude.

Shielding from cosmic rays because of sloped surfaces also results in a decrease of the production rate of  $^{10}\text{Be}$ . Therefore, production rates of  $^{10}\text{Be}$  were also corrected for shielding and slope following the methods described in Dunne et al. (1999) (see Figure 4.7).

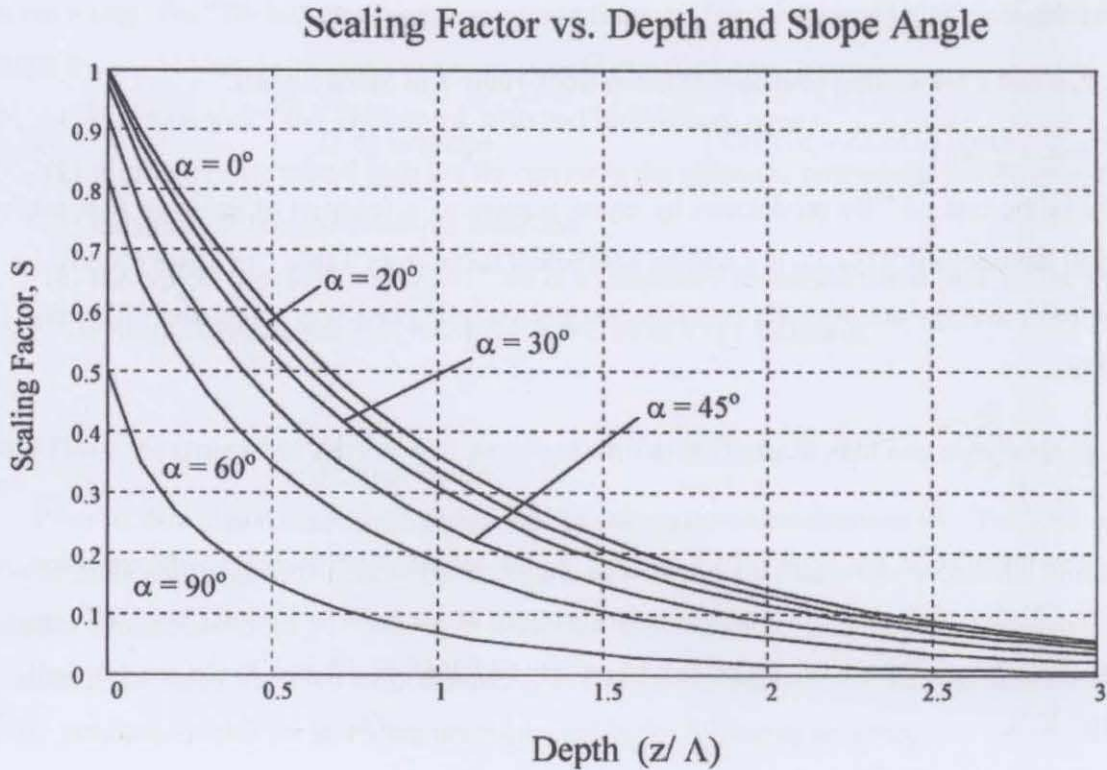


Fig. 4.7. Scaling factor for the rate of production as a function of sampling depth for various surface dip angles (with  $m = 2.3$ ). Depth is measured in fractions of the attenuation length normally used to model decrease in rate of production with depth as a simple exponential (taken from Dunne et al. 1999). Here, 'normalized depth' was calculated by ( $\text{Depth} = \frac{z\rho_{\text{rock}}}{\Lambda}$ ), where  $z$  is the thickness of the soil overburden,  $\rho_{\text{rock}}$  is the density of the rock and  $\Lambda$  is the attenuation of cosmic rays.

#### 4.3.3 Quantifying SPR using *in situ* $^{10}\text{Be}$ concentrations of soil parent materials

Normalized concentrations of  $^{10}\text{Be}$  in parent materials of soils were used to derive soil production rates (SPR) to ultimately investigate the rate of soil formation. To determine soil production rates the following needs to be known:

- (1) the rate of  $^{10}\text{Be}$  production in atoms  $\text{g}^{-1} \text{yr}^{-1}$  ( $5.1 \pm 0.3$  atoms  $\text{g}^{-1} \text{yr}^{-1}$  at sea level and high latitude), (Stone, 2000).
- (2) the half-life of  $^{10}\text{Be}$  ( $1.51 \pm 0.06 \times 10^6$  years), (Hofmann et al., 1987) and
- (3) the concentration of  $^{10}\text{Be}$  in atoms  $\text{g-quartz}^{-1}$  from the sampled parent materials.

Calculations of SPR in  $\text{mm kyr}^{-1}$  were based on a model of Nishiizumi et al. (1991), assuming that the concentration of  $^{10}\text{Be}$  in the sample of parent material was controlled by concentration increases with exposure time and also by the erosion rate ( $\epsilon$ ) of the parent material itself. Assuming constant erosion rates and cosmic ray intensities, the steady-state  $^{10}\text{Be}$  concentration ( $N$ ) in the sample of parent material in atoms  $\text{g-quartz}^{-1}$  can be calculated as:

$$N = \frac{P(h, \theta)}{\left( \lambda + \left( \frac{\rho_{parent} \varepsilon}{\Lambda} \right) \right)} \quad \text{equation (4.7),}$$

where  $P$  is the production rate of  $^{10}\text{Be}$  in the target mineral quartz at depth  $h$  and slope  $\theta$  in atoms gram-quartz $^{-1}$  year $^{-1}$ ,  $\rho_{parent}$  is the mean density of the parent material in g cm $^{-3}$ ,  $\lambda$  the decay constant of  $^{10}\text{Be}$  with  $\lambda$  equalizing  $\ln 2 / ^{10}\text{Be}$  half life, and  $\Lambda$  is the mean length of attenuation of cosmic rays with  $\Lambda$  equalizing 150 g cm $^{-2}$ . Rearranging equation 7 for  $\varepsilon$ , gives the equation for calculating soil production rates (SPR) in mm kyr $^{-1}$  (Heimsath et al., 1997; Lal, 1991):

$$SPR = \frac{\Lambda}{\rho_{parent}} \left( \frac{P(h, \theta)}{N} - \lambda \right) \quad \text{equation (4.8),}$$

As noted in equation 4.8 the annual production rate of  $^{10}\text{Be}$  ( $P$ ) needs to be normalized to production rates at the site sampled (elevation, latitude and longitude), and also needs to be corrected for the soil overburden and shielding by slope.

Soil production rates were calculated with the assumption that soil erosion and soil production are balanced and soil thickness is in steady state. Consequently, soil production rates are calculated assuming steady-state conditions (equal rates of soil formation and soil erosion) throughout the production of TCN.

The terms erosion rate (Lal, 1991) and soil production rate (Heimsath et al., 1997) are both used to describe TCN-derived denudation rates (physical and chemical processes combined). Heimsath et al. (1997) applied the concept of deriving TCN based erosion rates of rock (Lal, 1991) to investigate soil production. They derived erosion rates from soil parent materials, and subsequently called this calculation the rate of soil production. In pedology, soil weathering or the soil formation rate define the same process of the conversion of parent material (e. g. bedrock, saprolite) to soil, combining physical and chemical processes. However, here the physical breakdown of the parent material to soil is assumed to be the dominant process responsible for the thickening of the soil profile. Therefore, TCN-derived SPR primarily reflect the physical conversion of the parent material to soil. In this thesis, the term soil production rate (Heimsath et al., 1997) is used exclusively for TCN-derived rates of soil formation.

Theoretically, as discussed in von Blanckenburg (2006) only the term denudation rate is of correct use in this context, because unlike the term 'erosion' it defines the removal of mass through both physical and chemical processes. This definition is rectified with the explanation that the calculation of TCN-derived denudation rates also involves the combined effort of physical and chemical weathering processes. Therefore, the term erosion rate is used

inaccurately, because it generally describes only the mechanical processes of denudation. It can also be confused with erosion of soil. However, it was assumed that the physical conversion from parent material to soil is the main driver in soil production.

#### 4.4 Results

In the following, calculated concentrations of  $^{10}\text{Be}$  and subsequently estimates of rates of soil production at the study site are presented. Results from Werrikimbe National Park are then compared with soil production rates estimated for different environments in Australia and Northern America followed by discussion.

##### 4.4.1 *In situ* produced concentrations of $^{10}\text{Be}$ at Werrikimbe National Park

At Werrikimbe National Park measured  $^{10}\text{Be}$  concentrations ranged between  $0.103$  and  $0.450 \times 10^6$  atoms g-quartz $^{-1}$  (Table 4.3), normalized to sea level and high latitude ( $>60^\circ$ ). These results are derived from parent materials below different soil thicknesses and from one outcrop sample at zero soil depth. Measured *in situ* concentrations of  $^{10}\text{Be}$  of  $0.103$ - $0.150 \times 10^6$  atoms g-quartz $^{-1}$  are relatively low, i.e. for (outcrop) samples in south-central Australia concentrations of  $^{10}\text{Be}$  with values as high as  $5.3 \times 10^5$  atoms g-quartz $^{-1}$  have been estimated (Bierman and Caffee, 2002).

*In situ* produced concentrations of  $^{10}\text{Be}$  had the tendency to decrease with increasing soil depth, with the highest concentrations recorded for the outcrop sample at zero soil depth. This is presented graphically in Figure 4.8 using the unscaled  $^{10}\text{Be}$  concentrations.

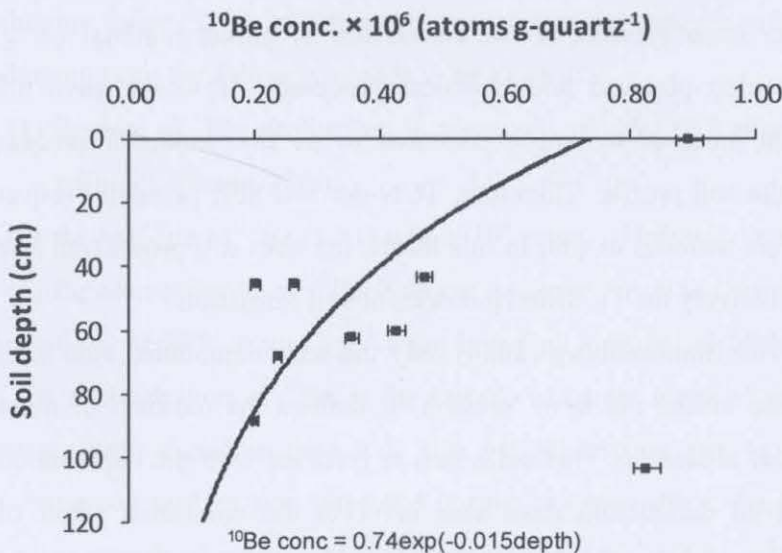


Fig. 4.8. *In situ* produced concentrations of  $^{10}\text{Be}$  for Werrikimbe National Park.



The decrease of *in situ* concentrations of  $^{10}\text{Be}$  with depth can be explained by the soil overburden that attenuated the production rate of  $^{10}\text{Be}$  over time.

#### 4.4.2 TCN-derived SPR at Werrikimbe National Park

At Werrikimbe National Park, rates of soil production derived from *in situ*  $^{10}\text{Be}$  concentrations were calculated following equation 4.8. Soil production rates varied between 3 and 18  $\text{mm kyr}^{-1}$ , equivalent to about 0.003 and 0.02  $\text{mm yr}^{-1}$ . At all sites rates of maximum soil production occurred between 0 and 50 cm of soil thickness. To quantify a function of soil production, estimated rates of soil production from parent materials were related to the thickness of soil. As evidenced in Figure 4.9 (and Table 4.3), there is no clear pattern of SPR with soil depth in any of the three individually sampled toposequences. Judging from field observations, the landscape that formed at the sites studied appeared to be most likely the result of exponentially influenced soil production, although some outcrops of parent material –modelled landscape features of humped soil formation (refer to study by Dietrich et al., 1995, discussed in the literature review)- were present at toposequence Spokes Mountain.

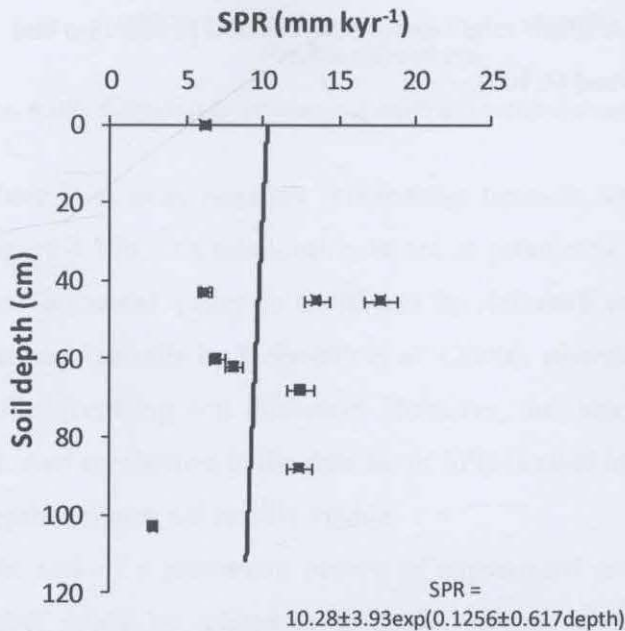


Fig. 4.9. Rates of soil production at Werrikimbe National Park. SPR are plotted as in soil science against depth. SPR were normalized to sea level and high latitude ( $>60^\circ$ ) and corrected for shielding by soil overburden and slope. Note: All calculations were made with SPR as the dependent variable.

However, under steady-state conditions it is assumed that the production rate of soil (SPR) can be modelled with an exponential function of the weathering of bedrock with increasing soil thickness (equation (2.12)):

$$SPR = P_0 \exp(-bh)$$

where  $P_0$  is the potential weathering rate of the parent material [ $L T^{-1}$ ] at depth  $h = \text{zero}$  [ $L$ ], and  $b$  is the rate constant [ $L$ ] (Heimsath et al., 1997; Minasny and McBratney, 1999).

It was attempted to fit the exponential function of soil production proposed in the literature for the set of soil production rates. For Werrikimbe National Park the potential weathering rate of the parent material of sedimentary rocks ( $P_0$ ) was estimated to be approximately  $10 \pm 4 \text{ mm kyr}^{-1}$  with  $b = 0.125 \pm 0.617 \text{ mm}^{-1}$ . The relatively high  $b$  value indicates that SPR vary slightly with depth, and that there is no certain pattern of soil production in relation to soil depth. However, the uncertainty in calculating SPR is also quite high since steady-state conditions of soil formation and soil erosion are assumed and soil production rates need to be corrected for the soil overburden and slope as discussed in section 4.3, meaning that the shape of the curve is not definite. The value of  $10 \pm 4 \text{ mm kyr}^{-1}$  therefore relates to a potential average weathering rate ( $P_0$ ). This estimated average weathering rate ( $P_0$ ) of  $10 \pm 4 \text{ mm kyr}^{-1}$  was relatively low for this warm-temperate to subtropical environment.

However, results also show that the rate of soil production is more closely related to the position of the toposequences in the landscape. A linear relationship between soil production and the terrain attribute, profile curvature, was observed (4.10a).

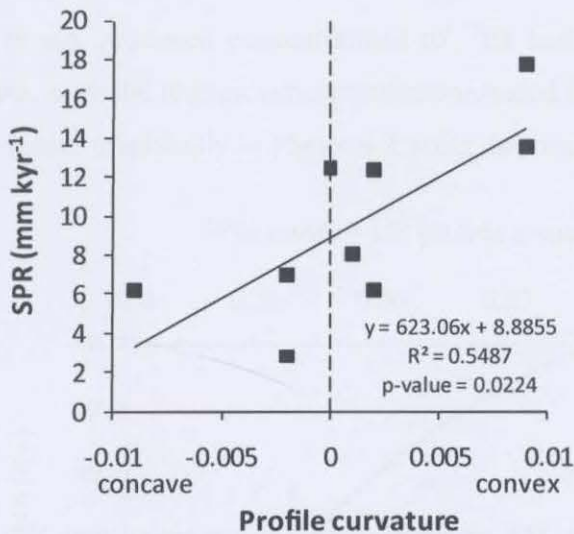


Fig. 4.10a. Relationship between soil production rate and profile curvature.

As shown in Figure 4.10a, soil production rates have a positive relationship with profile curvature. Soil production rates have the tendency to increase with changes in hillslope roundness from concave to convex. This relationship implies that convex hillslopes most likely

tend to lose soil materials (higher soil production rate) while in turn soil material tends to be gained on concave hillslopes (lower soil production).

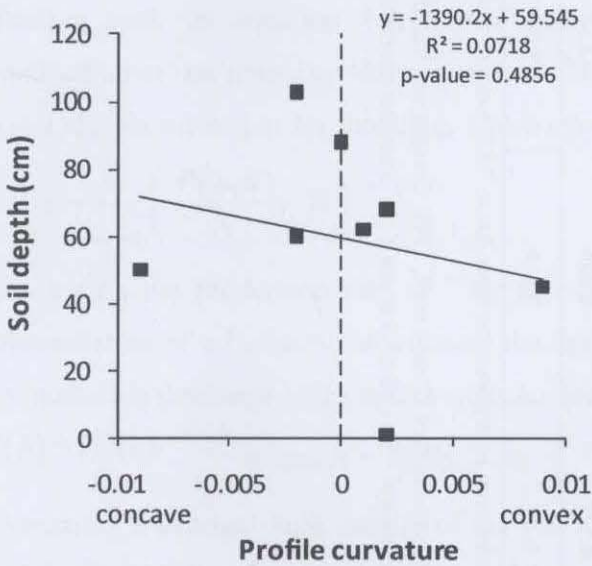


Fig. 4.10b. Relationship between soil depth and profile curvature.

There is a weak negative relationship between soil depth and profile curvature, displayed in Figure 4.10b, this relationship is not as prominent as demonstrated in other study sites, i.e. for the Tennessee Valley in California by Heimsath et al. (1999) or for the Bega Valley in south-eastern Australia by Heimsath et al. (2000), where SPR clearly followed an exponential decline with increasing soil thickness. However, the data set of SPR from Wilkinson et al. (2005b) showed similarities to the data set of SPR studied in this thesis. Here, a clear pattern of SPR with depth was also not readily visible.

The lack of a prominent pattern of exponential decline of soil production with increasing soil depth might be related to unsteady periods of soil production and soil erosion during the formation of the soil-mantled hillslopes in the subcatchment at Werrikimbe.

**Tab. 4.3.** Measurements of terrestrial cosmogenic nuclide concentrations ( $^{10}\text{Be}$ ), Werrikimbe National Park.

Sample	Latitude (deg)	Longitude (deg)	Elevation (m)	Depth (cm)	Weight purified quartz (g)	$^{10}\text{Be}$ conc.* ( $10^6$ atoms g-quartz $^{-1}$ )	$^{10}\text{Be}$ conc. error* ( $10^6$ atoms g-quartz $^{-1}$ )	Soil production rate** (mm kyr $^{-1}$ )	Soil production rate error** (mm kyr $^{-1}$ )
Ta17	31.12	152.34	1145	0	90.48	0.442	0.016	6.16	0.28
Ta2	31.13	152.34	931	43	42.45	0.272	0.011	6.20	0.43
Tb24a	31.20	152.39	979	45	47.07	0.146	0.006	13.50	0.84
Tb24b	31.20	152.39	979	45	40.51	0.112	0.0049	17.72	1.13
Tb12	31.20	152.38	931	60	41.64	0.245	0.011	6.96	0.50
Tb6	31.20	152.38	902	62	31.19	0.209	0.009	8.07	0.58
Te38	31.18	152.31	1092	88	89.35	0.103	0.004	12.43	0.93
TeM	31.18	152.32	1065	68	89.18	0.124	0.004	12.38	0.85
Te3	31.18	152.32	1008	103	47.69	0.45	0.018	2.78	0.23

\* $^{10}\text{Be}$  concentration normalized to sea level and high latitude (Stone, 2000), values of uncertainty incorporate the error due to AMS analysis and also the experimental uncertainties in production estimates for  $^{10}\text{Be}$  ( $\pm 5\%$ ), implemented in the scaling factor

\*\*Soil production rates calculated after Lal (1991), and corrected for slope and depth below the surface (Dunne et al., 1999; Granger and Muzikar, 2001), values of uncertainty incorporate the ones mentioned above and also the uncertainty for production rates of  $^{10}\text{Be}$  ( $5.1 \pm 0.3$  atoms  $\text{g}^{-1} \text{yr}^{-1}$ ) and the attenuation of cosmic rays ( $150 \pm 4$   $\text{g cm}^{-2}$ )

## 4.5 Discussion

### 4.5.1 Deriving SPR from soil parent materials *in situ*

'Dating' soil *in situ* from TCN concentrations in parent materials is useful for quantifying the rate of soil production. However, section 4.3 revealed that a lot of assumptions are involved in the process that leads to estimating soil production rates from accumulated  $^{10}\text{Be}$  concentrations. Reflecting back on equation 4.8, it was demonstrated that calculating SPR involved the normalization of the annual production rate of  $^{10}\text{Be}$  ( $P$ ) to the geographical position of the study site and also its correction for shielding, which attenuates the production rate of  $^{10}\text{Be}$ :

$$SPR = \frac{\Lambda}{\rho_{parent}} \left( \frac{P(h, \theta)}{N} - \lambda \right)$$

Correcting the production rate of  $^{10}\text{Be}$  for shielding by the soil overburden involved the implementation of a function that corrects the decline in production rates of  $^{10}\text{Be}$  exponentially with increasing thickness of the soil overburden (equation 4.6, Figure 4.11).

$$P_{Be}(h) = P_{Be}(0) e^{-h/\Lambda} \quad \text{where } \Lambda = 150/\rho_{soil} \text{ cm}$$

Assuming a constant bulk density of the soil overburden of  $1.3 \text{ g cm}^{-3}$  and an attenuation of cosmic rays of  $150 \text{ g cm}^{-2}$ , the exponent of the exponential decrease of the  $^{10}\text{Be}$  production is controlled by the thickness of the soil overburden,  $h$ , and the attenuation of cosmic rays through soil material,  $\Lambda$ , with a value of approximately 115.

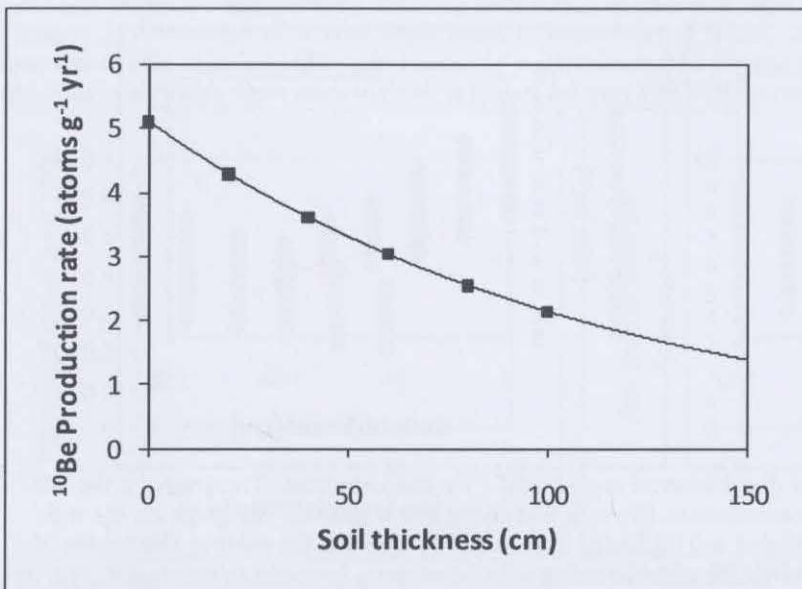


Fig. 4.11. Exponential decline of the annual  $^{10}\text{Be}$  production rate,  $P$ , with increasing soil overburden. This corrects for the attenuation of cosmic rays with increasing soil overburden.

Here, the influence of correcting the annual production rate of  $^{10}\text{Be}$ ,  $P$ , (in implementing a function that already behaves exponentially with depth) on the calculated soil production rate (SPR) will be explored. It was hypothesized that the calculated rate of soil production (SPR) might potentially be dependent on the correction for  $^{10}\text{Be}$  production with depth and not only on the observed 'attenuation' or distribution of the  $^{10}\text{Be}$  concentration in the parent materials ( $N$ ).

To test the hypothesis, a numerical experiment was conducted using simulations for two different scenarios (1) uniform, and (2) exponential decline of the observed distribution of  $^{10}\text{Be}$  concentrations,  $N$ . Firstly, a uniformly random  $^{10}\text{Be}$  concentration between  $0.3$  and  $0.6 \times 10^6$  atoms  $\text{g-quartz}^{-1}$  was generated at five depths based on TCN data from the site studied, and secondly, two different distributions with depth were applied to the data:

- (1) observed uniform distribution with depth (Figure 4.12), and
- (2) exponentially declining distribution with depth (Figure 4.13 to 4.15). For the exponent of the exponential distribution three different values were applied, because it is known that the value of the exponent controls the slope of the exponential fit. Therefore, the exponentially decreasing distribution with depth was applied at a rate (1) less than the attenuation of cosmic rays (2) equal to the attenuation of cosmic rays and (3) higher than the attenuation of cosmic rays.

Following on, SPR were calculated by implementing depth corrected  $^{10}\text{Be}$  production rates,  $P$ , (Figure 4.11) and the observed (1) uniform and (2) exponential distributions of  $^{10}\text{Be}$  concentrations,  $N$ , following equation 4.8. This process was repeated 100 times and is exemplified in the following graphs (Figure 4.12 to 4.15).

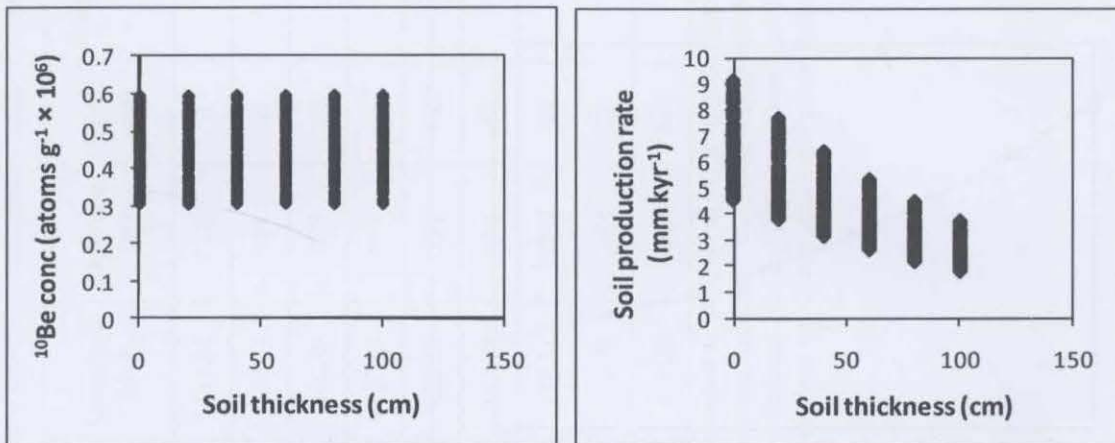


**Fig. 4.12.** Simulation of observed uniform distribution of randomized  $^{10}\text{Be}$  concentrations. The graph on the left shows the uniform distribution of  $^{10}\text{Be}$  concentrations ( $N$ ) with increasing soil thickness. The graph on the right demonstrates the calculated SPR with increasing soil thickness. Here, it can be seen that the uniform distribution of  $N$  with depth results in exponentially declining SPR with increasing soil thickness.

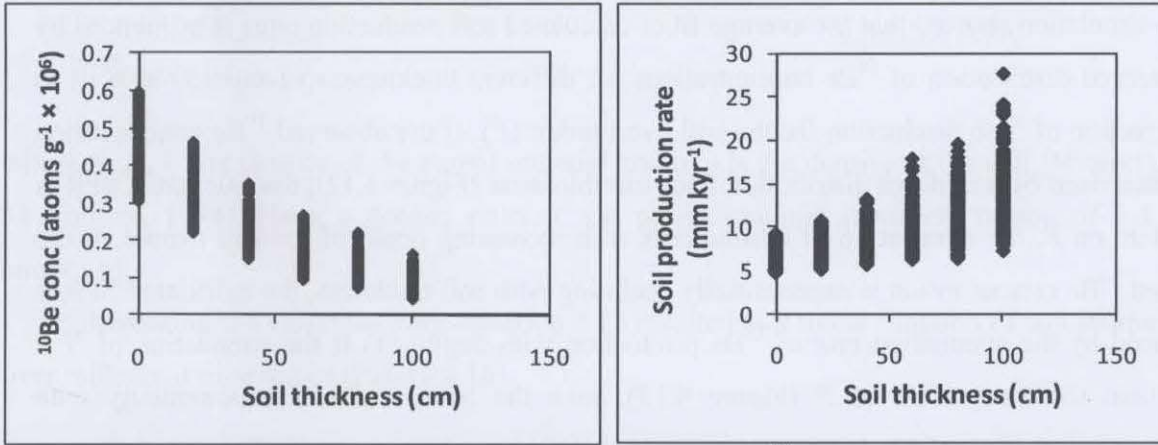


Fig. 4.13. Simulation of observed exponential distribution of randomized  $^{10}\text{Be}$  concentrations. The graph on the left shows the exponentially declining distribution of  $^{10}\text{Be}$  concentrations ( $N$ ) with increasing soil thickness. **Scenario 1:** Fast attenuation of  $N$  (at a rate greater than the  $^{10}\text{Be}$  attenuation) with depth. The graph on the right hand side demonstrates the calculated SPR with increasing soil thickness. SPR tend to result in exponential increase with increasing soil thickness.

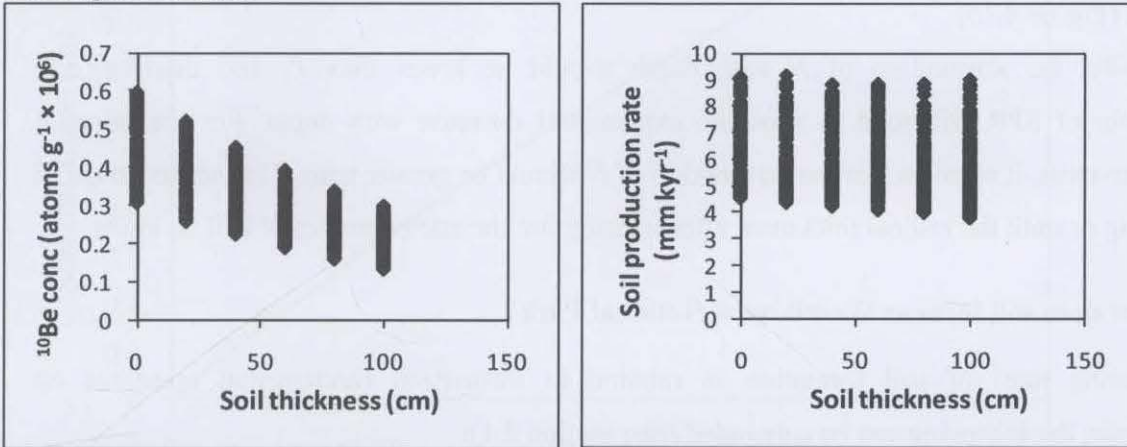


Fig. 4.14. Simulation of observed exponential distribution of randomized  $^{10}\text{Be}$  concentrations. The graph on the left hand side shows the exponentially declining distribution of  $^{10}\text{Be}$  concentrations ( $N$ ) with increasing soil thickness. **Scenario 2:** Attenuation of  $N$  with depth equal to attenuation of cosmic rays. The graph on the right hand side demonstrates the calculated SPR with increasing soil thickness. Here, it can be seen that the exponentially declining distribution of  $N$  with depth tends to result in almost uniform SPR with increasing soil thickness.

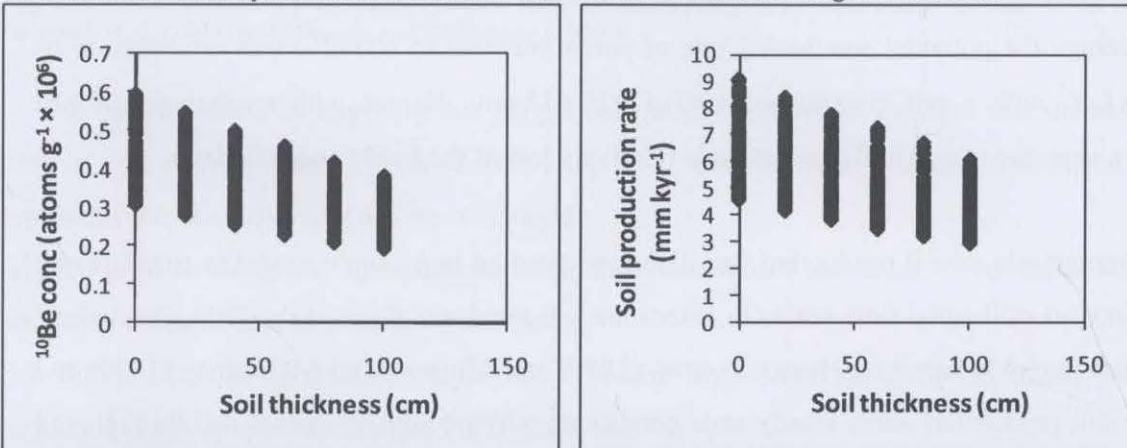


Fig. 4.15. Simulation of observed exponential distribution of randomized  $^{10}\text{Be}$  concentrations. The graph on the left hand side shows the exponentially declining distribution of  $^{10}\text{Be}$  concentrations ( $N$ ) with increasing soil thickness. **Scenario 3:** Slower attenuation compared to cosmic rays of  $N$  with depth. The graph on the right hand side demonstrates the calculated SPR with increasing soil thickness. Here, it can be seen that SPR tend to result in exponential decline with increasing soil thickness.

The simulation showed that the average fit of calculated soil production rates is influenced by the observed distribution of  $^{10}\text{Be}$  concentrations for different thicknesses of soil ( $N$ ) as well as the correction of  $^{10}\text{Be}$  production for the soil overburden ( $P$ ). If the observed  $^{10}\text{Be}$  concentration is characterized by a uniform distribution with soil thickness (Figure 4.12), the calculated SPR is dependent on  $P$ , the attenuation of cosmic rays with increasing depth of the soil mantle. If the observed  $^{10}\text{Be}$  concentration is exponentially declining with soil thickness, the calculated SPR is influenced by the attenuation rate of  $^{10}\text{Be}$  production with depth: (1) If the attenuation of  $N$  is faster than the attenuation of  $P$  (Figure 4.13), then the SPR increases exponentially with increasing soil thickness. (2) If attenuation of  $N$  is similar or the same as  $P$  (Figure 4.14), then the SPR shows almost uniform behaviour with increasing soil thickness. (3) If the attenuation of  $N$  is slower than the attenuation of  $P$ , then the SPR decreases exponentially with increasing soil thickness (Figure 4.15).

Naturally, the attenuation of  $N$  with depth should be lower than  $P$ , and therefore the relationship of SPR will tend to show an exponential decrease with depth. For the humped function to exist, it requires that the attenuation of  $N$  should be greater than  $P$  in the first stage of weathering or until the critical thickness, after which point the attenuation of  $N$  will be lower.

#### 4.5.2 How does soil form at Werrikimbe National Park?

Discussing rates of soil formation in relation to formalized fundamental questions on pedogenesis, the following can be concluded (See section 2.1):

- (1) Soil production rates derived for the study site at Werrikimbe National Park showed no clear pattern with soil depth, however, appeared to be related to the position of soil profiles in the landscape.
- (2) On average the potential weathering rate of parent material to soil ( $P_0$ ) was estimated to be  $10 \pm 4 \text{ mm kyr}^{-1}$  with a rate constant of  $b = 0.125 \pm 0.617 \text{ mm}$ . Hence, with an increase of just 0.01 mm a year, the rate of soil production is relatively low at the field site studied.

The average rate of soil production was also implemented in a simple model to simulate soil production over millennial time scales to determine soil residence times at the field site studied. The applied model is based on Heimsath et al. (1999) and Minasny and McBratney (1999) and predicted soil production under steady-state conditions with no gain or loss of soil through soil erosion and deposition and a constant bulk density throughout the soil profile:



$$dt = \frac{dh}{\frac{\rho_{\text{parent}}}{\rho_{\text{soil}}} P_0 \exp(-bt)} \quad \text{equation (4.9),}$$

where  $\rho_{\text{parent}}$  is the density of the parent material and  $\rho_{\text{soil}}$  is the density of the soil (Minasny and McBratney, 1999). Here, a density ratio of soil parent material (bedrock) to soil of 1.4 was employed.

Implementing the variables from equation 2.12 resulted in a linear function of soil production over millennial time scales (Figure 4.16).

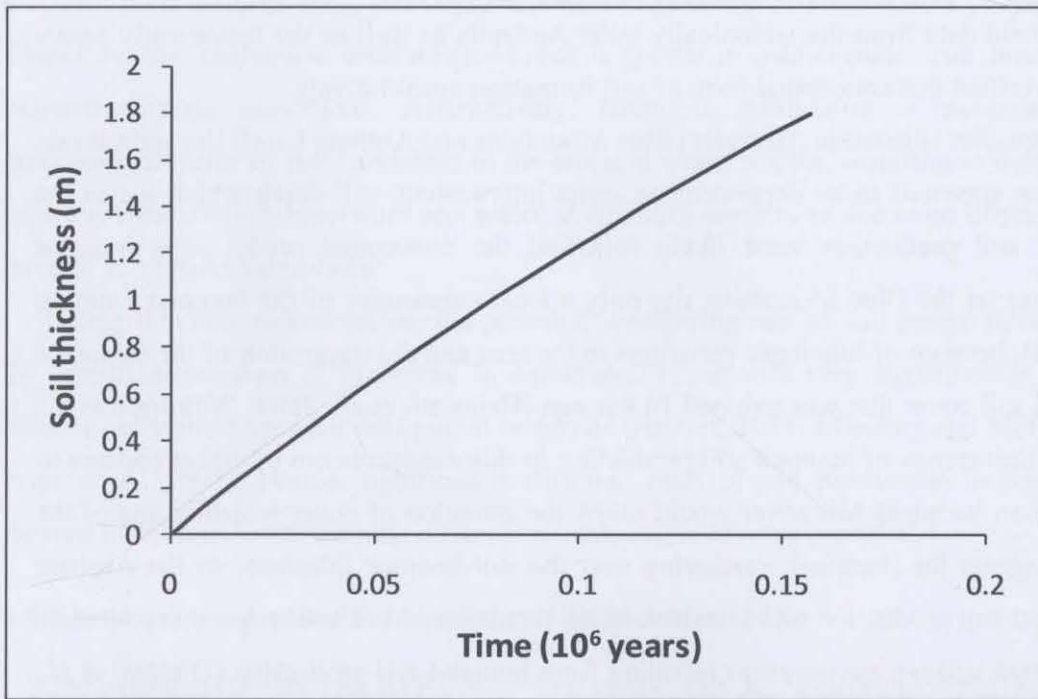


Fig. 4.16. Soil formation at Werrikimbe National Park, simulated applying a simple soil production model (based on Heimsath et al. (1999) and Minasny and McBratney (1999)).

The data obtained by applying this simple soil production model indicate that the residence time of soil at Werrikimbe National Park is up to 80 000 years. In relation to each individual toposequence, the following can be concluded:

- (a) Soil profiles along the toposequence of Spokes Mountain were about 45 cm thick, with soil residence times of approximately 29 000 years,
- (b) Soil profiles along the toposequence of Mount Boss were about 60 cm thick, with soil residence times of approximately 45 000 years, and
- (c) Soil profiles along the toposequence of Plateau Beech were about 1 m thick, with soil residence times of approximately 79 000 years.

However, soil residence times calculated for the soils at Werrikimbe National Park correspond to soil formation being in a steady-state, i.e. '*in situ*' soil production with no deposition or erosion. This assumption is based on the common perception that in steady-state a soil profile accumulates from weathered parent rock material only.

#### 4.5.3 Field observations of how soils form over time - based on TCN-derived SPR

As discussed in section 4.1.3, the compilation of TCN-derived SPR calculated for different locations with various lithologic conditions and climate regimes showed that the majority of TCN-derived SPR followed an exponential decline with increasing soil thickness (see Figure 4.1). Compiled field data from the tectonically quiet Australia as well as the tectonically active North America verified this conceptual form of soil formation quantitatively.

For two field studies situated in Australia (Blue Mountains and Arnhem Land) the highest rate of soil production appeared to be dependent on some intermediate soil depth which led to the assumption that soil production most likely followed the conceptual model of a humped function. However, at the Blue Mountains site only a local occurrence of the humped function was hypothesized, because of lithologic variations in the area and the suggestion of the existence of a hypothetical soil cover that was stripped 10 kyr ago (Heimsath et al., 2009; Wilkinson et al., 2005b). A local occurrence of humped soil production in this sandstone environment appears to be reasonable as an incipient soil cover would allow the retention of water which is one of the most important agents for chemical weathering near the soil-bedrock interface. At the Arnhem Land site, humped soil production was assumed, based on observed soil landscape characteristics that were consistent with an environment resulting from humped soil production (Dietrich et al., 1995). Soil thicknesses less than the peak in soil production at 35 cm could not be observed and rates of soil production decreased below and above 35 cm. The Arnhem Land study site was characterized by soil-mantled convex hillslopes or outcropping bedrock almost free of tors and rocky cliffs (Heimsath et al., 2009).

Evidence for the existence of a humped function of soil production comes from observations in the field where weathering rates were highest under an incipient soil cover (cryoturbation, bioturbation) (Anderson et al., 2007). The unequivocal field evidence for soil production following a humped model is still to be verified with TCN data although it has been discussed widely in the literature either as a conceptual model (Gilbert, 1877; Humphreys and Wilkinson, 2007; Wilkinson et al., 2005b) or incorporated in soil-landscape evolution models (Carson and Kirkby, 1972; Heimsath et al., 2009; Pelletier and Rasmussen, 2009; Small et al., 1999).

#### 4.5.4 Assumptions on the extent of soil production

The extent of soil production is believed to be dependent on local site characteristics including climate, parent material, vegetation and topography as discussed in Jenny (1941). It is assumed that soil production varies with the strength and composition of the parent material, the soil temperature and the water penetration through the soil profile. Theories on the extent of weathering of parent materials *in situ* and consequently on the rate of soil production are mainly based on observed geographical variations in climate and weathering characteristics. Existing climatic theories on the extent of weathering discuss the variability of pedogenesis as a result of different rock disintegration and decay because of different climatic zones (Pope et al., 1995). Therefore, the mechanical breakdown of rock is greater in cold climates and deserts because of extreme climate conditions. Alternatively, chemical weathering is assumed to be the predominant factor of soil formation in the wet and warm tropics, resulting in deeply weathered profiles. Ultimately, temperature and water availability seem to be the main drivers for different rates of soil production *in situ*.

Taking this into consideration, the potential weathering rate of soil parent materials ( $P_0$ ) and the empirical constant  $b$ , presented in equation 2.12, should vary significantly in relation to different climatic zones and soil parent materials (Ahnert, 1977; Minasny and McBratney, 1999; Pope et al., 1995). Hence, significantly different rates of soil production in compiling TCN-derived SPR from locations with different climate regimes were expected.

#### 4.5.5 Indications of a similar behaviour of TCN-derived SPR

Comparing TCN-derived SPR from the study site at Werrikimbe National Park with previously published field data, it can be observed that the site at Werrikimbe National Park exhibits the lowest observed TCN-derived SPR, with a  $P_0$  value of  $10 \pm 4 \text{ mm kyr}^{-1}$ .

Nevertheless, the obtained data fit well within the range of TCN-derived SPR of the various environments studied. Despite the different environments with different climatic conditions and parent materials the conversion rates of soil parent materials to soil ( $P_0$ ) appear to be similar (Figure 4.17). The only anomaly is the dataset from the Oregon coast range in North America, where non-steady erosion rates account for high values in SPR. Generally, for field studies set in a tectonically active environment with fluctuating erosion rates, the assumption of steady-state erosion for calculating SPR does not apply. This is a suggested explanation for an order of magnitude higher SPR in Heimsath (2006). With regards to the field sites in the Bega Valley of south-eastern Australia there is also the possibility that erosion rates were non-steady during

periods of dramatic climate change in the Pleistocene (Heimsath, 2006). However, this is not seen in the compiled SPR data. With the exception of one dataset (Heimsath et al., 2001b) all TCN-derived SPR fall within the same range and do not vary as much as expected with recent climate and differing underlying soil parent materials. As exemplified in Figure 4.17, differences fall within one order of magnitude.

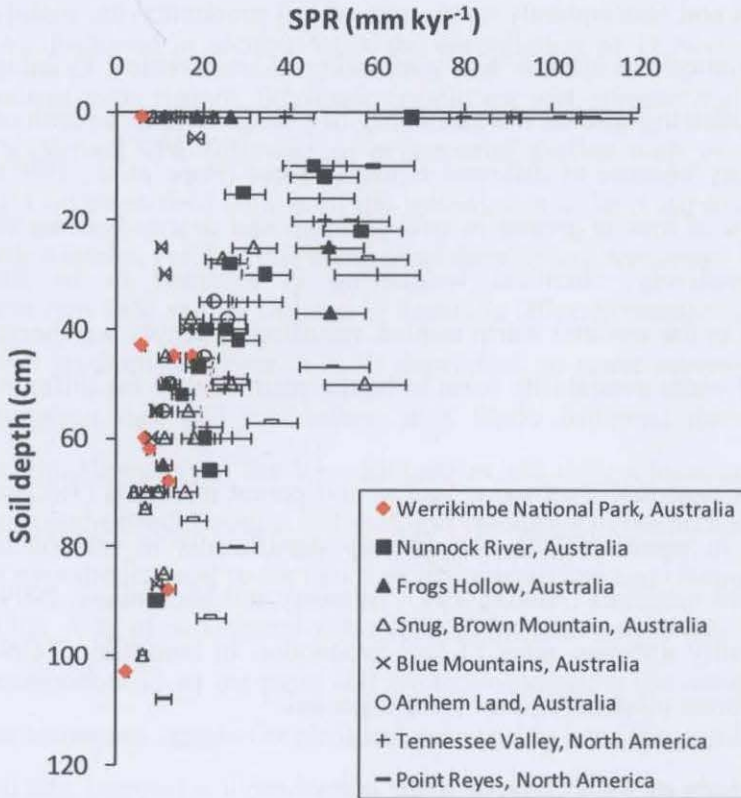
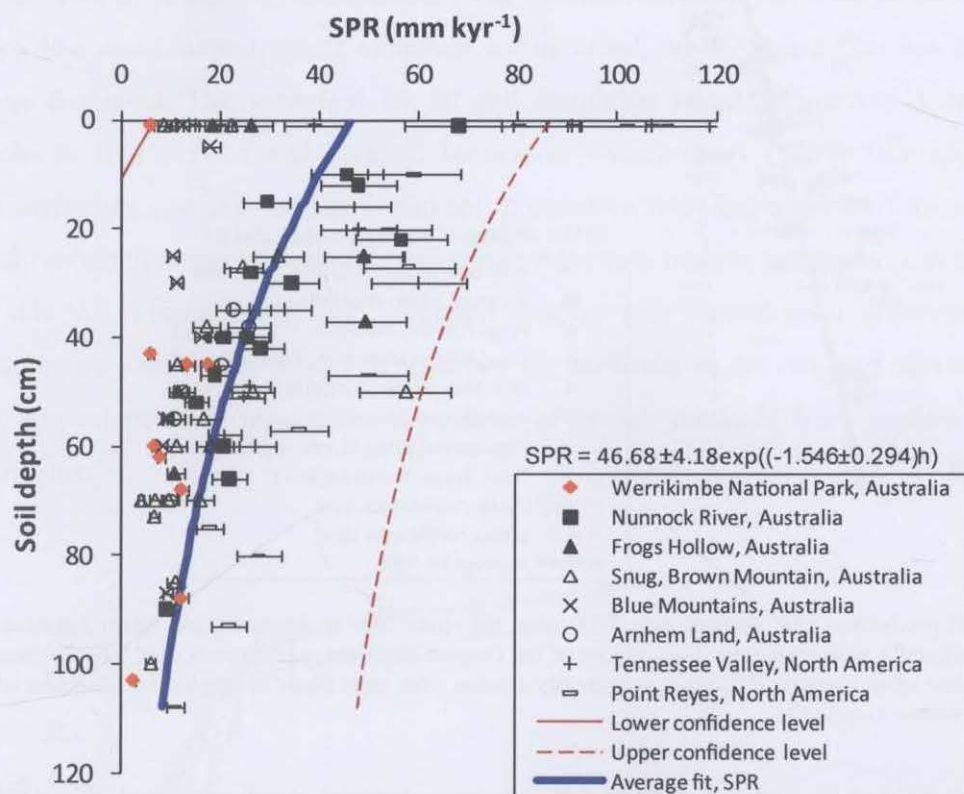


Fig. 4.17. Soil production rates derived with TCN data, for study sites in Australia and North America. The dataset from the Oregon Coast Range is not included in the graph. It can be seen that TCN-derived SPR fall within the same range and do not vary much in orders of magnitude. SPR are plotted conventionally as in pedology, demonstrating the behaviour of a parameter down the soil profile.

This observation concurs with other studies, which used different methods to investigate rates of soil formation. Pope et al. (1995) reviewed quantitative weathering data based on chemical weathering studies (solutes, mass-balance approach) for a wide range of climates from polar to tropical humid. Their data did not reveal a climatic signal, sparking the question of whether the top-down assumption of weathering being based on climatic zones is overrated. Pope et al. (1995) then proposed a bottom-up perception of weathering processes where geographic variability in weathering is controlled by the variability in weathering processes that operate at microscale. Furthermore, a study based on uranium-series isotopes (Dosseto et al., 2008) suggested that the rate of bedrock weathering at a study site in temperate Australia was defined through the same order of magnitude as the rate inferred for laterites in tropical climates.

Taking this into consideration, it was concluded that an average rate of soil formation can be formulated based on TCN-derived SPR for semi-arid to tropical environments. Thus, implementing the discussed field studies an average best fit of the data was calculated to generate an average potential weathering rate of the soil parent materials of  $47 \pm 4 \text{ mm kyr}^{-1}$  for  $P_0$  with  $b = -1.546 \pm 0.294 \text{ mm}^{-1}$  (Figure 4.18a (displays original values) and 4.18b (displays the log-scale)).



**Fig. 4.18a.** Average soil production rate, derived with TCN data, for study sites in Australia and North America. SPR are plotted conventionally as in pedology. The data set of the Oregon coast range (Heimsath et al., 2001a) was excluded from calculations of an average SPR. Here, non-steady erosion rates most likely accounted for one order of magnitude higher SPR values. Original values.

The value for  $P_0$  of  $47 \pm 4 \text{ mm kyr}^{-1}$  represents a mean SPR and is useful for indications of the magnitude of (global) soil production. The estimated average rate of soil formation from TCN-derived SPR is within the range of proposed global rates of soil formation of  $58 \text{ mm kyr}^{-1}$  and  $83 \text{ mm kyr}^{-1}$  (Montgomery, 2007; Wakatsuki and Rasyidin, 1992). In suggesting an average TCN-derived SPR, it needs to be clarified here that the soil production rate mostly reflects the physical interactions that develop a soil profile by converting parent material to soil (Burke et al., 2007). Therefore, the variation in chemical weathering of different soil parent materials does not have a major input (White and Brantley, 2003) as SPR are mainly related to the thickness of the soil profile. Consequently, processes that lead to alterations of the soil profile, eventually

forming a particular soil horizon or soil type, are not considered. Hence, formulating an average soil production rate does not imply uniform soil profiles or soil types.

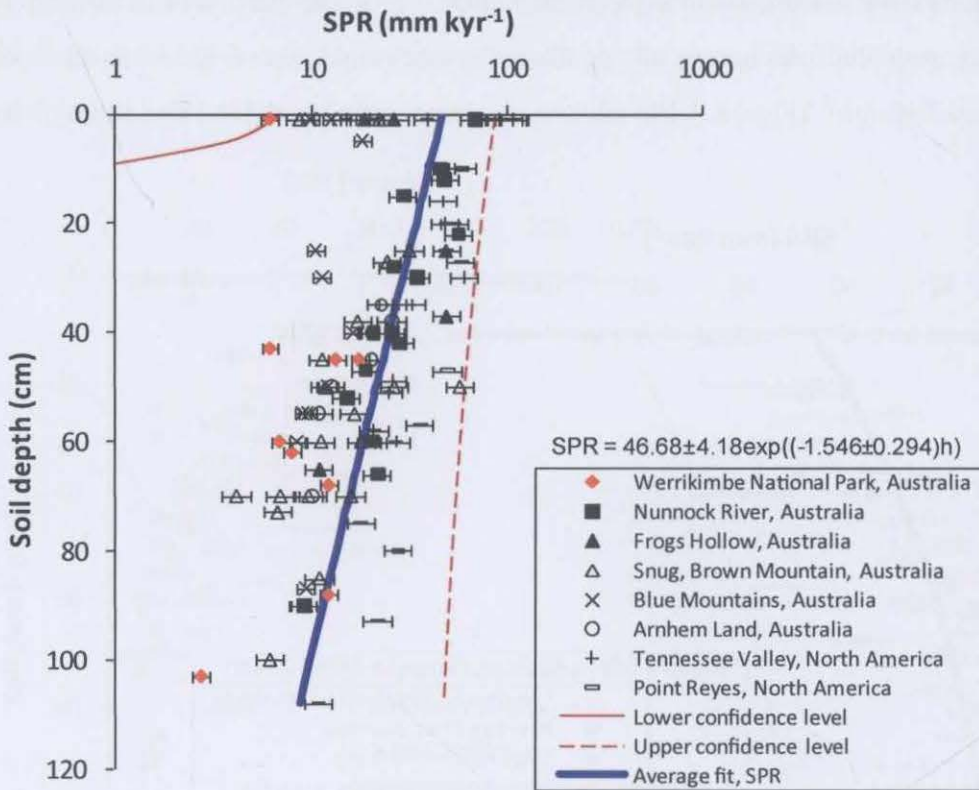


**Fig. 4.18b.** Average soil production rate, derived with TCN data, for study sites in Australia and North America. SPR are plotted conventionally as in pedology. The data set of the Oregon coast range (Heimsath et al., 2001a) was excluded from calculations of an average SPR. Here, non-steady erosion rates most likely accounted for one order of magnitude higher SPR values. Log-scale.

Recent studies have investigated the relationship between physical weathering and chemical weathering in the conversion process of soil parent materials to soil. These studies applied TCN-derived SPR in combination with various weathering indices. For example, Burke et al. (2007) and Yoo et al. (2007) found that chemical weathering accounts for 13 to 51 % of total weathering in soils, respectively. Green et al. (2006) published similar percentages for the study site at Nunnock River in the Bega Valley, south-eastern Australia (Heimsath et al., 2000), implying that mass loss in solution accounted for 35 to 55 % of the total mass loss from the investigated hillslope. Another study examined the extent of chemical weathering, comparing field sites in the lowlands and highlands around the area of the Bega Valley (Burke et al., 2009). This study indicated that the extent of chemical weathering is lower in the highland sites (47 %) than in lowland sites (57 %). Similarly, results comparing weathering rates (chemical and physical) along a transect from low to high elevation by Dixon et al. (2009) for the Sierra Nevada Mountains, California imply that chemical weathering peaks at mid elevations compared

to high and low elevation sites and that physical erosion rates increase with both saprolite weathering rates and intensity. These studies indeed confirm that physical weathering is the dominant process in converting parent materials to soil.

#### 4.5.6 Comparison of SPR with soil formation rates derived from other methods

Furthermore, TCN-derived SPR were also compared with soil formation rates derived with other field methods (e.g. denudation, mass balance, solutes). Here, only soil formation rates on rock-like consolidated parent materials are included, which means that volcanic ash and loess were excluded. The compiled list of soil formation rates (in  $\text{mm kyr}^{-1}$ ) derived from other methods is a revised and updated version of Montgomery (2007) (see appendix, Table 2). Characteristics of soil formation and soil production rate distributions of the compiled data sets and probability distribution plots show that there is a relative consistency in the collective data (Table 4.4, Figure 4.19). The compiled data on soil formation or weathering rates confirm assumptions made that there is a tendency for similarity in the range of data on soil weathering on the micro- and mesoscale, regardless of which methods were applied to quantify soil formation.

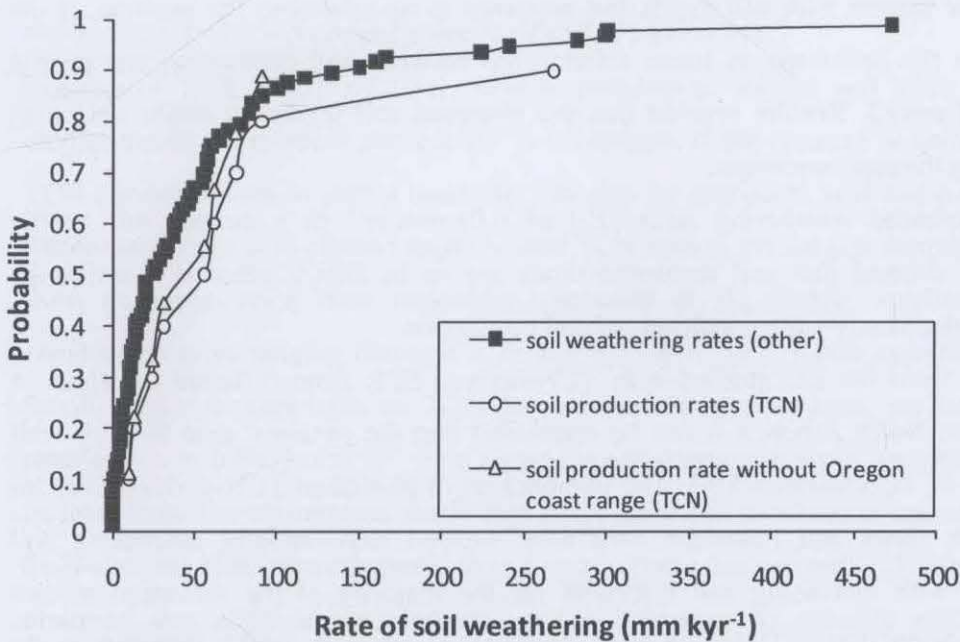


Fig. 4.19. Probability distribution plots of rates of soil production derived with *in situ* TCN data and weathering rates of soil derived with other methods. Probability distribution plots show that there is a relative consistency in the datasets.

**Tab. 4.4.** Characteristics of soil formation and soil production rate distributions for the compiled data sets.

	Method	Sample size, n	Median [mm kyr <sup>-1</sup> ]	Mean [mm kyr <sup>-1</sup> ]	Standard error [mm kyr <sup>-1</sup> ]
Soil production rate (SPR)	TCN ( <sup>10</sup> Be)	127	25.99	50.37	5.54
Soil weathering rate	Other (denudation, mass-balance, solutes)	125	14.80	41.83	6.34

#### 4.6 Conclusions

1. The rate of soil formation over time has been discussed extensively in the literature on pedogenesis. In recent years, with the application of TCN techniques in pedogenesis it has become possible to quantify the formation of a soil profile *in situ* over millennial time scales. The TCN dating method was applied to derive soil production rates for the high country rainforest park of Werrikimbe National Park in south-eastern Australia. At the studied site SPR varied between 3 and 18 mm kyr<sup>-1</sup> under 43 to 103 cm thick soils. These results represent the lowest SPR determined to date, with a potential average weathering rate ( $P_0$ ) of the soil parent material of 10 mm kyr<sup>-1</sup>. At Werrikimbe National Park soil production followed no clear pattern with soil depth, but appeared to be related to the position of the toposequences in the landscape. A linear relationship between soil production and profile curvature was observed. Results implied that the observed soil thickness might not be in equilibrium along the toposequences.
2. Implementing potential weathering rates ( $P_0$ ) of 0.01 mm yr<sup>-1</sup> in a simple soil profile evolution model showed that soil residence times are up to 80000 years at Werrikimbe National Park under steady-state conditions of soil production.
3. Comparing SPR from the site studied with TCN-derived SPR from different locations in Australia and also North America it can be concluded that the obtained data fit very well within the range of TCN-derived SPR. The compilation of published TCN-derived SPR for different climatic zones and lithologic conditions showed exponentially decreasing soil production rates with increasing soil thickness for the majority of the discussed studies (Heimsath et al., 2000, 2001a; Heimsath et al., 2006; Heimsath et al., 1997; Heimsath et al., 1999; Heimsath et al., 2001b; Heimsath et al., 2005). At two study sites the interpretation of the SPR implied that soil formation followed a humped function because soil production rates were greatest under an incipient soil thickness (Heimsath et al., 2009; Wilkinson et al., 2005b). Nevertheless, the unequivocal field evidence for the conceptual model of a humped



soil formation and its parameterization from field data (Gilbert, 1877) is yet to be achieved with TCN-derived SPR.

4. The conclusion was drawn that the calculation of SPR with soil thickness is influenced by the observed distribution of TCN concentrations at different thicknesses of soil as well as the production rate of  $^{10}\text{Be}$ . For soil parent materials the annual TCN production needs to be corrected for the soil overburden, which attenuates the cosmic rays. By using equation 4.6 (Granger and Muzikar, 2001) to correct for TCN production as a function of depth, functions are applied which behave in an exponential way. The performed simulation showed that the slope of an exponential decline of soil production with increasing soil thickness is influenced by the attenuation of the observed TCN concentrations, as compared to the attenuation of the TCN production rate.
5. The presented compilation of TCN-derived SPR showed that the values of potential weathering rates ( $P_0$ ) appeared to be very similar for the investigated environments. Values of conversion rates of parent materials to soil did indeed vary, though not as much over orders of magnitude as expected. It is not implied, however, that SPR did not vary, just not as much in orders of magnitude. The observed trend in the data set on SPR resulted in the assumption that an average soil production rate can be formulated for semi-arid to tropical environments with a proposed value for  $P_0$  of  $47 \pm 4 \text{ mm kyr}^{-1}$ .
6. The use of TCN is still relatively new in pedological studies and more data for different environments are needed, particularly to investigate if the concept of calculating SPR from TCN concentrations in parent materials can also be applied to arid and polar environments. Recent studies in cold climate regimes used TCN data to investigate denudation rates derived from moraines since their deposition (Schaller et al., 2009a; Schaller et al., 2009b). Denudation rates ranging between  $4.78$  and  $8.15 \text{ g m}^{-2} \text{ yr}^{-1}$  ( $0.004$  and  $0.007 \text{ mm yr}^{-1}$ ) were found. And reflecting back on TCN-derived outcrop erosion rates, we learned that erosion rates as low as  $0.0003 \text{ mm yr}^{-1}$  were found for outcropping rocks in Antarctica.
7. In relation to the assumption made that an average soil production rate can be formulated, TCN-derived SPR were compared to soil weathering rates derived with other methods. It was observed that none of the methods used in pedology to quantify soil weathering rates detected significant differences related to different climatic zones.
8. The assumption of an insensitive soil production rate is rather counter-intuitive and leads to the question, to what extent are limitations or uncertainties in the field methods (i.e. corrections for the soil overburden and slope) actually masking possible geographical variations in soil production data. And therefore is the relative consistency of SPR a function

of the uncertainty of the TCN methods or a real consistency in weathering? It was hypothesized that uncertainties in the methods of determining soil production rates or soil weathering rates from real-world data may potentially mask climatic variations.

## Chapter 5 Optically stimulated luminescence

In this chapter the application of optically stimulated luminescence (OSL) to investigate ‘*in situ*’ soil formation over millennial time scales is reviewed followed by the presentation and discussion of OSL derived single-grain age estimates for the area studied. Subsequently, estimates of pedogenic processes (vertical and lateral soil mixing rates) from OSL data will be discussed. Furthermore, the principles and results of the analysis of fallout radionuclides ( $^{137}\text{Cs}$ ,  $^{210}\text{Pb}_{\text{ex}}$ ), determined during OSL analysis are presented.

### 5.1 Principles of OSL for investigating pedogenesis

Optically stimulated luminescence is a dating method based on the exposure of mineral grains to solar radiation, which occurs due to the movement of soil particles on or close to the soil surface. This technique relies on the ability of some mineral grains to trap electrons in their crystal structure and accumulate a charge over thousands of years. The capacity of mineral grains to trap electrons in their crystal structure is the result of imperfections in their crystal lattice which has the potential to accommodate a population of electrons. The size of the electron population, which equals the amount of radiation received, relates to the dose the grains received when they were last exposed to sunlight (Aitken, 1994).

The overall dose the grains received is the result of small quantities of cosmic radiation and the natural ionising radiation that is emitted from the soil surrounding the mineral grains. The flux of ionising radiation (alpha-, beta- and gamma-rays) results from very low concentrations of uranium ( $^{235}\text{U}$ ,  $^{238}\text{U}$ ), thorium ( $^{232}\text{Th}$ ), potassium ( $^{40}\text{K}$ ) and rubidium ( $^{87}\text{Rb}$ ) in the soil. The population of electrons trapped in the crystal structure increases in response to the ionizing radiation the minerals are exposed to after being buried and shielded away from sunlight. Therefore, the more light or energy emitted by the mineral grains after being exposed to light of a specific wavelength, the longer the mineral grains have been buried away from sunlight (Aitken, 1998; Olley et al., 2004).

The advantage of the OSL technique is that the ‘clock’, which started ‘ticking’ after burial can be set back to zero by exposing the mineral grains to light, which is commonly referred to as resetting, zeroing or bleaching (Madsen et al., 2005). During the bleaching process the emitted radiation level is measured by a photomultiplier in units of gray (Gy), where the unit gray is defined as the energy per unit mass that the mineral grains absorbed from the flux of surrounding radiation (1 Gy stands for  $1 \text{ J kg}^{-1}$ ).

However, to calculate a burial age for each mineral grain, the weighted annual radiation flux it received over time also needs to be known. The annual radiation flux or dose rate can be determined by measuring the concentration of radionuclides in the sample via gamma spectrometry. The evaluation of the total annual dose rate therefore includes a combination of the average cosmic ray dose rate and the total terrestrial dose rate that the sample received over time. The total terrestrial dose rate consists of the dose rate from alpha-rays, the dose rate from beta-rays and the dose rate from gamma-rays, which is calculated from element concentrations of uranium ( $^{238}\text{U}$ ), radium ( $^{226}\text{Ra}$ ), lead ( $^{210}\text{Pb}$ ), potassium ( $^{40}\text{K}$ ) and thorium ( $^{232}\text{Th}$ ) in the soil sample.

For the accurate calculation of the annual dose rate, both the bulk density and the moisture content of the sample material have to be considered to adjust for effects of compaction and soil moisture, because water can absorb parts of the radiation that would otherwise reach the mineral grains in dry conditions. The natural dose of wet soil is lower than in dry conditions. Therefore it is necessary to document the water content in the field and also to estimate the average wetness of the soil during burial time (Aitken, 1998).

Combining the dose and the annual dose rate makes it possible to calculate a burial age for individual mineral grains:

$$\text{Burial age (yr)} = \frac{\text{Dose, } D_e \text{ (Gy)}}{\text{Dose rate, } D_r \text{ (Gy yr}^{-1}\text{)}} \quad \text{equation (5.1)}$$

Some terms that are often used in publications on OSL research need to be clarified. The dose the grain received since its burial is also called the Paleodose or the equivalent dose (ED), whereas the dose rate is often also referred to as the annual radiation dose. Here, the terms 'dose' and 'dose rate' will be used exclusively.

### 5.1.1 Mineral grains used for OSL

It is very important for OSL dating that the mineral grains studied have the capacity to produce a luminescence signal in their crystal structure and are relatively abundant in the sample materials (Duller, 1996). Both quartz and feldspar fulfil these requirements and are subsequently the primary minerals used for luminescence dating.

Another important factor when considering OSL dating is to work with minerals that are known for bleaching fast, since dating is based on the exposure to sunlight. Generally, mineral grains need to be sufficiently exposed to enough light in order to be completely reset to zero.

This is especially important for dating younger mineral grains (around 100 years) and for the application of OSL in pedology.

Quartz has preferentially been chosen for luminescence studies because it is known for bleaching fast and its bleaching process is faster than that of feldspars (Madsen et al., 2005). Additionally quartz grains unlike feldspars are more or less free of internal radioactivity, which would otherwise contribute to the total radioactivity received (Aitken, 1998).

Quartz grains sampled from relatively stable environments like forest soils can have reduced luminescence intensities because they were not exposed to adequate amounts of sunlight (Bush and Feathers, 2003). This is in contrast to soil samples from depositional environments (i.e. fluvial) or sand dunes where quartz grains stay in suspension, in either air or water, for an extended period of exposure to sunlight prior to deposition and burial.

### **5.1.2 Development of the luminescence technique for dating Quaternary sediments**

This is a brief review about the development of the luminescence dating technique and its application for dating Quaternary sediments (up to 500 kyr). More detailed reviews on this topic can be found in Aitken (1994, 1998), Duller (1996) or Murray and Olley (2002).

Luminescence dating has been used since the 1960s to provide chronological information for minerals from sedimentary environments. Early applications of luminescence dating were based on thermoluminescence techniques. In thermoluminescence dating, the luminescence signal of mineral grains is set back to zero through exposure to heat instead of light (Duller, 1996).

Techniques of optically stimulated luminescence were developed in the mid 1980s (Huntley et al., 1985). Since then OSL has become preferable to thermoluminescence dating because only the signal received from light-emitted traps is used after stimulation. With thermoluminescence it was not possible to distinguish the individual signals received from thermal and optical sources. In the past decade OSL analysis has been mainly based on infrared (IR) stimulation of feldspars. Working with quartz grains still had its limitations, because of the insensitivity of quartz to IR stimulation and the high costs of visible light stimulation. Subsequent improvements in visible light stimulation due to the development of cost-effective visible lasers made it possible to use the mineral quartz in optical dating (Murray and Olley, 2002).

Occurring simultaneously with the changes in the luminescence technique were significant changes in measurement protocols for OSL analysis; the development of the single-aliquot method in the late 1990s, allowed single grains (aliquots) to be measured (Murray and Roberts, 1997). Up until the development of the single-grain approach, OSL analysis was based on

multiple aliquots with 20 to 80 sub-samples (aliquots) per sample. Per aliquot around 10 mg of quartz (equivalent to 1000 grains) was measured to determine the dose the sample received since burial. To compensate for the variation between aliquots some form of normalization was required, which increased the uncertainty of the data. Using multiple aliquots often resulted in an over or underestimation of mean depositional ages especially in environments where the distribution of the OSL data may have been skewed rather than normal (Duller, 2006).

Measurements of single aliquots became valuable in luminescence dating because uncertainties were reduced when calculating the mean exposure or deposition ages, especially for poorly bleached samples like soil. This technique allows for a single grain to be used for repeated measurements to gradually generate a calibration curve for the particular grain. This is possible because the luminescence signal accumulated in the crystal structure of the mineral grain is not removed completely as in thermoluminescence dating. Hence, the dose is calculated for each single grain, and mean dose ages from the same sampling depth can be estimated based on the distribution of individual doses the grains received (Jacobs et al., 2006).

With single grain OSL analysis, both the single-aliquot additive dose protocol and the single-aliquot regenerative-dose (SAR) protocol are available (Murray and Roberts, 1997; Murray and Roberts, 1998). The single-aliquot additive dose protocol adds known laboratory doses to the natural dose before the OSL measurement, while in the regenerative dose protocol the OSL signal is measured from the natural dose and then known doses are added. In recent years the SAR protocol has been revised and improved (Murray and Wintle, 2000; Olley et al., 2004) and is now the principal method used for OSL research. In this thesis the SAR protocol of Olley et al. (2004) was applied. Olley et al. (2004) modified the SAR protocol by introducing an IR stimulation at 125°C before OSL stimulation to completely isolate the OSL signal received from quartz grains from the signal received from feldspars. This new improved method increased the reliability of age estimations from OSL data.

The development of the SAR protocol opened up the possibility of applying OSL techniques in pedology. With OSL, individual quartz grains from a soil profile can now be dated. Hence, it is possible to study the distribution of ages from individual quartz grains down the soil profile. This distribution can be used as a direct measurement of possible soil mixing rates, particularly from the surface layers of the soil profile. Therefore, the application of the OSL technique for pedology has made it possible to quantify vertical processes of soil formation (Bush and Feathers, 2003; Wilkinson et al., 2009).

### 5.1.3 Applications of OSL to pedogenesis

As emphasised in the previous section, single-grain OSL analysis can be used to calculate the burial time of individual quartz grains in a soil profile. These data can then be used to estimate the age of quartz grains distributed down the soil profile. This offers the opportunity to investigate pedogenesis quantitatively by estimating soil mixing rates and the age of soil horizons directly from field data. In theory, dating soil horizons can be achieved by calculating an appropriate mean age by running different statistical models (Bateman et al., 2003; Galbraith et al., 1999; Jacobs et al., 2006; Lepper and McGeever, 2002). But this approach has its limitations if single grain dose distributions are not normally distributed, which is common in soils where adjacent mineral grains could be from different origins because of pedoturbation processes (Wilkinson and Humphreys, 2005). Mixing rates of soil can be identified by studying the age distribution from individual quartz grains in the soil profile and along the hillslope.

For instance, Wilkinson and Humphreys (2005) proposed that with OSL the occurrence of soil mixing by faunal agents can now be investigated directly from field data to verify frequent rates of bioturbation suggested in the literature (see Box 2.2). They hypothesized that with a lack of mixing agents soil profile development along a hillslope might occur in a similar manner to the mechanisms of an 'elevator', where weathering of bedrock to soil takes place at the soil-bedrock or soil-saprolite interface. In this scenario weathering products might only 'see' the soil surface via downslope transport. Consequently, soil particles are the youngest at the base of the soil profile with ages increasing linearly towards the soil surface, which is frequently bleached by processes like rainwash. Therefore, it was argued that most likely only near surface grains would return an OSL age whereas all other grains further down the profile would be undateable. However, reflecting back on section 2.3.3 field observations suggested that the 'elevator'-like soil profile development is abundantly disrupted by soil mixing agents, who revise the allocation of soil particles throughout the soil profile. These mechanisms need to be clarified further with dating mineral grains *in situ*.

The single-grain OSL technique has been applied widely in dating of aeolian, fluvial, marine, glacial and colluvial sediments of Holocene and Late Pleistocene origin (i.e. Madsen et al., 2005; Murray and Olley, 2002; Olley et al., 1999), but its application in conjunction with pedology to improve our understanding of pedogenic processes is still limited (Wilkinson and Humphreys, 2005).

Single grain OSL has been used in pedological studies to investigate creeping soil (Heimsath et al., 2002), to study the effect of pedobioturbation (Bateman et al., 2003; Bush and Feathers,

2003; Forrest et al., 2003; Heimsath et al., 2002; Wilkinson et al., 2005b), to date Paleosols and loess (i.e. Priori et al., 2008; Schmidt et al., 2009), to better understand soil evolution in young floodplains (i.e. Lair et al., 2009) and to study soil erosion and alluvial or colluvial deposition (i.e. Eriksson et al., 2000; Fuchs et al., 2010). Most of these studies used the single grain OSL technique to estimate the age of soil layers in order to investigate the Quaternary history of the field site.

The research by Heimsath et al. (2002), Bush and Feathers (2003) and Bateman et al. (2003) focused on age estimations, and attempts were also made to model the distribution of dose values down the soil profile. Heimsath et al. (2002) explored soil erosion processes associated with soil creep in south-eastern Australia. At the study site in the Bega Valley, OSL dating indicated transport of sand sized grains from 1 m down the soil profile up to the soil surface and vice versa with calculated vertical rates of downward movement between 0.1 and 0.4 mm yr<sup>-1</sup> and much higher lateral downslope depth-averaged velocities of between 5.9 and 12.0 mm yr<sup>-1</sup>. Distributions of mean ages of sand-sized grains down the profile showed that mean ages increased with soil depth, with grains younger than a 1000 years in the top 10 cm and grains of 10000 years of age at 85 cm. Comparing mean grain ages with soil residence times, calculated from TCN-derived soil production rates, they hypothesized that soil grains visited the soil surface repeatedly. Heimsath et al. (2002) suggested that bioturbation, especially burrowing agents, played a dynamic role in increasing the transport velocities measured at the site and demonstrated the hypothesis of a soil creep model based on Monte Carlo stimulations.

Bush and Feathers (2003) examined the distribution of single-aliquot and single-grain derived dose values in anthropogenic soil profiles and concluded that pedoturbation was the main driver for resetting the luminescence signal at the site. Their study also exemplified the tendency for the population of near-zero aged grains to decrease down the soil profile. The authors proposed a three-zone model, to explain the processes of surface bleaching of mineral grains, where the surface layer of the topsoil is continuously stressed by subaerial and subsurface mechanisms creating surface relief (Figure 5.1).



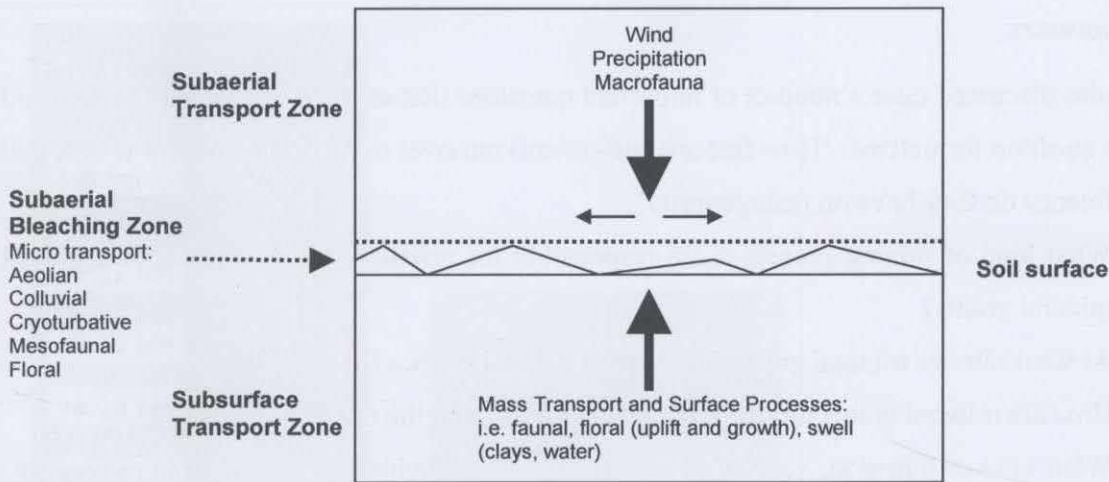


Fig. 5.1. A three-zone model for soil-surface disturbances (after Bush and Feathers (2003)).

Bateman et al. (2003) investigated the effects of pedoturbation on luminescence dating of sedimentary deposits. They concluded that near-surface pedoturbation was the main transport mechanism disturbing the distribution of dose values in deposits. Bateman et al. (2003) proposed three hypothetical effects of bioturbation on dose distributions in the profile (Figure 5.2):

- (1) Undisturbed well-bleached deposits have the tendency to be normally distributed.
- (2) The occurrence of minor bioturbation processes has the tendency to mix younger or older grains and consequently dose distributions may be skewed.
- (3) Frequent mixing of grains has the tendency to lead towards homogeneity, which may be displayed by a wide range of dose values with low frequencies.

This work by Bateman et al. (2003) has important implications for understanding the distribution of dose values sampled from different depths within a soil profile.

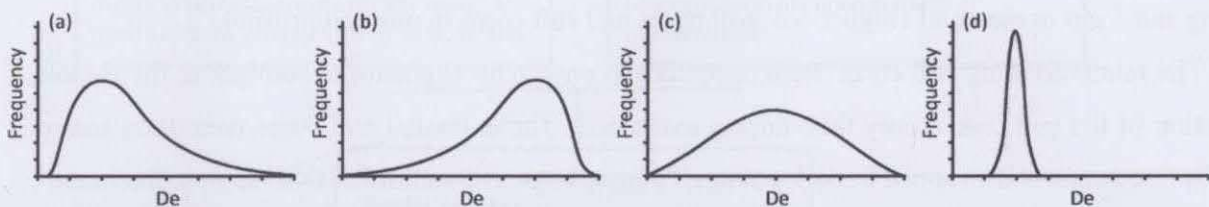


Fig. 5.2. Proposed effects of pedoturbation on the distribution of dose values,  $D_e$  in Gy, measured with OSL (source: graph and captions based on Bateman et al. (2003)). (a) A sample into which older material has been mixed giving rise to a high  $D_e$  tail or skewed distribution. (b) A sample into which younger and exhumed material has been mixed giving rise to a low  $D_e$  tail or skewed distribution. (c) A sample in which mixing has caused near homogeneity giving a wide range of  $D_e$  values with a low frequency at any single value. (d) Undisturbed well bleached sample with a small  $D_e$  distribution and high reproducibility.

### 5.1.4 Summary

The studies discussed raise a number of important questions that are directly relevant to the third research question formalized: 'How fast are rates of soil turnover occurring in the soil profile and what influence do they have on pedogenesis?'.

- What kind of mixing processes are responsible for resetting the luminescence signal of mineral grains?
- At what rate are mineral grains bleached at the soil surface?
- How are mineral grains mixed in the bleaching zone of the upper soil profile?
- What kind of transport, vertical or lateral, is the predominant driver of grain movements in the soil profile?
- Do mixing processes lead to a homogenization of soil layers in the profile? Is there field evidence for such behaviour? Alternatively, does bioturbation lead to horizonation and texture contrast soils?
- Are mixing rates caused by pedoturbation as fast as the literature implies? Are soil mixing rates faster than the rate of soil production?

## 5.2 Materials and Methods

### 5.2.1 Sampling in the field for OSL analysis

The following sampling strategy was undertaken to eliminate the exposure of mineral grains to sunlight. Undisturbed soil samples for optically stimulated luminescence (OSL) were taken from the first 50 cm of each soil profile (5 cm, 20 cm, 30 cm, and 50 cm) using soil cores 26 cm long and 5 cm in diameter (Figure 5.3, soil cores and soil cores in one soil profile).

The relatively long soil cores were necessary to ensure no exposure to sunlight at the middle section of the soil core at any time during extraction. The extracted soil cores were then sealed with fitted caps and wrapped in dark coloured plastic bags. All additional OSL sample treatments and the sample analysis were carried out in a darkroom.

Ages for individual quartz grains were analysed for a dense increment of soil depths to investigate single-grain behaviour in the soil profile down to 50 cm depth.

OSL analysis was carried out at the luminescence laboratory at CSIRO Land and Water in Canberra, in collaboration with Dr Tim Pietsch, Prof. John Olley, Mr Ken McMillan and Dr Chris Leslie.

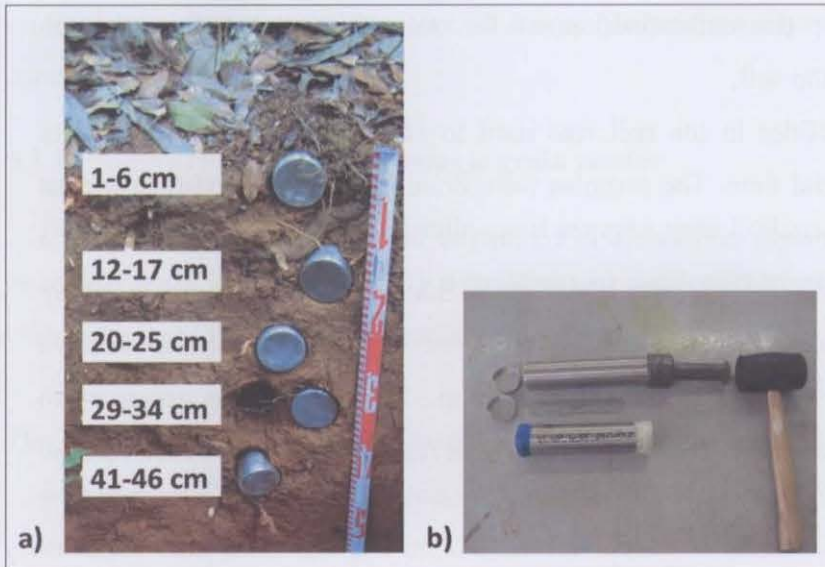


Fig. 5.3. Sampling in the field for OSL analysis. (a) Soil cores used (26 cm long and 5 cm in diameter). (b) Sampled soil depths exemplified with soil profile Te38.

### 5.2.2 Sample preparations for OSL analysis

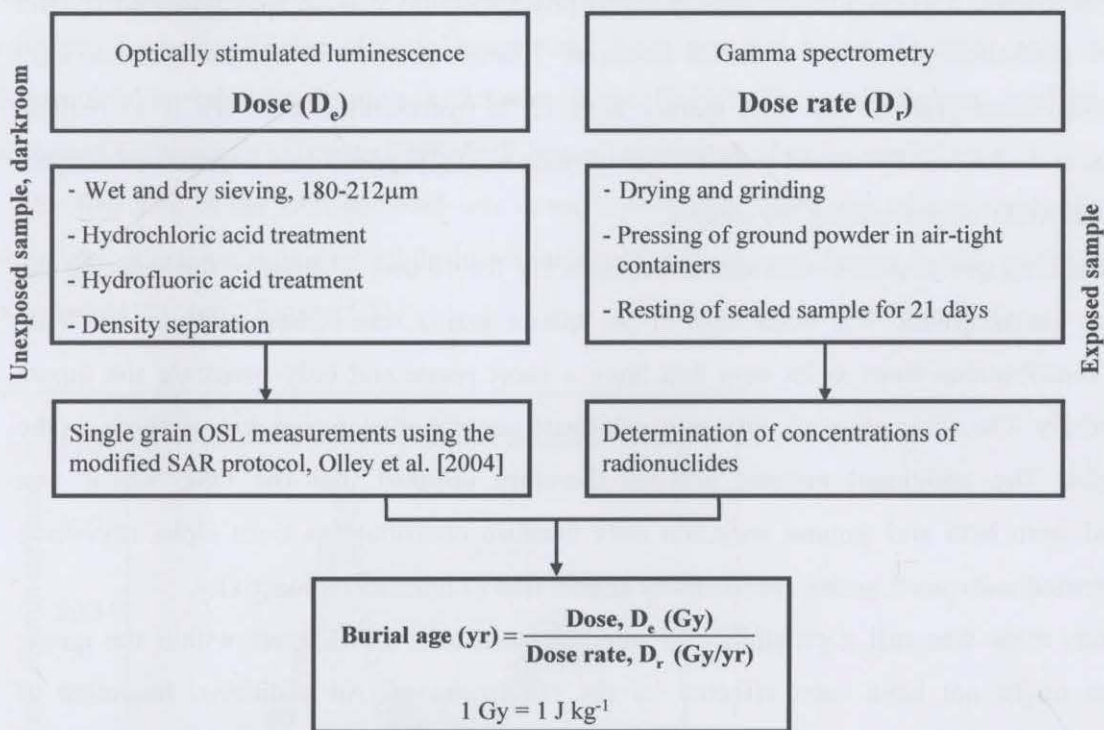


Fig. 5.4. Flowchart of OSL analysis

#### Sample preparations for gamma spectrometry

All soil sample pre-treatments and OSL analysis were carried out in a darkroom. In the darkroom, approximately 5 cm from the exposed ends of the sampled soil cores was removed.

These ends were then used for the determination of the soil moisture content and the concentration of radionuclides in the soil.

The concentration of radionuclides in the soil was used to calculate the annual dose rate received by the grains during burial time. The samples were dried, ground to an almost talcum like powder and pressed into air-tight containers to retain the inert gas radon-222 ( $^{222}\text{Rn}$ ), a daughter radionuclide of radium-226 ( $^{226}\text{Ra}$ ) with a half-life of 3.8 days (He and Walling, 1996). The sealed powder samples needed to rest for a minimum of 21 days in order to achieve radioactive equilibrium between  $^{226}\text{Ra}$  and  $^{222}\text{Rn}$  (Madsen et al., 2005). This was necessary to ensure precise measurement of the radionuclide content via high resolution gamma spectrometry.

#### *Sample preparations for OSL*

The unexposed part of the soil core sample was used for OSL analysis to determine the dose individual quartz grains received since burial. This section explains the method of isolating quartz grains from the soil samples for analysis on the OSL photomultiplier.

In the darkroom, a 10 % sodium hexametaphosphate solution was applied followed by wet sieving the sand-sized grains into different fractions. The fraction of 180-212  $\mu\text{m}$  (particle size: medium-sized sand grains) was then treated with 15 % hydrochloric acid (HCl) to remove carbonates, and additionally etched in 40 % hydrofluoric acid (HF) for 5 min to remove feldspars and other minerals contaminating the sample.

The remaining quartz grains were again etched in HF for 40 min to dissolve the outer 10  $\mu\text{m}$  rind of the quartz grains. The outer rind of the quartz grains was etched away to eliminate radiation contributions from alpha rays that have a short range and only penetrate the quartz grains partially. The attenuation of alpha rays can cause uncertainties during dose analysis on the OSL reader. The additional etching process therefore ensured that the OSL signal was determined from beta and gamma radiation only because contributions from alpha rays have been eliminated and quartz grains are naturally almost free of internal radioactivity.

However, there was still a possibility of internal inclusions of feldspars within the quartz grains that might not have been affected by the HF treatment. An additional treatment of hydrochloric acid (HCl) was applied for 10 min to remove possible acid soluble fluorides. Complete elimination of minerals lighter (feldspar) or heavier (black magnetite minerals and zircon) than quartz ( $2.65 \text{ g cm}^{-3}$ ) was ensured by density separation using a solution of lithium heteropolytungstates heavy liquids (LST).

The final steps of the laboratory treatment involved sieving through a 180  $\mu\text{m}$  sieve to remove fractional grains followed by drying of the quartz grains. Isolated quartz grains were then placed

on five aluminium discs with a 10 x 10 array of holes for analysis on the OSL reader. Each disc contained 100 quartz grains.

### 5.2.3 Procedure of OSL on the single grain reader

Because of the difficulties of dating soil samples with OSL, a minimum of 500 quartz grains were analysed for each sample. This strategy was applied to ensure an adequate number of grains with sufficient OSL signals for statistical analysis.

#### *The single aliquot-regenerative dose protocol*

Single grain OSL measurements were made on a Risø TL/OSL DA-15 reader that applied a green laser with a wavelength of 532 nm for optical stimulation and using the modified SAR protocol from Olley et al. (2004) (Table 5.1). As demonstrated in Table 5.1, the SAR protocol compares the OSL signal resulting from a natural dose to the OSL signals resulting from regenerated and therefore artificial doses to ultimately calculate a date or dose for a single grain. The regenerated or artificial OSL dose was induced in the sample by a known dose of laboratory radiation. Emissions in the ultraviolet spectrum were detected by an Electron Tube 9235QA photomultiplier tube fitted with a 7.5 mm Hoya U-340 filter. Irradiations applied in the laboratory employed a calibrated  $^{90}\text{Sr}/^{90}\text{Y}$  beta source attached to the reader.

The first step of the SAR protocol was to run a preheat at 240°C for 10 s to empty the ‘traps’ within the quartz crystals that might have been partially emptied during burial, particularly the so-called 110°C trap (Figure 5.5).

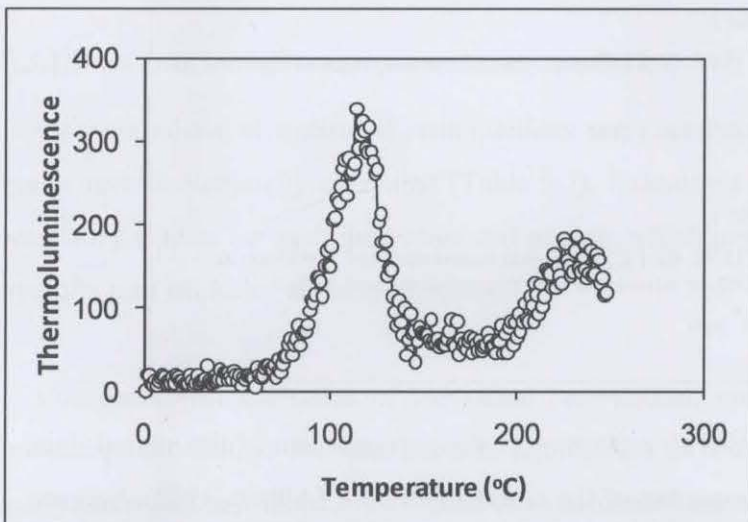


Fig. 5.5. Thermoluminescence. Peak from the so-called 110°C trap observed after natural irradiation.

The charge at 110°C has a lifetime of less than a day and therefore does not contribute to the natural dose. However, laboratory artificially-produced regenerated doses will record contributions from the 110°C trap since the grains were stimulated within a few hours of measuring their dose. Preheating is therefore necessary to ensure that the natural and artificial doses both result only from traps with very long half lives.

After the preheating process infrared radiation was applied to the quartz grains for 40 s at 125°C. The purpose of this infrared wash was to remove all charges from any remaining feldspars that might still be trapped in the sample after chemical elimination. This IR wash did not affect the quartz grains themselves in any way. Throughout the SAR protocol a small, constant test dose was applied followed by the stimulation and measurement of the natural or the regenerated OSL signal (Table 5.1) (Murray and Wintle, 2000).

**Tab. 5.1.** Modified single-aliquot regenerative-dose (SAR) protocol (after Olley et al. 1994).

<b>Run 1 Set 2</b>	Preheat at 240°C for 10 s to empty traps which might have partially emptied during burial
<b>Run 1 Set 3</b>	Infrared radiation at 125°C for 40 s to remove any remaining feldspars and therefore possible trapped charges that might contaminate the OSL signal
<b>Run 1 Set 4</b>	Stimulation with green laser at 125°C for 1 s, single grain OSL measurement of the 'Natural Dose', hence the trapped charge population built up during burial
<b>Run 1 Set 5</b>	Application of the Test Dose, beta radiation for 10 or 50 s, standard dose which is applied throughout the sequence to monitor changes in sensitivity
<b>Run 1 Set 6</b>	Preheat at 160°C for 10 s to remove the charge from very short lived traps (110 °C trap)
<b>Run 1 Set 7</b>	Infrared radiation as in Run 1 Set 3
<b>Run 1 Set 8</b>	Stimulation with green laser at 125°C for 1 s, single grain measurement of the Test Dose, to calculate sensitivity corrected OSL as $OSL_{Natural}/OSL_{Test\ Dose}$
<b>Run 2 Set 1</b>	Application of the First Regeneration Dose to create a 'growth curve' (standards curve)
<b>Run 2 Set 2</b>	Preheat as in Run 1 Set 2
<b>Run 2 Set 3</b>	Infrared radiation as in Run 1 Set 3
<b>Run 2 Set 4</b>	Stimulation with green laser at 125°C for 1 s, single grain OSL measurement of First Regeneration Dose
<b>Run 2 Set 5</b>	Application of same Test Dose as in Run 1 Set 5
<b>Run 2 Set 6</b>	Preheat as in Run 1 Set 6
<b>Run 2 Set 7</b>	Infrared radiation as in Run 1 Set 3
<b>Run 2 Set 8</b>	Stimulation with green laser at 125°C for 1 s, single grain measurement of Test Dose, to calculate sensitivity corrected OSL in response to First Regeneration Dose with: $OSL_{1^{st}\ Regen}/OSL_{Test\ Dose\ following\ 1^{st}\ Regen}$
<b>Run 3 Set 1</b>	Return to Run 2 Set 1 etc.

This was necessary to relate the sensitivity pertaining to the measurement of the natural dose to the sensitivity pertaining to the measurement of the regenerated dose (Aitken, 1998), because laboratory treatments such as heating, bleaching and irradiating can change the sensitivity of quartz grains to OSL stimulation (Pietsch et al., 2008). Each natural and regenerated dose was

therefore corrected for possible changes in sensitivity using the applied test dose to monitor possible changes in grain sensitivity during the OSL analysis:

$$OSL_{\text{sensitivity corrected}} = \frac{OSL_{\text{natural}} \text{ or } OSL_{\text{regenerated}}}{OSL_{\text{Test Dose}}} \quad \text{equation (5.2).}$$

If an adequate test dose was used during analysis the OSL response should be independent of prior measurements and thermal or optical treatment (Murray and Wintle, 2000).

### 5.3 Results and discussion

Dose rates and single-grain doses were determined for the Mount Boss and Plateau Beech toposequences. Measured radionuclide concentrations from gamma spectrometry were used to derive annual dose rates and to interpret short-term patterns of pedogenesis. Annual dose rates were also applied to determine the age of individual quartz grains in conjunction with dose values from OSL analysis. The distribution of these individual grain ages was analysed.

Furthermore, tools used in geomorphologic studies such as radial plots and age models were implemented to display OSL dose data and to explore whether these tools can be readily used for analysing dose values from individual quartz grains taken from undisturbed soil samples. Finally, pedogenic processes are parameterized from OSL data and discussed.

#### 5.3.1 Dose rate and gamma spectrometry analysis

Concentrations of measured radionuclides were used to determine the dose rate the quartz grains received annually over time (Table 5.2). Calculated dose rates from different soil depths were very similar for each individual soil profile, which implies stable environmental conditions over the past centuries at the study site.

Comparison of the ratios of individual radionuclide concentrations can also be used as an indication of whether soil has been in equilibrium at site studied. This method relies on the assumption that soil materials evolved without disturbances with respect to the Uranium-decay-series chain. Within a 'closed' system uranium-238 ( $^{238}\text{U}$ ) and its daughter decay products should be in equilibrium.

Tab. 5.2. Dose rate data calculated from gamma spectrometry data.

Sample ID	$^{238}\text{U}$ [Bq kg $^{-1}$ ]	$^{226}\text{Ra}$ [Bq kg $^{-1}$ ]	$^{228}\text{Ra}$ [Bq kg $^{-1}$ ]	$^{210}\text{Pb}$ [Bq kg $^{-1}$ ]	$^{228}\text{Th}$ [Bq kg $^{-1}$ ]	$^{232}\text{Th}$ [Bq kg $^{-1}$ ]	$^{40}\text{K}$ [Bq kg $^{-1}$ ]	Dose rate [Gy kyr $^{-1}$ ]
<b>Toposequence Mount Boss (Tb)</b>								
Tb24 2.5-7.5	54±4	54±1	57±1	56±5	60±1	59±2	123±6	2.52±0.24
Tb24 11-16	55±3	56±1	63±1	54±3	62±1	62±1	125±4	2.48±0.23
Tb24 23.5-28.5	54±4	60±1	65±2	54±5	67±1	66±2	111±7	2.43±0.24
Tb24 43-48	60±3	60±1	75±1	45±3	76±1	75±1	119±4	2.45±0.24
Tb12 5-10	58±3	61±1	67±1	46±3	66±1	67±1	98±4	2.45±0.23
Tb12 18-23	60±3	63±1	67±1	53±4	70±1	69±2	98±5	2.49±0.24
Tb12 27-32	61±3	64±1	69±1	47±4	72±1	70±1	118±4	2.46±0.24
Tb12 42-47	66±3	66±1	75±1	40±3	74±1	75±1	106±4	2.37±0.24
Tb6 2.5-7.5	41±2	42±1	48±1	91±4	50±1	49±1	83±4	2.68±0.24
Tb6 13-18	50±3	51±1	52±1	63±3	56±1	54±2	99±4	2.39±0.22
Tb6 27-32	49±2	51±1	54±1	59±3	54±1	54±1	94±4	2.26±0.22
Tb6 40.5-45.5	51±3	54±1	58±1	39±3	56±1	57±1	100±4	2.02±0.20
<b>Toposequence Plateau Beech (Te)</b>								
Te38 1.5-6.5	61±4	58±1	57±1	58±5	60±1	59±1	20±3	2.28±0.23
Te38 12-17	54±3	56±1	60±2	45±4	60±1	60±1	15±3	1.98±0.20
Te38 29.5-34.5	68±3	58±1	69±2	48±4	71±2	70±2	14±4	2.15±0.23
TeM 4-9	59±3	59±1	55±1	60±3	57±1	56±1	29±2	2.26±0.22
TeM 12-16	60±3	67±1	61±1	53±4	60±1	60±1	26±3	2.15±0.22
TeM 21.5-26.5	64±3	64±1	66±1	47±3	68±1	67±1	23±3	2.13±0.22
TeM 29-34	63±4	63±1	72±2	51±4	71±2	71±1	27±5	2.24±0.24
Te3 4-8	50±4	50±1	57±1	49±4	57±1	57±1	65±4	2.20±0.21
Te3 10-15	46±3	52±1	56±2	52±4	56±1	56±1	65±5	2.14±0.21
Te3 18-23	47±3	51±1	56±1	41±3	58±1	57±1	71±3	1.98±0.20
Te3 31-36	51±3	54±1	59±1	37±3	61±1	61±1	56±4	1.91±0.20

Relevant ratios of radionuclide concentrations (radium-226, uranium-238, thorium-228, lead-210) are shown in Figures 5.6, 5.7 and 5.8 and will be discussed according to the following information:

- (1) Equal concentrations of naturally occurring  $^{238}\text{U}$  (half-life of 4.5 billion yr) and  $^{226}\text{Ra}$  (half-life of 1.6 kyr).  $^{226}\text{Ra}$  is a daughter product of the  $^{238}\text{U}$  decay series. Both radionuclides are produced in soil *in situ* and should therefore be in natural equilibrium if no intensive leaching or salinisation occurred during their decay period.
- (2) Equal concentrations of  $^{228}\text{Th}$  (half-life of 1.9 yr) and  $^{228}\text{Ra}$  (half-life of 5.8 yr). Both isotopes have similar half-lives and should be in equilibrium.
- (3) The ratio of naturally occurring  $^{226}\text{Ra}$  to  $^{210}\text{Pb}$  should also be in equilibrium.  $^{210}\text{Pb}$  (half-life of 22 yr) is a decay product of its *in situ* parent  $^{226}\text{Ra}$  and is derived from gaseous radon-222 ( $^{222}\text{Rn}$ , half-life of 3.8 days), which introduces  $^{210}\text{Pb}$  into the atmosphere.



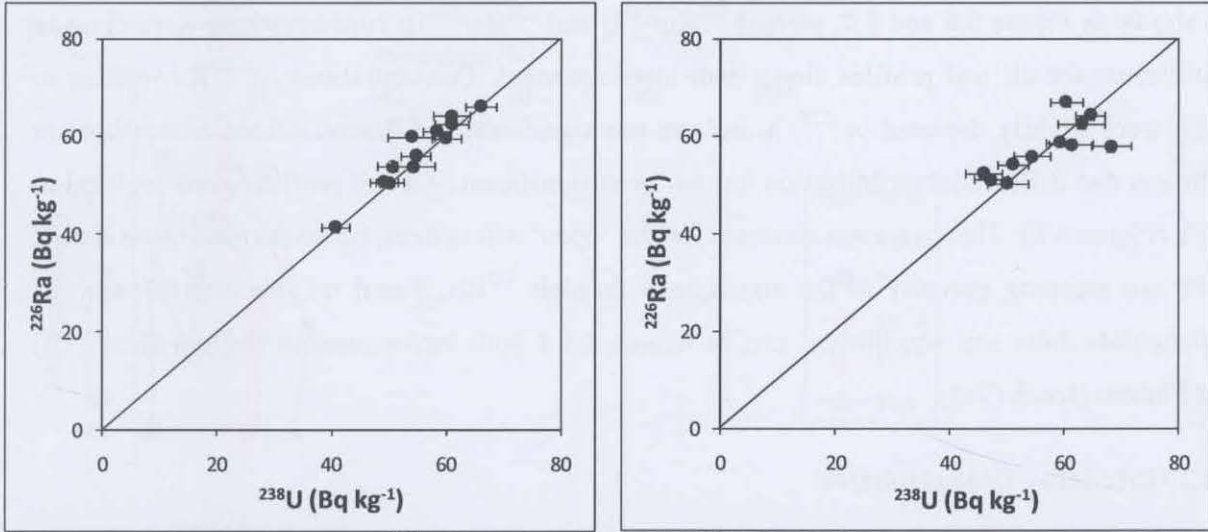


Fig. 5.6. Concentrations of measured  $^{238}\text{U}$  ( $\text{Bq kg}^{-1}$ ) plotted against  $^{226}\text{Ra}$  ( $\text{Bq kg}^{-1}$ ). Left: Toposequence Mount Boss Tb. Right: Toposequence Plateau Beech Te.

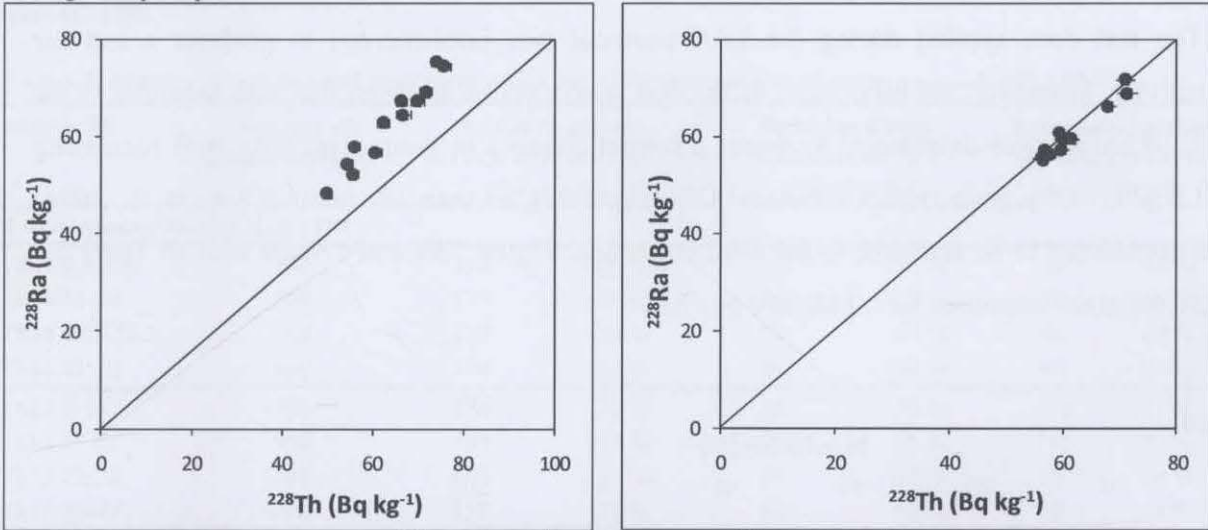


Fig. 5.7. Concentrations of measured  $^{228}\text{Th}$  ( $\text{Bq kg}^{-1}$ ) plotted against  $^{228}\text{Ra}$  ( $\text{Bq kg}^{-1}$ ). Left: Toposequence Mount Boss Tb. Right: Toposequence Plateau Beech Te.

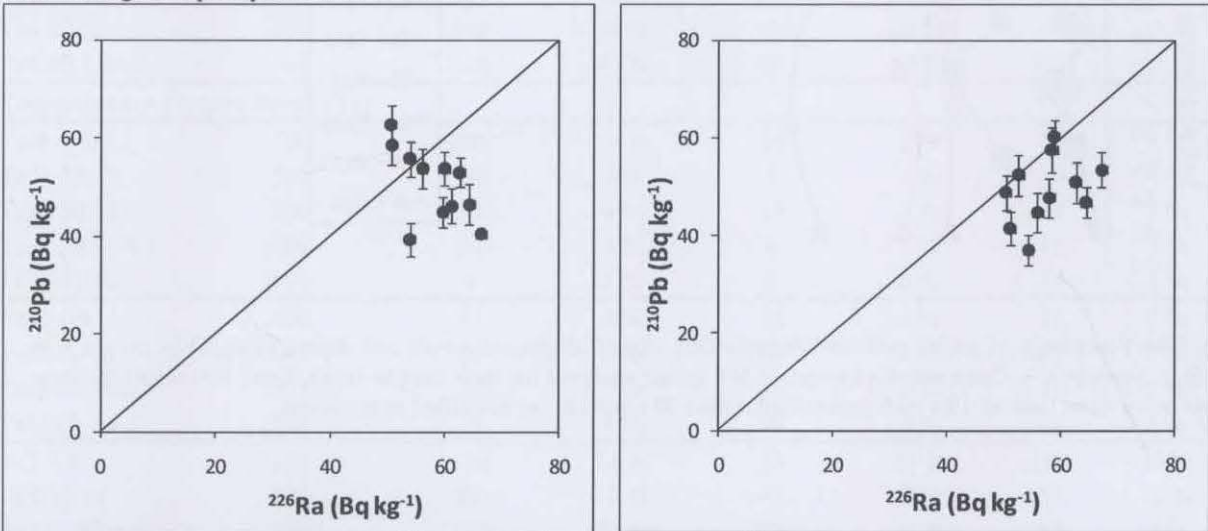


Fig. 5.8. Concentrations of measured  $^{210}\text{Pb}$  ( $\text{Bq kg}^{-1}$ ) plotted against  $^{226}\text{Ra}$  ( $\text{Bq kg}^{-1}$ ). Left: Toposequence Mount Boss Tb. Right: Toposequence Plateau Beech Te.

As shown in Figure 5.6 and 5.7, plotted  $^{226}\text{Ra}/^{238}\text{U}$  and  $^{228}\text{Ra}/^{228}\text{Th}$  concentrations were close to equilibrium for all soil profiles along both toposequences. Concentrations of  $^{228}\text{Ra}$  relative to  $^{228}\text{Th}$  were slightly depleted in  $^{228}\text{Th}$ , but are not significantly different. Minor disequilibrium indicates that differential mobilisation has not been significant. All soil profiles were depleted in  $^{210}\text{Pb}$  (Figure 5.8). This pattern is common for the ‘open’ soil system, because small quantities of  $^{210}\text{Pb}$  are escaping partially to the atmosphere through  $^{222}\text{Rn}$ . Based on this interpretation of radionuclide data, soil equilibrium can be assumed for both toposequences (Mount Boss (Tb) and Plateau Beech (Te)).

### 5.3.2 OSL data - Dose estimates

#### 5.3.2.1 Test for OSL sensitivity of quartz grains

The test dose applied during the SAR protocol was implemented to perform a test for sensitivity. Moreover, the proportion of the 500 quartz grains analysed that was sensitive to the OSL technique was determined to detect potential changes in grain sensitivity with increasing soil depth. Every grain with a measured OSL signal higher than 30 counts (Olley et al., 2004) was considered to be sensitive to the OSL technique. Figure 5.9a and 5.9b as well as Table 5.3 show the grain responses for all six soil profiles.

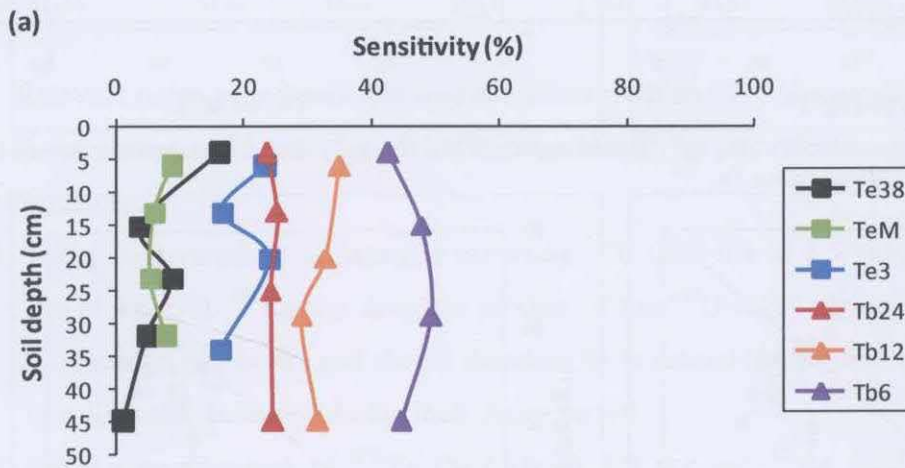


**Fig. 5.9a.** Percentage of grains with an adequate OSL signal, displayed for all soil depths sampled in the six soil profiles. Sensitivity – Grain sensitivity, out of 500 grains analysed for each sample depth. Tests for sensitivity were made using a test dose of 10 s with grains higher than 30 counts being classified as sensitive.

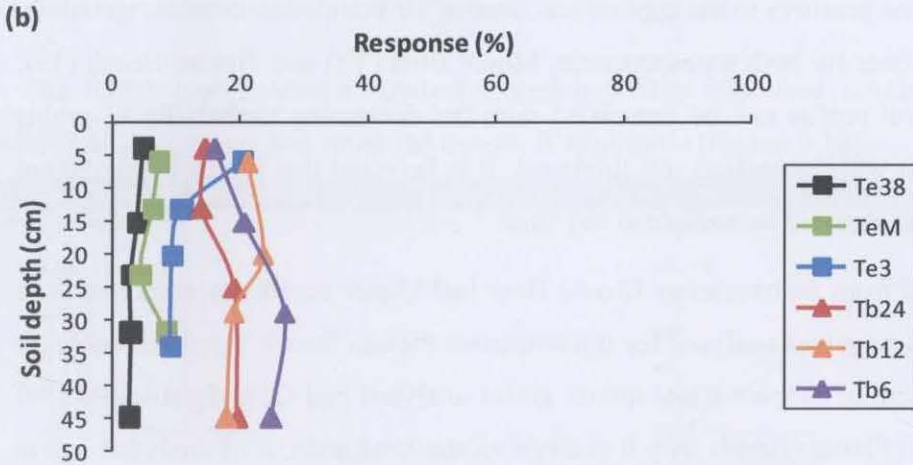


Fig. 5.9b. Percentage of grains with an adequate OSL signal, displayed for all soil depths sampled in the six soil profiles. Response – Responsive grains out of 500 grains analysed for each sample, for which a dose value in Gy was calculated.

Tab. 5.3. Amount of sensitive and responsive grains out of the total number of grains analysed with OSL.

Sample ID	Number of grains analysed	Sensitive grains (Test dose of 10 s, >30 counts)		Sensitive grains (Test dose of 10 s, >100 counts)		Responsive grains (Dose in Gy could be calculated)	
<b>Toposequence Mount Boss (Tb)</b>							
Tb24 2.5-7.5	500	119	24 %	52	10 %	73	15 %
Tb24 11-16	500	127	25 %	55	11 %	70	14 %
Tb24 23.5-28.5	500	122	24 %	52	10 %	96	19 %
Tb24 43-48	500	124	24 %	48	10 %	98	20 %
Tb12 5-10	500	176	35 %	82	16 %	106	21 %
Tb12 18-23	500	165	33 %	77	15 %	118	24 %
Tb12 27-32	500	146	29 %	59	12 %	95	19 %
Tb12 42-47	500	159	32 %	66	13 %	90	18 %
Tb6 2.5-7.5	500	214	43 %	82	16 %	80	16 %
Tb6 13-18	500	239	48 %	107	21 %	104	21 %
Tb6 27-32	500	248	50 %	103	21 %	135	27 %
Tb6 40.5-45.5	500	224	45 %	91	18 %	125	25 %
<b>Toposequence Plateau Beech (Te)</b>							
Te38 1.5-6.5	500	80	16 %	29	6 %	24	5 %
Te38 12-17	500	20	4 %	5	1 %	19	4 %
Te38 20-25	500	44	9 %	15	3 %	14	3 %
Te38 29.5-34.5	500	24	5 %	6	1 %	15	3 %
Te38 41-46	500	6	1 %	0	0 %	13	3 %
TeM 4-9	500	44	9 %	15	3 %	36	7 %
TeM 12-16	500	30	6 %	10	2 %	31	6 %
TeM 21.5-26.5	500	27	5 %	15	3 %	23	4 %
TeM 29-34	500	39	8 %	19	4 %	42	8 %
Te3 4-8	500	118	24 %	54	11 %	102	20 %
Te3 10-15	500	83	17 %	44	9 %	55	11 %
Te3 18-23	500	120	24 %	52	10 %	47	9 %
Te3 31-36	500	82	16 %	37	7 %	45	9 %

The proportion of grains sensitive to the applied test dose of 10 s tended to decrease gradually with increasing soil thickness for both toposequences, Mount Boss (Tb) and Plateau Beech (Te). This pattern down the soil profile can be associated with the decreasing probability of grains being exposed to sunlight with increasing soil thickness. It is believed that grains below 50 cm depth might not have been exposed to sunlight at any time.

Quartz grains sampled from toposequence Mount Boss had higher sensitivity responses to a test dose of 10 s than quartz grains analysed for toposequence Plateau Beech. Approximately 20 to 40 % of the total amount of 'Mount Boss' quartz grains analysed had OSL signals above 30 counts. For toposequence Plateau Beech only 0 to 20 % of the total amount of analysed quartz grains was sensitive to the test dose.

Responses of individual quartz grains to the test dose may also be used as an indication for repeated cycles of irradiation and heating of grains, which was posited to correspond to repeated exposure of grains at the soil surface. Research on fluvial deposits of the Castlereagh River in Australia confirmed that the sensitivity of quartz grains increased linearly with distance downstream reflecting both a proportional increase of luminescence grains as well as an increase in the sensitivity of individual grains (Pietsch et al., 2008). An additional test for sensitivity was performed, where OSL signal counts above 100 were classified as a high response or high sensitivity to a test dose of 10 s for the analysed samples. Results showed that grains with a 'high' sensitivity decreased proportionally with luminescence grains with increasing soil thickness. It can therefore be assumed that the probability of grains experiencing repeated cycles of exposure and therefore becoming more sensitized to sunlight decreases down the soil profile.

The dose could only be determined for a relatively small proportion of the total analysed grains (Figure 5.9). Here, this fraction of quartz grains will be referred to as 'responsive grains'. A dose was calculated for about 15 to 25 % of the 500 quartz grains analysed for soil profiles along toposequence Mount Boss, and for about 3 to 10 % of the 500 quartz grains analysed for soil profiles along toposequence Plateau Beech. The amount of responsive grains decreased down the soil profile for toposequence Plateau Beech. This trend was also visible for toposequence Mount Boss. However, here, grain responses increased slightly at about 25 cm of soil depth before they decreased with increasing soil thickness.

### 5.3.2.2 Dose calculations in units of gray

The RISØ Luminescence Analyst (Version 3.04b) was used (Duller, 2001) to calculate individual grain doses and weighted means, if applicable (Figure 5.10).

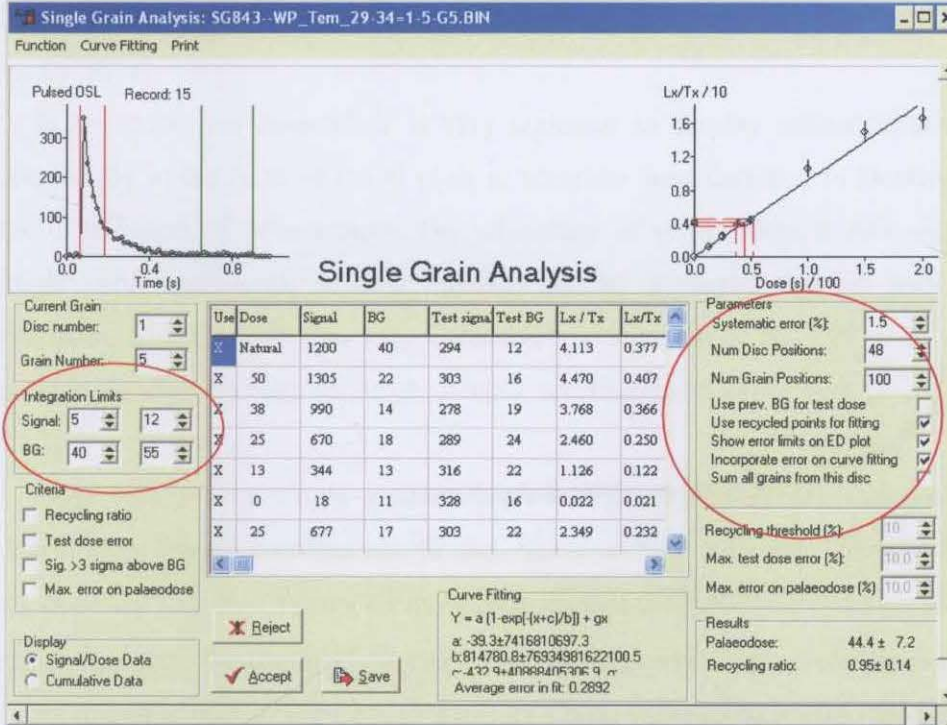


**Fig. 5.10.** RISØ Luminescence Analyst (Version 3.04b) after Duller (2001). Criteria used throughout the procedure of rejecting and accepting quartz grains for dose calculations are circled. The data window shows the 'dose' applied in each sets, the 'signal' and 'background' counts from OSL measurements within the set integration limits, followed by the 'test signal' and 'test background' counts from the applied test dose; and the ratio of the 'signal' to the 'test signal' ('Lx/Tx') and its uncertainty ('Lx/Tx error'), minus the 'background' counts, respectively.

The majority of grains analysed did not have an adequate shine-down curve to calculate a dose and had to be excluded from further analysis. After performing the sensitivity analysis, this behaviour was expected since quartz grains might not have seen the light or might not have been sufficiently bleached to create an ideal shine-down curve. A shine-down curve is defined by the depletion of the (natural) OSL signal as stimulation continues over time. This process corresponds to the exhaustion of supply of electrons from the OSL trap(s) (Aitken, 1998). For each grain with a good shine-down curve a growth curve or standard curve was created using the natural and regenerated dose values (Figure 5.11). As shown in Figure 5.11 the growth curve is defined as a plot of the sensitivity corrected OSL signal ('Lx/Tx') against the applied dose ('Dose'). Accordingly, a weighted mean dose for each grain was calculated by adjusting the best fit of the data (linear, quadric, cubic, exponential, exponential + linear). However, an actual dose value could not be calculated for every grain with a good shine-down curve because of rejection criteria based on statistical uncertainty.

After the completion of the statistical analysis of each individual quartz grain, the calculated dose values and their uncertainties were converted from seconds (s) to gray (Gy) by multiplying each value by 0.105. The value of 0.105 represented the dose rate used on the OSL reader of  $0.105 \text{ Gy s}^{-1}$ .

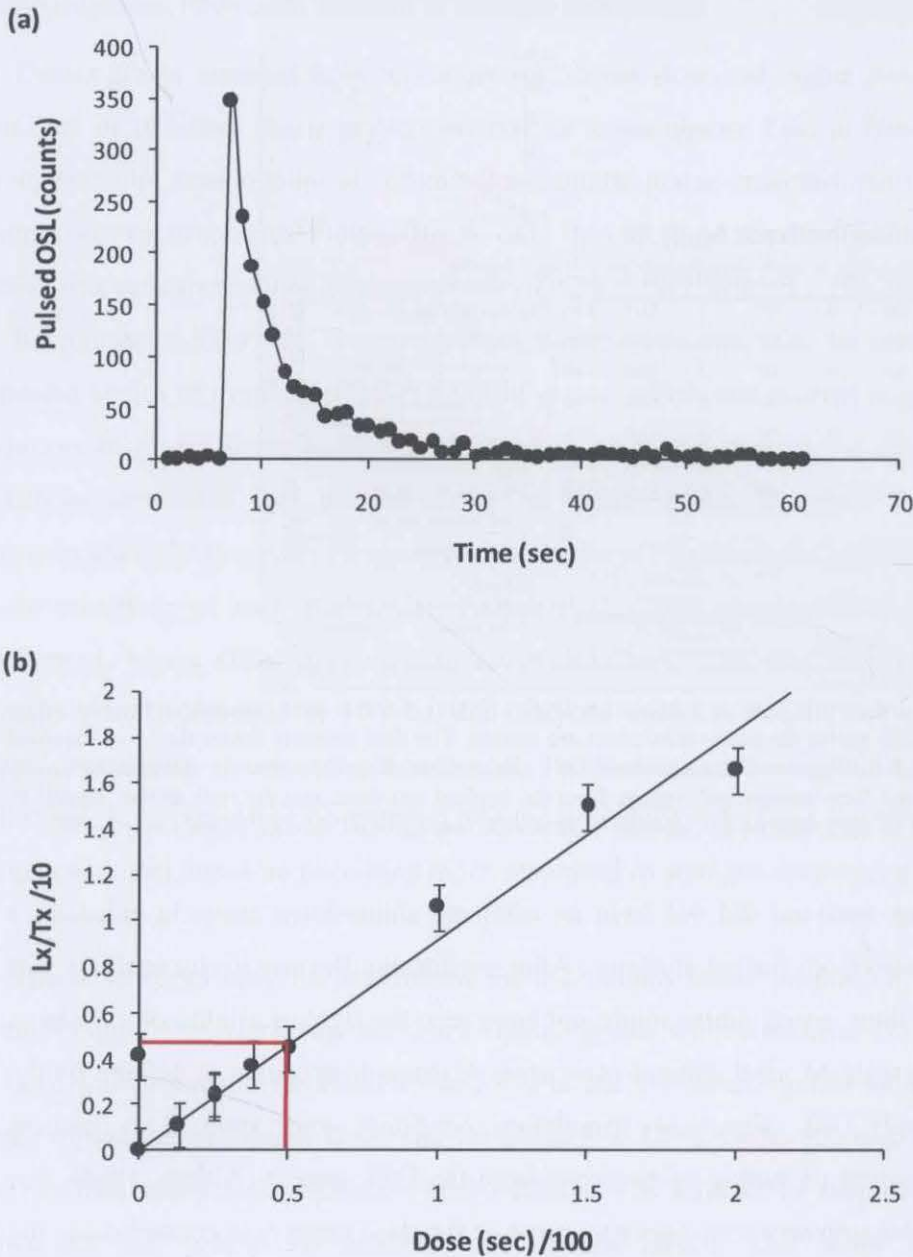


**Fig. 5.11.** (a) Shine down curve of the natural OSL signal in OSL reader counts per seconds. (b) Growth curve plot of the sensitivity corrected OSL signal ( $L_x/T_x$ ) against the applied dose. Plotted data were fitted with the linear + exponential curve fitting option to generate a value for the natural dose received during burial of  $44.3 \pm 7.2$  s. Shine down and growth curves are exemplified using single grain data from the soil profile TeM (depth 29-34 cm for disc 1 and grain 5 from toposequence Plateau Beech).

### 5.3.2.3 Dose distributions for individual quartz grains

Dose distributions from single grain measurements of the sampled soil depths are presented and discussed in the following, using radial plots and equally spaced dose density estimates.

#### *Radial Plots*

In luminescence research it is very common to display estimated dose ( $D_e$ ) distributions graphically in the form of radial plots to compare dose data and to identify possible patterns in the distribution of dose values. The advantage of radial plots is that single-grain data which might vary significantly in their intensity can be displayed together with the precision of the estimates which might also vary extensively (Galbraith et al., 1999). In the following, single grain dose distributions for each sample are displayed using this graphical platform (Figure 5.12).

Dose values from single grains are plotted around the central value of the estimated dose distribution which corresponds to the mean of the data set. In other words, plotting the standardised log dose values on the y-axis against the precision ( $1/\sigma$ ) on the x-axis. The shaded region indicates the standard error ( $2\sigma$ ) around the central value (Galbraith et al., 1999).

As demonstrated in Figure 5.12 measured dose values (in Gy) for single grains can be read by tracing a line from the y-axis origin throughout the point studied until the line intersects the radial axis (log scale) on the inside of the right-hand side. The corresponding standard error (in %) can be estimated by extending a vertical line from the point studied to the x-axis. In addition to the relative standard error, the precision, a reciprocal of the standard error can be estimated. Accordingly, values with the highest precision and the smallest relative errors are plotted closest to the radial axis on the right whereas the least precise dose estimates are plotted furthest to the left (Olley et al., 2004).

For instance, if individual dose estimates are consistent with one common dose, most of the points should fall within the  $\pm 2$  radial band. If dose estimates arose from 2 distinct populations (two true doses), then points should lie within two radial bands (Galbraith et al., 1999).

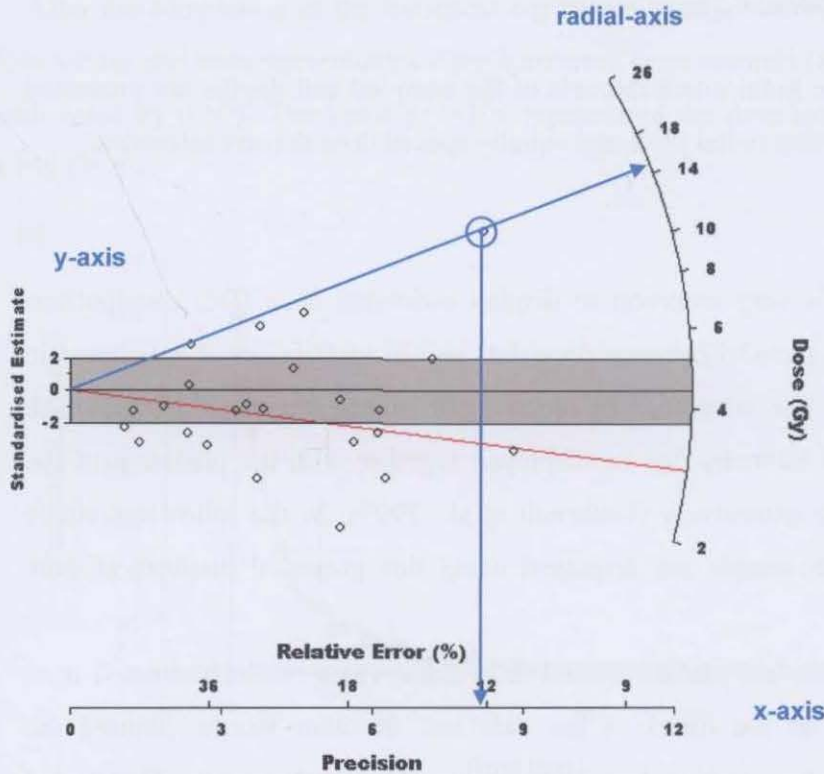


Fig. 5.12. The use of radial plots for displaying OSL data, exemplified with dose values from soil profile Te38 (1-6 cm depth). The estimated dose the grains received since burial can be read by tracing the blue line from the y-axis origin through the point studied until it intersects with the radial-axis (log scale). The corresponding standard error can be read by extending the blue vertical line to the x-axis. The precision, which plots the reciprocal standard error, can also be read on the x-axis. For example, the circled point corresponds to a dose value of 14.34 Gy (2.7, log scale) with a standard error of more or less 1.74 Gy (12.13 %). The black line indicates the mean value of the estimated dose values of 4.41 Gy with a standard error of 0.88 Gy (shaded region, 2 sigma ( $\sigma$ )). The red line corresponds to the median of the dose distributions of 2.91 Gy.

Radial plots for each sample depth are presented graphically in Figures 5.13 to 5.18, plotted separately for each soil profile sampled along Mount Boss and Plateau Beech toposequences. Comparing radial plots, it can be seen graphically that samples from toposequence Mount Boss were characterised by a larger amount of responsive quartz grains than samples from toposequence Plateau Beech. Furthermore, displaying dose values in the form of radial plots showed that dose distributions potentially belonged to more than one population, because of the wide spread in the data around the mean. This pattern was more prominent for toposequence Mount Boss. Here, single grain dose distributions implied the occurrence of additional grain populations for the range of low dose values (up to 3 Gy). Comparing the central value of all dose populations down the soil profile the conclusion was made that the central dose value is similar for all soil depths except for dose distributions from the deepest soil depths sampled (around 50 cm). Radial plots also demonstrated graphically that the uncertainty of dose estimates was relatively high for the majority of individual grains sampled. Relative standard errors exceeded 15 % for most of the single grain estimates.



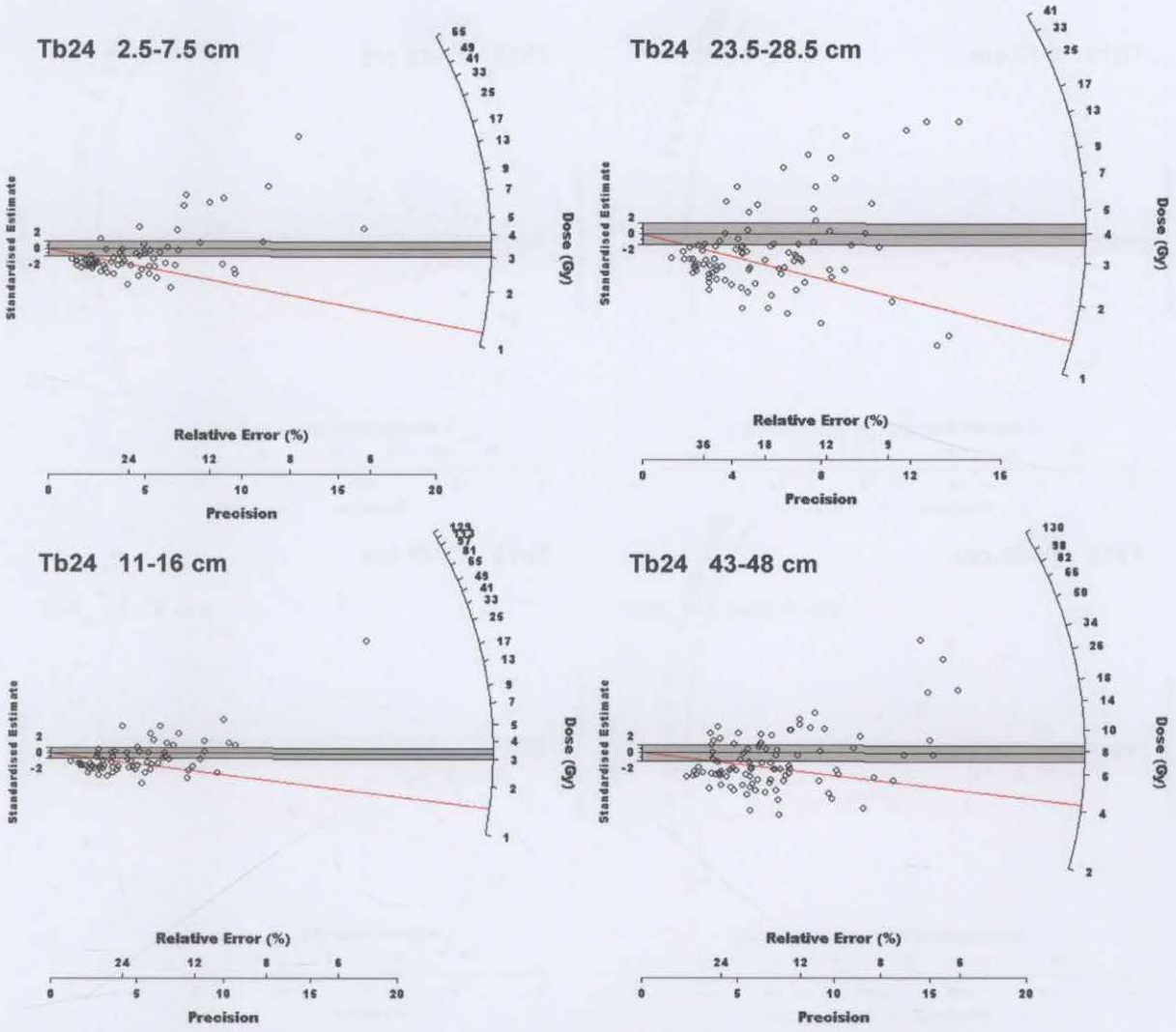


Fig. 5.13. Radial plots of single-grain dose ( $D_e$ ) estimates in Gy for different depths of the soil profile Tb24 along the toposequence Mount Boss.

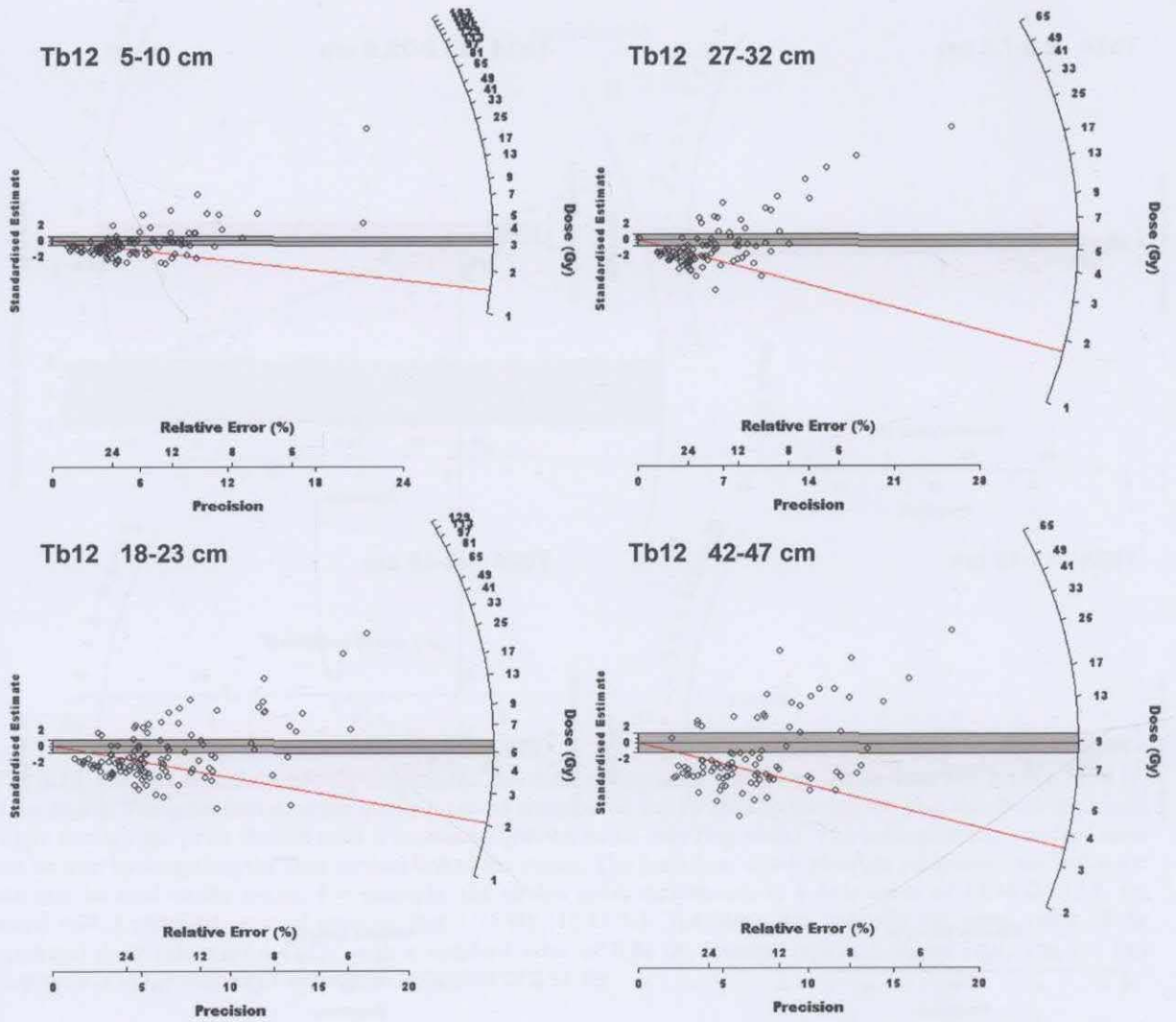


Fig. 5.14. Radial plots of single-grain dose ( $D_e$ ) estimates in Gy for different depths of the soil profile Tb12 along the toposquence Mount Boss.

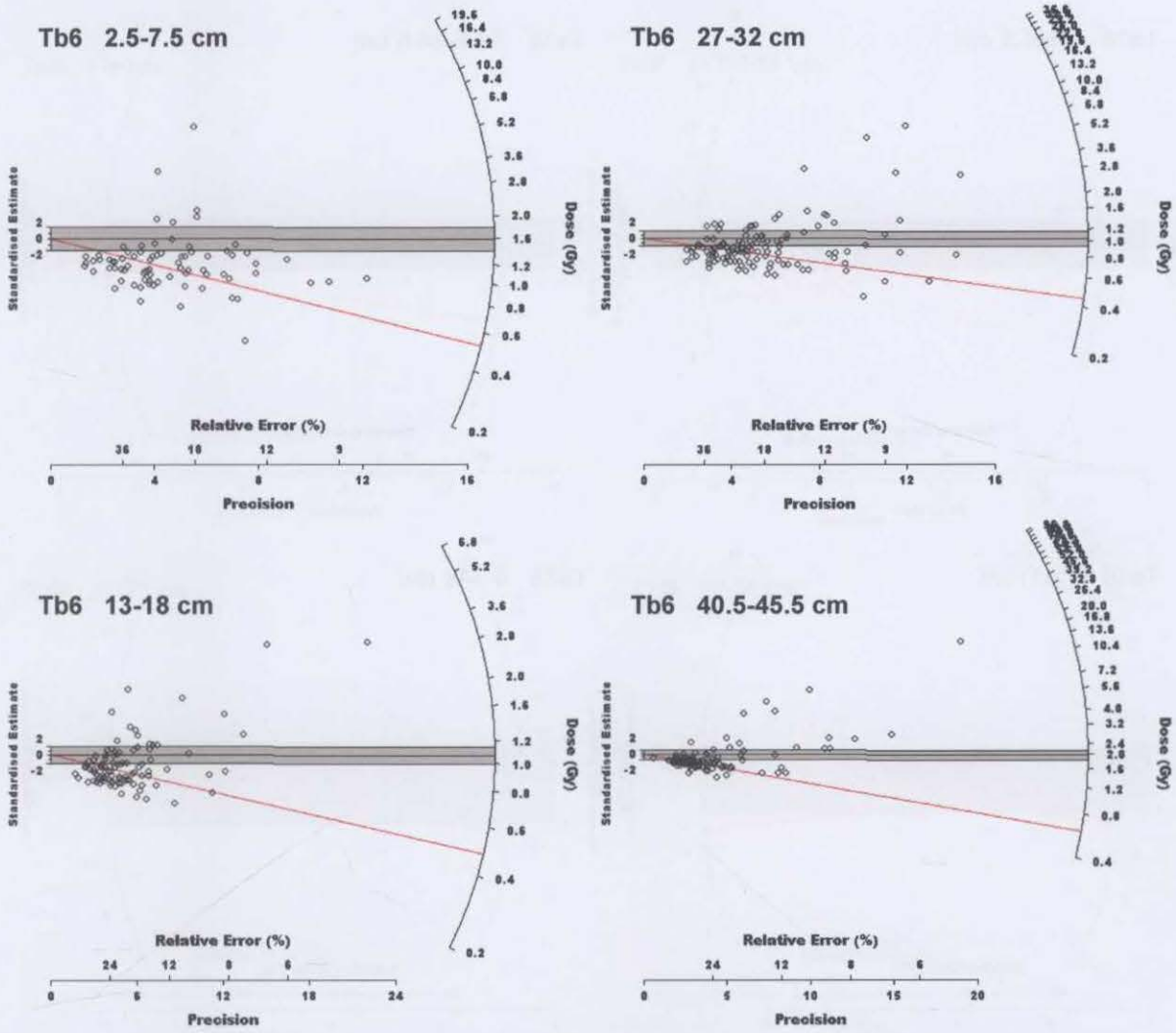


Fig. 5.15. Radial plots of single-grain dose ( $D_e$ ) estimates in Gy for different depths of the soil profile Tb6 along the toposequence Mount Boss.

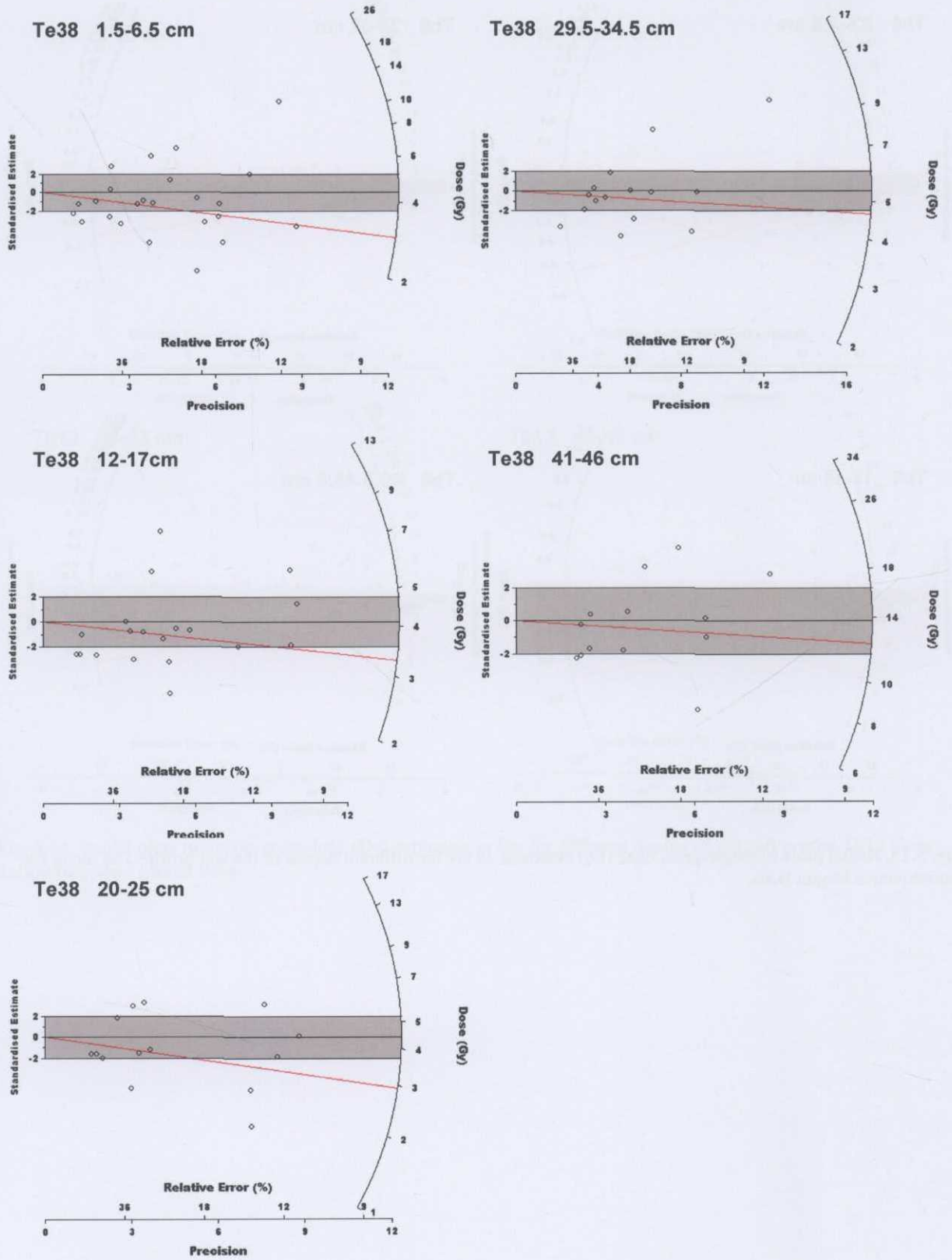


Fig. 5.16. Radial plots of single-grain dose ( $D_e$ ) estimates in Gy for different depths of the soil profile Te38 along the toposequence Plateau Beech.

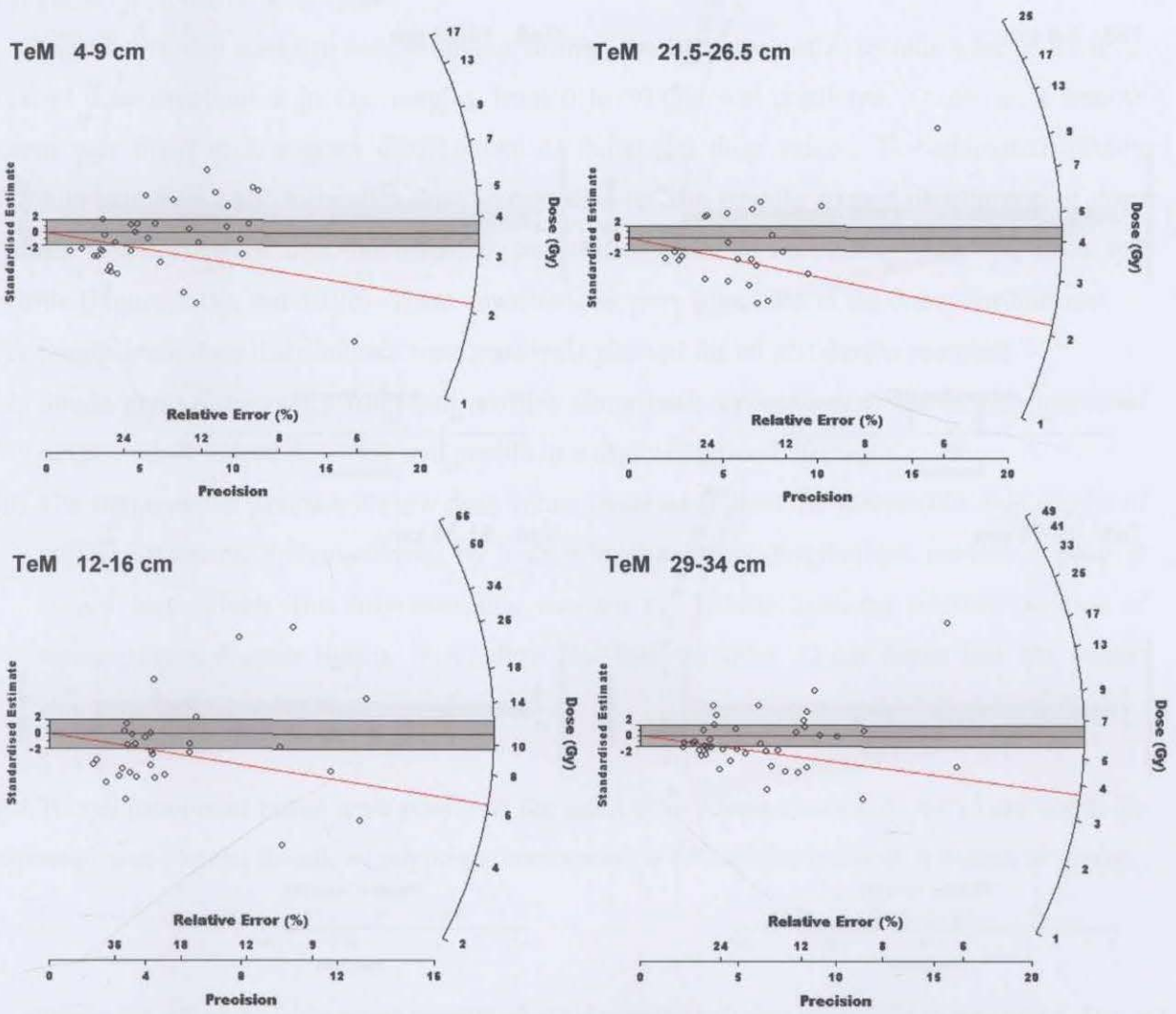


Fig. 5.17. Radial plots of single-grain dose ( $D_e$ ) estimates in Gy for different depths of the soil profile TeM along the toposequence Plateau Beech.

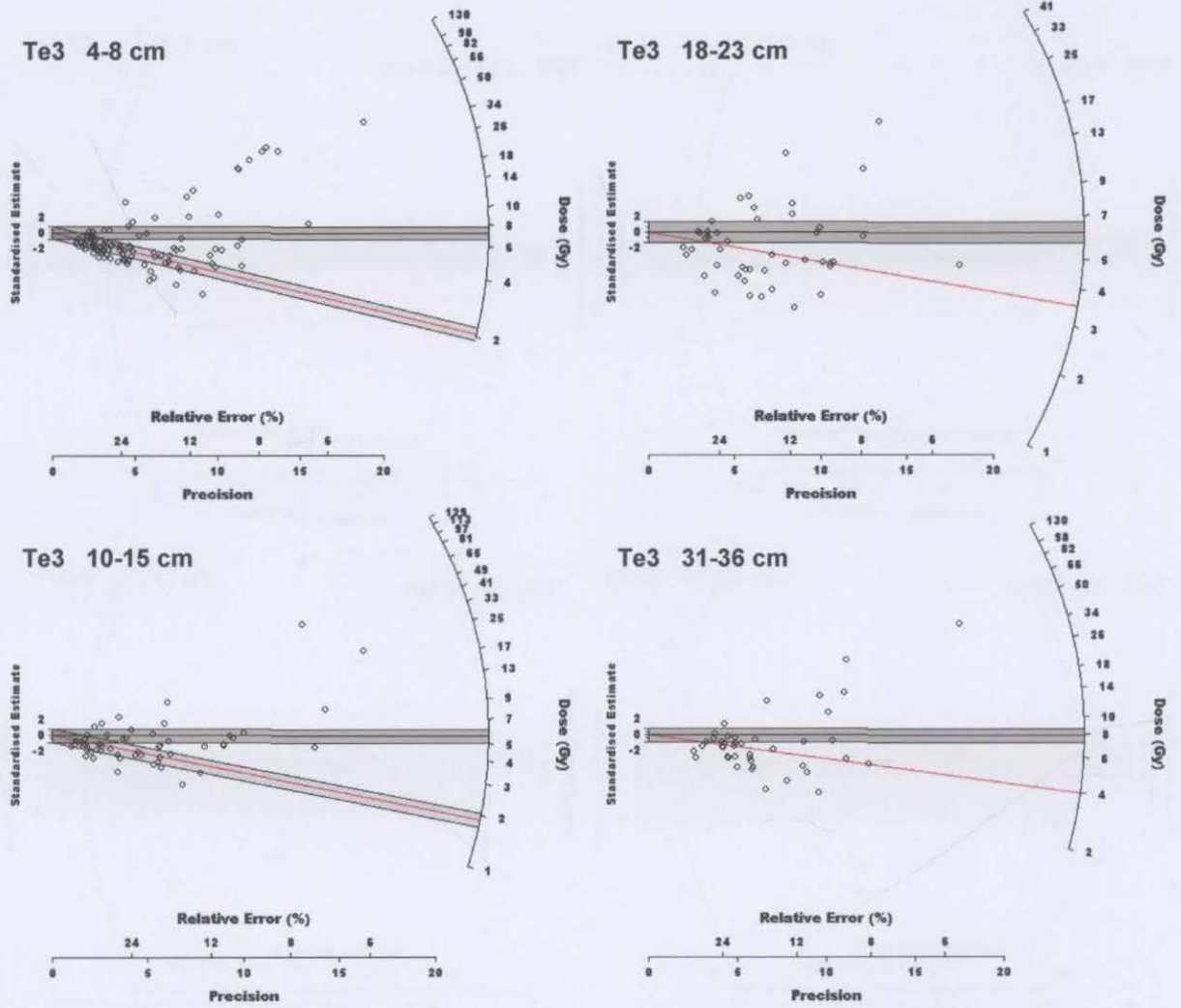


Fig. 5.18. Radial plots of single-grain dose ( $D_e$ ) estimates in Gy for different depths of the soil profile Te3 along the toposequence Plateau Beech.

*Frequency distributed dose values*

To visualize and compare dose estimates further, the frequency of dose values for an equally-spaced dose distribution in Gy, ranging from 0 to 50 Gy, was predicted. To do so, a smooth curve was fitted to histogram distributions of individual dose values. The estimated density formula was then used to predict dose frequencies for the equally spaced distribution of dose values. Equally spaced dose distributions were then plotted in an overlay graph for each soil profile (Figure 5.19a and 5.19b). Three consistencies were identified in the dose distributions:

- (1) Single-grain dose distributions were positively skewed for all soil depths sampled.
- (2) Single-grain dose values from soil profiles along both toposequences showed an increased range of dose values down the soil profile to a depth of around 50 cm.
- (3) The frequency of grains with low dose values decreased down the soil profile. Soil depths of around 50 cm were characterized by a shift in dose grain distributions towards a peak at higher dose values. The only exception was the soil profile from the mid-hill position of toposequence Plateau Beech. Here, dose distributions from 13 cm depth had the lowest amount of younger grains.

Additional prominent peaks were predicted for grain dose distributions at 4 and 23 cm depth for toposequence Plateau Beech, which might correspond to two modes in the distribution of grains.

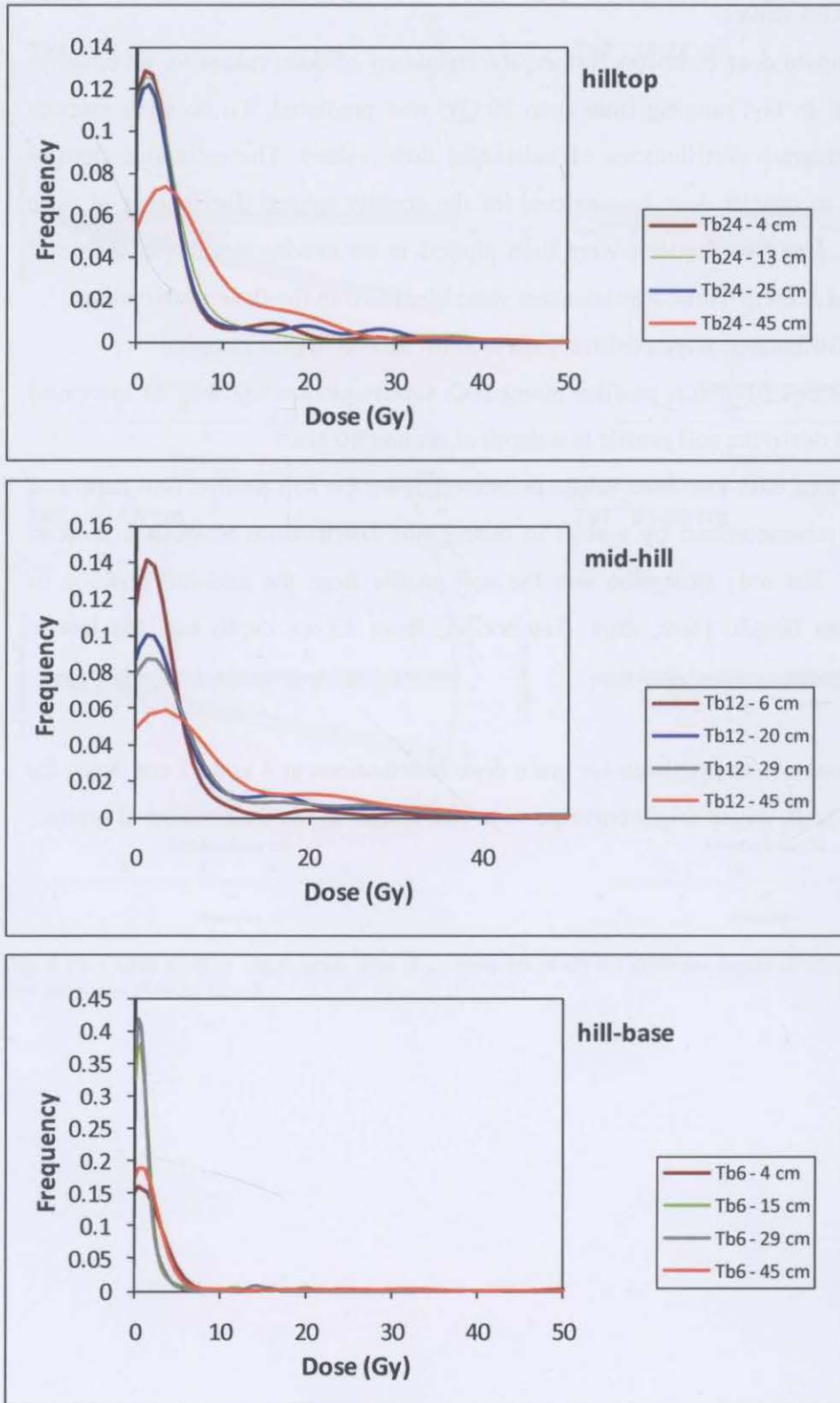


**Fig. 5.19a.** Dose distributions for soil profiles along toposequence Mount Boss. Frequency distributed dose values, ranging between 0 and 50 Gy. The fit of a 'smooth curve' to dose distributions from each soil depth was used to predict the density formula for interpolating equally spaced dose distributions.



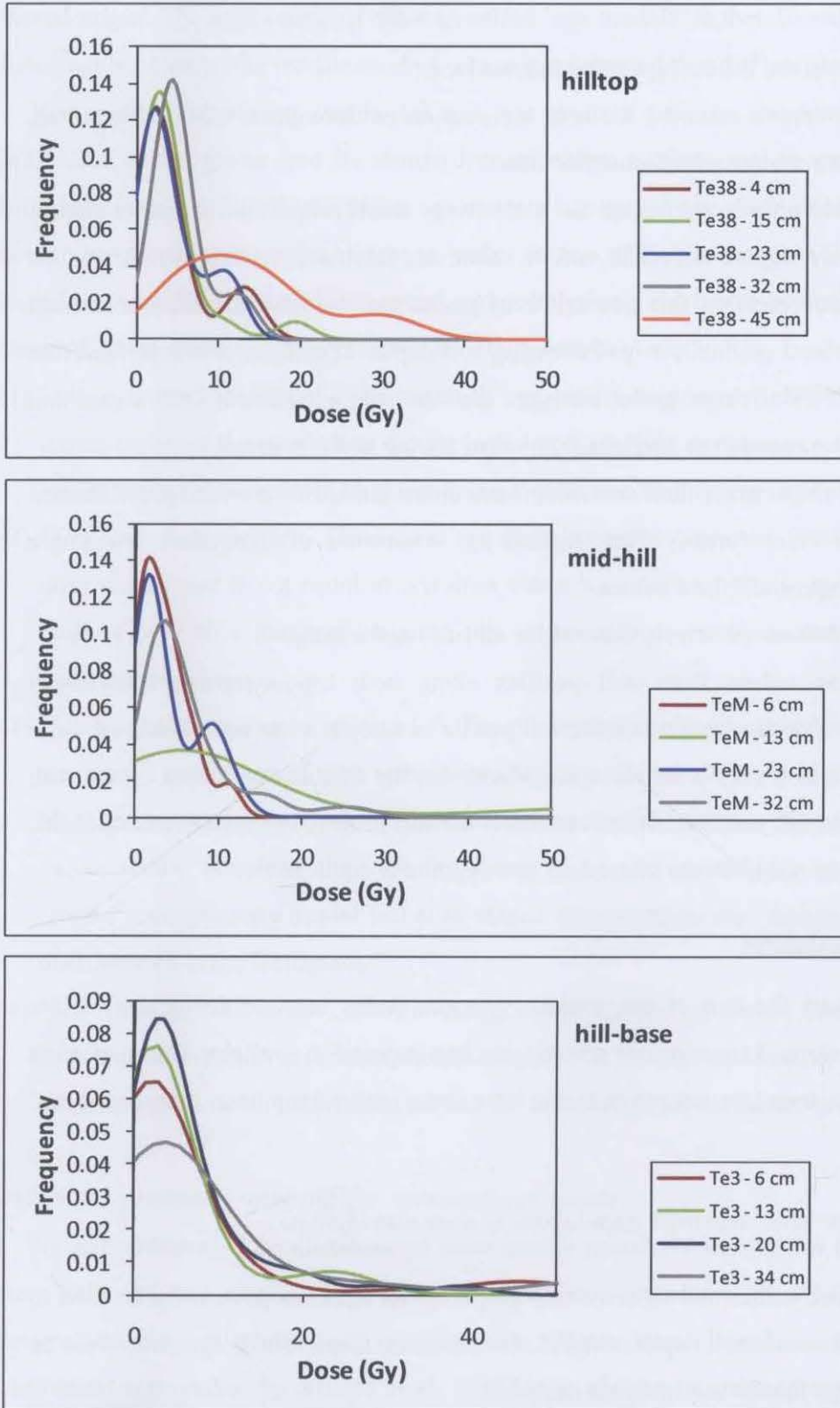


**Fig. 5.19b.** Dose distributions for soil profiles along toposquence Plateau Beech. Frequency distributed dose values, ranging between 0 and 50 Gy. The fit of a 'smooth curve' to dose distributions from each soil depth was used to predict the density formula for interpolating equally spaced dose distributions.

### Summary

From the previous sections the following can be summarized:

- Soil equilibrium can be assumed for both toposequences throughout the past centuries, based on the interpretation of radionuclide data.
- Dose values could only be estimated for a relatively small proportion of quartz grains. Out of 500 grains analysed with OSL, a dose value was calculated for less than 25 %. For the majority of soil profiles, this proportion of grains that did have a sufficient enough dose value decreased gradually with increasing soil depth. Therefore, it was posited that approximately 75 % of single-grains analysed did not have a sufficient OSL signal and may not have been exposed to sunlight at any time during soil formation.
- Distributions of single grain dose estimates were characterized by a wide spread around the central dose value (mean). This implied the occurrence of more than one single population of single grain dose values.
- Dose distributions were positively skewed for all soil depths sampled.
- Single-grain dose values from soil profiles along both toposequences showed an increased range of dose values down the soil profile to a depth of around 50 cm, i.e. dose values of more than 50 Gy were recorded. Moreover, the frequency of dose values with low or close to zero Gy values, decreased down the soil profile. For both toposequences, there seemed to be a shift in the mean dose at a depth of around 50 cm.

### 5.3.3 OSL data - Age estimates

In the following sections the use of the words 'younger grains' and 'older grains' refers exclusively to the time elapsed since quartz grains were last exposed to sunlight. The discussion of grain age results does therefore not relate to the time since grains have been 'weathered out' of the parent material.

#### 5.3.3.1 Estimation of one 'true' age from populations of dose distributions

Calculating single dose values and subsequently single burial ages can potentially be used to determine a mean age for each soil depth sampled. Furthermore, single burial ages may then be applied to estimate an age for the soil horizons sampled.

Statistical models have been formulated to calculate one appropriate burial age for all single grains analysed from one sample material (Galbraith et al., 1999). However, these models are mainly applicable in geomorphologic studies and generally not applicable in pedogenic studies, because they were developed to calculate a depositional age for sediments, i.e. of aeolian or

fluvial origin. The application of these so called ‘age models’ is therefore limited in undisturbed forest environments like the site studied where it is assumed that soil profiles formed *in situ*.

Rather than calculating one burial age, age models estimate one burial dose received by individual quartz grains and its standard error, which is then used to determine a burial age following equation 5.1. Furthermore, age models implement one mean dose rate for all grains to determine one dose value for all quartz grains from a particular sample (Galbraith et al., 1999). Based on dose distributions (histograms and radial plots), the burial dose can be calculated by a range of different models (Galbraith et al., 1999; Jacobs et al., 2006):

- (1) ‘*The common age model*’. The common age model assumes an ideal distribution where all grains received the same dose during burial and possible variations in the dataset are due to measurement uncertainties only (i.e. instrumental uncertainty, curve fitting).
- (2) ‘*The central age model*’. The central age model assumes a normal distribution of logarithmic dose values that is not equal to one dose value but rather randomly spread around a central dose value with a standard variation that is too wide to be accounted for by measurement uncertainties alone.
- (3) ‘*The minimum/maximum age model*’. The minimum/maximum age model assumes more than one single population of dose values, which can be due to different bleaching histories (well bleached, partially bleached, unbleached) or irradiation histories. The most appropriate dose values would therefore either be the lowest range (‘minimum age model’) or the highest range (‘maximum age model’) of dose values, depending on the ‘skewness’ of the dose value distributions in the histogram.
- (4) ‘*The finite mixture model*’. The finite age model assumes different dose components within one dose distribution and calculates dose values for each component by treating the standard deviation as a known parameter that has the same range for all the different components.

#### *Burial dose estimates applying the ‘minimum age model’*

As demonstrated, dose distributions were mostly positively skewed for the samples analysed from different soil depths. This pattern was seen in particular for single-grain dose values determined for soil profiles of toposequence Mount Boss. Based on this distribution, the ‘minimum age model’ by Arnold et al. (2009) was chosen to estimate one burial dose for the range of dose distributions determined from one soil depth (see Table 5.4). As described above, this model assumes a positively skewed distribution of dose values and is applicable for depositional environments. The estimated burial dose or age therefore corresponds to the most recent event of deposition.

**Tab. 5.4.** Single dose data calculated in applying the Minimum Age Model using an overdispersion of 10 % (after Arnold et al. (2009)), the mean and median of single-grain age distributions are also listed.

Sample ID	Single dose [Gy]	Dose rate [Gy kyr <sup>-1</sup> ]	'Minimum' age [yr]	Mean age [yr]	Median age [yr]
<b>Toposequence Mount Boss (Tb)</b>					
Tb24 2.5-7.5	0.43	2.52±0.24	170	1323	470
Tb24 11-16	0.33	2.48±0.23	130	1297	570
Tb24 23.5-28.5	0.36	2.43±0.24	150	1544	550
Tb24 43-48	0.79	2.45±0.24	320	3024	1665
Tb12 5-10	0.34	2.45±0.23	140	1277	562
Tb12 18-23	0.47	2.49±0.24	190	2086	788
Tb12 27-32	0.49	2.46±0.24	200	2186	696
Tb12 42-47	0.57	2.37±0.24	240	3405	1376
Tb6 2.5-7.5	0.24	2.68±0.24	70	652	214
Tb6 13-18	0.29	2.39±0.22	120	440	195
Tb6 27-32	0.30	2.26±0.22	130	430	184
Tb6 40.5-45.5	0.49	2.02±0.20	240	832	253
<b>Toposequence Plateau Beech (Te)</b>					
Te38 1.5-6.5	0.87	2.28±0.23	440	1961	1295
Te38 12-17	1.00	1.98±0.20	510	1836	1456
Te38 20-25				1973	1314
Te38 29.5-34.5	1.00	2.15±0.23	470	2392	2072
Te38 41-46				6144	5441
TeM 4-9	0.70	2.26±0.22	310	1480	1248
TeM 12-16	0.80	2.15±0.22	370	4720	2771
TeM 21.5-26.5	0.89	2.13±0.22	420	1777	942
TeM 29-34	0.83	2.24±0.24	370	2631	1595
Te3 4-8	0.86	2.20±0.21	390	3309	961
Te3 10-15	0.47	2.14±0.21	220	2582	867
Te3 18-23	0.40	1.98±0.20	200	2841	1623
Te3 31-36	0.40	1.91±0.20	210	4686	1845

The minimum age model assumes that the true logarithms of the doses are a random sample from a mixed truncated normal distribution. If  $p$  denotes the unknown proportions of grains that were completely bleached before burial, each of these grains acquires the minimum log paleodose denoted by  $\gamma$ . Thus, the minimum paleodose is defined as  $\exp(\gamma)$ . The partially bleached grains have larger log doses, drawn from a truncated normal distribution with parameters  $\mu$  and  $\sigma$ . If the distribution was not truncated,  $\mu$  will be the mean and  $\sigma$  will be the standard deviation. However, for the truncated distribution,  $\mu$  and  $\sigma$  are simply adjustable parameters that capture the unknown spread in the log doses of the partially bleached grains. The details of the model are presented in Galbraith et al. (1999).

The parameters in this model are  $p$ ,  $\gamma$ ,  $\mu$  and  $\sigma$ , which need to be computed numerically using an optimization program. The model was written in R using different levels of overdispersion. The term overdispersed refers to data sets that are characterised by having more than one true

dose value. This refers to more than one prominent peak in the distribution of dose values. Consequently, for a distribution to be overdispersed more than 5 % of the dose values must lie outside the range of the two sigma error band (Jacobs et al., 2006).

As discussed previously, this pattern was assumed for almost all dose distributions of the sampled forest soils. Using the minimum age model, the lowest 'true' burial age for different depths in the soil profile was calculated. However, it needs to be taken into consideration that calculations were based on estimating an appropriate 'minimum' depositional age. Consequently, calculated 'minimum burial ages' can not be readily translated into ages of soil horizons and can therefore only be used as an estimate of the lowest age range for the soil depths sampled. Hence, proposed 'minimum burial ages' can only be used to estimate how long ago the youngest grains were exposed at the soil surface.

However, running the minimum age model resulted in 'reasonable' estimates only for toposequence Mount Boss, whose single-grain dose distributions were more similar to distributions from depositional environments for which the minimum age model was designed, exhibiting an 'abundance' of younger or recently bleached grains with the occasional older grains.

Minimum ages estimated for toposequence Mount Boss ranged between 100 and 300 years and were lower than minimum ages estimated for toposequence Plateau Beech. They increased down the soil profile. For toposequence Plateau Beech minimum ages ranged between 200 and 500 years and showed no distinct pattern down the profile. However, parameters applied in the minimum age model did not fit the distribution of single-grain ages for toposequence Plateau Beech. Predicted minimum ages were clearly underestimated when compared to mean and median ages of single-grain age distributions for the relevant soil depths.

#### *5.3.3.1 Age distributions for individual quartz grains*

In the following, the distributions of OSL age estimates is visualized and discussed for every soil depth sampled using probability plots, box plots and density plots. Because of the wide range of dose distributions and subsequently age distributions in the data sets, it was necessary to apply a range of different statistical methods to interpret the single grain data in relation to pedogenic processes.

### *Probability plots*

For both toposequences, single-grain age distributions were compared from each soil depth sampled using probability plots (Figure 5.20a and 5.20b). Probability plots confirmed patterns that were identified for the corresponding dose distributions:

- (1) Probability distributions for single-grain age estimates from 50 cm depth were inconsistent with distributions in the surface layers of the soil profiles. Age distributions at 50 cm depth were generally greater than age distributions between 0 and 30 cm. This behaviour was particularly prominent for soil profiles situated at the hilltop. Here, ages ranged between 0 to 22000 years and 2000 to 14000 years for toposequence Mount Boss and Plateau Beech, respectively.
- (2) Probability plots of single-grain age distributions from 0 to 30 cm tended to be similar, displaying a relative consistency in age distributions.
- (3) Probability plots of age distributions from the mid-hill position of toposequence Plateau Beech revealed a different trend compared to the other soil profiles. Here, single-grain distributions from the surface layer at 13 cm depth appeared to be reasonably different, having the highest median age of around 3000 years.

### *Box Plots*

Distributions of age estimates were also compared using box plots to get additional information about the distribution of single-grain ages and to display the change in the median of age distributions graphically down the soil profile. Figure 5.21 and 5.22 display box-plots for every soil depth sampled down the profile, for both toposequences. For easier interpretation, lower horizon boundaries are indicated.

The line in the middle of the box refers to the median and the box refers to the interquartile range. The box plot rectangle therefore represents the distance between the lower and the upper quartile. The distance between the two lines extending from the box plots equals the data points that are still within a 1.5 interquartile range from the quartiles of the distribution. Points plotted independently are shown as 'outliers' of the distribution.

Comparing box plots down the soil profiles, it is readily seen that median ages increase down the soil profile. It can also be observed that the majority of age estimates lies below an estimated age of 5000 years and that all age distributions have the occasional very old grains, particularly at toposequence Mount Boss. The occurrence of very old grains appeared to be increasing downslope.

Comparing box plot distributions in conjunction with probability plots revealed the tendency for similar distributions to occur in the equivalent soil horizons for both toposequences. It can therefore be posited that single-grain distributions reflect individual soil horizons in the profile.

#### *Density plots*

Because of the wide spread in age distributions and the skewness of the data, the hypothesis was made that age distributions could potentially be characterized by more than two distinct peaks and subsequently more than one mode. Therefore, age distributions were also plotted in form of density plots (Figure 5.23 to 5.28). However, no significant additional peaks were recognized for the single-grain age distributions. Some distributions showed minor additional peaks which may indicate the existence of more than one population of single-grain ages. More than one population of ages might correspond to more than one 'significant' event of alterations in single-grain age distributions.

The interpretation of single-grain age distributions applying different statistical methods revealed and confirmed a number of distinct patterns for the range of soil depth increments sampled:

The median of age distributions from single-grains increased down the soil profile. Subsequently, the amount of near-zero quartz grains declined down the soil profile. These trends were expected. The probability of quartz grains buried at depth reaching the soil surface and being set back to zero was likely to decrease down the soil profile (Bush and Feathers, 2003; Heimsath et al., 2002).

Single-grain age distributions from 50 cm of soil depth were significantly different to depth increments closer to the soil surface, being characterized by an increased amount of older grains present and a shift towards an older median age. This trend indicated a potential change in soil mixing processes at this depth.

Grains near the soil surface were generally much younger, but occasional older grains were also present. The apparent accumulation of a relatively high amount of younger grains near the soil surface is the result of constant bleaching of these grains, demonstrated in Figure 5.1.

Similar grain distributions at soil depths belonging to the same soil horizon may be an indication of mixing processes occurring in the upper half of the soil profile that did not lead to homogenisation of adjacent soil horizons.

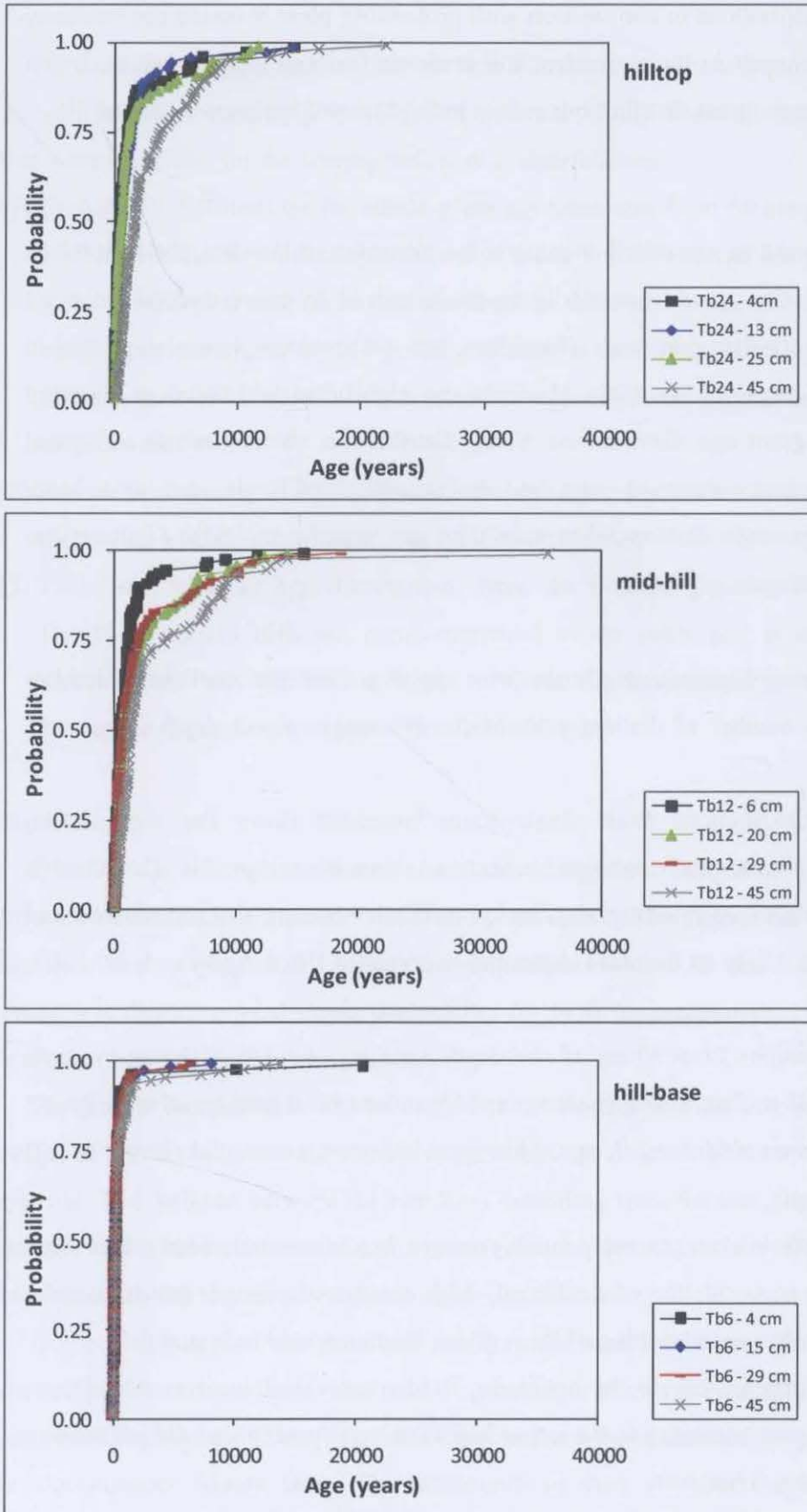


Fig. 5.20a. Toposequence Mount Boss. Probability distribution plots of depth distributions of individual quartz grain ages.



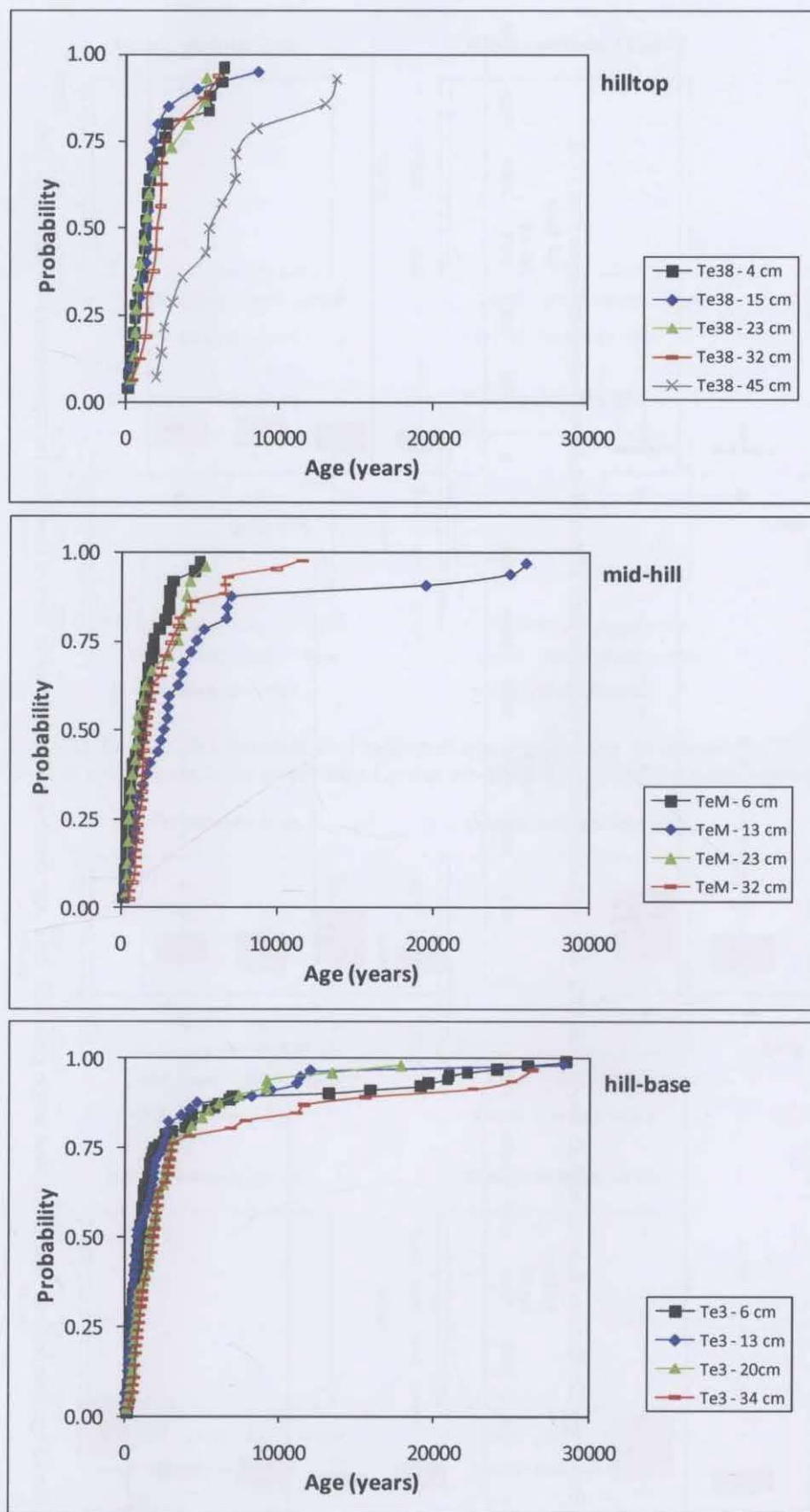


Fig. 5.20b. Toposequence Plateau Beech. Probability distribution plots of depth distributions of individual quartz grain ages.

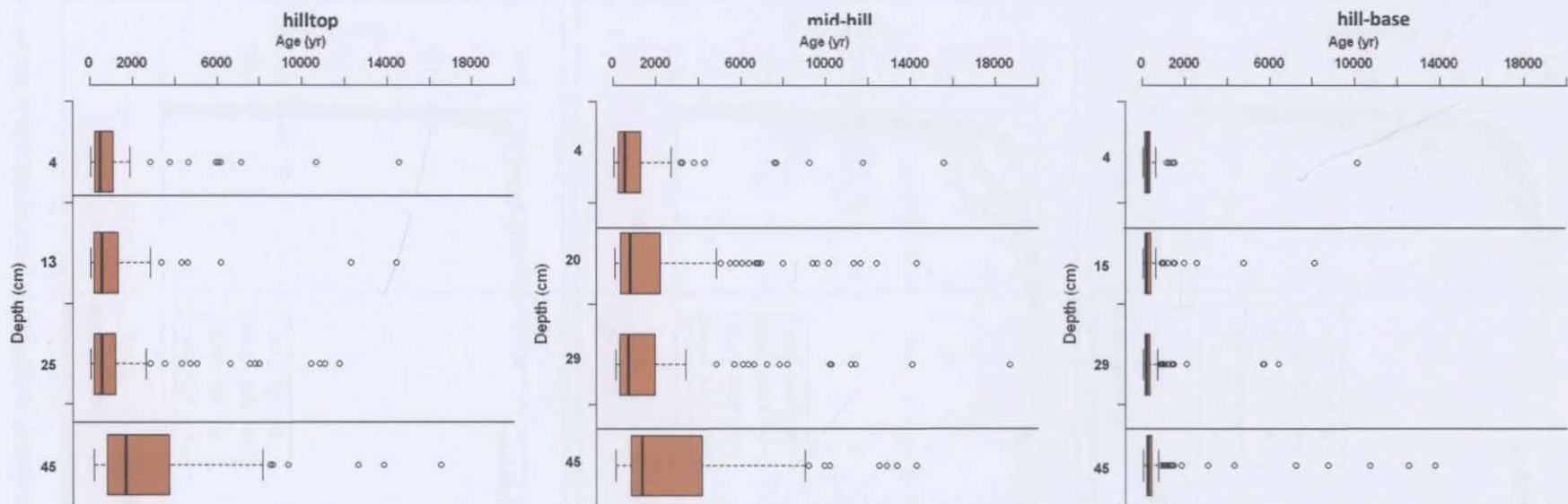


Fig. 5.21. Burial age distributions determined from single grain OSL data. Age distributions are plotted in form of Box Plots for toposequence Mount Boss (Tb).



Fig. 5.22. Burial age distributions determined from single grain OSL data. Age distributions are plotted in form of Box Plots for toposequence Plateau Beech (Te).

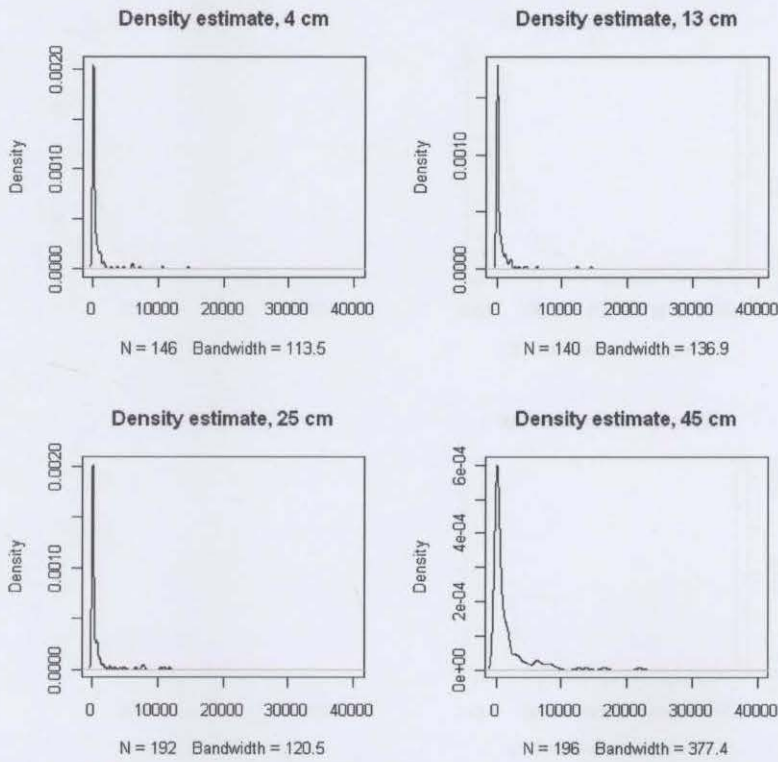


Fig. 5.23. Density plot distribution of individual quartz grain ages for soil profile Tb24 along toposequence Mount Boss. N corresponds to the proportion of grains out of 500 grains with finite age estimates from OSL data.

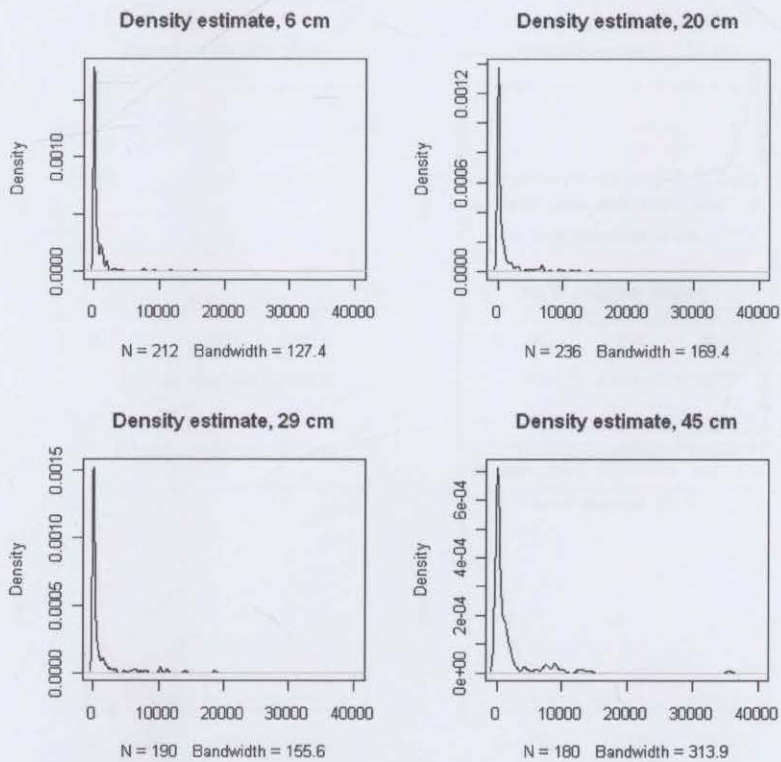
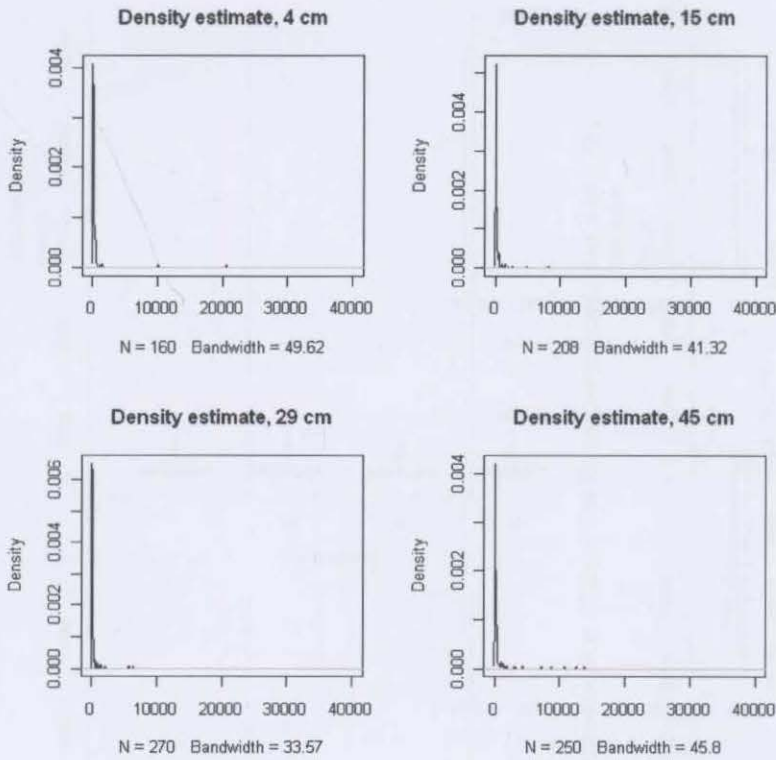
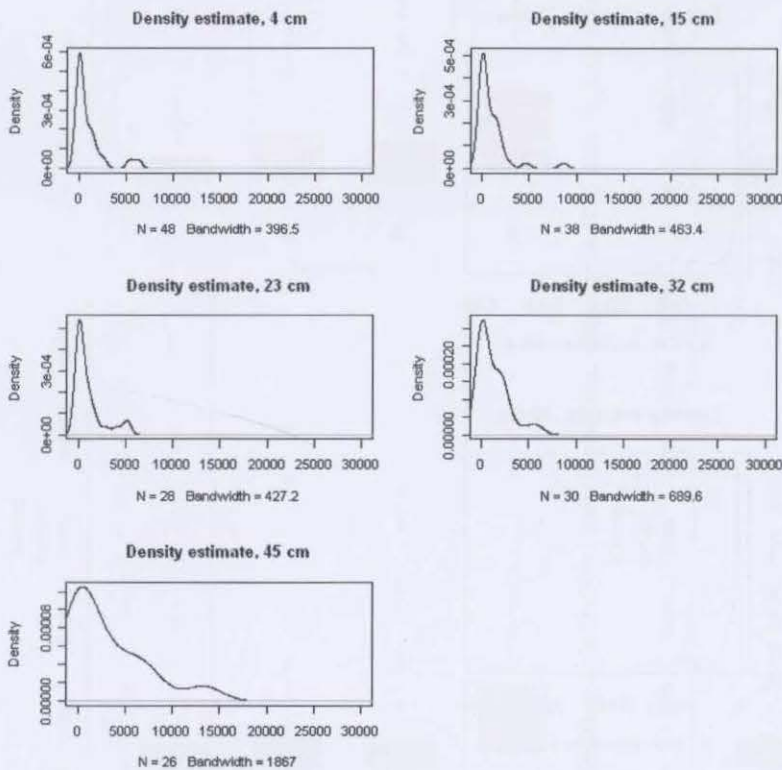


Fig. 5.24. Density plot distribution of individual quartz grain ages for soil profile Tb12 along toposequence Mount Boss. N corresponds to the proportion of grains out of 500 grains with finite age estimates from OSL data.



**Fig. 5.25.** Density plot distribution of individual quartz grain ages for soil profile Tb6 along toposequence Mount Boss. N corresponds to the proportion of grains out of 500 grains with finite age estimates from OSL data.



**Fig. 5.26.** Density plot distribution of individual quartz grain ages for soil profile Te38 along toposequence Plateau Beech. N corresponds to the proportion of grains out of 500 grains with finite age estimates from OSL data.

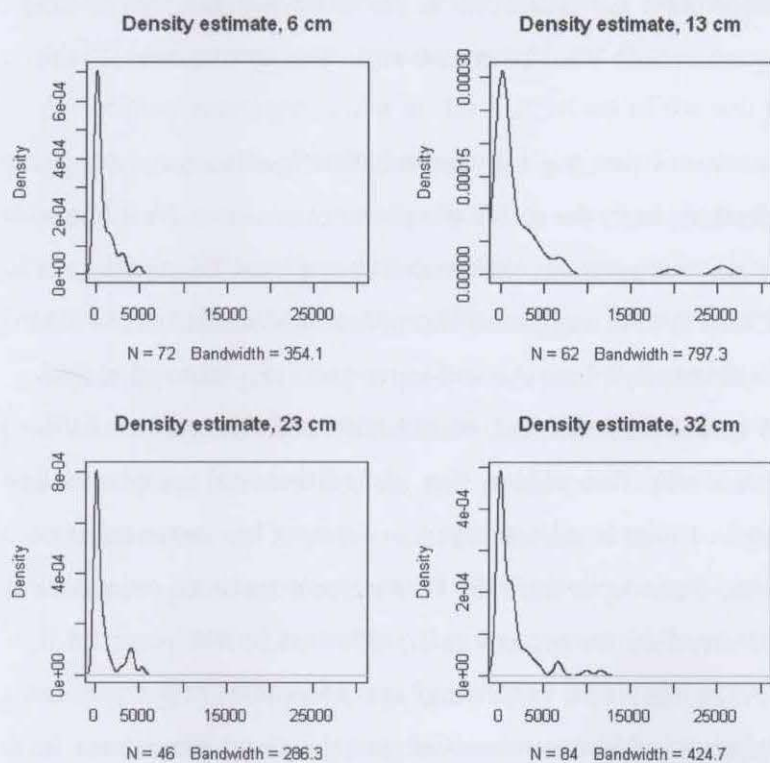


**Fig. 5.27.** Density plot distribution of individual quartz grain ages for soil profile TeM along toposequence Plateau Beech. N corresponds to the proportion of grains out of 500 grains with finite age estimates from OSL data.

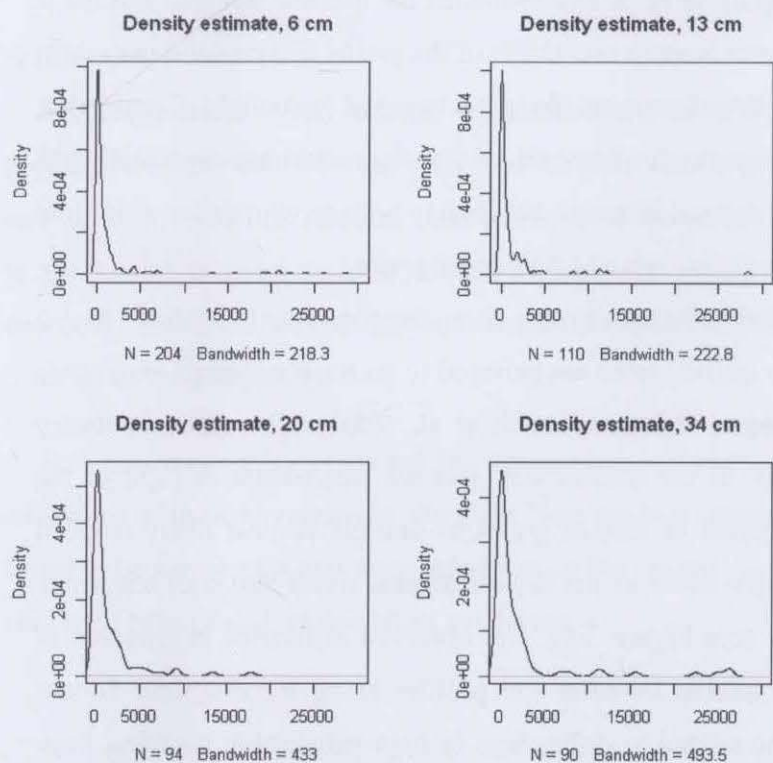


**Fig. 5.28.** Density plot distribution of individual quartz grain ages for soil profile Te3 along toposequence Plateau Beech. N corresponds to the proportion of grains out of 500 grains with finite age estimates from OSL data.

Resulting from the interpretation of single-grain age distributions, the following conclusions can be made in relation to the proposed questions on the occurrence and velocity of potential soil mixing rates:

Reflecting back on the literature review of pedologically related OSL publications, single-grain age and subsequently dose distributions from the native forest environment of Werrikimbe are consistent with distributions for an environment influenced by minor frequencies of pedoturbation (Bush and Feathers, 2003). It was suggested that minor pedoturbations would result in positively or negatively skewed density plots. Accordingly, positively skewed single-grain age distributions, present for all soil depths sampled, would have been the result of low frequency mixing of older grains into the soil. This implies that the soil material sampled at a certain soil depth is as 'old' as the range of data around the median value of the distribution of ages. For instance, soil material at about 50 cm depth from the hilltop positions of toposequence Mount Boss and Plateau Beech would therefore be approximately 2000 and 5500 years 'old', respectively (Figure 5.21 and Figure 5.22). As stated earlier this age refers to the time elapsed since soil material out of 50 cm of depth has last seen the sunlight. However, it needs to be considered that the single-grain dose distributions proposed by Bush and Feathers (2003) were for sedimentary deposits where exposure histories are different to those of undisturbed stable soil environments. In interpreting single-grain dose or age estimates for the soil samples studied it needs to be taken into account that approximately two-thirds of the grains analysed did not return an OSL signal on the reader and were therefore most likely not exposed to sunlight. Considering this relatively high amount of infinite ages in the distribution of grains would hypothetically shift age distributions towards a negatively skewed bimodal distribution with an abundance of infinite grains interspersed with lower frequencies of 'mixed in' younger grains.

To comprehend the exposure history of single-grains from the forest soils studied, it also needs to be considered that Australian quartz grains are believed to be some orders of magnitude brighter than samples from for example, Europe (Pietsch et al., 2008). Therefore, in theory 'bleaching' opportunities are 'optimal' at the studied site. But the penetration of light to the forest floor and subsequently the exposure of surface grains to sunlight is most likely reduced due to understorey and foremost canopy cover of the dry eucalyptus forest and cool temperate rainforest where sampling took place (see Figure 3.8). The observed difference in amounts of single-grains responsive to OSL stimulation between soil profiles along toposequence Mount Boss and Plateau Beech might also be related to differences in light penetration resulting from different vegetation patterns. Lower responses for the cool temperate rainforest environment at

toposequence Plateau Beech may be caused by denser canopy cover compared to the dry eucalyptus forest present at toposequence Mount Boss.

A complete homogenisation of the first 50 cm of the soil profile was not visible in this set of single-grain age data. Pedoturbations did not seem to impact the distribution of grains to the extent of homogenizing grain distributions, which are hypothesized to be visible in a wide range of age data with low frequencies at any single value (Bush and Feathers, 2003). This is in contrast to conclusions drawn by Wilkinson and Humphreys (2005).

Reflecting back on Chapter 3, it was stated that profile differentiation was observed for all profiles studied and that horizonation was most prominent along toposequence Plateau Beech. Soil horizons were identified by soil profile descriptions in the field based on changes in soil colour, structure and strength. Comparing distributions of single-grains in relation to identified soil horizons, similar patterns in the distribution of single-grain estimates were recognized.

It is hypothesized that along the toposequences lateral downwards movement of medium-sized quartz grains may potentially be faster than vertical movements in the soil profile and may drive the distribution of grains in the soil profiles located at the mid-hill and base-of-the-hill positions.

#### *5.3.3.2 Determination of mixing rates from ages of individual quartz grains*

##### *Soil residence time*

Residence times of soil material were calculated for equivalent soil depths applying the soil-production model derived from TCN (see Chapter 4.5.2). In addition to the thickness of the soil and the soil production rate, the bulk densities of the parent material and the soil were included in the model to generate soil residence times. As anticipated, potential soil residence times decreased down the soil profile with surface layers being characterised by possibly the oldest material in the soil profile.

Soil residence times predicted for toposequence Plateau Beech were generally higher. This concurred with observations in the field. Soil profiles along toposequence Plateau Beech were found to be the deepest and were subsequently the 'oldest' soil profiles with up to 80000 years of residence time of soil, as described in Chapter 4.

Tab. 5.5. Soil residence times for equivalent soil depths.

ID	Depth [cm]	Soil residence time [yr]	ID	Depth [cm]	Soil residence time [yr]	ID	Depth [cm]	Soil residence time [yr]
<b>Toposequence Mount Boss (Tb)</b>								
Tb24	4	33 893	Tb12	6	40 188	Tb6	4	43 381
Tb24	13	26 957	Tb12	20	29 252	Tb6	15	34 674
Tb24	25	17 943	Tb12	29	22 417	Tb6	29	23 923
Tb24	45	3 500	Tb12	45	10 632	Tb6	45	12 080
<b>Toposequence Plateau Beech (Te)</b>								
Te38	4	64 904	TeM	6	46 605	Te3	6	76 176
Te38	15	55 634	TeM	13	40 983	Te3	13	70 063
Te38	23	49 044	TeM	23	33 115	Te3	20	64 051
Te38	32	41 781	TeM	32	26 196	Te3	34	52 323
Te38	45	31 564						

*Soil mixing rates*

Calculated individual single-grain age estimates from each soil depth sampled were used to calculate rates of soil mixing for each grain:

$$\text{Soil mixing rates} = \frac{\text{Depth of burial (mm)}}{\text{OSL age (yr)}} \quad \text{equation (5.3).}$$

These estimates were then employed to generate average soil mixing rates (Table 5.6, Figure 5.29 and 5.30). Additional estimates of vertical and lateral rates of soil mixing for each toposequence were based on the following:

- (1) Similar rates of bioturbation were posited for all soil profiles.
- (2) It was assumed that soil profiles located at the hilltop were influenced by constant removal of soil material and bioturbation only. Therefore, it was hypothesized that the observed distribution of grain age estimates resulted solely from vertical movements in the soil profile.
- (3) Accordingly, mixing rates calculated for the hilltop positions were used to estimate vertical rates of soil turnover.
- (4) For soil profiles situated at the mid-hill position rates of bioturbation as well as constant removal and deposition of soil material at the soil surface due to bioturbation as well as potential erosion-deposition processes were assumed.
- (5) Soil profiles at the base of the hill were believed to be influenced by bioturbation and deposition of upper slope material only.
- (6) Hence, it was concluded that by assuming equal rates of bioturbation along the hillslope, rates of lateral displacement of soil particles can be estimated by calculating the difference in soil mixing rates for soil profiles located at the mid-hill and hill-base positions.



**Tab. 5.6.** Calculated average rates of soil mixing for toposequence Mount Boss and Plateau Beech. Average soil mixing rates in  $\text{mm yr}^{-1}$  were calculated from individual mixing rates for single quartz grains for each soil depth, following equation 5.3. The distribution of these individual mixing rates for all depth increments sampled at each hillslope position is shown in the histograms in Figure 5.29 and 5.30.

Depth [cm]	Vertical mixing rates [ $\text{mm yr}^{-1}$ ]	Lateral mixing rates [ $\text{mm yr}^{-1}$ ]	Depth [cm]	Vertical mixing rates [ $\text{mm yr}^{-1}$ ]	Lateral mixing rates [ $\text{mm yr}^{-1}$ ]
<b>Toposequence Mount Boss (Tb)</b>			<b>Toposequence Plateau Beech (Te)</b>		
4	0.085	0.177	4	0.031	0.014
13	0.228	0.515	15	0.103	0.103
25	0.456	1.157	23	0.176	-0.121
32	N. A.	N.A.	32	0.154	-0.017
45	0.270	1.452	45	0.083	N.A.
Mean <sup>1)</sup>	0.263	0.897	Mean <sup>1)</sup>	0.092	-0.008

<sup>1)</sup>Mean values were calculated implementing individual vertical mixing rates determined for single-grains from each soil depth sampled.

Results showed that soil mixing rates determined for toposequence Plateau Beech were slower than rates calculated for toposequence Mount Boss (Figure 5.29 and 5.30).

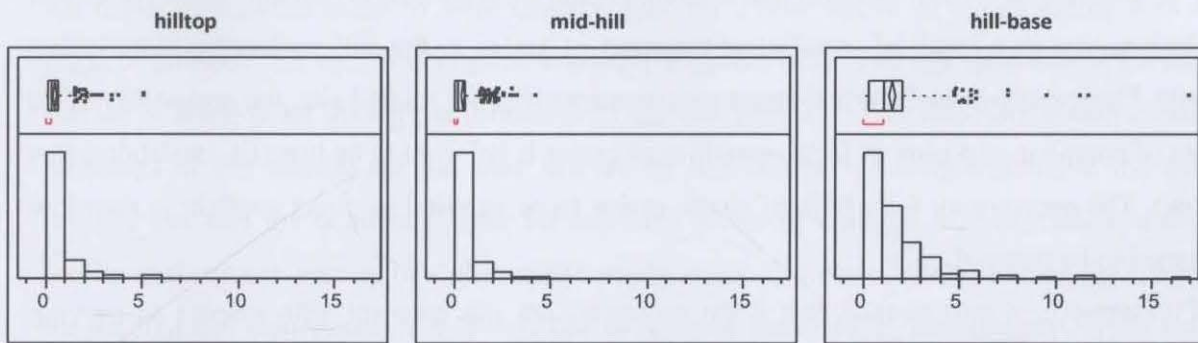


**Fig. 5.29.** Histograms of soil mixing rates in  $\text{mm yr}^{-1}$  for toposequence Mount Boss (includes all depth increments).

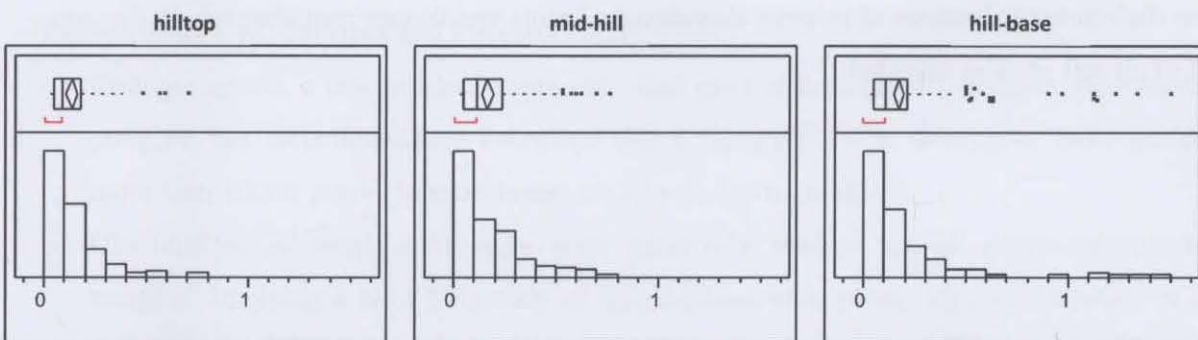


**Fig. 5.30.** Histograms of soil mixing rates in  $\text{mm yr}^{-1}$  for toposequence Plateau Beech (includes all depth increments).

Vertical mixing rates of soil ranged between 0.03 and 0.2  $\text{mm yr}^{-1}$  and 0.1 and 0.5  $\text{mm yr}^{-1}$ , respectively. Both toposequences revealed the tendency for vertical mixing rates to increase (in terms of being faster) with soil thickness to a depth of about 25 cm and to subsequently decrease (in terms of being slower) with soil thickness down to a depth of 50 cm. Vertical mixing rates

were as high or as 'fast' as  $0.5$  and  $0.2 \text{ mm yr}^{-1}$  at  $25 \text{ cm}$  of soil depth and as low or as 'slow' as  $0.3$  and  $0.1 \text{ mm yr}^{-1}$  at  $50 \text{ cm}$  at toposequence Mount Boss and Plateau Beech, respectively.

Lateral mixing rates appeared to be potentially faster down the soil profile for toposequence Mount Boss. Here, rates of lateral transport of single-grains exceeded the vertical displacement of individual grains. This pattern could not be observed for toposequence Plateau Beech where the velocity of lateral movements of single-grains was only estimated to occur down to  $15 \text{ cm}$  of depth. Furthermore, lateral rates in the top two soil depths were much slower than vertical rates.

Comparing soil residence times with rates of vertical and lateral displacement of single-grains suggested that some grains may have visited the soil surface repeatedly and that most grains were not exposed to sunlight at any time during the formation of the soil profile or were not sufficiently bleached during exposure at the soil surface. Insufficient exposure histories of grains can be anticipated for soil samples due to grains being incorporated in soil aggregates or in soil inclusions and as a result of insufficient transport of grains to the soil surface by bioturbating agents. Particularly in undisturbed forest environments like the studied site, the probability of an event of complete exposure of large quantities of grains is believed to be low (i.e. landslides, tree throw). The opportunity for a bulk of single-grains to be exposed to direct sunlight is therefore assumed to be reduced.

Furthermore, it was posited that grain velocities are not constant with respect to moving grains up and down the soil profile in a circular motion. Moreover, it was hypothesized that at the field site studied downwards vertical movements were the dominant factor in generating grain distributions, because of relative abundance of roots and former root channels in the upper half of all soil profiles sampled.

## 5.4 Conclusions

Analysing distributions of single-grain OSL age estimates from soil samples of Werrikimbe National Park revealed that tools used for interpreting distributions in depositional environments, i.e. fluvial or aeolian, cannot be applied readily for interpreting soil samples from natural, undisturbed forested environments.

In relation to the research question on pedogenesis 'How fast are rates of soil turnover occurring in the soil profile and what influence do they have on pedogenesis?' the following can be concluded from single-grain OSL age estimates:

1. The observed good agreement of dose rate calculations at the depth increments sampled is an indication of relatively stable environmental conditions at toposequence Mount Boss and Plateau Beech over the past centuries.
2. All depth increments sampled were characterized by a distribution of single grains with a finite or infinite OSL age. This implied exposure of grains with finite age estimates at the soil surface at some point during the formation of the soil profile. It was therefore assumed that processes of soil mixing are the main drivers for displacement of single-grains in the soil profiles and also the dominant factor for exposing grains to sunlight. Hypothetically, a soil profile without any mixing of soil material would result in a distribution of finite OSL ages for the first few centimetres of soil only due to constant bleaching by disturbances of the soil surface, i.e. by rainsplash, macrofauna or microfauna.
3. The distribution of single-grain age estimates varied in the first 50 cm of soil for both toposequences, Mount Boss and Plateau Beech.
  - a. Younger grains, a few hundred years old, were present throughout the depth increments sampled, but their abundance decreased down the profile. The occasional older grains more than 10000 years old were found for all soil depths analysed.
  - b. Distributions of single-grain ages were positively skewed for all depth increments sampled, implying a high frequency of single-grains with young ages in the range of a few hundred to a few thousand years. However, grain distributions did not correspond to the total amount of 500 grains analysed for each depth increment. They referred to the proportion of single-grains for which a finite age could be calculated. Approximately two-thirds of the grains analysed were characterised by infinite ages because they did not have a sufficient enough OSL signal, which implied no exposure to sunlight during the formation of the soil profile or insufficient bleaching during transport.

- c. Positively skewed distributions of single-grain age estimates implied low mixing velocities of soil grains. Considering the high proportion of grains with an infinite age in interpreting grain distributions, it was hypothesized that younger grains were mixed into much 'older' soil material that might have not been exposed to sunlight at any time. High frequent mixing would have resulted in similar grain distributions throughout the depth increments sampled, with a wide range of age estimates with low frequencies at any single grain value. And possibly higher percentages of finite grains compared to infinite grains.
  - d. Calculated vertical mixing velocities indicated soil turnover rates of 0.2 and 0.5 mm yr<sup>-1</sup> in the first 25 cm of soil. Results revealed that vertical mixing rates within close distance to the soil surface seemed to be lower than rates deeper down the profile. This implied the following for mixing rates in the upper soil profile: Soil mixing rates are most likely varying with depth, with rates increasing down to 25 cm and subsequently decreasing down to 50 cm. Varying vertical displacements of grains may have been anticipated because turbation rates in the field are almost certainly not following constant circular motions of moving grains up and down in the soil profile. If equal downwards movement of grains is assumed, it would take about 500 and 1250 years to transport the proportion of grains that has been exposed to sunlight from the soil surface down to 25 cm of depth for toposequence Mount Boss and Plateau Beech, respectively. These rates are relatively low when compared to rates of complete turnover of the top 50 cm of soil of approximately 700 years, found in the literature (Amundson, 2004).
  - e. Furthermore, it can be posited that only the first few centimetres of the soil profile were bleached frequently since a high frequency of zero and close to zero ages was not visible for the first 3 to 6 cm of soil. And that soil material close to the parent material would have never been exposed to sunlight.
4. Based on field observations, it is believed that at the field site studied vertical grain distributions were mainly driven by downward transport directed by floral agents. Consequently, plant roots may control the observed changes in single-grain age distributions present at approximately 50 cm of soil depth. Soil profiles along toposequence Mount Boss and Plateau Beech were characterized by an abundance of root channels in the first 30 to 50 cm of the soil profile (see profile pictures of Figure 5.31 and 5.32). Translocation of sand-sized grains through former root channels would explain the occurrence of younger grains deeper down the soil profile. Vertical transport of sand-sized grains to deeper parts of the soil profile predominantly along voids and channels after root-decay was also proposed for a

study of periglacial slope deposits in Germany where younger grains were present in layers of much older deposits. Here, micromorphological analysis confirmed the presence of root channels and voids of up to 5 mm in size and macropores within the diameter of some centimetres (Hülle et al., 2009).

5. The occurrence of faunal agents, in particular earthworms, was also observed in the soil profiles during field work. Nevertheless, earthworms did not seem to be as 'active' as estimated in some of the studies referred to in Chapter 2. As discussed, soil mixing rates resulting from earthworm activities can be as low as approximately  $0.5 \text{ mm yr}^{-1}$  and as high as approximately  $10 \text{ mm yr}^{-1}$ . Earthworms have the ability to produce higher rates of soil alteration because they also ingest the soil material in addition to moving soil particles by mounding and burrowing. There is the possibility that at the studied site earthworm activities were impeded by particle size or the observed occurrence of relatively high amounts of tree roots and stones in the topsoils.
6. There is also the possibility of aeolian deposition of grains on the toposequences. However, the probability of transport of surface grains by wind is most likely eliminated in this forested environment, because of biotic ground cover (Dietrich and Perron, 2006).
7. Our estimates of vertical soil mixing rates fell into the lower range of published soil mixing rates from various turbating agents that were estimated using other methods than *in situ* numerical dating. As concluded in Chapter 2, the majority of published rates were characterized by higher values than  $0.5 \text{ mm yr}^{-1}$ . However, estimates are similar to grain velocities that were estimated for south-eastern Australia by applying numerical dating (Heimsath et al., 2002).
8. Estimated rates of lateral transport were higher than vertical mixing rates for toposequence Mount Boss and lower for toposequence Plateau Beech. This observation agreed with differences in grain distributions for both toposequences. It appeared that grain distributions for soil profiles along toposequence Mount Boss were influenced by dominance in lateral transport. Grain distributions at Mount Boss were more similar to distributions from depositional environments, with an abundance of younger grains and the occasional older grains. Hence grain distributions derived for soil profiles along toposequence Mount Boss potentially resulted from frequent rates of erosion and deposition along the hillslope.
9. Even though the first 50 cm of all soil profiles were influenced by processes of soil mixing, displacement of grains did not result in a homogenisation of the first 50 cm for any of the six soil profiles analysed. Surface and subsurface soil layers were present in all soil profiles (see

Figure 5.31 and 5.32). Subsequently, rates of bioturbation did not prevent horizonation processes.

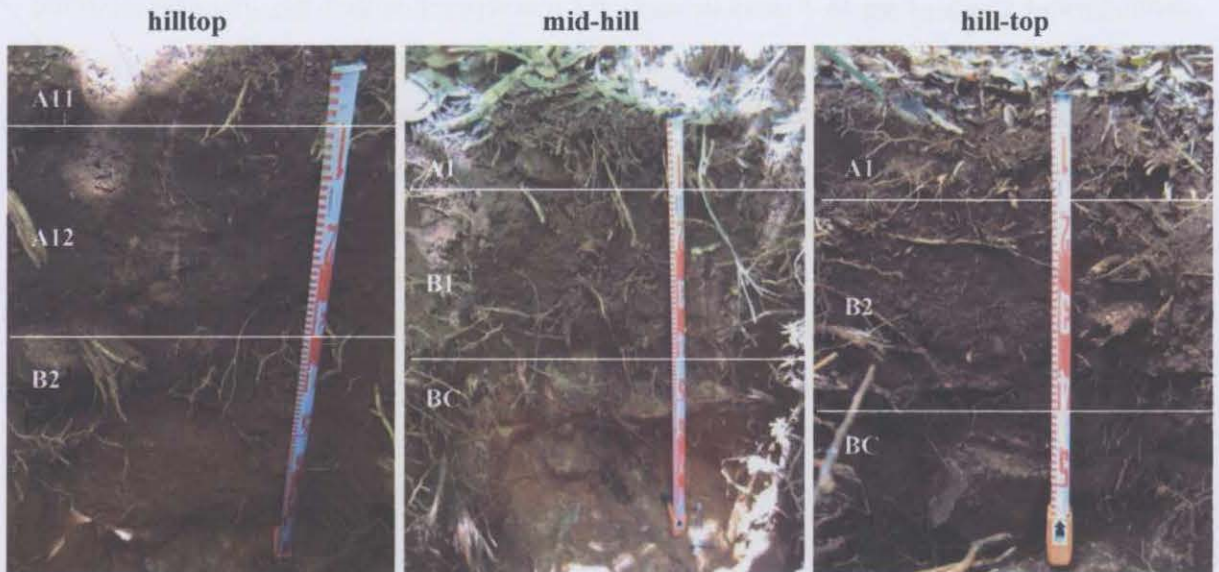


Fig. 5.31. Soil profiles along toposequence Mount Boss.

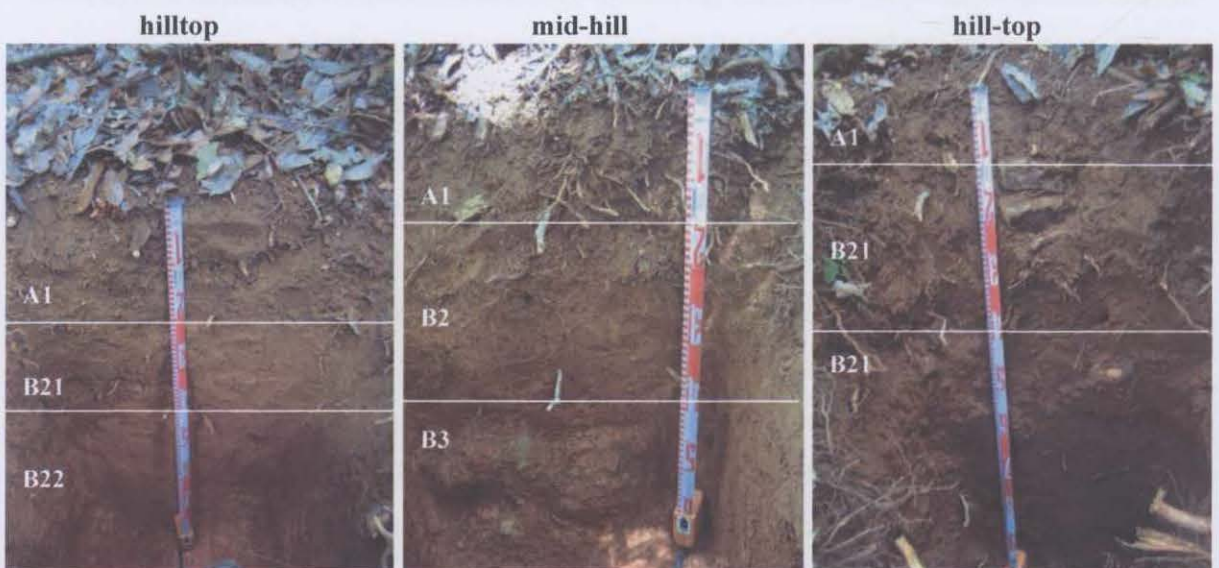


Fig.5.32. Soil profiles along toposequence Plateau Beech.

Determining soil horizons in the field was based on the field morphology, particularly structure and strength, and a noticeable colour change between layers. Comparing soil profile pictures of both toposequences, it is clearly visible that soil horizons at toposequence Mount Boss were defined by observed changes in soil structure and only minor changes in soil colour, whereas soil horizons were readily identified through differences in colour for soil profiles along toposequence Plateau Beech. These differences are most likely related to the proposed differences in displacement velocities of single-grains within the soil.

The vertical distribution of soil particles, in particular soil organic carbon, is in good agreement with vertical distributions of single-grains detected by age estimates. The presence of significant amounts of soil organic carbon in the surface as well as the subsurface soil (Figure 5.33) corresponds to root decay, but also to translocations along channels and macropores and translocations within the soil-solution. Recalling the analysis of soil chemical properties more or less significant amounts of soil organic carbon were found for all soil profiles. Along toposequence Mount Boss hard nodules of charcoal were also present, particularly at the hill-base position. The vertical distribution of soil organic carbon, in particular charcoal, in the soil profiles therefore most likely confirms the occurrence of translocations of soil particles.

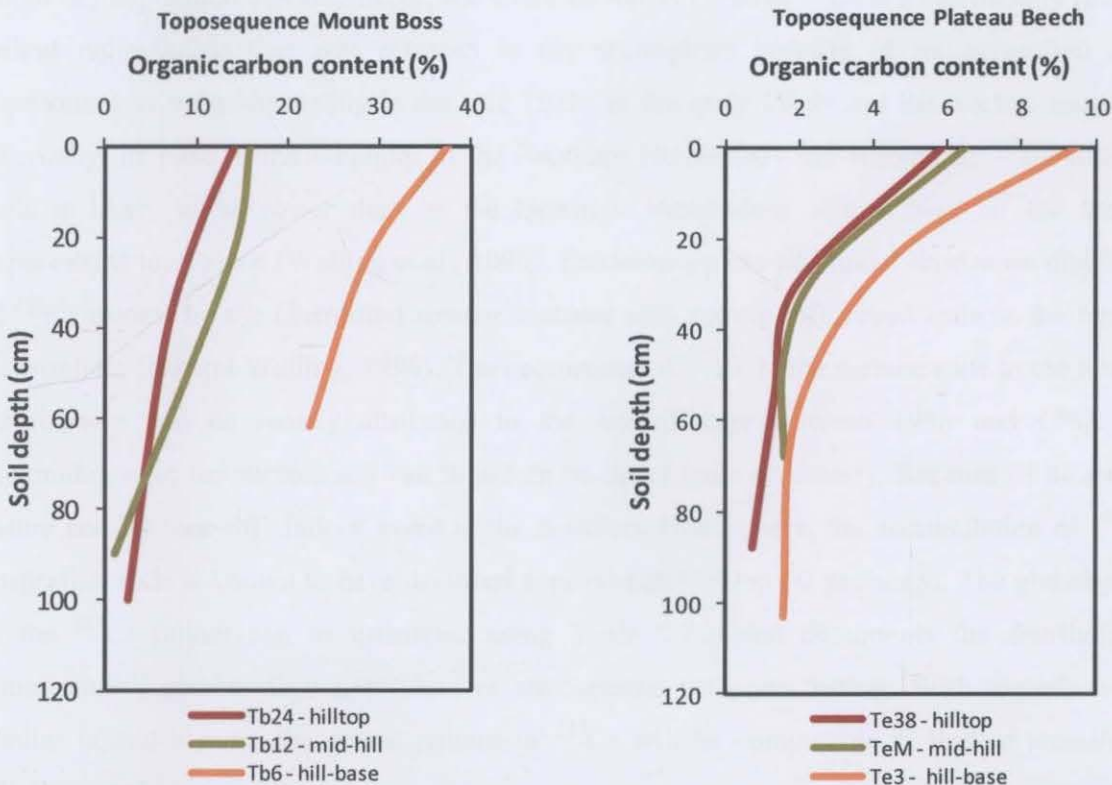
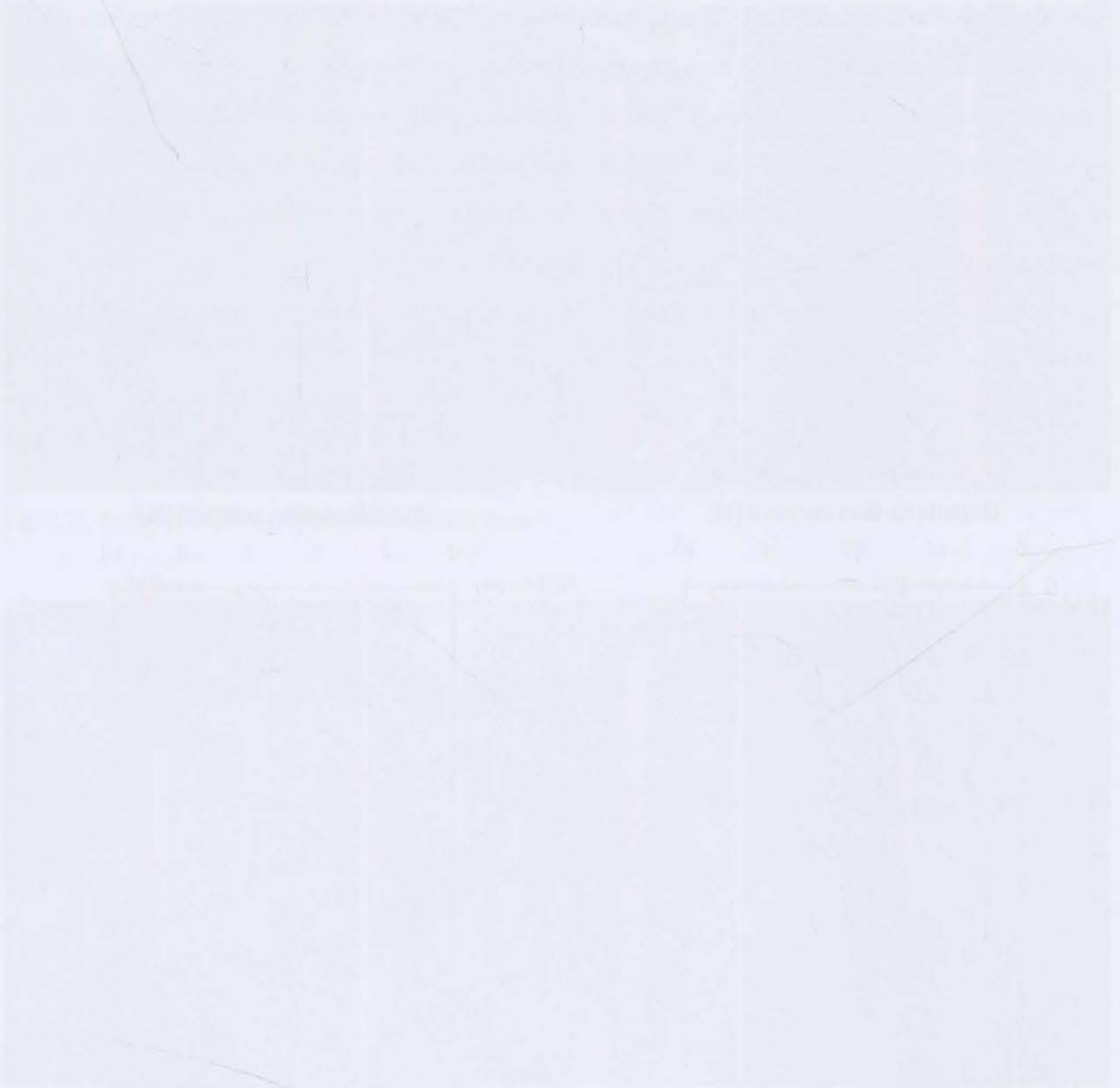


Fig. 5.33. Distribution of soil organic carbon for soil profiles along toposequence Mount Boss and Plateau Beech.

10. Based on the proportion of grains with finite, compared to, infinite ages, together with the actual ages estimated for single-grains it could be argued that soils at the studied field site evolved 'in situ' about 40000 years ago. Approximately 40000 years was estimated for quartz grains that had accumulated the greatest population of electrons in their crystal structure since last exposed to sunlight. Single-grains with ages older than 40000 years were

not present in the bulk samples. This might relate to grains not being exposed to the soil surface.





## 5.5 Fallout radionuclides – Caesium-137 ( $^{137}\text{Cs}$ ) and excess lead-210 ( $^{210}\text{Pb}_{\text{ex}}$ )

### 5.5.1 Introduction

As described in section 5.1, in order to calculate the annual dose rate quartz grains have received over time, the concentration of radionuclides was measured through gamma spectrometry. During gamma spectrometry analysis, the concentration of the fallout radionuclides caesium-137 ( $^{137}\text{Cs}$ ) and excess lead-210 ( $^{210}\text{Pb}$ ) was also determined. The concentration of these fallout radionuclides was used in conjunction with OSL age estimates to further investigate potential short-term vertical and lateral mixing rates of soil.

### 5.5.2 Principles of the input of $^{137}\text{Cs}$ and $^{210}\text{Pb}_{\text{ex}}$ to surface soils

$^{137}\text{Cs}$  and  $^{210}\text{Pb}_{\text{ex}}$  are dominantly deposited to the earth surface via precipitation (some very minor dry deposition can also occur, see Clark and Smith (1988)).  $^{137}\text{Cs}$  is an artificially produced fallout radionuclide that was released to the atmosphere because of its generation during thermonuclear weapons testing in the mid 1950s to the early 1960s and the nuclear accident of Chernobyl in 1986 in the Ukraine. In the Southern Hemisphere the amount of  $^{137}\text{Cs}$  in surface soils is likely to be lower than in the Northern Hemisphere where most of the bombing experiments took place (Walling et al., 1995). Furthermore, the additional short-term distribution of  $^{137}\text{Cs}$  caused by the Chernobyl reactor accident also mainly influenced soils in the Northern Hemisphere (He and Walling, 1996). The occurrence of  $^{137}\text{Cs}$  in the surface soils in the Southern Hemisphere can be mostly attributed to the fallout time between 1955 and 1963.  $^{137}\text{Cs}$  accumulation in the surface soil can therefore be dated quite accurately. Because of its artificial nature and its 'one-off' fallout event in the Southern Hemisphere, the accumulation of  $^{137}\text{Cs}$  in Australian soils is known to have occurred approximately 50 to 60 years ago. The global pattern of the  $^{137}\text{Cs}$  fallout can be estimated using Table 5.7 which documents the distribution of strontium-90, another fission product of atmospheric weapons testing. With regards to their similar fallout history, the global pattern of  $^{137}\text{Cs}$  will be comparable to that of strontium-90 (Walling et al., 1995).

To date,  $^{137}\text{Cs}$  has been the most widely applied fallout radionuclide in soil erosion studies. But with a half-life of 30.17 years the artificially-produced  $^{137}\text{Cs}$  will not be available some time in the future because of its radioactive decay.  $^{137}\text{Cs}$  is therefore often used in conjunction with  $^{210}\text{Pb}_{\text{ex}}$ , a naturally produced fallout radionuclide, whose use as an alternative to  $^{137}\text{Cs}$  is currently being further explored (Mabit et al., 2008).

$^{210}\text{Pb}$  is a natural product of the Uranium-238 ( $^{238}\text{U}$ ) decay series and is derived from the decay of gaseous radon-222 ( $^{222}\text{Rn}$ ), a daughter radionuclide of radium-226 ( $^{226}\text{Ra}$ ).  $^{226}\text{Ra}$  occurs naturally in soils and rocks and generates  $^{210}\text{Pb}$ , which will be in equilibrium with its parent ( $^{226}\text{Ra}$ ). The diffusion of a small quantity of  $^{222}\text{Rn}$  from the soil introduces  $^{210}\text{Pb}$  into the atmosphere. The fallout of this quantity of  $^{210}\text{Pb}$  onto the soil surface is called the unsupported or excess  $^{210}\text{Pb}$  and can not be accounted for because its concentration in the surface soil is in disequilibrium with its *in situ* parent  $^{226}\text{Ra}$ . The amount of  $^{210}\text{Pb}_{\text{ex}}$  in the soil sample can be determined by measuring the concentration of  $^{210}\text{Pb}$  and  $^{226}\text{Ra}$  and then subtracting the *in situ* parent.  $^{210}\text{Pb}_{\text{ex}}$  is continuously replenished on the soil surface because of its constant generation and fallout from the atmosphere. The annual variation of its global distribution is presented in Table 5.8 With a half-life of 22.26 years  $^{210}\text{Pb}_{\text{ex}}$  can be used to assess short-term (< 100 years) pedogenic processes (Kaste et al., 2007; Mabit et al., 2008; Walling et al., 1995).

**Tab. 5.7.** Latitudinal variation of mean bomb-derived strontium-90 inventories at the end of 1983 (after Walling et al. (1995)).

Latitude band	Mean strontium-90 inventory [Bq m <sup>-2</sup> ]	Mean strontium-90 inventory [Bq m <sup>-2</sup> ]
	Northern hemisphere	Southern hemisphere
0-10	953	526
10-20	1370	491
20-30	2075	841
<b>30-40</b>	<b>2862</b>	<b>967</b>
40-50	3867	1124
50-60	3585	672
60-70	2084	455
70-80	897	276
80-90	409	154

**Tab. 5.8.** Global variation in the total annual deposition of lead-210 (after Walling et al. (1995), and using a conversion rate of 1 dpm cm<sup>-2</sup> yr<sup>-1</sup> equal to 166 2/3 Bq m<sup>-2</sup> yr<sup>-1</sup>).

Location	Mean $^{210}\text{Pb}$ deposition rate [dpm cm <sup>-2</sup> yr <sup>-1</sup> ]	Mean $^{210}\text{Pb}$ deposition rate [Bq m <sup>-2</sup> yr <sup>-1</sup> ]
Suva, Fiji	0.48	80
Auckland, New Zealand	0.30	50
Delhi, India	0.80	133
Calcutta, India	0.61	102
Bombay, India	1.50	250
<b>Sydney, Australia</b>	<b>0.32</b>	<b>53</b>
Alice Springs, Australia	0.34	57
Darwin, Australia	0.57	95
Hokkaido, Japan	2.20	367
Milford Haven, UK	0.51	85
Moscow, Russia	0.69	115
New Haven, USA	0.92	153

### 5.5.3 Using $^{137}\text{Cs}$ and $^{210}\text{Pb}_{\text{ex}}$ to investigate short-term processes of pedogenesis

Precipitated  $^{210}\text{Pb}_{\text{ex}}$  and  $^{137}\text{Cs}$  are absorbed by the surface soil and redistributed down the soil profile predominantly through their strong affinity to other soil particles (He and Walling, 1996).

Applications based on  $^{210}\text{Pb}$  in soils have shown that  $^{210}\text{Pb}$  is passively transported down the soil profile using soil particles as carrier substances. Soil organic matter is believed to be one of the main carriers for lead. Dörr (1995) observed  $^{210}\text{Pb}$  migration velocities that were almost identical to organic matter sedimentation in forest soils. Consequently, it is likely that movement of  $^{210}\text{Pb}$  down a soil profile is caused by processes of bioturbation and soil erosion.

$^{137}\text{Cs}$  is transported passively in the soil profile attached to particles of the fine soil fraction, particularly clay minerals and humic materials (Zapata, 2003). In addition to passive transport,  $^{137}\text{Cs}$  is also transported actively down the soil profile due to mobilization from the solid into the liquid phase (Dörr, 1995). He and Walling (1996) reported that  $^{137}\text{Cs}$  can percolate down the profile through infiltrating or leaching processes. However, the concentration of  $^{137}\text{Cs}$  in the infiltrating water will decrease with increasing depth because some of the radionuclide will be adsorbed through its direct contact with the pore walls in the soil. Consequently, studying the distribution of  $^{137}\text{Cs}$  down the soil profile can be important for observing infiltration and leaching processes in surface soils.

Fallout radionuclides have been widely used to study soil erosion and sediment transport in agricultural and 'natural' environments (Blake et al., 2009; Hancock et al., 2010; He and Walling, 1996; Martinez et al., 2009; Walling et al., 1995; Zapata, 2003). The redistribution of fallout radionuclides in the soil is believed to be a result of erosion, transport and deposition of soil particles that occurred after the main phase of atmospheric deposition (Zapata, 2003). Calculating soil erosion rates using fallout radionuclides requires a stable, locally representative reference site of the area studied. Sites with an inventory lower or higher than the reference site are assumed to be erosional or depositional, respectively (Martinez et al., 2009). Vertical distributions of fallout radionuclides of the soil profiles studied are often compared to simulated vertical fallout radionuclide distributions (i.e. exponential decline of concentrations with increasing soil depth, advection diffusion model, and diffusion and migration model).

Fallout radionuclides can also be used to trace possible mixing processes down the soil profile because of their initial accumulation on the soil surface.

Kaste et al. (2007) used fallout radionuclides to investigate short-term (< 100 years) soil mixing processes. For this study they revisited the field site of the Bega Valley in south-eastern Australia and calculated diffusion-like mixing coefficients of  $0.1\text{--}0.2\text{ mm yr}^{-1}$ , which were

comparable to  $0.1\text{-}0.4\text{ mm yr}^{-1}$  grain-scale velocities calculated from a previous study with luminescence dating (Heimsath et al., 2002). Kaste et al. (2007) used depth profiling and advection-diffusion modelling of the short-lived isotopes Berrilium-7 ( $^7\text{Be}$ ) and  $^{210}\text{Pb}$  to quantify differences in physical soil mixing across different landscapes with contrasting climate, geology and vegetation. The study sites were situated in a forested landscape in the Bega Valley, Australia; on grasslands in Marin County, California; and in montane forests in northern New England. The sites in the Bega Valley and Marin County showed that bioturbation was the dominant soil mixing process with rates of  $5\text{-}10\text{ cm kyr}^{-1}$ . For the New England site significantly slower mixing rates of around  $0.2\text{ cm kyr}^{-1}$  were derived. The difference in soil mixing rates for the New England site could be explained by a possible lack of soil stirring processes in the landscape. The advection-diffusion model failed under coniferous forest cover in New England.

Concentrations of  $^{137}\text{Cs}$  and  $^{210}\text{Pb}_{\text{ex}}$  were interpreted in terms of the following questions:

How far down the soil profiles are  $^{137}\text{Cs}$  and  $^{210}\text{Pb}_{\text{ex}}$  detectable?

Is an accumulation of  $^{137}\text{Cs}$  and  $^{210}\text{Pb}_{\text{ex}}$  down the hillslope visible for each toposequence?

## 5.5.4 Results and discussion

### 5.5.4.1 Vertical and lateral distribution of $^{137}\text{Cs}$ and $^{210}\text{Pb}_{\text{ex}}$

In the following the vertical and lateral distribution of  $^{137}\text{Cs}$  and  $^{210}\text{Pb}_{\text{ex}}$  will be presented and discussed in relation to measured soil properties. As seen in Table 5.9, concentrations of fallout radionuclides decreased with increasing soil depth, with the majority of  $^{137}\text{Cs}$  and  $^{210}\text{Pb}_{\text{ex}}$  present in the first 15 cm of soil, an indication for undisturbed sites (Martinez et al., 2009, 2010).

**Tab. 5.9.** Fallout radionuclide data analysed with gamma spectrometry, displayed in conjunction with relevant soil properties.

Sample ID	$^{226}\text{Ra}$ [Bq kg <sup>-1</sup> ]	$^{210}\text{Pb}$ [Bq kg <sup>-1</sup> ]	$^{210}\text{Pb}_{\text{ex}}$ [Bq kg <sup>-1</sup> ]	$^{137}\text{Cs}$ [Bq kg <sup>-1</sup> ]	Clay [%]	Organic carbon content [%]
<b>Toposequence Mount Boss (Tb)</b>						
Tb24 2.5-7.5	54±1	56±5	1.9±5.5	6.5±0.4	43	14.2
Tb24 11-16	56±1	54±3	0	5.0±0.3	32	10.3
Tb24 23.5-28.5	60±1	54±5	0	2.4±0.3	31	9.2
Tb24 43-48	60±1	45±3	0	0	35	3.3
Tb12 5-10	61±1	46±3	0	4.7±0.2	24	15.8
Tb12 18-23	63±1	53±4	0	3.3±0.3	24	14.4
Tb12 27-32	64±1	47±4	0	1.7±0.2	29	11.1
Tb12 42-47	66±1	40±3	0	0.3±0.1	34	5.2
Tb6 2.5-7.5	42±1	91±4	49.9±4.4	11.2±0.4	14	46.2
Tb6 13-18	51±1	63±3	12.4±3.6	10.0±0.4	13	27.5
Tb6 27-32	51±1	59±3	7.97±3.4	7.4±0.3	14	27.1
Tb6 40.5-45.5	54±1	39±3	0	1.7±0.2	14	22.7
<b>Toposequence Plateau Beech (Te)</b>						
Te38 1.5-6.5	58±1	58±5	0	3.1±0.3	36	7.7
Te38 12-17	56±1	45±4	0	1.4±0.3	39	4.8
Te38 29.5-34.5	58±1	48±4	0	0	43	1.9
TeM 4-9	59±1	60±3	1.6±3.5	3.5±0.2	33	5.5
TeM 12-16	67±1	53±4	0	0.9±0.2	33	5.1
TeM 21.5-26.5	64±1	47±3	0	0.1±0.2	37	3.2
TeM 29-34	63±1	51±4	0	0	37	1.6
Te3 4-8	50±1	49±4	0	4.3±0.3	40	9.5
Te3 10-15	52±1	52±4	0	4.0±0.4	38	6.3
Te3 18-23	51±1	41±3	0	1.8±0.2	41	4.2
Te3 31-36	54±1	37±3	0	0.2±0.2	53	2.0

In order to compare measured  $^{137}\text{Cs}$  and  $^{210}\text{Pb}_{\text{ex}}$  from the study site with published deposition rates of the fallout radionuclides, concentrations in Bq kg<sup>-1</sup> were converted to Bq m<sup>-2</sup> based on the following assumptions:

- (1) Concentrations of fallout radionuclides were calculated following equation 5.4 (Loughran et al., 1990):

$$S = \frac{CM}{A} \quad \text{equation (5.4),}$$

where  $S$  is the  $^{137}\text{Cs}/^{210}\text{Pb}_{\text{ex}}$  content at the site [ $\text{Bq m}^{-2}$ ],  $C$  is the  $^{137}\text{Cs}/^{210}\text{Pb}_{\text{ex}}$  concentration in the sample ( $<2$  mm) [ $\text{Bq kg}^{-1}$ ],  $M$  is the sample mass [kg] and  $A$  is the area of the sample cylinder ( $\text{m}^2$ ).

- (2) The area,  $A$ , for the sampling cores of  $0.0157 \text{ m}^2$  was calculated by using their radius of 2.5 cm and assuming a height of 10 cm. As noted in the 'Materials and Methods' section of this chapter, the outer 5 cm from each end of the sampling core were used for gamma spectrometry analysis.

Concentrations of fallout radionuclides were relatively low when compared to estimated global deposition rates (Table 5.7 and 5.8) and results from different studies in south-eastern Australia, i.e. concentrations as high as  $140 \text{ Bq m}^{-2}$  were recorded for the first 5 cm of soil in the greater area of the Hunter Valley (Martinez et al., 2009). However, the study of Martinez et al. (2009) was conducted in open areas with minor occurrence of trees. Tree canopy, trunk- and stem flow most likely influenced the concentration of fallout radionuclides in the forested environment of Werrikimbe which would explain the relatively low concentrations.

#### *Short-term vertical distribution of $^{137}\text{Cs}$ and $^{210}\text{Pb}_{\text{ex}}$ in the soil profiles*

$^{137}\text{Cs}$  was present in all near surface layers of the six soil profiles analysed (Figure 5.34a and 5.34b). Comparing its vertical distribution, it can be seen that concentrations of  $^{137}\text{Cs}$  of toposequence Mount Boss exceeded concentrations of  $^{137}\text{Cs}$  of toposequence Plateau Beech. It can also be observed that amounts of  $^{137}\text{Cs}$  were the highest at the hill-base position for both toposequences. This may relate to lateral movements of soil material down the hillslope.

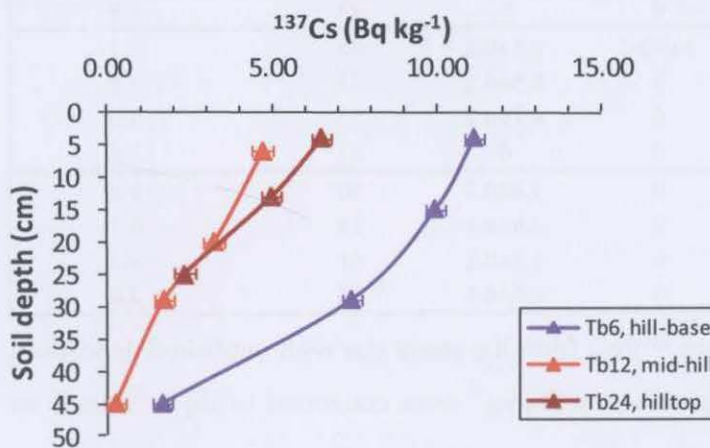


Fig. 5.34a. Vertical distribution of  $^{137}\text{Cs}$  concentrations in the soil profile. Toposequence Mount Boss.

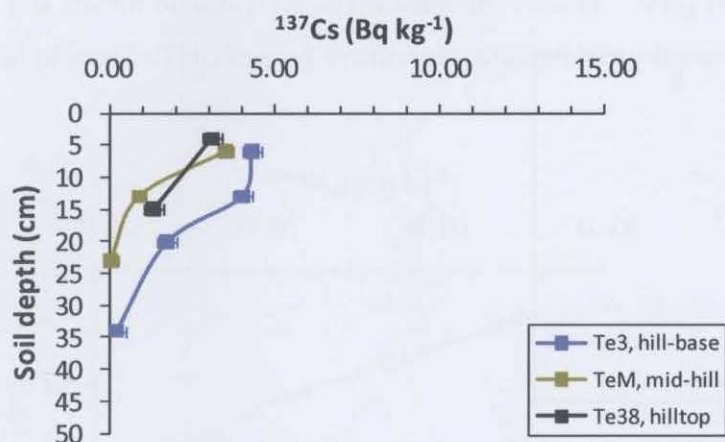


Fig. 5.34b. Vertical distribution of  $^{137}\text{Cs}$  concentrations in the soil profile. Toposequence Plateau Beech.

For all six soil profiles concentrations of  $^{137}\text{Cs}$  were the highest at 3-6 cm of soil depth with gradually decreasing concentrations with increasing soil thickness. Significant amounts of  $^{137}\text{Cs}$  were detected down to about 30 cm of soil depth for profiles in hilltop and mid-hill position of toposequence Mount Boss. However, for the hill-base position of toposequence Mount Boss  $^{137}\text{Cs}$  was present down to approximately 50 cm.

In contrast to toposequence Mount Boss, for all soil profiles along toposequence Plateau Beech significant amounts of  $^{137}\text{Cs}$  were only observed down to about 25 cm.

It can be assumed that the main fallout time of  $^{137}\text{Cs}$  occurred about 50 years ago and that  $^{137}\text{Cs}$  was fixated on soil particles like soil organic carbon and clay particles shortly after its deposition from the atmosphere. However, the redistribution of  $^{137}\text{Cs}$  in the soil profiles is most likely a combination of initial active migration through infiltration and leaching processes in conjunction with passive transport (Eguchi et al., 2010).  $^{137}\text{Cs}$  concentrations correlated significantly ( $R^2 = 0.73$ ) with contents of soil organic carbon indicating a potential relationship between  $^{137}\text{Cs}$  concentrations and contents of soil organic carbon that might relate to preferential passive transport of  $^{137}\text{Cs}$  attached to particles of soil organic carbon (Figure 5.35a). The adsorption of  $^{137}\text{Cs}$  by direct contact with pore walls of the soil during active transport might be one explanation for the gradual decrease in concentrations of  $^{137}\text{Cs}$  with increasing soil depth (He and Walling, 1996), which was observed for all surface layers of the soil profiles studied.

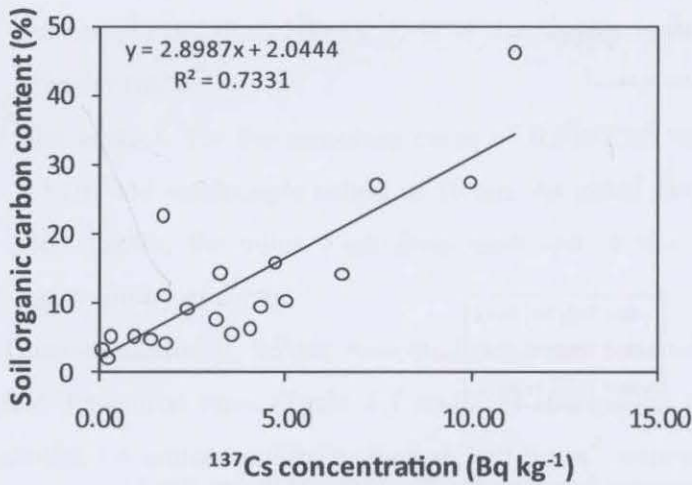


Fig. 5.35a. Relationship (linear) between  $^{137}\text{Cs}$  concentrations and soil organic carbon contents in the soil profiles.

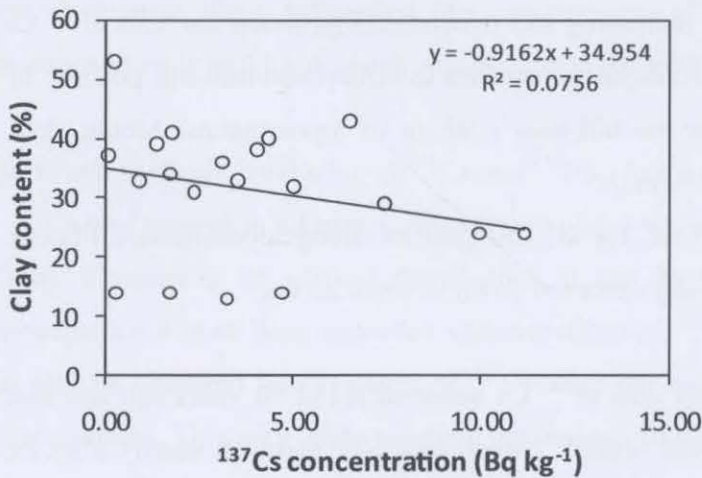


Fig. 5.35b. Relationship (linear) between  $^{137}\text{Cs}$  concentrations and clay contents in the soil profiles.

A recent study explored the relationship between  $^{137}\text{Cs}$  and soil organic carbon for a site in south-eastern Australia (Martinez et al., 2010). In contrast to previous studies, results from this study indicated that for uncultivated grasslands in dry climatic settings, soil organic carbon and  $^{137}\text{Cs}$  most likely do not move along the same physical pathways or by the same mechanisms. The lack of a relationship between the two was suggested to be a result of biological factors that might drive the spatial distribution of soil organic carbon in the soil profile (i.e. biological oxidation, mineralization). It was also assumed that increased soil organic carbon contents found near the soil surface of most of the uncultivated soils studied could have ‘diluted’  $^{137}\text{Cs}$  concentrations in the soil profile.



As shown in Table 5.9, significant amounts of  $^{210}\text{Pb}_{\text{ex}}$  were only present in the first 50 cm of soil of profile Tb6, located in hill-base position along toposequence Mount Boss (Figure 5.36).

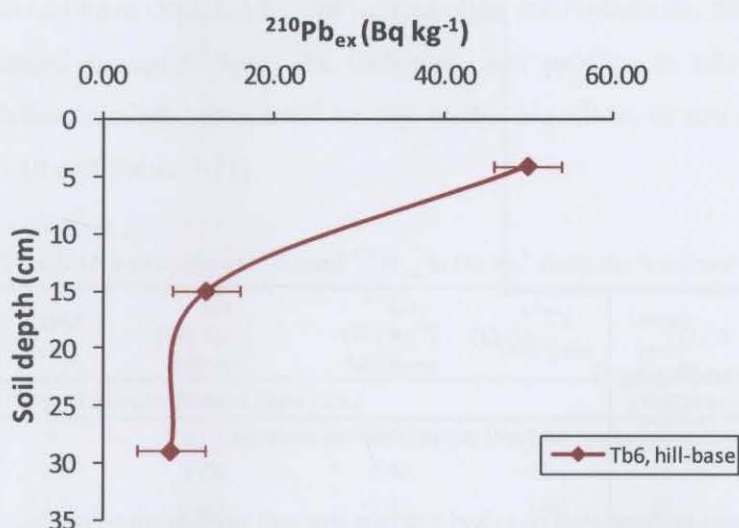


Fig. 5.36. Vertical distribution of  $^{210}\text{Pb}_{\text{ex}}$  concentrations in the soil profile for soil profile T6; located in hill-base position of toposequence Mount Boss.

The presence of  $^{210}\text{Pb}_{\text{ex}}$  beyond the first few centimetres of the soil surface is usually an indication of transport of soil along a hillslope in environments affected by severe soil erosion due to the immobility of  $^{210}\text{Pb}_{\text{ex}}$ . However, the accumulation of  $^{210}\text{Pb}_{\text{ex}}$  concurs with very high concentrations of soil organic carbon (> 20 %) in all layers of this particular profile (Figure 5.37a and 5.37b).

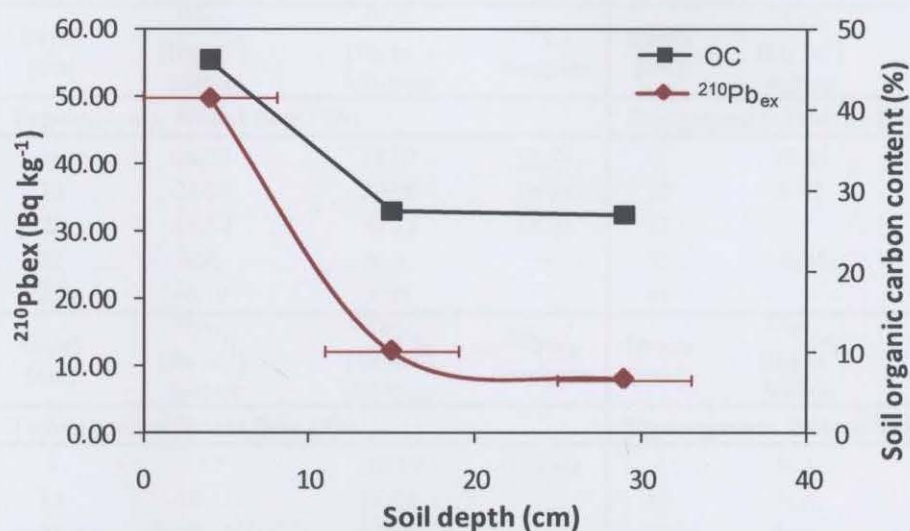


Fig. 5.37a. Vertical distribution of  $^{210}\text{Pb}_{\text{ex}}$  concentrations plotted in conjunction with contents of organic carbon in the soil profile for soil profile T6; located in hill-base position of toposequence Mount Boss.

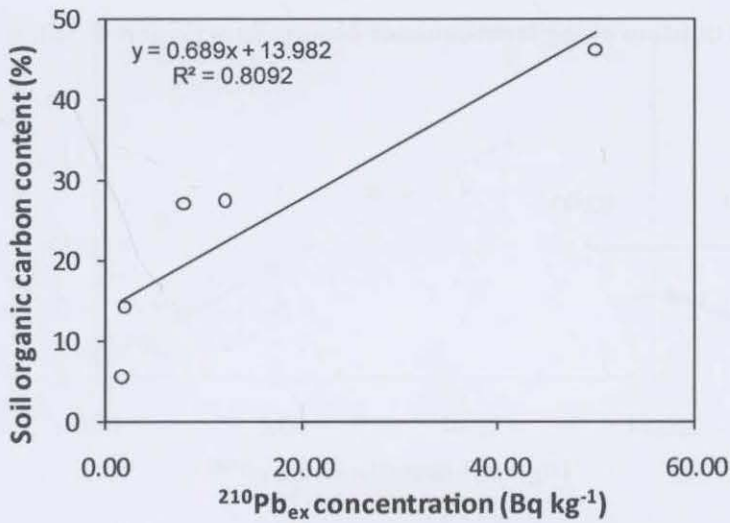


Fig. 5.37b. Relationship (linear) between  $^{210}\text{Pb}_{\text{ex}}$  concentrations and soil organic carbon contents.

It was therefore posited that  $^{210}\text{Pb}_{\text{ex}}$  was transported passively down the soil profile attached to particles of soil organic matter, possibly along former root channels. The affinity and most likely passive transport of  $^{210}\text{Pb}_{\text{ex}}$  in relation to soil organic matter sedimentation in forest soils has been indicated in the literature, i.e. by Dörr (1995). Furthermore, the occurrence of  $^{210}\text{Pb}_{\text{ex}}$  in 50 cm of soil depth is in agreement with vertical distributions of  $^{137}\text{Cs}$  at the hill-base position of toposequence Mount Boss.

*Lateral distribution of  $^{137}\text{Cs}$  and  $^{210}\text{Pb}_{\text{ex}}$  along the toposequences: Estimation of loss/gain*

It was also attempted to estimate potential amounts of loss/gain of  $^{137}\text{Cs}$  and  $^{210}\text{Pb}_{\text{ex}}$  in  $\text{Bq kg}^{-1}$  and  $\text{Bq m}^{-2}$  along the hillslopes based on the assumption that soil profiles in hilltop positions would have depleted fallout radionuclide concentrations, because of loss of soil material through lateral transport down the hillslope. Soil profiles in hill-base position would have enriched fallout nuclide concentrations due to the deposition of soil material from the upper slope (Table 5.10 and Table 5.11).

**Tab. 5.10.** Loss/gain of  $^{137}\text{Cs}$  and  $^{210}\text{Pb}_{\text{ex}}$  in  $\text{Bq kg}^{-1}$  along the hillslopes.

Depth [cm]	$^{137}\text{Cs}$ [Bq kg <sup>-1</sup> ] hilltop	$^{137}\text{Cs}$ [Bq kg <sup>-1</sup> ] hill-base	$^{137}\text{Cs}$ loss/gain	Depth [cm]	$^{137}\text{Cs}$ [Bq kg <sup>-1</sup> ] hilltop	$^{137}\text{Cs}$ [Bq kg <sup>-1</sup> ] hill-base	$^{137}\text{Cs}$ loss/gain
<b>Toposequence Mount Boss (Tb)</b>				<b>Toposequence Plateau Beech (Te)</b>			
4	6.51	11.15	4.64	4	3.13	4.34	1.21
13	5.00	9.96	4.96	15	1.36	4.04	2.68
25	2.37	7.43	5.06	23		1.77	
32	N.A.	N.A.		32	-0.43	0.23	
45	-0.02	1.71		45			
Depth [cm]	$^{210}\text{Pb}_{\text{ex}}$ [Bq m <sup>-2</sup> ] hilltop	$^{210}\text{Pb}_{\text{ex}}$ [Bq m <sup>-2</sup> ] hill-base	$^{210}\text{Pb}_{\text{ex}}$ loss/gain	Depth [cm]	$^{210}\text{Pb}_{\text{ex}}$ [Bq m <sup>-2</sup> ] hilltop	$^{210}\text{Pb}_{\text{ex}}$ [Bq m <sup>-2</sup> ] hill-base	$^{210}\text{Pb}_{\text{ex}}$ loss/gain
<b>Toposequence Mount Boss (Tb)</b>				<b>Toposequence Plateau Beech (Te)</b>			
4	1.90	49.86	47.96	4	N.A.	N.A.	N.A.
13	-2.30	12.14		15	N.A.	N.A.	N.A.
25	-6.15	7.97		23	N.A.	N.A.	N.A.
32	N.A.	N.A.		32	N.A.	N.A.	N.A.
45	-14.80	-14.56		45	N.A.	N.A.	N.A.

**Tab. 5.11.** Loss/gain of  $^{137}\text{Cs}$  and  $^{210}\text{Pb}_{\text{ex}}$  in  $\text{Bq m}^{-2}$  along the hillslopes.

Depth [cm]	$^{137}\text{Cs}$ [Bq m <sup>-2</sup> ] hilltop	$^{137}\text{Cs}$ [Bq m <sup>-2</sup> ] hill-base	$^{137}\text{Cs}$ loss/gain	Depth [cm]	$^{137}\text{Cs}$ [Bq m <sup>-2</sup> ] hilltop	$^{137}\text{Cs}$ [Bq m <sup>-2</sup> ] hill-base	$^{137}\text{Cs}$ loss/gain
<b>Toposequence Mount Boss (Tb)</b>				<b>Toposequence Plateau Beech (Te)</b>			
4	26.29	38.03	11.74	4	12.65	22.38	9.72
13	21.98	38.36	16.38	15	6.72	19.54	12.83
25	11.32	30.23	18.91	23		10.09	
32	N.A.	N.A.		32	-2.02	1.41	
45	-0.10	8.28		45			
Depth [cm]	$^{210}\text{Pb}_{\text{ex}}$ [Bq m <sup>-2</sup> ] hilltop	$^{210}\text{Pb}_{\text{ex}}$ [Bq m <sup>-2</sup> ] hill-base	$^{210}\text{Pb}_{\text{ex}}$ loss/gain	Depth [cm]	$^{210}\text{Pb}_{\text{ex}}$ [Bq m <sup>-2</sup> ] hilltop	$^{210}\text{Pb}_{\text{ex}}$ [Bq m <sup>-2</sup> ] hill-base	$^{210}\text{Pb}_{\text{ex}}$ loss/gain
<b>Toposequence Mount Boss (Tb)</b>				<b>Toposequence Plateau Beech (Te)</b>			
4	7.67	170.07	162.40	4	N.A.	N.A.	N.A.
13	-10.11	46.76		15	N.A.	N.A.	N.A.
25	-29.38	32.43		23	N.A.	N.A.	N.A.
32	N.A.	N.A.		32	N.A.	N.A.	N.A.
45	-77.37	-70.53		45	N.A.	N.A.	N.A.

Based on the set of data, calculations of lateral distributions showed that hill-base positions potentially gained concentrations of  $^{137}\text{Cs}$  when compared to total concentrations at the hilltop position. Alternatively, the observed variability in  $^{137}\text{Cs}$  may not necessarily be the result of erosion-deposition processes. Looking at the total activities for Toposequence Mount Boss (values range between 13.89-30.25 Bq kg<sup>-1</sup> or 59.59-104.62 Bq m<sup>-2</sup> for the hilltop-hillbase positions, respectively) and Plateau Beech (values range between 4.49-10.38 Bq kg<sup>-1</sup> or 9.37-53.42 Bq m<sup>-2</sup> for the hilltop-hillbase positions, respectively), the absolute values are very low and the actual differences are not reasonably high. These differences could be explained by site variability due to infiltration variation rather than movement of soil particles (i.e. see study by Wallbrink et al., 1994, here, fallout variability potentially added to or accounted for observed differences in areal concentrations).

The identification of potential lateral distributions of  $^{210}\text{Pb}_{\text{ex}}$  was not possible due to lack of detection. In relation to toposequence Mount Boss it may be plausible to argue that moderate concentrations of  $^{210}\text{Pb}_{\text{ex}}$  in the surface layer of the soil profile in hill-base position might be the result of deposition of surface soil material from the upper slope positions. However, the vertical distribution of  $^{210}\text{Pb}_{\text{ex}}$  attached to particles of soil organic matter appears to be more reasonable for the detection of relatively high concentrations down to 30 cm of soil depth.

### 5.5.5 Summary

The decrease of concentrations of fallout radionuclides with increasing soil depth most likely reflected the adsorption of  $^{137}\text{Cs}$  and  $^{210}\text{Pb}_{\text{ex}}$  to soil particles.

$^{137}\text{Cs}$  was present in all surface layers of the soil profiles studied, implying short-term vertical and/or lateral redistribution of the radionuclide in the forest soils. Most likely, vertical distributions down the soil profile are the result of initial active transport through leaching processes after deposition from the atmosphere and passive transport attached to soil particles.

Comparing the occurrence of  $^{137}\text{Cs}$  in conjunction with  $^{210}\text{Pb}_{\text{ex}}$ , similar patterns of distributions were only present in the lowest profile in toposequence Mount Boss. In all other soil profiles significant amounts of  $^{210}\text{Pb}_{\text{ex}}$  were not present. This pattern may indicate that  $^{137}\text{Cs}$  was predominantly transported down the soil profile in the liquid phase by infiltration of rainwater, whereas  $^{210}\text{Pb}_{\text{ex}}$  was passively transported attached to particles of soil organic carbon. Simulating the initial deposition of  $^{137}\text{Cs}$  and  $^{210}\text{Pb}_{\text{ex}}$  onto the soil surface from the atmosphere

He and Walling (1996) found that more than 90 % of both radionuclides was contained in the first 1.5 cm of soil. It can therefore be presumed that  $^{210}\text{Pb}_{\text{ex}}$  may only be present in the first few centimetres (<2 cm) of soil that have not been sampled. The lack of  $^{210}\text{Pb}_{\text{ex}}$  in the near surface soil may also be an indicator for short-term (<100 yr) lateral transport processes along both toposequences.

The observed variability in  $^{137}\text{Cs}$  along the hillslopes is most likely not necessarily the result of erosion-deposition processes. Soil material along hillslopes is most likely 'preserved' by plant cover and surface litter covering the topsoil of the forested environment studied. Estimation of total activities showed that absolute values are low and actual differences were not significantly high. It was therefore posited that the variability in  $^{137}\text{Cs}$  concentrations potentially resulted from site variability rather than erosion-deposition processes.

The first part of the paper discusses the importance of the study and the objectives of the research. It highlights the need for a comprehensive understanding of the subject matter and the role of the researcher in this process. The second part of the paper presents the methodology used in the study, including the data collection methods and the analysis techniques. The third part of the paper discusses the results of the study and the conclusions drawn from the data. The final part of the paper provides a summary of the findings and offers suggestions for future research.

The results of the study indicate that there is a significant relationship between the variables studied. The findings suggest that the independent variable has a positive effect on the dependent variable. This relationship is supported by the statistical analysis conducted in the study. The conclusions drawn from the data are consistent with the hypotheses of the study. The study also identifies some limitations and suggests areas for further research.

The study has several limitations, including the sample size and the scope of the research. The sample size was limited to a specific group of individuals, which may not be representative of the entire population. The scope of the research was also limited to a specific area of the subject matter. Despite these limitations, the study provides valuable insights into the relationship between the variables studied. The findings of the study have implications for practice and policy. The study also identifies some areas for further research, including the need for a larger sample size and a more comprehensive scope of research.

## Chapter 6 General discussion - Quantifying pedogenesis using sophisticated dating methods – TCN and OSL

### 6.1 Modelling ‘global’ soil production based on the TCN-derived average SPR

The calculated average soil production rate of  $47 \pm 4 \text{ mm kyr}^{-1}$  was implemented in the estimation of the production of soil over tens of thousands of years. For this purpose the model of Heimsath et al. (1999) and Minasny and McBratney (1999) was used to determine the residence time of the soil. In the application of this model, steady-state conditions of soil production with no gain or loss of soil through erosion and deposition, and a constant bulk density throughout the soil profile were assumed. A density ratio of soil parent material (bedrock) to soil of 1.4 was employed. The data obtained by using this simple soil production model indicate that the soil residence time for a soil profile of 1m depth is approximately 69,000 years, if soil is produced at a rate of approximately  $0.05 \text{ mm yr}^{-1}$  (Figure 6.1).

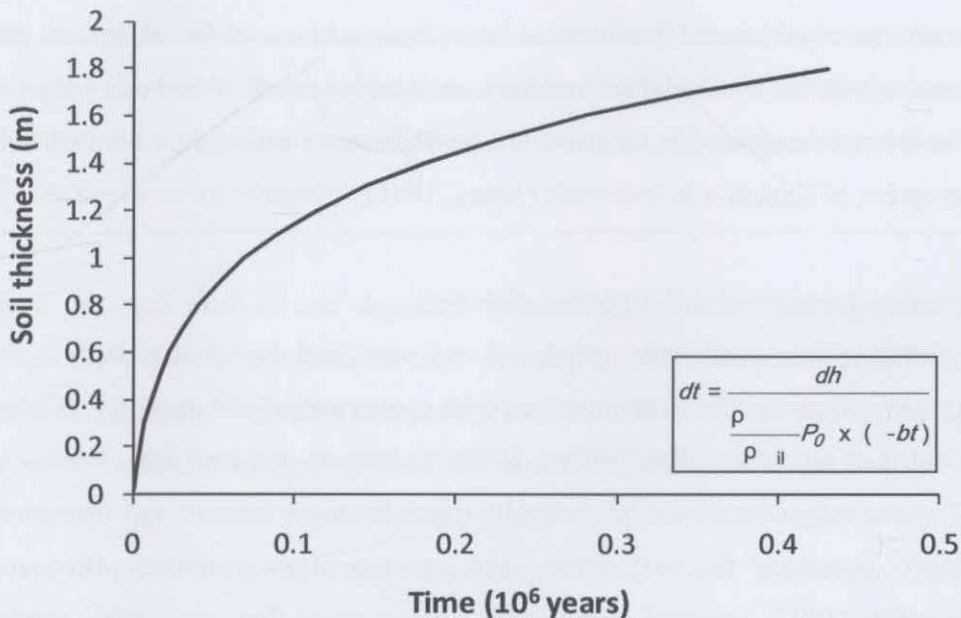


**Fig. 6.1.** Soil profile development over tens of thousands of years assuming steady-state conditions with no soil gain or loss and constant bulk density of the soil profile, applying the average SPR for semi-arid to tropical environments. Equation 4.9 was revised after Minasny and McBratney (1999), where  $\rho_{\text{parent}}$  is the density of the parent material and  $\rho_{\text{soil}}$  is the density of the soil,  $P_0$  is the potential weathering rate of the parent material and  $b$  is an empirical constant.

Under this average rate of soil production, only 3 mm of soil would be produced in about 50 years. The production of soil from parent materials is therefore relatively slow when employing the in Chapter 4 proposed TCN-derived average rate of soil production. Pimentel et al. (1995)

presented rates of between 200 and 1000 years to form 2.5 cm of topsoil under agricultural conditions and discussed that it would take even longer to form this amount of topsoil under grassland or forested conditions. This argument seems to underestimate the formation of topsoil under native vegetation, where soil formation and especially soil organic matter formation can take place more rapidly due to undisturbed conditions. By applying the proposed soil production model it would take approximately 400 years to produce 2.5 cm of soil from bedrock under native conditions.

These rates of soil production would suggest that soil is not renewable in societal time scales. This supposition is only applicable however, where soil ‘renewal’ results from weathering of unaltered bedrock without ‘human interventions’. Soil conservation programs have been initiated worldwide to improve the fertility of (top)-soil after agricultural practises (i.e. the US Conservation Reserve Program, (Pimentel et al., 1995)). Furthermore, soil reclamation or rehabilitation is practised after major environmental disturbances (i.e. mining, see Grigg et al., 2006). It remains to be seen whether or not these conservation programs will be successful in the long-run.

It is also important to consider soil production rates from unconsolidated materials like volcanic ash and loess, which are much higher than from unaltered bedrock. Weathering rates as high as  $8 \text{ mm yr}^{-1}$  have been recognized in the literature for Indonesian soils formed on volcanic ash after the 1883 eruption of Krakatoa in Indonesia (Jenny, 1941).

#### *How much soil is produced or formed and degraded globally?*

To address the question ‘How much soil is produced or formed and degraded globally?’, the proposed average rate of soil production was compared with mean rates of soil erosion published in the literature (Collins et al., 2010; Montgomery, 2007; Wakatsuki and Rasyidin, 1992). As shown in Table 6.1, mean rates of soil erosion generally exceeded mean rates of soil formation, and this relationship is consistent for both natural and agricultural environments. However, Wakatsuki and Rasyidin (1992) reported global soil erosion rates that were very similar compared to global soil formation rates, which supports the hypothesis that landscapes evolve towards an equilibrium of soil formation and erosion (denudation). Montgomery (2007) reviewed soil erosion rates resulting from different land uses, compared to the rate of soil formation. Soil erosion rates under conservation agriculture were about 3 times as fast as soil formation rates, whereas soil erosion rates from conventional agriculture were about 68 times faster than soil formation rates (Montgomery, 2007). Erosion rates from conventionally ploughed agricultural fields were therefore estimated to be approximately 1 order of magnitude greater



than soil formation rates as well as soil erosion rates estimated for natural environments (Table 6.1 and Figure 6.2). Montgomery (2007) therefore concluded that conservation agriculture practises such as no-till or reduced-till could provide a foundation for sustainable agricultural practices due to reduced rates of soil erosion.

#### *Definition of the term 'Anthropocene'*

The term 'Anthropocene' was introduced in 2000 by Paul J. Crutzen and Eugene F. Stoermer in the Newsletter of the International Geosphere-Biosphere Programme to emphasize the role of mankind in the current geological epoch of the Holocene (Crutzen and Stoermer, 2000). Crutzen and Stoermer (2000) assigned a more specific date to the 'Anthropocene' by proposing that it started in the latter part of the 18<sup>th</sup> century where "global effects of human activities have become clearly noticeable". In addition to the linkage with the industrial revolution, the date has also been linked to the rise of agriculture (about 8000 years ago).

#### *What is 'Peak Soil'?*

In the current literature on 'Anthropocene'-induced soil erosion the term 'peak soil' is often used. In the Macquarie Dictionary the term 'peak soil' is defined as "that point in time when the world's soil for agriculture is not sufficient to sustain crop productivity, either through loss of topsoil or depletion of nutrients".

How fast soil evolves and degrades, especially since the Anthropocene is an important question that needs to be addressed more thoroughly. Have we reached *peak soil*? Are the soils of the world actually degrading to a point that there will be no soil left on the Earth's surface in the next 60 to 100 years (quoted from the Australian newspaper 'The Land', 12<sup>th</sup> of November 2009, "...the world could run out of usable soil within about 60 years".)? – A number that has been published in the media and seems exaggerated, almost a dystopia. This statement was surely intended to raise awareness of the fragility of soil. However, does it refer to the loss of topsoil or stripping of the soil-mantle so that only parent material is left behind?

It has been discussed widely that soil, especially the topsoil, is degrading faster than it can be replenished. This is particularly worrying for agricultural purposes, where a loss of the soils fertile capacity has major effects on (crop) productivity. Quinton et al. (2010) discussed that the removal of soil by erosion might also bring the subsoil and parent materials closer to the Earth's surface. Consequently, soil erosion could also be associated with increasing rates of chemical

weathering of silicate-rich parent materials under steady state conditions, which may result in weathering accelerated carbon dioxide release to the atmosphere (Quinton et al., 2010).

**Tab. 6.1.** Compilation of global rates of river sediment flux, sediment discharge to the oceans, global rates of soil erosion and soil formation (estimates for native vegetation, conservation agriculture and conventional agriculture).

Reference	Method	Surface area	Published rate units	Rate (mm yr <sup>-1</sup> )
<b>Sediment flux (to the oceans, watercourses)</b>				
Buchan, 2010 <sup>1)</sup>	Global soil erosion	N.A.	75 Gt yr <sup>-1</sup>	0.6
Buchan, 2010 <sup>1)</sup>	Global soil erosion	150 × 10 <sup>6</sup> km <sup>2</sup> (earth surface)	68-75 Gt yr <sup>-1</sup>	0.38-0.42 <sup>2)</sup>
Buchan, 2010 <sup>1)</sup>	Discharge of sediment (soil) to the oceans	60 major rivers 3.39 × 10 <sup>6</sup> km <sup>2</sup>	15-16 Gt yr <sup>-1</sup>	0.28
	Redistribution of sediment (soil) to the landscape or storage in reservoirs or dams		53-59 Gt yr <sup>-1</sup>	0.29-0.33
Collins et al., 2010	Net sediment delivered to watercourses from cultivated topsoils	135 samples	30 to 1995 kg ha <sup>-1</sup> yr <sup>-1</sup>	0.003 to 0.2
Collins et al., 2010	Net sediment delivered to watercourses from pasture topsoils	135 samples	33 to 829 kg ha <sup>-1</sup> yr <sup>-1</sup>	0.003 to 0.07
Ludwig and Probst, 1998	Discharge of sediment to the oceans	60 major rivers 43.39 × 10 <sup>6</sup> km <sup>2</sup>	14.8-16 Gt yr <sup>-1</sup>	0.28-0.31
Ludwig and Probst, 1998 <sup>3)</sup>	Redistribution of sediment (soil) to the landscape or storage in reservoirs or dams		59 to 60 Gt yr <sup>-1</sup>	
Pimentel et al., 1995	Global soil erosion (one-third natural and two-thirds agricultural)	150 × 10 <sup>6</sup> km <sup>2</sup> (earth surface)	75 Gt yr <sup>-1</sup>	0.42 <sup>2)</sup>
Pimentel et al., 1995	Soil erosion rates (Asia, Africa and South America)	N.A.	30-40 t ha <sup>-1</sup> yr <sup>-1</sup>	2.5-3.0 <sup>4)</sup>
Pimentel et al., 1995	Soil erosion rates (United States, Europe)	N.A.	17 t ha <sup>-1</sup> yr <sup>-1</sup>	1.4 <sup>4)</sup>
Pimentel et al., 1995	Soil erosion rates (undisturbed forests)	N.A.	0.004-0.05 t ha <sup>-1</sup> yr <sup>-1</sup>	0.0003-0.004 <sup>4)</sup>
Pimentel et al., 1995	Average rate of soil formation	N.A.	1 t ha <sup>-1</sup> yr <sup>-1</sup>	0.083 <sup>4)</sup>
Syvitski et al., 2005	Estimates of global river sediment discharge	4462 rivers 106 × 10 <sup>6</sup> km <sup>2</sup>	38 540 km <sup>3</sup> yr <sup>-1</sup>	364 <sup>5)</sup>
Syvitski et al., 2005	Estimate of global river sediment discharge to the oceans (prehuman)	4462 rivers 106 × 10 <sup>6</sup> km <sup>2</sup>	14 Gt yr <sup>-1</sup>	0.11 <sup>5)</sup>
Syvitski et al., 2005	Estimate of global river sediment discharge to the oceans (modern, anthropocene) minus sediment retention in reservoirs	4462 rivers 106 × 10 <sup>6</sup> km <sup>2</sup>	12.6 Gt yr <sup>-1</sup>	0.099 <sup>5)</sup>

Reference	Method	Surface area	Published rate units	Rate (mm yr <sup>-1</sup> )
<b>Sediment flux (to the oceans, watercourses)</b>				
Syvitski et al., 2005	Estimate of global river sediment discharge to the oceans (modern, anthropocene) plus sediment retention in reservoirs	4462 rivers	16.2 Gt yr <sup>-1</sup>	0.127 <sup>5)</sup>
Syvitski et al., 2005	Redistribution of sediment (soil) to the landscape or storage in reservoirs or dams		3.6 Gt yr <sup>-1</sup>	0.028 <sup>5)</sup>
Wilkinson and McElroy, 2007	Global agricultural erosion <sup>6)</sup>	N.A.	75 Gt yr <sup>-1</sup>	0.6
Wilkinson and McElroy, 2007	Global natural sediment flux (river loads, rock volumes)	N.A.	21 Gt yr <sup>-1</sup>	0.062
Wilkinson and McElroy, 2007	Accumulation of postsettlement alluvium from eroding croplands on tributary channels and floodplains	N.A.	12,600 m Myr <sup>-1</sup>	12.6
Wilkinson and McElroy, 2007	Phanerozoic natural sediment flux (sedimentary rocks)	N.A.	5 Gt yr <sup>-1</sup>	0.016
Wilkinson and McElroy, 2007	Pliocene natural sediment flux (sedimentary rocks)	N.A.	16 Gt yr <sup>-1</sup>	0.053
Reference	Method	Sample size, n	Published rate units	Mean rate (mm yr <sup>-1</sup> )
<b>Soil erosion and soil formation</b>				
Montgomery, 2007	Erosion rates for conventional agriculture	448		4.0
Montgomery, 2007	Erosion rates for conservation agriculture	47		0.124
Montgomery, 2007	Erosion rates for native vegetation	65		0.053
Wakatsuki and Rasydyidin, 1992	Global mean rate of soil erosion	N.A.	906 kg ha <sup>-1</sup> yr <sup>-1</sup>	0.076
Wakatsuki and Rasydyidin, 1992	Global mean rate of soil formation	N.A.	695 kg ha <sup>-1</sup> yr <sup>-1</sup>	0.058
Montgomery, 2007, revised (section 4.5.6)	Average soil formation rate, other (denudation, mass-balance, solutes)	125		0.042
This research study	Average rate of soil production (TCN)	96		0.047

Note:

<sup>1)</sup>Values were cited from Pimentel et al., 1995; Ludwig and Probst, 1997; Syvitski et al., 2005 and Wilkinson and McElroy, 2007

<sup>2)</sup>Conversions from Gt yr<sup>-1</sup> to mm kyr<sup>-1</sup> were based on a surface of the earth of  $150 \times 10^6$  km<sup>2</sup> and a bulk density of 1200 kg m<sup>-3</sup>

<sup>3)</sup>Calculations were based on the global rate of soil erosion published by Wilkinson and McElroy, 2007

<sup>4)</sup>Values of t ha<sup>-1</sup> yr<sup>-1</sup> were converted to mm kyr<sup>-1</sup> or mm yr<sup>-1</sup> assuming an average soil bulk density of 1200 kg m<sup>-3</sup>

<sup>5)</sup>Conversions from Gt yr<sup>-1</sup> to mm kyr<sup>-1</sup> were based on a surface of the earth of  $106 \times 10^6$  km<sup>2</sup> and a bulk density of 1200 kg m<sup>-3</sup>

<sup>6)</sup>USLE estimates for the USA

A common perception is that all eroded soil material, caused by natural or agriculturally induced soil erosion, is eventually transported to the oceans of the world through river sediment discharge. But this is far from the case. Eroded soil is not necessarily lost in the sediment load of rivers and directly transported to the oceans. A relatively large amount is deposited and accumulated in areas with reduced slope, in sediment traps or reservoirs, in dams or wetlands. This eroded soil material is therefore eventually converted to colluvial and alluvial soils. Consequently, the impact of humans on global soil erosion rates and sedimentation rates needs to be discussed in conjunction with river sediment loads and sediment discharges to the oceans (Buchan, 2010; Ludwig and Probst, 1998; Pimentel et al., 1995; Syvitski et al., 2005; Wilkinson and McElroy, 2007). Values of global soil erosion (natural as well as agricultural induced) and soil formation were therefore compiled and compared, together with global river sediment loads and global river sediment discharge to the oceans published in the literature over the past 10 years (Table 6.1 and Figure 6.2).

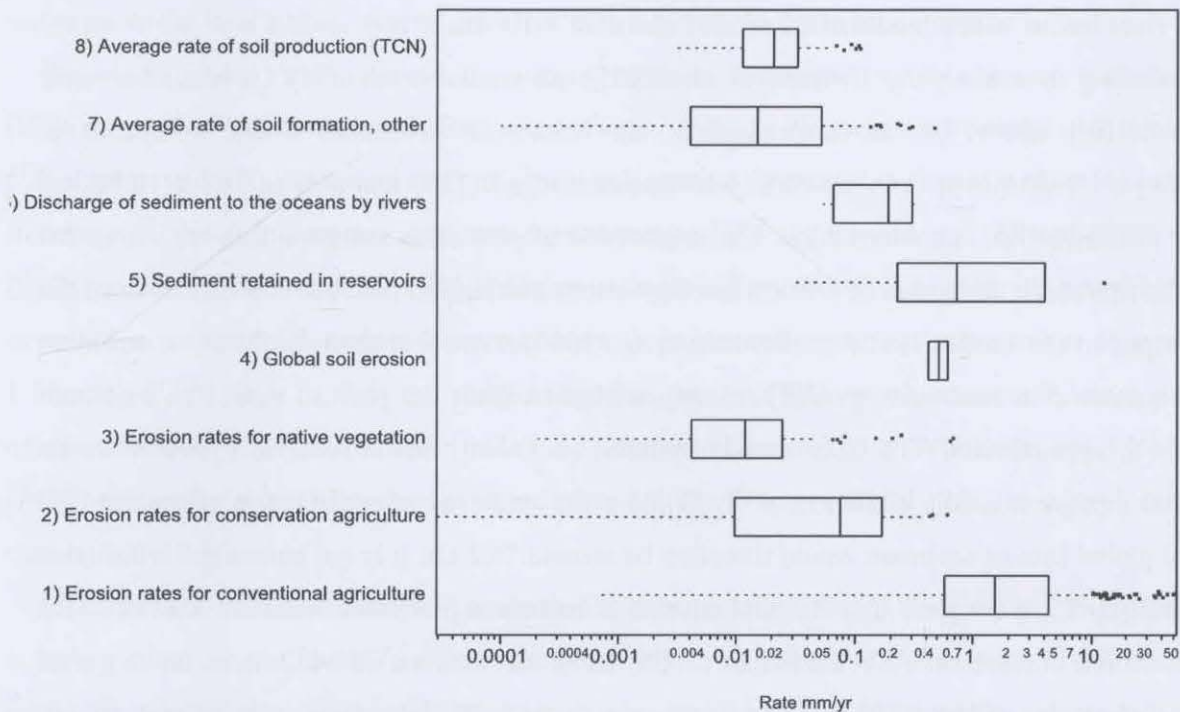


**Fig. 6.2.** Box plots of compiled rates of soil erosion, soil formation and river sediment discharge to the oceans and river sediment retained on the land surface in reservoirs, based on Table 6.1, plotted on the log-scale.

*Note:* Erosion rates from conventional or conservation agriculture and native vegetation are from Montgomery (2007); Global erosion rates are from Buchan (2010) and Pimentel et al. (1995); Amounts of sediment retained in reservoirs are from Buchan (2010), Ludwig and Probst (1998), Syvitski et al. (2005) and Wilkinson and McElroy (2007); Rates of discharge of sediments to the oceans by rivers are from Buchan (2010), Ludwig and Probst (1998), Syvitski et al. (2005) and Wilkinson and McElroy (2007); Average rates of soil formation (other) is a revised version of Montgomery (2007) used in section 4.5.6; and average rates of soil production (TCN) are based on compilations from this study, section 4.5.5.

Pimentel et al. (1995) argued that approximately  $12 \times 10^6$  ha of arable land are degrading annually as result of unsuitable agricultural practices, and that only  $1.5 \times 10^9$  ha of land in total are being cultivated each year. The highest soil erosion rates were presented for Asia, Africa and

South America, at about  $30$  to  $40 \text{ t ha}^{-1} \text{ yr}^{-1}$  ( $2.5$  to  $3 \text{ mm yr}^{-1}$ ) and the lowest rates were reported for the United States of America and Europe, about  $17 \text{ t ha}^{-1} \text{ yr}^{-1}$  ( $1.4 \text{ mm yr}^{-1}$ ). These average soil erosion rates greatly exceed the assumed average rate of soil formation of  $1 \text{ t ha}^{-1} \text{ yr}^{-1}$  ( $0.083 \text{ mm yr}^{-1}$ ). However, in an undisturbed forest soil erosion values of only  $0.004$  to  $0.05 \text{ t ha}^{-1} \text{ yr}^{-1}$  were proposed equating to  $0.0003$  to  $0.004 \text{ mm yr}^{-1}$ . It can therefore be assumed that rates of soil erosion and soil formation are most likely in a dynamic equilibrium in undisturbed natural environments.

Ludwig and Probst (1998) discussed that between  $14.8$  and  $16 \text{ Gt}$  of sediment are discharged to the oceans every year ( $0.28$  and  $0.31 \text{ mm yr}^{-1}$ ) via major rivers (about  $68 \%$  is delivered to the Pacific and the Indian Ocean). However, a global rate of soil erosion was estimated to be about  $75 \text{ Gt yr}^{-1}$  ( $1.44 \text{ mm yr}^{-1}$ ) (Wilkinson and McElroy, 2007), that means a much larger amount of sediment of about  $59$  to  $60 \text{ Gt yr}^{-1}$  ( $1.13$  to  $1.15 \text{ mm yr}^{-1}$ ) is redistributed to the landscape or stored in reservoirs or dams. Ludwig and Probst (1998) based their calculations on  $60$  major world river basins with a total surface area of about  $44 \times 10^6 \text{ km}^2$ .

According to a study by Syvitski et al. (2005), an annual total of  $14 \text{ Gt}$  of global river sediment ( $0.1 \text{ mm yr}^{-1}$ ) was discharged to the oceans in prehuman times, compared to  $12.6 \text{ Gt yr}^{-1}$  ( $0.09 \text{ mm yr}^{-1}$ ) in modern, anthropocene times. This amounts to about  $10 \%$  less global sediment flux in modern times. Estimated rates of prehuman sediment flux are connected to geomorphologic processes of erosion and deposition that shaped (and are still influencing) the landscapes of the Earth. However, Syvitski et al. (2005) noted that around  $100 \text{ Gt}$  of sediment are sequestered in reservoirs globally, mostly initiated within the past  $50$  years. This amount equates to approximately  $3.6 \text{ Gt}$  of eroded material (sediment) that is retained in reservoirs on the land surface annually ( $0.03 \text{ mm yr}^{-1}$ ). Without the retention of sediment in reservoirs, the annual global flux of sediment would therefore be around  $16.2 \text{ Gt}$ . It is not quite clear within this publication, if it is assumed that the total amount of increased prehuman sediment load of rivers is now stored in reservoirs. Syvitski et al. (2005) based calculations on  $4462$  rivers and a global Earth surface area of  $106 \times 10^6 \text{ km}^2$ .

Wilkinson and McElroy (2007) stated that around  $83 \%$  of soil erosion induced by agricultural practices occurs on the lower  $65 \%$  of the Earth's surface area with a rate of about  $75 \text{ Gt yr}^{-1}$  ( $0.6 \text{ mm yr}^{-1}$ ). A total of about  $21 \text{ Gt yr}^{-1}$  ( $0.062 \text{ mm yr}^{-1}$ ) of sediment load is assumed for rivers globally. The discrepancy between the rate of global soil erosion and the rate of global river sediment flux is explained by the accumulation of alluvial sediment from eroded croplands on tributary channels and floodplains at a rate of approximately  $12.6 \text{ mm yr}^{-1}$  since 'post-settlement' (anthropocene times) (Wilkinson and McElroy, 2007).

Buchan (2010) stated that 68 to 75 Gt of soil are removed by soil erosion globally each year. A great amount of this eroded soil (about 80 %) is redistributed or concentrated in the landscape or in reservoirs and dams; whereas only approximately 15-16 Gt of eroded soil or sediment is discharged by rivers to the oceans each year. The rate of soil erosion and the rate of discharge of sediment to the oceans presented in Buchan (2010) were based on published rates by Ludwig and Probst (1998), Pimentel et al. (1995) and Wilkinson and McElroy (2007).

### *Summary*

Various rates of global soil erosion and global soil formation, river sediment discharge to the oceans and redistribution of sediment to the landscapes or storage in reservoirs or dams have been published in the cited literature. An inter-comparison of different rates and conversions to  $\text{mm yr}^{-1}$  as demonstrated in Table 6.1 (also see Figure 6.2) proved difficult, because of differing or unknown surface areas. In particular, rates of global soil erosion and rates of redistribution of sediment to the land surface when converted to  $\text{mm yr}^{-1}$  differ by great amounts.

Rates of global soil erosion in  $\text{mm yr}^{-1}$  varied considerably, the lowest rate being  $0.076 \text{ mm yr}^{-1}$  (Wakatsuki and Rasyidin, 1992) and the highest rate about  $4.1 \text{ mm yr}^{-1}$  (Montgomery, 2007). Assumed rates of global soil erosion discussed in fluvial studies lay within the range of global soil erosion rates and ranged between  $0.4$  and  $0.6 \text{ mm yr}^{-1}$  ( $68$  and  $75 \text{ Gt yr}^{-1}$ ) (Buchan, 2010; Pimentel et al., 1995; Wilkinson and McElroy, 2007). The rates of redistribution of sediment to the land surface were consistent in most studies with a mean value of around  $1.11 \text{ mm yr}^{-1}$  ( $58 \text{ Gt yr}^{-1}$ ). Only the study of Syvitski et al. (2005) presented a much lower value of around  $3.6 \text{ Gt yr}^{-1}$  ( $0.028 \text{ mm yr}^{-1}$ ). On the other hand the study of Wilkinson and McElroy (2007) assumed a much higher value of sediment storage in reservoirs of  $12600 \text{ mm kyr}^{-1}$ , which translates to  $12.6 \text{ mm yr}^{-1}$ .

Nevertheless, the conclusion was made that approximately 80 to 90 % of eroded soil material is redistributed on the Earth's surface. Consequently, it appears that the impact of soil erosion might be smaller than suggested, because of sequestration. The sequestration of eroded soil material has increased, particularly with the introduction of preservation programs over the past 50 years (Syvitski et al., 2005). Pimentel et al. (1995) hypothesized that it costs about 2.10 US dollars to 'save' or sequester 1 t of soil.

### *Concluding remarks*

After studying published soil erosion and soil formation rates, it can be concluded that global soil erosion rates need to be discussed in conjunction with river sediment loads and discharges of

river sediment to the oceans. However, this discussion showed that a comparison of different published rates is challenging because of different units and surface areas used in the studies. Nevertheless, it can be concluded that it is essential to consider net rates of sediment flux to the oceans or watercourses when discussing global rates of soil erosion, because a large amount (more than 80 %) of eroded soil is redistributed or preserved as colluvial or alluvial soil. Even though soil erosion has increased significantly since anthropocene times, a large amount of eroded soil material is indeed sequestered on the land surface (Buchan, 2010).

There is no doubt that human intervention has accelerated rates of soil erosion, but this acceleration does not directly translate to the complete loss of soil as commonly reported in the media. When interpreted in relation to sediment (soil) sequestration on the land surface the total loss of sediment load to the oceans is smaller than expected. Even though rates of soil production are relatively slow compared to rates of soil erosion, rates of soil erosion may be closer to soil formation rates than posited.

## **6.2 How did soil form at the undisturbed forested environment of Werrikimbe National Park?**

### *How did soil form at Werrikimbe?*

At Werrikimbe National Park, steady-state conditions for soil formation over the past tens of thousands of years can be assumed due to the lack of major tectonic disturbances since the formation of the landscape, and the high probability that this mid-mountain range was not affected by the Last Glacial Maximum.

Soil properties determined in the field and by laboratory analysis confirmed the assumption made. Based predominantly on field morphology, soil horizons were identified for all soil profiles sampled. It may be plausible to argue that the observed development of soil horizonation along the toposequences sampled already confirms the occurrence of soil formation over a relatively long time in a more or less 'stable' environment. Reflecting back on Chapter 2 where mechanistic modelling of soil formation processes has been discussed, we learned that some soil horizons can form after 20000 years (Salvador-Blanes et al., 2007). This time period also falls into the range of assumed B horizon formation rates of Australian environments that ranged from decades to tens of thousands of years (McKenzie et al., 2004).



*At what rate was soil produced at Werrikimbe?*

TCN-derived SPR indicated that soil was produced at a rate of  $0.01 \text{ mm yr}^{-1}$  or  $10 \text{ mm kyr}^{-1}$ . This soil production rate is higher than the average rate proposed for most soils in the Australian continent of less than  $1 \text{ mm kyr}^{-1}$ , but falls within the range of assumed rates of soil formation of  $10\text{-}50 \text{ mm kyr}^{-1}$  for the Southern Tablelands in NSW, Australia (McKenzie et al., 2004).

A clear pattern of soil production rates related to soil depth could not be identified. However, the observed soil production rates appeared to be related to the terrain attribute curvature. It was posited that at the field site studied soil thickness was most likely not in equilibrium, i.e. soil erosion and deposition are still actively happening. This was confirmed by distributions of  $^{137}\text{Cs}$  in the top 50 cm of the soil profiles along the toposequences analysed.

Nevertheless, when this rate ( $0.01 \text{ mm yr}^{-1}$ ) was applied in a simple model of soil production that incorporated the bulk density of soil and parent materials, soil residence times at Werrikimbe of up to 80000 years were determined, for soil profiles of about 1 m in depth. However, these residence times were calculated with the assumption of no gain or loss of soil material and refer to '*in situ*' rates of soil production. Soil residence times can therefore only be used as an estimation of the age of the 'oldest' soil material present along the toposequences.

Based on the thickness of soil observed in the field, the time for '*in situ*' soil production ranged between 29000 and 79000 years for solum depths of 45 cm and 100 cm, respectively. Implementing gain and loss of soil material in soil production models would most likely accelerate soil profile formation along hillslopes and would better predict soil production in these soil-mantled environments. Although the soil production rate was estimated to be  $10 \text{ mm kyr}^{-1}$ , the absolute age of the soil at Werrikimbe can not be determined confidently as the soil depths are most likely not in equilibrium.

*How fast were rates of soil turnover occurring in the soil profile?*

The distribution of individual quartz grains estimated from soil burial age calculations along Mount Boss and Plateau Beech toposequences confirmed the occurrence of soil mixing in the top 50 cm of soil. Vertical as well as lateral displacements of grains were calculated for both toposequences. Soil mixing rates of  $0.5 \text{ mm yr}^{-1}$  and  $0.2 \text{ mm yr}^{-1}$  were calculated for the Mount Boss and Plateau Beech toposequences, respectively, and the velocity of vertical grain movements appeared to be higher in the top 25 cm of the soil profile compared to rates calculated for about 50 cm of depth.

At Werrikimbe, rates of soil mixing exceeded rates of soil production by about one order of magnitude, which is less than assumed for different study sites in south-eastern Australia where

up to 3 orders of magnitude difference (Wilkinson and Humphreys, 2005) have been reported. Vertical rates of soil mixing were 50 times faster than soil production rates at Mount Boss, and 20 times more rapid than rates of soil production at Plateau Beech.

*What influence did soil turnover rates have on pedogenesis?*

The occurrence of soil mixing was confirmed for the uncultivated forest soils. However, soil mixing did not operate to the extent of homogenising the top 50 cm of the soil profile and therefore did not impede the presence of soil horizons. One could argue that the differentiation of soil horizons appeared to be blurred on the Mount Boss toposequence when compared to the Plateau Beech toposequence where horizonation was more prominent. This discrepancy also seemed to be reflected in grain responses, age distributions and consequently grain velocities discussed for both toposequences. Accordingly, it was posited that the Mount Boss toposequence was influenced by higher rates of vertical and lateral mixing and therefore greater disturbances by turbation or gravitational processes.

Observed changes in grain distributions (at approximately 50 cm of depth) are potentially controlled by floral agents. An active faunal, i.e. earthworm community, would have most likely resulted in a homogenisation of the soil material from the top-horizon and adjacent soil-horizons.

### **6.3 Relationship between soil properties with soil forming factors and topography**

In order to identify potential correlations, a multivariate analysis of topsoil or subsoil properties was performed together with rates of soil production and terrain attributes (covariates) calculated for the site studied. Correlations were estimated by linear correlation analysis. Predicted relationships between soil properties or soil forming factors with terrain attributes will be discussed in more detail.

This analysis identified the following significant relationships (see appendix, Figure 1 and 2):

- (1) Negative correlation between bulk density and soil organic carbon content (topsoil: -0.824, subsoil: -0.881),
- (2) Negative correlation between bulk density and amount of  $^{137}\text{Cs}$  (topsoil: -0.842)
- (3) Negative correlation between bulk density and slope (topsoil: -0.789)
- (4) Negative correlation between clay content and aspect (topsoil: -0.699)
- (5) Negative correlation between clay content and amount of  $^{137}\text{Cs}$  (topsoil: -0.849)
- (6) Positive correlation between clay content and solum depth (topsoil: 0.707, subsoil: 0.586)
- (7) Negative correlation between solum depth and aspect (-0.702)
- (8) Positive correlation between soil organic carbon content and amount of  $^{137}\text{Cs}$  (topsoil: 0.973)
- (9) Positive correlation between SPR and curvature (0.784)

For the parameters bulk density and slope a negative relationship was predicted, where the bulk density increased with decreasing slope. This is most certainly related to the increased probability of thicker soil profiles occurring in reduced slope positions, which is connected to a greater 'compactness' of soil material, because of increased soil thicknesses. A positive relationship between clay content and solum depth can be attributed to the higher clay contents in the subsoil, attributed to argilluviation. The negative correlation between the clay content as well as the solum depth with aspect could be related to soil profiles with north-eastern (0-90°) positions being influenced by higher rainfall than profiles in north-western (270-360°) positions. However, the predicted relationships could also be an artefact in the dataset.

The positive relationship between rates of soil production and curvature appears to be counter-intuitive and has been discussed in section 4.4.2. Accordingly, soil production rates increase with changes in hillslope roundness from concave to convex. However, it can be assumed that convex hillslopes tend to lose soil material while in turn soil material is gained on concave hillslopes. The tendency for a negative relationship between solum depth and curvature seems to confirm these trends. Solum depths tended to increase with decreasing curvature towards a concave roundness of hillslopes.

By applying the linear correlation analysis, correlations were also obtained between the soil organic carbon content, the amount of  $^{137}\text{Cs}$  and the median age of single-grains determined for depth increments in the top 50 cm of soil profiles along the Mount Boss and Plateau Beech toposequences.

This analysis identified the following significant relationships (see appendix Figure 3):

- (1) Negative correlation between the median age and amounts of  $^{137}\text{Cs}$  (-0.848)
- (2) Negative correlation between the median age and soil organic carbon content (-0.858)
- (3) Positive correlation between amount of  $^{137}\text{Cs}$  and soil organic carbon (0.921)

These relationships were expected. For the top 50 cm analysed, median ages of single-grains increased down the soil profile. This trend is related to the decreasing probability of quartz grains buried at depth reaching the soil surface. Simultaneously, contents of organic carbon and amount of  $^{137}\text{Cs}$  in the soil bulk samples decreased down the soil profile, which is related to their initial accumulation near the soil surface and their subsequent vertical translocation discussed in section 5.5.

## 6.4 Performance of sophisticated dating methods to investigate pedogenesis

### *TCN*

The determination of soil production rates from TCN data is based on the assumption that the soil landscape studied evolved under steady-state conditions of soil production and soil erosion. Subsequently, soil depths along a hillslope need to be relatively constant or in equilibrium over the period of TCN-production in parent materials, in order to ‘correctly’ estimate the long-term production rate at the site studied. Assuming constant soil depths along hillslopes over time is linked to presuming linear transport functions along these hillslopes. Deriving SPR from TCN-data is therefore only applicable in landscapes that have a significant relief and are in steady-state condition in relation to rates of soil production and soil erosion. Humphreys and Wilkinson (2007) discussed that for TCN measurements these conditions need to be maintained over an average period of about  $10^4$  to  $10^5$  years in the subsoil.

Calculated soil production rates are arguable because of these assumptions. The occurrence of stable conditions of soil depths along hillslopes over the majority of TCN accumulation in parent materials over time, resulting from steady soil erosion and soil formation might not always be the case, although it was discussed that uncertainties would not be higher than 20 % (Riebe et al., 2003). As discussed in Chapter 4, annual rates of TCN production were corrected by the soil overburden, and it was therefore posited that the present soil depths occurred for the main period of TCN accumulation. However, in contrast, the probability of stable conditions for the target material itself over the time where TCN accumulate is high when deriving soil production rates of soil by ‘dating’ soil parent materials.

Moreover, using TCN to ‘date’ soil material and subsequently estimate rates of total soil denudation along hillslopes is even more challenging than estimating SPR from soil parent materials. For the target soil material, stable conditions for the accumulation of TCN over time can not be assumed, because of lateral movements of the soil material. In addition, there is also the difficulty of estimating annual rates of TCN production, because of the unsteady soil overburden. Estimating denudation rates from soil samples using TCN was predominantly applied together with geochemical mass balance approaches in order to investigate the extent of chemical weathering compared to physical weathering, which was discussed in Chapter 2.

Uncertainties for TCN-derived SPR ranged between 6 and 10 %, including AMS measurement errors and additional uncertainty resulting from normalization to sea level and high latitude and also from corrections for shielding by slope and soil overburden. Currently, research

is focused on the refinement of nuclide production rates to further reduce the uncertainties in denudation rate and consequently soil production rate calculations (NAS, 2010).

### *OSL*

In order to estimate the OSL age and consequently the distribution of mid-sized sand grains from soil samples, a sampling size of at least 500 single quartz grains was necessary. The quantity of quartz grains was restricted, because of difficulties with the OSL reader performance. An increase of the single-grain sampling size for all depth increments sampled was therefore not possible.

The exposure history of single grains in undisturbed soil-mantled environments and therefore their response to OSL is different to depositional environments. In fluvial or aeolian depositional environments it is believed that all grains from the bulk sample analysed were translocated and most likely sufficiently exposed to sunlight during the transport process. In undisturbed soil environments it is believed that the exposure of single grains to sunlight occurs only near the soil surface and consequently by transport of grains to the soil surface through bioturbating agents or gravitationally induced lateral movements along the hillslope. The bleaching history of these grains is therefore reduced. Results confirmed these assumptions, because of the low ratio of finite to infinite ages.

Uncertainties in single-grain age estimates were quite high, most likely resulting from discrepancies in the exposure of single grains to sunlight at the soil surface. With uncertainties of over 18 %, single-grain age estimates can only be used as an indication of the age of soil particles and not for absolute age interpretations.

The potential for estimation of soil horizon ages by determination of one 'true' dose age from single-grain OSL data was limited, because of the heterogeneous nature of age estimates from individual grains and also due to the fact that a relatively large amount of single grains did not have a natural OSL signal. If it is assumed that this fraction of single-grains was never exposed to sunlight since its production, soil horizons should be as old as soil residence times calculated for relevant soil depths, applying the simple soil production model (see section 4.5.2). Surface horizons would therefore be between 33000 and 76000 years old, whereas the age of adjacent subsurface horizons would range from 10000 to 50000 years. This time period concurs with supposed time periods for soil horizon formation (McKenzie et al., 2004; Salvador-Blanes et al., 2007).



## Chapter 7 Overall conclusions and suggestions for future work

The research presented here confirms that dating methods developed to investigate geomorphologic processes are applicable to derive rates of pedogenic processes. The applied sampling scheme of sampling along toposequences proved to be ideal for investigating processes of pedogenesis quantitatively in the forested environment studied. Applying TCN to estimate rates of soil production, and OSL to derive rates of soil mixing was challenging however, because of increased uncertainties in the determination of 'exposure times of parent materials' or 'ages of single-grains' in soil-mantled environments.

The automated use of TCN and OSL is still restricted by the high costs that are involved in conducting research that applies these tools. Currently, research is focused on developing significantly smaller and more affordable AMS facilities in order to reduce the cost and the sample throughput of TCN analysis (NAS, 2010).

### 7.1 Key findings

Key findings presented in this research thesis are first summarized in relation to the proposed questions about pedogenesis:

Questions or challenges posited within this research	Answers and examples
What is the rate of soil production at Werrikimbe National Park?	Relatively slow potential weathering rate, $P_0$ , of $10 \pm 4 \text{ mm kyr}^{-1}$ , with $b = 0.125 \pm 0.617 \text{ mm}^{-1}$
Which concept did soil production follow at Werrikimbe National Park?	No clear pattern of SPR related to soil depth was observed. SPR neither followed a clear exponential nor humped soil production function as proposed in the literature. SPR appeared to be closely related to the terrain attribute profile curvature. This implied that soil erosion and deposition were not in equilibrium.
Did soil mixing occur in the first 50 cm of the soil profile?	Yes

How fast were rates of soil mixing in the first 50 cm of soil?

Vertical mixing: 0.2 to 0.5 mm yr<sup>-1</sup>

Lateral transport: 0.01 to 1.2 mm yr<sup>-1</sup>

Did soil mixing prevent the occurrence of soil horizons in the soil profile?

No.

Horizonation was present at all soil profiles sampled. These results imply that the occurrence of minor soil mixing (mostly related to floral agents) does not necessarily lead to a homogenisation of the topsoil and adjacent horizons.

Resulting from this research the following findings have also been achieved:

- The compilation of TCN-derived SPR showed that values of conversion rates of parent materials to soil varied, but not over several orders of magnitude as expected. Differences were within one order of magnitude for diverse climate regimes and parent materials. An average rate of soil production of 47±4 mm kyr<sup>-1</sup> resulting from the compilation of TCN-derived SPR was therefore posited.
- Analysing OSL single-grain distributions from natural soil-mantled forested environments revealed that tools used for analysing distributions in depositional environments cannot be applied readily for interpreting soil data from these environments. In order to interpret the range of age distributions of single-grains a combination of different statistical tools was required. Probability plots, box plots and density plots seemed to work the best for analysing the OSL single-grain age dataset.
- Out of 500 single grains analysed with OSL from each depth increment, for less than 25 % a finite age was estimated. This proportion of finite grains to infinite grains had the tendency to decrease gradually with increasing soil depth.
- The median of age distributions from single grains increased down the soil profile. Subsequently, the amount of near zero single grains decreased down the soil profile. These trends were related to the declining probability of quartz grains buried at depth reaching the soil surface and being set back to zero.



## 7.2 Suggestions for future work

There are many opportunities for future work:

### *TCN*

#### *Calculating SPR implementing recent advances in the refinement of the half-life of $^{10}\text{Be}$*

Recently, a new half-life of  $^{10}\text{Be}$  has been proposed that might alter the precision in calculations of SPR (Chmeleff et al., 2009).

### *OSL*

#### *OSL analysis for larger quantities of grains*

To improve the performance of single-grain age estimates from soil samples, measurements should be made on quantities of more than 500 quartz grains. However, this aim is limited by the availability of more than 500 purified quartz grains after sample preparations. Bulk samples of soil from cores of 26 cm in length and 5 cm in diameter resulted in more or less 700 grains for OSL analysis, with a sand content of the soil materials sampled of about 20-40 %. The taking of more than one bulk sample of soil for the same depth increment for OSL analysis is therefore proposed here.

#### *OSL analysis for different mineral fractions*

To improve the interpretation of soil mixing rates, OSL ages should be estimated for different mineral fractions. This might reveal equal or different grain distributions with respect to grain sizes and might also detect preferential mixing of soil particles. During sample preparations sand-sized quartz grains were separated into three fractions, 90-180  $\mu\text{m}$  (fine sand), 180-212  $\mu\text{m}$  (medium-sand) and >212  $\mu\text{m}$  (coarse sand), but only the mid-sized sand fraction was used for analysis on the OSL reader. Only grains of the 180-212  $\mu\text{m}$  fraction fit readily in the array of holes of discs that habituate 100 grains for 'automated' analysis on the OSL reader. For coarser fractions single-aliquots have to be used resulting in a very tedious work of analysing each grain individually. Nevertheless, it would be feasible to conduct such a study for different grain-sizes of quartz to identify possible differences in grain velocities given that some burrowing agents perform selective transfer of certain soil particle sizes.

#### *Test for sensitivity of quartz grains from soil samples*

An opportunity exists to conduct further tests of the sensitivity of quartz grains following procedures presented in Pietsch et al. (2008) for fluvial environments. Applying different test doses in the laboratory might reveal if and how often quartz grains visited the soil surface. Repetitive natural processes of irradiation and heating that the grains have experienced since

weathering from bedrock would increase their sensitivity. Low sensitivity was suggested for colluvial samples because of short bleaching histories during their final pre-burial bleach (Pietsch et al., 2008). Increased sensitivity of single-grains might therefore correspond to repeated events of exposure to the soil surface. A test for sensitivity of quartz grains would involve the identification of grains with a high natural sensitivity. This would equate to high responses with respect to OSL reader counts per second, and subsequently replicating the natural cycle of irradiation in the laboratory, based on grains from the interface of parent material to soil.

#### *Conducting micromorphological analysis together with OSL analysis*

Analysing undisturbed thin sections together with OSL will most certainly improve the interpretation of grain distributions and consequently the interpretation of their displacement in the soil profile. Micromorphological analysis of thin sections would be very useful to identify macropores, voids and channels that most certainly act as translocation agents for soil particles. Furthermore, soil thin sections would be helpful to better explore the distribution of organic matter and therefore the translocation of soil particles in the soil profile through identifying organic coatings on pore walls.

#### *Fallout radionuclides*

The quantitative assessment of fallout radionuclides resulted from data obtained for OSL analysis. In order to conduct an erosion/sediment transport study as performed by for instance Martinez et al. (2009; 2010) total fallout radionuclide activities would have to be determined for a flat plateau site without soil erosion. Comparing the variability of this natural, flat and highly likely uneroded reference site with the fallout variability determined for the hillslope transects would definitely rule out the occurrence of present-day soil erosion.

#### *Quantitative-mechanistic modelling of soil formation*

##### *Implementing derived rates of pedogenic processes in a quantitative-mechanistic soil formation model*

The next step resulting from this research is to implement the derived rates of soil production and soil mixing in a quantitative-mechanistic model that should be based on soil formation models discussed in Chapter 2, i.e. Minasny and McBratney (1999) and Salvador-Blanes et al. (2007).

The derived parameters for pedogenic processes should be used to verify the soil formation model. The model should be tested for its ability to predict the current soil landscape of the subcatchment analysed at Werrikimbe National Park. Also worthy of investigation is whether the

implementation of estimated rates of soil mixing that differ at certain soil depths would improve the simulation of horizonation in the soil profile. Would the estimated lower rates of soil mixing of 0.2 to 0.5 mm yr<sup>-1</sup> 'prevent' the formation of stone layers that were predicted when using relatively high soil mixing rates of 0.8 to 4.2 mm yr<sup>-1</sup>?

The Board of Directors of the American Telephone and Telegraph Company has the honor to acknowledge the many suggestions and criticisms of the public which have been received during the past year. It is gratifying to find that the public interest in the Company's affairs is so widespread and that the public opinion is so well informed. The Board is confident that the suggestions and criticisms received will be of great value in the improvement of the Company's service to the public. It is the policy of the Company to keep the public advised of its activities and to invite their suggestions and criticisms. The Board is confident that the public interest in the Company's affairs will continue to grow and that the public opinion will continue to be well informed.

The Board of Directors of the American Telephone and Telegraph Company has the honor to acknowledge the many suggestions and criticisms of the public which have been received during the past year. It is gratifying to find that the public interest in the Company's affairs is so widespread and that the public opinion is so well informed. The Board is confident that the suggestions and criticisms received will be of great value in the improvement of the Company's service to the public. It is the policy of the Company to keep the public advised of its activities and to invite their suggestions and criticisms. The Board is confident that the public interest in the Company's affairs will continue to grow and that the public opinion will continue to be well informed.

Public Relations

The Board of Directors of the American Telephone and Telegraph Company has the honor to acknowledge the many suggestions and criticisms of the public which have been received during the past year. It is gratifying to find that the public interest in the Company's affairs is so widespread and that the public opinion is so well informed. The Board is confident that the suggestions and criticisms received will be of great value in the improvement of the Company's service to the public. It is the policy of the Company to keep the public advised of its activities and to invite their suggestions and criticisms. The Board is confident that the public interest in the Company's affairs will continue to grow and that the public opinion will continue to be well informed.

Financial Statement

The Board of Directors of the American Telephone and Telegraph Company has the honor to acknowledge the many suggestions and criticisms of the public which have been received during the past year. It is gratifying to find that the public interest in the Company's affairs is so widespread and that the public opinion is so well informed. The Board is confident that the suggestions and criticisms received will be of great value in the improvement of the Company's service to the public. It is the policy of the Company to keep the public advised of its activities and to invite their suggestions and criticisms. The Board is confident that the public interest in the Company's affairs will continue to grow and that the public opinion will continue to be well informed.

The Board of Directors of the American Telephone and Telegraph Company has the honor to acknowledge the many suggestions and criticisms of the public which have been received during the past year. It is gratifying to find that the public interest in the Company's affairs is so widespread and that the public opinion is so well informed. The Board is confident that the suggestions and criticisms received will be of great value in the improvement of the Company's service to the public. It is the policy of the Company to keep the public advised of its activities and to invite their suggestions and criticisms. The Board is confident that the public interest in the Company's affairs will continue to grow and that the public opinion will continue to be well informed.

The Board of Directors of the American Telephone and Telegraph Company has the honor to acknowledge the many suggestions and criticisms of the public which have been received during the past year. It is gratifying to find that the public interest in the Company's affairs is so widespread and that the public opinion is so well informed. The Board is confident that the suggestions and criticisms received will be of great value in the improvement of the Company's service to the public. It is the policy of the Company to keep the public advised of its activities and to invite their suggestions and criticisms. The Board is confident that the public interest in the Company's affairs will continue to grow and that the public opinion will continue to be well informed.

## Bibliography

- Ahnert, F. (1977). Some comments on the quantitative formulation of geomorphological processes in a theoretical model. *Earth Surface Processes* **2**, 191-201.
- Aitken, M. J. (1994). Optical dating: A non-specialist review. *Quaternary Geochronology* **13**, 503.
- Aitken, M. J. (1998). "An introduction to optical dating. The dating of Quaternary sediments by the use of photon-stimulated luminescence," Oxford University Press, Oxford, New York, Tokyo.
- Alexander, E. B. (1985). Rates of soil formation from bedrock or consolidated sediments *Physical Geography* **6**, 25-42.
- Alexander, E. B. (1988). Rates of soil formation: Implications for soil-loss tolerance. *Soil Science* **145**, 37-45.
- Amundson, R. (2004). Soil formation. In "Treatise on Geochemistry" (H. D. Holland and K. K. Turekian, eds.), Vol. 5, pp. 1-35. Elsevier Press, Amsterdam.
- Amundson, R., and Jenny, H. (1997). On a State Factor Model of Ecosystems. *BioScience* **47**, 536-543.
- Amundson, R., Richter, D. D., Humphreys, G. S., Jobbágy, E. G., and Gaillardet, J. (2007). Coupling between Biota and Earth Materials in the Critical Zone. *Elements* **3**, 327-332.
- Anderson, J. M. (1988). Section 1. Interactions between invertebrates and microorganisms in organic-matter decomposition, energy flux and nutrient cycling in ecosystems. Invertebrate-mediated transport processes in soils. *Agriculture, Ecosystems and Environment* **24**, 5-19.
- Anderson, S. P., von Blanckenburg, F., and White, A. F. (2007). Physical and chemical controls on the critical zone. *Elements* **3**, 315-319.
- Arnold, L. J., Roberts, R. G., Galbraith, R. F., and DeLong, S. B. (2009). A revised burial dose estimation procedure for optical dating of young and modern-age sediments. *Quaternary Geochronology* **4**, 306-325.
- Atkinson, G. (1999). "Soil Landscapes of the Kempsey-Korogoro Point 1:100 000 Sheet Report," Department of Land and Water Conservation, Sydney.
- Balco, G. (2006). Converting Al and Be isotope ratio measurements to nuclide concentrations in quartz. *Cosmogenic Nuclide Lab, University of Washington*.
- Barrows, T. T., Stone, J. O., Fifield, L. K., and Cresswell, R. G. (2000). The timing of the Last Glacial Maximum in Australia. *Quaternary Science Reviews* **21**, 159-173.
- Bateman, M. D., Frederick, C. D., Jaiswal, M. K., and Singhvi, A. K. (2003). Investigations into the potential effects of pedoturbation on luminescence dating. *Quaternary Science Reviews* **22**, 1169-1176.

- Bierman, P. R. (1994). Using in situ produced cosmogenic isotopes to estimate rates of landscape evolution: A review from the geomorphic perspective. *Journal of Geophysical Research* **99**, 13885-13896.
- Bierman, P. R., and Caffee, M. (2002). Cosmogenic exposure and erosion history of Australian bedrock landforms. *Geological Society of America Bulletin* **114**, 787-803.
- Bierman, P. R., and Nichols, K. K. (2004). Rock to sediment - Slope to sea with  $^{10}\text{Be}$  - Rates of landscape change. *Annual Review of Earth and Planetary Sciences*. **32**, 215-255.
- Bierman, P. R., Reuter, J. M., Pavich, M., Gellies, A. C., Caffee, M. W., and Larsen, J. (2005). Using cosmogenic nuclides to contrast rates of erosion and sediment yield in a semi-arid, arroyodominated landscape, Rio Puerco Basin, New Mexico. *Earth Surface Processes and Landforms* **30**, 935-953.
- Blake, W. H., Wallbrink, P. J., Wilkinson, S. N., Humphreys, G. S., Doerr, S. H., Shakesby, R. A., and Tomkins, K. M. (2009). Deriving hillslope sediment budgets in wildfire-affected forests using fallout radionuclide tracers. *Geomorphology* **104**, 105-116.
- Blum, W. E., and Ganssen, R. (1972). Bodenbildende Prozesse der Erde, ihre Erscheinungsformen und diagnostischen Merkmale in tabellarischer Darstellung. *Die Erde. Zeitschrift der Gesellschaft für Erdkunde zu Berlin* **103**, 7-20.
- Bockheim, J. G., and Gennadiyev, A. N. (2000). The role of soil-forming processes in the definition of taxa in Soil Taxonomy and the World Soil Reference Base. *Geoderma* **95**, 53-72.
- Bockheim, J. G., and Gennadiyev, A. N. (2009). The value of controlled experiments in studying soil-forming processes: A review. *Geoderma* **152**, 208-217.
- Branagan, D. F., and Packham, G. H. (2000). "Field geology of New South Wales," Department of Mineral Resources New South Wales, Sydney, Australia.
- Brantley, S. L. (2010). Weathering: Rock to regolith. *Nature Geoscience* **3**, 305-306.
- Brantley, S. L., Goldhaber, M. B., and Ragnarsdottir, K. V. (2007). Crossing disciplines and scales to understand the critical zone. *Elements* **3**, 307-314.
- Brantley, S. L., White, T. S., White, A. F., Sparks, D., Richter, D., Pregitzer, K., Derry, L., Chorover, J., Chadwick, O., April, R., Anderson, S., and Amundson, R. (2006). "Frontiers in exploration of the Critical Zone: A workshop sponsored by the National Science Foundation (NSF)," Newark, DE.
- Brindley, G. W., and Brown, G. (1980). "Crystal structures of clay minerals and their X-ray identification " Mineralogical Society, London.
- Brown, E. T., Colin, F., and Bournès, D. L. (2003). Quantitative evaluation of soil processes using in situ-produced cosmogenic nuclides. *Comptes Rendus Geoscience* **335**, 1161-1171.
- Buchan, G. (2010). Ode to soil. *Journal of Soil and Water Conservation* **65**, 48A-54A.

- Burke, B. C., Heimsath, A. M., Dixon, J. L., Chappell, J., and Yoo, K. (2009). Weathering the escarpment: chemical and physical rates and processes, south-eastern Australia. *Earth Surface Processes and Landforms* **34**, 768-785.
- Burke, B. C., Heimsath, A. M., and White, A. F. (2007). Coupling chemical weathering with soil production across soil-mantled landscapes. *Earth Surface Processes and Landforms* **32**, 853-873.
- Bush, D. A., and Feathers, J. K. (2003). Application of OSL single-aliquot and single-grain dating to quartz from anthropogenic soil profiles in the SE United States. *Quaternary Science Reviews* **22**, 1153-1159.
- Carson, M. A., and Kirkby, M. J. (1972). "Hillslope form and process," Cambridge University Press, Cambridge.
- Child, D., Elliott, G., Mifsud, C., Smith, A. M., and Fink, D. (2000). Sample processing for Earth science studies at ANTARES. *Nuclear Instruments and Methods in Physics Research Section B: Beam Interactions with Materials and Atoms* **172**, 856-860.
- Chmeleff, J., von Blanckenburg, F., Kossert, K., and Jakob, D. (2009). Determination of the  $^{10}\text{Be}$  half-life by Multi Collector ICP-mass spectrometry and liquid scintillation counting. *Goldschmidt Abstracts 2009 - C. Geochimica et Cosmochimica Acta* **73**, A221-A221.
- Churchman, G. J. (2010). The philosophical status of soil science. *Geoderma* **157**, 214-221.
- Clapp, E., Bierman, P. R., and Caffee, M. (2002). Using  $^{10}\text{Be}$  and  $^{26}\text{Al}$  to determine sediment generation rates and identify sediment source in an arid region drainage basin. *Geomorphology* **45**, 67-87.
- Clapp, E. M., Bierman, P. R., Schick, A. P., Lekach, J., Enzel, Y., and Caffee, M. (2000). Sediment yield exceeds sediment production in arid region drainage basins. *Geology* **28**, 995-998.
- Clark, M. J., and Smith, F. B. (1988). Wet and dry deposition of Chernobyl releases. *Nature* **332**, 245-249.
- Cleaves, E. T. (1993). Climatic impact on isovolumetric weathering of a coarse-grained schist in the northern Piedmont Province of the central Atlantic states. *Geomorphology* **8**, 191-198.
- Cockburn, H. A. P., Brown, R. W., Summerfield, M. A., and Seidl, M. A. (2000). Quantifying passive margin denudation and landscape development using a combined fission-track thermochronology and cosmogenic isotope analysis approach. *Earth and Planetary Science Letters* **179**, 429-435.
- Cockburn, H. A. P., Seidl, M. A., and Summerfield, M. A. (1999). Quantifying denudation rates on inselbergs in the central Namib Desert using in situ-produced cosmogenic  $^{10}\text{Be}$  and  $^{26}\text{Al}$ . *Geology* **27**, 399-402.
- Colgan, P. M., Bierman, P. R., Mickelson, D. M., and Caffee, M. (2002). Variation in glacial erosion near the southern margin of the Laurentide Ice Sheet, south-central Wisconsin, USA: Implications for cosmogenic dating of glacial terrains. *Geological Society of America Bulletin* **114**, 1581-1591.

- Collins, A. L., Walling, D. E., Webb, L., and King, P. (2010). Apportioning catchment scale sediment sources using a modified composite fingerprinting technique incorporating property weightings and prior information. *Geoderma* **155**, 249-261.
- Colman, S. M. (1981). Rock-weathering rates as functions of time. *Quaternary Research* **15**, 250-264.
- Colman, S. M., and Dethier, D. P. (1986). An overview of rates of chemical weathering. In "Rates of chemical weathering of rocks and minerals" (S. M. Colman and D. P. Dethier, eds.), pp. 1-18. Academic Press, Orlando.
- Corkery, N. A. (1993). "Environmental impact statement. Kempsey/Wauchope management areas. Proposed forest management.." Truyard Pty Ltd, Crows Nest.
- Crutzen, P. J., and Stoermer, E. F. (2000). The "Anthropocene". *IGBP Newsletter* **41**, 17-18.
- Dethier, D. P. (1986). Weathering Rates and the Chemical Flux from Catchments in the Pacific Northwest, U.S.A. In "Rates of Chemical Weathering of Rocks and Minerals" (S. M. Colman and D. P. Dethier, eds.), pp. 503-530. Academic Press, Orlando.
- DiBiase, R. A., Whipple, K. X., Heimsath, A. M., and Ouimet, W. B. (2010). Landscape form and millennial erosion rates in the San Gabriel Mountains, CA. *Earth and Planetary Science Letters* **289**, 134-144.
- Dietrich, W. E., and Perron, T. J. (2006). The search for a topographic signature of life. *Nature* **439**, 411-418.
- Dietrich, W. E., Reiss, R., Hsu, M.-L., and Montgomery, D. R. (1995). A process-based model for colluvial soil depth and shallow landsliding using digital elevation data. *Hydrological Processes* **9**, 383-400.
- Dixon, J. L., Heimsath, A. M., and Amundson, R. (2009). The critical role of climate and saprolite weathering in landscape evolution. *Earth Surface Processes and Landforms* **34**, 1507-1521.
- Dörr, H. (1995). Application of  $^{210}\text{Pb}$  in soils. *Journal of Paleolimnology* **13**, 157-168.
- Dosseto, A., Turner, S. P., and Chappell, J. (2008). The evolution of weathering profiles through time: New insights from uranium-series isotopes. *Earth and Planetary Science Letters* **274**, 359-371.
- Duller, G. A. T. (1996). Recent developments in luminescence dating of Quaternary sediments. *Progress in Physical Geography* **20**, 127-145.
- Duller, G. A. T. (2001). Luminescence Analyst Version 3.04b. *University of Wales, Aberystwyth*.
- Duller, G. A. T. (2006). Single grain optical dating of glacial deposits. *Quaternary Geochronology* **1**, 296-304.
- Dunai, T. J. (2000). Scaling factors for production rates of in situ produced cosmogenic nuclides: a critical reevaluation. *Earth and Planetary Science Letters* **176**, 157-169.



- Dunne, J., Elmore, D., and Muzikar, P. (1999). Scaling factors for the rates of production of cosmogenic nuclides for geometric shielding and attenuation at depth on sloped surfaces. *Geomorphology* **27**, 3-11.
- Edmond, J. M., Palmer, M. R., Measures, C. I., Grant, B., and Stallard, R. F. (1995). The fluvial geochemistry and denudation rate of the Guayana Shield in Venezuela, Colombia, and Brazil. *Geochimica et Cosmochimica Acta* **59**, 3301-3325.
- Eguchi, S., Yamaguchi, N., Fujiwara, H., Fukuyama, T., Mori, Y., Seki, K., Suzuki, K., and Adachi, K. (2010). Cosmogenic, anthropogenic, and airborne radionuclides for tracing the mobile soil particles in a tile-drained heavy clay soil. *19<sup>th</sup> World Congress of Soil Science, Soil Solutions for a Changing World 1 – 6 August 2010, Brisbane, Australia. Published on DVD.*
- Elmore, D., and Phillips, F. M. (1987). Accelerator mass spectrometry for measurement of long-lived radioisotopes. *Science* **236**, 543-550.
- Eriksson, M. G., Olley, J. M., and Payton, R. W. (2000). Soil erosion history in central Tanzania based on OSL dating of colluvial and alluvial hillslope deposits. *Geomorphology* **36**, 107-128.
- Fink, D., and Smith, A. (2007). An inter-comparison of  $^{10}\text{Be}$  and  $^{26}\text{Al}$  AMS reference standards and the  $^{10}\text{Be}$  half-life. *Nuclear Instruments and Methods in Physics Research Section B: Beam Interactions with Materials and Atoms* **259**, 600-609.
- Finke, P. A., and Hutson, J. L. (2008). Modelling soil genesis in calcareous loess. *Geoderma* **145**, 462-479.
- Forrest, B., Rink, W. J., Bicho, N., and Ferring, C. R. (2003). OSL ages and possible bioturbation signals at the Upper Paleolithic site of Lagoa do Bordoal, Algarve, Portugal. *Quaternary Science Reviews* **22**, 1279-1285.
- Fuchs, M., Fischer, M., and Reverman, R. (2010). Colluvial and alluvial sediment archives temporal resolved by OSL dating: Implications for reconstructing soil erosion. *Quaternary Geochronology* **5**, 269-273.
- Furbish, D. J., and Fagherazzi, S. (2001). Stability of creeping soil and implications for hillslope evolution. *Water Resources Research* **37**, 2607-2618.
- Gabet, E. J., Reichman, O. J., and Seabloom, E. W. (2003). The effects of bioturbation on soil processes and sediment transport. *Annual Review of Earth and Planetary Sciences* **31**, 249-274.
- Galbraith, R. F., Roberts, R. G., Laslett, G. M., Yoshida, H., and Olley, J. M. (1999). Optical dating of single and multiple grains of quartz from Jinmium Rock Shelter, Northern Australia: Part I. Experimental design and statistical models. *Archaeometry* **41**, 339-364.
- Gilbert, G. K. (1877). "Report on the geology of the Henry Mountains (Utah)," United States Geological Survey, Washington DC.
- Gill, R. A., and Jackson, R. B. (2000). Global patterns of root turnover for terrestrial ecosystems. *New Phytologist* **147**, 13-31.

- Glendon, W. G., and Dani, O. (2002). Particle-size analysis. In "Methods of soil analysis. Part 4 Physical Methods" (J. H. Dane and G. C. Topp, eds.), pp. 255-293. Soil Science Society of America, Madison.
- Gosse, J. C., and Phillips, F. M. (2001). Terrestrial in situ cosmogenic nuclides: theory and application. *Quaternary Science Reviews* **20**, 1475-1560.
- Graham, R. C., Rossi, A. M., and Hubbert, K. R. (2010). Rock to regolith conversion: Producing hospitable substrates for terrestrial ecosystems. *GSA Today* **20**, 4-9.
- Granger, D. E., and Muzikar, P. F. (2001). Dating sediment burial with in situ-produced cosmogenic nuclides: theory, techniques, and limitations. *Earth and Planetary Science Letters* **188**, 269-281.
- Granger, D. E., Riebe, C. S., Kirchner, J. W., and Finkel, R. C. (2001). Modulation of erosion on steep granitic slopes by boulder armoring, as revealed by cosmogenic  $^{26}\text{Al}$  and  $^{10}\text{Be}$ . *Earth and Planetary Science Letters* **186**, 269-281.
- Green, E. G., Dietrich, W. E., and Banfield, J. F. (2006). Quantification of chemical weathering rates across an actively eroding hillslope. *Earth and Planetary Science Letters* **242**, 155-169.
- Grigg, A. H., Sheridan, G. J., Pearce, A. B., and Mulligan, D. R. (2006). The effect of organic mulch amendments on the physical and chemical properties and revegetation success of a saline-sodic minespoil from central Queensland, Australia. *Australian Journal of Soil Research* **44**, 97-105
- Grossman, R. B., and Reinsch, T. G. (2002). Bulk density and linear extensibility. In "Methods of soil analysis. Part 4 Physical Methods" (J. H. Dane and G. C. Topp, eds.). Soil Science Society of America, Madison.
- Hancock, G. R., Murphy, D., and Evans, K. G. (2010). Hillslope and catchment scale soil organic carbon concentration: An assessment of the role of geomorphology and soil erosion in an undisturbed environment. *Geoderma* **155**, 36-45.
- Hazelton, P., and Murphy, B. (2007). "Interpreting Soil Test Results. What do all the numbers mean?," 2nd/Ed. CSIRO Publishing, Collingwood.
- He, Q., and Walling, D. E. (1996). Interpreting particle size effects in the adsorption of  $^{137}\text{Cs}$  and unsupported  $^{210}\text{Pb}$  by mineral soils and sediments. *Journal of Environmental Radioactivity* **30**, 117-137.
- Heimsath, A. M. (2006). Eroding the land: Steady-state and stochastic rates and processes through a cosmogenic lens. *Geological Society of America* **415**, 111-129.
- Heimsath, A. M., Chappell, J., Dietrich, W. E., Nishiizumi, K., and Finkel, R. C. (2000). Soil production on a retreating escarpment in southeastern Australia. *Geology* **28**, 787-790.
- Heimsath, A. M., Chappell, J., Dietrich, W. E., Nishiizumi, K., and Finkel, R. C. (2001a). Late Quaternary erosion in southeastern Australia: A field example using cosmogenic nuclides. *Quaternary International* **83-85**, 169-185.

- Heimsath, A. M., Chappell, J., Finkel, R. C., Fifield, K., and Alimanovic, A. (2006). Escarpment erosion and landscape evolution in southeastern Australia. *Geological Society of America* **398**, 173-190.
- Heimsath, A. M., Chappell, J., Spooner, N. A., and Questiaux, D. G. (2002). Creeping soil. *Geology* **30**, 111-114.
- Heimsath, A. M., Dietrich, W. E., Nishiizumi, K., and Finkel, R. C. (1997). The soil production function and landscape equilibrium. *Nature* **388**, 358-361.
- Heimsath, A. M., Dietrich, W. E., Nishiizumi, K., and Finkel, R. C. (1999). Cosmogenic nuclides, topography, and the spatial variation of soil depth. *Geomorphology* **27**, 151-172.
- Heimsath, A. M., Dietrich, W. E., Nishiizumi, K., and Finkel, R. C. (2001b). Stochastic processes of soil production and transport: erosion rates, topographic variation and cosmogenic nuclides in the Oregon Coast Range. *Earth Surface Processes and Landforms* **26**, 531-552.
- Heimsath, A. M., Fink, D., and Hancock, G. R. (2009). The 'humped' soil production function: eroding Arnhem Land, Australia. *Earth Surface Processes and Landforms* **34**, 1674-1684.
- Heimsath, A. M., Furbish, D. J., and Dietrich, W. E. (2005). The illusion of diffusion: Field evidence for depth-dependent sediment transport. *Geology* **33**, 949-952.
- Hofmann, H. J., Beer, J., Bonani, G., von Gunten, H. R., Raman, S., Suter, M., Walker, R. L., Wölfli, W., and Zimmermann, D. (1987).  $^{10}\text{Be}$ : Half-life and AMS-Standards. *Nuclear Instruments and Methods in Physics Research B29* 32-36.
- Hole, F. D. (1981). Effects of animals on soil. *Geoderma* **25**, 75-112.
- Hoosbeek, M. R., and Bryant, R. B. (1992). Towards the quantitative modeling of pedogenesis - A review. *Geoderma* **55**, 183-210.
- Huggett, R. J. (1975). Soil landscape systems: A model of soil genesis. *Geoderma* **13**, 1-22.
- Huggett, R. J. (1998). Soil chronosequences, soil development, and soil evolution: a critical review. *CATENA* **32**, 155-172.
- Hülle, D., Hilgers, A., Kühn, P., and Radtke, U. (2009). The potential of optically stimulated luminescence for dating periglacial slope deposits — A case study from the Taunus area, Germany. *Geomorphology* **2009**, 66-78.
- Humphreys, G. S., and Wilkinson, M. T. (2007). The soil production function: A brief history and its rediscovery. *Geoderma* **139**, 73-78.
- Hunter, R. J. (2004). World heritage and associative natural values of the central eastern rainforest reserves of Australia. NSW National Parks and Wildlife Service.
- Huntley, D. J., Godfrey-Smith, D. I., and Thewalt, M. L. W. (1985). Optical dating of sediments. *Nature* **313**, 105-107.
- Isbell, R. F., McDonald, W. S., and Ashton, L. J. (1997). "Concepts and Rationale of the Australian Soil Classification.," ACLEP, CSIRO Land and Water, Canberra.

- Jacobs, Z., Duller, G. A. T., and Wintle, A. G. (2006). Interpretation of single grain  $D_e$  distributions and calculation of  $D_e$ . *Radiation Measurements* **41**, 264-277.
- Jenny, H. (1941). "Factors of soil formation. A system of quantitative pedology," McGraw-Hill Book Company, New York, London.
- Johnson, D. L. (1990). Biomantle evolution and the redistribution of earth materials and artifacts. *Soil Science* **149**, 84-102.
- Johnson, D. L., and Watson-Stegner, D. (1987). Evolution model of pedogenesis. *Soil Science* **143**, 349-366.
- Johnston, R. M., Barry, S. J., Bley, E., Bui, E. N., Moran, C. J., Simon, D. A. P., Carlile, P., McKenzie, N. J., Henderson, B. L., Chapman, G., Imhoff, M., Maschmedt, D., Howe, D., Grose, C., Schoknecht, N., Powell, B., and Grundy, M. (2003). ASRIS: The database. *Australian Journal of Soil Research* **41**, 1021-1036.
- Kaste, J. M., Heimsath, A. M., and Bostick, B. C. (2007). Short-term soil mixing quantified with fallout radionuclides. *Geology* **35**, 243-246.
- Kirkby, M. J. (1977). Soil development models as a component of slope models. *Earth Surface Processes* **2**, 203-230.
- Kirkby, M. J. (1985). A basis for soil profile modelling in a geomorphic context. *Journal of Soil Science* **36**, 97-121.
- Lair, G. J., Zehetner, F., Hrachowitz, M., Franz, N., Maringer, F.-J., and Gerzabek, M. H. (2009). Dating of soil layers in a young floodplain using iron oxide crystallinity. *Quaternary Geochronology* **4**, 260-266.
- Lal, D. (1991). Cosmic ray labeling of erosion surfaces: in situ nuclide production rates and erosion models. *Earth and Planetary Science Letters* **104**, 424-439.
- Lasaga, A. C., Soler, J. M., Ganor, J., Burch, T. E., and Nagy, K. L. (1994). Chemical weathering rate laws and global geochemical cycles. *Geochimica et Cosmochimica Acta* **58**, 2361-2386.
- Lepper, K., and McGeever, S. W. S. (2002). An objective methodology for dose distribution analysis. *Radiation Protection Dosimetry* **101**, 349.
- Lindsay, J. (2008). Terrain Analysis System (TAS): GIS software. <http://www.uoguelph.ca/~hydrogeo/TAS/index.html>, University of Guelph, Canada.
- Lobry de Bruyn, L. A., and Conacher, A. J. (1990). The role of termites and ants in soil modification: A review. *Australian Journal of Soil Research* **28**, 55-93.
- Loughran, R. J., Campbell, B. L., Elliott, G. L., and Shelly, D. J. (1990). Determination of the rate of sheet erosion on grazing land using caesium-137. *Applied Geography* **10**, 125-133.
- Ludwig, W., and Probst, J. L. (1998). River sediment discharge to the oceans: present-day controls and global budget. *American Journal of Science* **298**, 265-295.

- Mabit, L., Benmansour, M., and Walling, D. E. (2008). Comparative advantages and limitations of the fallout radionuclides  $^{137}\text{Cs}$ ,  $^{210}\text{Pb}_{\text{ex}}$  and  $^7\text{Be}$  for assessing soil erosion and sedimentation. *Journal of Environmental Radioactivity* **99**, 1799–1807.
- Madsen, A. T., Murray, A. S., Andersen, T. J., Pejrup, M., and Breuning-Madsen, H. (2005). Optically stimulated luminescence dating of young estuarine sediments: a comparison with  $^{210}\text{Pb}$  and  $^{137}\text{Cs}$  dating. *Marine Geology* **214**, 251-268.
- Martinez, C., Hancock, G. R., and Kalma, J. D. (2009). Comparison of fallout radionuclide (caesium-137) and modelling approaches for the assessment of soil erosion rates for an uncultivated site in south-eastern Australia. *Geoderma* **151**, 128-140.
- Martinez, C., Hancock, G. R., and Kalma, J. D. (2010). Relationships between  $^{137}\text{Cs}$  and soil organic carbon (SOC) in cultivated and never-cultivated soils: An Australian example. *Geoderma* **158**, 137-147.
- McBratney, A. B., Mendonca Santos, M. L., and Minasny, B. (2003). On digital soil mapping. *Geoderma* **117**, 3-52.
- McKean, J. A., Dietrich, W. E., Finkel, R. C., Southon, J. R., and Caffee, M. W. (1993). Quantification of soil production and downslope creep rates from cosmogenic  $^{10}\text{Be}$  accumulations on a hillslope profile. *Geology* **21**, 343-346.
- McKenzie, N., Jacquier, D., Isbell, R., and Brown, K. (2004). "Australian soils and landscapes. An illustrated compendium," CSIRO Publishing, Collingwood.
- Milne, G. (1935). Some suggested units for classification and mapping, particularly for East African Soils. *Soil Research* **4**, 183-198.
- Minasny, B., and McBratney, A. B. (1999). A rudimentary mechanistic model for soil production and landscape development. *Geoderma* **90**, 3-21.
- Minasny, B., and McBratney, A. B. (2001). A rudimentary mechanistic model for soil formation and landscape development: II. A two-dimensional model incorporating chemical weathering. *Geoderma* **103**, 161-179.
- Minasny, B., McBratney, A. B., and Salvador-Blanes, S. (2008). Quantitative models for pedogenesis - A review. *Geoderma* **144**, 140-157.
- Montgomery, D. R. (2007). Soil erosion and agricultural sustainability. *Proceedings of the National Academy of Science* **104**, 13268-13272.
- Moore, D. M., and Reynolds, R. C., Jr. (1989). "X-ray diffraction and the identification and analysis of clay minerals," Oxford University Press, Oxford, New York.
- Muller-Lemans, H., and van Dorp, F. (1996). Bioturbation as a mechanism for radionuclide transport in soil: Relevance of earthworms. *Journal of Environmental Radioactivity* **31**, 7-20.
- Murray, A. S., and Olley, J. M. (2002). Precision and accuracy in the optically stimulated luminescence dating of sedimentary quartz: A status review. *Geochronometria* **21**, 1-16.

- Murray, A. S., and Roberts, R. G. (1997). Determining the burial time of single grains of quartz using optically stimulated luminescence. *Earth and Planetary Science Letters* **152**, 163-180.
- Murray, A. S., and Roberts, R. G. (1998). Measurement of the equivalent dose in quartz using a regenerative-dose single-aliquot protocol. *Radiation Measurements* **29**, 503-515.
- Murray, A. S., and Wintle, A. G. (2000). Luminescence dating of quartz using an improved single-aliquot regenerative-dose protocol. *Radiation Measurements* **32**, 57-73.
- NAS (2010). "Landscapes on the edge. New horizons for research on Earth's surface," The National Academy Press, Washington, D.C.
- Nichols, K. K., Bierman, P. R., Eppes, M. C., Caffee, M., Finkel, R. C., and Larsen, J. (2005). Late Quaternary history of the Chemehuevi Mountain piedmont, Mojave Desert, deciphered using  $^{10}\text{Be}$  and  $^{26}\text{Al}$ . *American Journal of Science* **305**, 345-368.
- Nichols, K. K., Bierman, P. R., Foniri, W. R., Gillespie, A. R., Caffee, M., and Finkel, R. C. (2006). Dates and rates of arid region geomorphic processes. *GSA Today* **16**, 4-11.
- Nishiizumi, K., Kohl, C. P., Arnold, J. R., Klein, J., Fink, D., and Middleton, R. (1991). Cosmic ray produced  $^{10}\text{Be}$  and  $^{26}\text{Al}$  in Antarctic rocks: exposure and erosion history. *Earth and Planetary Science Letters* **104**, 440-454.
- Nishiizumi, K., Winterer, E. L., Kohl, C. P., Klein, J., Middleton, R., Lal, D., and Arnold, J. R. (1989). Cosmic ray production rates of  $^{10}\text{Be}$  and  $^{26}\text{Al}$  in quartz from glacially polished rocks. *Journal of Geophysical Research* **94**, 17907-17915.
- Odgers, N. P., McBratney, A. B., and Minasny, B. (2008). Generation of kth-order random toposequences. *Computers & Geosciences* **34**, 479-490.
- Olley, J. M., Caitcheon, G. G., and Roberts, R. G. (1999). The origin of dose distributions in fluvial sediments, and the prospect of dating single grains from fluvial deposits using optically stimulated luminescence. *Radiation Measurements* **30**, 207-217.
- Olley, J. M., Pietsch, T., and Roberts, R. G. (2004). Optical dating of Holocene sediments from a variety of geomorphic settings using single grains of quartz. *Geomorphology* **60**, 337-358.
- Ollier, C. D. (1995). Tectonics and landscape evolution in southeast Australia. *Geomorphology* **12**, 37-44.
- Owens, L. B., and Watson, J. P. (1979). Landscape reduction by weathering in small Rhodesian watersheds. *Geology* **7**, 281-284.
- Pačes, T. (1986). Rates of weathering and erosion derived from mass balance in small drainage basins. In "Rates of Chemical Weathering of Rocks and Minerals" (S. M. Colman and D. P. Dethier, eds.), pp. 531-550. Academic Press, Orlando.
- Palm, C., Sanchez, P. A., Ahamed, S., and Awiti, A. (2007). Soils: A contemporary perspective. *Annual Review of Environmental Resources* **32**, 99-129.

- Paton, T. R., Humphreys, G. S., and Mitchell, P. B. (1995). "Soils: A new global view," University College London Press, London.
- Pavich, M. J. (1986). Processes and rates of saprolite production and erosion on a foliated granitic rock of the Virginia Piedmont. In "Rates of Chemical weathering of Rocks and Minerals" (S. M. Colman and D. P. Dethier, eds.), pp. 552-590. Academic Press, Orlando.
- Pelletier, J. D., and Rasmussen, C. (2009). Geomorphically based predictive mapping of soil thickness in upland watersheds. *Water Resources Research* **45**.
- Pietsch, T. J., Olley, J. M., and Nanson, G. C. (2008). Fluvial transport as a natural luminescence sensitiser of quartz. *Quaternary Geochronology* **3**, 365-376.
- Pimentel, D., Harvey, C., Resosudarmo, P., Sinclair, K., Kurz, D., McNair, M., Crist, S., Shpritz, L., Fitton, I., Saffouri, R., and Blair, R. (1995). Environmental and economic costs of soil erosion and conservation benefits. *Science* **v267**, p1117(7).
- Pope, G. A., Dorn, R. I., and Dixon, J. C. (1995). A new conceptual model for understanding geographical variations in weathering. *Annals of the Association of American Geographers* **85**, 38-64.
- Priori, S., Costantini, E. A. C., Capezzuoli, E., Protano, G., Hilgers, A., Sauer, D., and Sandrelli, F. (2008). Pedostratigraphy of Terra Rossa and Quaternary geological evolution of a lacustrine limestone plateau in central Italy. *Journal of Plant Nutrition and Soil Science* **171**, 509-523.
- Quinton, J. N., Govers, G., Van Oost, K., and Bardgett, R. D. (2010). The impact of agricultural soil erosion on biogeochemical cycling. *Nature Geoscience* **3**, 311-314.
- Rayment, G. E., and Higginson, F. R. (1992). "Australian laboratory handbook of soil and water chemical methods," Inkata Press, Melbourne, Sydney.
- Regan, E. J. (1977). The natural energy basis for soils and urban growth in Florida, University of Florida, Florida.
- Riebe, C. S., Kirchner, J. W., and Finkel, R. C. (2003). Long-term rates of chemical weathering and physical erosion from cosmogenic nuclides and geochemical mass balance. *Geochimica et Cosmochimica Acta* **67**, 4411-4427.
- Riebe, C. S., Kirchner, J. W., and Finkel, R. C. (2004a). Erosional and climatic effects on long-term chemical weathering rates in granitic landscapes spanning diverse climate regimes. *Earth and Planetary Science Letters* **224**, 547-562.
- Riebe, C. S., Kirchner, J. W., and Finkel, R. C. (2004b). Sharp decrease in long-term chemical weathering rates along an altitudinal transect. *Earth and Planetary Science Letters* **218**, 421-434.
- Riebe, C. S., Kirchner, J. W., Granger, D. E., and Finkel, R. C. (2001). Minimal climatic control on erosion rates in the Sierra Nevada, California. *Geology* **29**, 447-450.
- Runge, E. C. A. (1973). Soil development sequences and energy models. *Soil Science* **115**, 183-193.

- Ruxton, B. P. (1968). Measures of the Degree of Chemical Weathering of Rocks. *The Journal of Geology* **76**, 518-527.
- Salvador-Blanes, S., Minasny, B., and McBratney, A. B. (2007). Modelling long-term in situ soil profile evolution: application to the genesis of soil profiles containing stone layers. *European Journal of Soil Science* **58**, 1535-1548.
- Samedov, P. A., and Nadirov, F. T. (1990). Effect of earthworms and woodlice on the physicochemical and surface properties of soils. *Soil Biology* **22**, 48-55.
- Saunders, I., and Young, A. (1983). Rates of surface processes on slopes, slope retreat and denudation. *Earth Surface Processes and Landforms* **8**, 473-501.
- Schaetzl, R., and Anderson, S. (2005). "Soils. Genesis and geomorphology," Cambridge University Press, New York.
- Schaetzl, R. J., Barrett, L. R., and Winkler, J. A. (1994). Choosing models for soil chronofunctions and fitting them to data. *European Journal of Soil Science* **45**, 219-232.
- Schaller, M., Blum, J. D., and Ehlers, T. A. (2009a). Combining cosmogenic nuclides and major elements from moraine soil profiles to improve weathering rate estimates. *Geomorphology* **106**, 198-205.
- Schaller, M., Ehlers, T. A., Blum, J. D., and Kallenberg, M. A. (2009b). Quantifying glacial moraine age, denudation, and soil mixing with cosmogenic nuclide depth profiles. *Journal of Geophysical Research* **114**.
- Schmidt, E. D., Machalet, B., Markovic, S. B., Tsukamoto, S., and Frechen, M. (2009). Luminescence chronology of the upper part of the Stari Slankamen loess sequence (Vojvodina, Serbia). *Quaternary Geochronology* **5**, 137-142.
- Seidl, M. A., Weissel, J. K., and Pratson, L. F. (1996). The kinematics and pattern of escarpment retreat across the rifted continental margin of SE Australia. *Basin Research* **8**, 301-316.
- Shaw, C. F. (1930). Potent factors in soil formation. *Ecology* **11** (XI), 239-245.
- Simonson, R. W. (1959). Modern concepts of soil genesis. Outline of a generalized theory of soil genesis. *Soil Science Society Proceedings*, 152-156.
- Small, E. E., Anderson, R. S., and Hancock, G. S. (1999). Estimates of the rate of regolith production using  $^{10}\text{Be}$  and  $^{26}\text{Al}$  from an alpine hillslope. *Geomorphology* **27**, 131-150.
- Sommer, M., Gerke, H. H., and Deumlich, D. (2008). Modelling soil landscape genesis - A "time split" approach for hummocky agricultural landscapes. *Geoderma* **145**, 480-493.
- Stone, J. O. (2000). Air pressure and cosmogenic isotope production. *Journal of Geophysical Research* **105**, 23,753-23,759.
- Strahler, A. N. (1957). Quantitative analysis of watershed geomorphology. *Transactions of the American Geophysical Union* **38**, 913-920.



- Stroeven, A. P., Fabel, D., Hättestrand, C., and Harbor, J. (2002). A relict landscape in the centre of Fennoscandian glaciation: cosmogenic radionuclide evidence of tors preserved through multiple glacial cycles. *Geomorphology* **44**, 145-154.
- Syvitski, J. P. M., Vorosmarty, C. J., Kettner, A. J., and Green, P. (2005). Impact of humans on the flux of terrestrial sediment to the global coastal ocean. *Science* **308**, 376-380.
- Taylor, G., and Eggleton, R. A. (2001). "Regolith geology and geomorphology," John Wiley & Sons, Ltd, Chichester.
- Tonneijck, F. H., and Jongmans, A. G. (2008). The influence of bioturbation on the vertical distribution of soil organic matter in volcanic ash soils: a case study in northern Ecuador. *European Journal of Soil Science* **59**, 1063-1075.
- Velbel, M. A. (1986). The mathematical basis for determining rates of geochemical and geomorphic processes in small forested watersheds by mass balance: examples and implications. In "Rates of Chemical Weathering of Rocks and Minerals" (S. M. Colman and D. P. Dethier, eds.), pp. 439-451. Academic Press, Orlando.
- Volobuyev, V. R. (1974). Main concepts of ecology. *Geoderma* **12**, 27-33.
- Volobuyev, V. R. (1984). Two key solutions of the energetics of soil formation. *Soviet Soil Science* **16**, 1-8.
- Volobuyev, V. R., and Ponomarev, D. G. (1977). Some thermodynamic characteristics of the mineral associations of soils. *Soviet Soil Science - Genesis and Geography of Soils*, 1-11.
- Volobuyev, V. R., Ponomarev, D. G., and Mikailov, F. D. (1980). Relation between the thermodynamic functions of soils, their mineral composition and infiltration capacity. *Soviet Soil Science - Soil Physics*, 210-212.
- von Blanckenburg, F. (2006). The control mechanisms of erosion and weathering at basin scale from cosmogenic nuclides in river sediment. *Earth and Planetary Science Letters* **242**, 224-239.
- Wakatsuki, T., and Rasyidin, A. (1992). Rates of weathering and soil formation. *Geoderma* **52**, 251-263.
- Wallbrink, P. J., Olley, J. M., and Murray, A. S. (1994). Measuring soil movement using <sup>137</sup>Cs: implications of reference site variability. *IAHS Publications* **224**, 95-102.
- Walling, D. E., He, Q., and Quine, T. A. (1995). Use of caesium-137 and lead-210 as tracers in soil erosion investigations. In "Tracer Technologies for Hydrological Systems (Proceedings of a Boulder Symposium, July 1995)" (C. Leibundgut, ed.), Vol. 229, pp. 163-172. IAHS Publications.
- Weissel, J. K., and Seidl, M. A. (1997). Influence of rock strength properties on escarpment retreat across passive continental margins. *Geology* **25**, 631-634.
- White, A. F., and Blum, A. E. (1995). Effects of climate on chemical weathering in watersheds. *Geochimica et Cosmochimica Acta* **59**, 1729-1747.

- White, A. F., and Brantley, S. L. (2003). The effect of time on the weathering of silicate minerals: why do weathering rates differ in the laboratory and field? *Chemical Geology* **202**, 479-506.
- Wilkinson, B. H., and McElroy, B. J. (2007). The impact of humans on continental erosion and sedimentation. *Geological Society of America Bulletin* **119**, 140-156.
- Wilkinson, M. T., Chappell, J., Humphreys, G. S., Fifield, K., Smith, B., and Hesse, P. (2005a). Erratum for soil production in heath and forest, Blue Mountains, Australia: influence of lithology and palaeoclimate. *Earth Surface Processes and Landforms* **30**, 1683-1685.
- Wilkinson, M. T., Chappell, J., Humphreys, G. S., Fifield, K., Smith, B., and Hesse, P. (2005b). Soil production in heath and forest, Blue Mountains, Australia: influence of lithology and palaeoclimate. *Earth Surface Processes and Landforms* **30**, 923-934.
- Wilkinson, M. T., and Humphreys, G. S. (2005). Exploring pedogenesis via nuclide-based soil production rates and OSL-based bioturbation rates. *Australian Journal of Soil Research* **43**, 767-779.
- Wilkinson, M. T., Richards, P. J., and Humphreys, G. S. (2009). Breaking ground: Pedological, geological, and ecological implications of soil bioturbation. *Earth Science Reviews* **97**, 257.
- Willgoose, G. (2005). Mathematical modeling of whole landscape evolution. *Annual Review of Earth and Planetary Sciences*. **33**, 443-459.
- Yaalon, D. H. (1975). Conceptual models in pedogenesis: Can soil-forming functions be solved? *Geoderma* **14**, 189-205.
- Yoo, K., Amundson, R., Heimsath, A. M., and Dietrich, W. E. (2005). Process-based model linking pocket gopher (*Thomomys bottae*) activity to sediment transport and soil thickness. *Geology* **33**, 917-920.
- Yoo, K., Amundson, R., Heimsath, A. M., Dietrich, W. E., and Brimhall, G. H. (2007). Integration of geochemical mass balance with sediment transport to calculate rates of soil chemical weathering and transport on hillslopes. *Journal of Geophysical Research* **112**.
- Zapata, F. (2003). The use of environmental radionuclides as tracers in soil erosion and sedimentation investigations: recent advances and future developments. *Soil & Tillage Research* **69**, 3-13.

## Appendix

### Soil profile descriptions (field morphology) (Chapter 3)

#### Toposequence Spokes Mountain (Ta)

##### *Soil Profile Ta16*

**Soil type:** Grey Kandosol

**Location:** Spokes Mountain, Spokes Mountain Trail, map reference: 437399E 6556424N (GDA1994, MGA56)

**Landform:** top of the hill

**Slope:** 1°

**Parent material:** fine lithic sandstone / siltstone

**Elevation:** 1145 m

**Vegetation:** dry sclerophyll forest, 80 % ground cover

**Land use:** old growth native forest

Layer 1 – A11(h), 0-5 cm	moist and dry: very dark brown (10YR 2/1) silty loam; weak 2-5 mm crumb rough-faced peds; weak force; less than 10-50 % sub-angular shaped stones (60-200 mm); 2-10 % roots (1-2, 2-5 mm); sharp (<5 mm) even boundary to...
Layer 2 – A12, 5-32 cm	moist and dry: brown (10YR 5/3), silty loam; diffuse inclusions of manganese; weak 2-5 mm crumb rough-faced peds; weak force; less than 10 % sub-rounded shaped stones (20-60 mm); 10-50 % roots (1-2, 2-5, mm); clear (20-50 mm) wavy boundary to...
Layer 3 – B21, 32-55 cm	moist: black (7.5YR 2.5/1), dry: very dark greyish brown (2.5Y 3/2) silty loam; diffuse inclusions of manganese; moderate 5-10 mm sub-angular blocky rough-faced peds; weak force; 10-50 % sub-angular and angular stones (20-60, 60-200 mm); 2-10 % roots (2-5, >5 mm); clear (20-50 mm) irregular boundary to the substrate.

##### *Soil Profile Ta12*

**Soil type:** Black Kandosol

**Location:** Spokes Mountain, Spokes Mountain Trail, map reference: 437679E 6556251N (GDA1994, MGA56)

**Landform:** mid- hill

**Slope:** 20°

**Parent material:** fine lithic sandstone / siltstone

**Elevation:** 1104 m

**Vegetation:** dry sclerophyll forest, 80 % ground cover

**Land use:** old growth native forest

**Other:** high amount of organic matter/leaves in first 5 cm of the profile, earthworms observed at site

Layer 1 – A11(h), 0-5 cm	moist and dry: very dark brown (10YR 2/1) silty loam; weak 2-5 mm crumb rough-faced peds; weak force; less than 10-50 % sub-angular shaped stones (60-200 mm); 10-50 % roots (1-2, 2-5 mm); sharp (<5 mm) even boundary to...
Layer 2 – A12, 5-25 cm	moist and dry: brown (10YR 5/3), silty loam; weak 2-5 mm crumb rough-faced peds; weak force; less than 10 % sub-rounded shaped stones (20-60 mm); 10-50 % roots (1-2, 2-5, mm); clear (20-50 mm) irregular boundary to...
Layer 3 – B21, 25-39 cm	moist: black (7.5YR 2.5/1), dry: very dark greyish brown (2.5Y 3/2) silty loam, mottles present: 20 % greyish brown (2.5Y 5/2) pale faint; diffuse inclusions of manganese; moderate 2-5 mm crumb rough-faced peds; moderate force; 10-50 % sub-angular and angular stones (20-60 mm); 10-50 % roots (2-5, >5 mm); clear (20-50 mm) boundary to...
Layer 4 – B22, 39-59 cm	moist: brownish yellow (10YR 6/8), dry: yellow (10YR 7/8) silty clay loam, mottles present: 20 % grey (10YR 4/1) pale distinct; moderate 5-10 mm sub-angular blocky peds; moderate force; 10-50 % angular stones (200-600 mm); 2-10 % roots (2-5, >5 mm); clear even boundary to the substrate.

**Soil Profile Ta2****Soil type:** Brown Kandosol**Location:** Spokes Mountain, Spokes Mountain Trail, map reference: 437996E 6555615N (GDA1994, MGA56)**Landform:** base of the hill**Slope:** 22°**Parent material:** fine lithic sandstone / siltstone**Elevation:** 1024 m**Vegetation:** dry sclerophyll forest, 80 % ground cover**Land use:** old growth native forest**Other:** moist in field condition, spiders and earthworms observed at site, stones parallel aligned throughout the profile

Litter layer – O, 2-0 cm

Layer 1 – A1, 0-15 cm

moist: very dark brown (10YR 2/2) silty loam; weak 2-5 mm polyhedral rough-faced peds; weak force; 10-50 % angular, sub-angular shaped stones (6-20, 20-60 mm); 10-50 % roots (1-2, 2-5, &gt;5 mm); clear (20-50 mm) even boundary to...

Layer 2 – B21, 15-40 cm

moist: very dark greyish brown (10YR 3/2) silty loam; weak 2-5 mm sub-angular blocky/crumb rough-faced peds; weak force; less than 10 % sub-rounded shaped stones (6-20, 20-60 mm); 10-50 % roots (1-2, 2-5, &gt;5 mm); clear (20-50 mm) even boundary to...

Layer 3 – B22, 40-50 cm

moist: dark grey (10YR 4/1) silty loam; weak 2-5 mm sub-angular/crumb rough-faced peds; weak force; 10-50 % sub-angular shaped stones (6-20, 20-60 mm); 10-50 % roots (1-2, 2-5, &gt;5 mm); clear (20-50 mm) wavy boundary to the substrate (rock).

**Toposequence Mount Boss (Tb)*****Soil Profile Tb24*****Soil type:** Brown Dermosol**Location:** Mount Boss, Upper Forbes road, map reference: 441941E 6547645N (GDA1994, MGA56)**Landform:** top of the hill**Slope:** 1°**Parent material:** fine lithic sandstone / siltstone**Elevation:** 979 m**Vegetation:** wet sclerophyll forest, 50 % ground cover**Land use:** old growth native forest**Other:** abundance of earthworms visible at the site

Layer 1 – A11(h), 0-5 cm	moist: very dark brown (7.5YR 2.5/2), dry: very dark brown (7.5YR 2.5/3) silty clay; moderate 5-10 mm polyhedral rough-faced peds; weak force; less than 10 % sub-angular shaped stones (20-60 mm); 10-50 % roots (1-2 mm); sharp (<5 mm) even boundary to...
Layer 2 – A12, 5-35 cm	moist: very dark brown (10YR 2/2), dry: dark brown (10YR 3/3) silty clay; moderate 5-10 mm polyhedral rough-faced peds; weak force; less than 10 % sub-angular shaped stones (20-60 mm); 2-10 % roots (1-2 mm); clear (20-50 mm) even boundary to...
Layer 3 – B2, 35-(45)55 cm	moist: dark brown (10YR 3/3), dry: dark brown (7.5YR 3/3) silty clay; moderate 5-10 mm sub-angular blocky rough-faced peds; moderate force; 10-50 % sub-angular and angular shaped stones (60-200 mm); 2-10 % roots (2-5 mm); gradual (50-100 mm) irregular boundary to the substrate...
Layer 4 – BC, 55-100 cm	moist and dry: strong brown (7.5YR 5/6) silty clay; weak 5-10 mm polyhedral rough-faced peds; moderate force; less than 10 % sub-angular shaped stones (60-200 mm); 2-10 % roots (2-5 mm); gradual (50-100 mm) irregular boundary to the substrate throughout this layer.

***Soil Profile Tb12*****Soil type:** Brown Dermosol**Location:** Mount Boss, Upper Forbes road, map reference: 441725E 6547639N (GDA1994, MGA56)**Landform:** mid- hill**Slope:** 15°**Parent material:** fine lithic sandstone / siltstone**Elevation:** 931 m**Vegetation:** wet sclerophyll forest, 50 % ground cover**Land use:** old growth native forest**Other:** hard nodules of charcoal, grubs observed at the site

Layer 1 – A1, 0-10 cm	moist and dry: very dark brown (7.5YR 2.5/3) silty clay loam; weak 5-10 mm polyhedral rough-faced peds; weak force; less than 10 % sub-rounded shaped stones (20-60, 60-200 mm); 10-50 % roots (2-5 mm); clear (20-50 mm) even boundary to...
Layer 2 – B1, 10-40 cm	moist: very dark brown (7.5YR 2.5/2), dry: very dark brown (7.5YR 2.5/3) silty clay loam; moderate 10-20 mm polyhedral rough-faced peds; weak force; less than 10 % sub-rounded shaped stones (60-200 mm); 2-10 % roots (2-5, >5 mm); clear (20-50 mm) even boundary to the substrate...
Layer 3 – BC, 40-60(90) cm	moist: strong brown (7.5YR 5/6), dry: strong brown (7.5YR 5/8) silty clay loam; moderate 20-50 mm sub-angular rough-faced peds; moderate force; 10-50 % sub-angular shaped stones (200-600, >600 mm); 2-10 % roots (2-5, >5 mm); diffuse (>100 mm) irregular boundary to the substrate throughout this layer.

**Soil Profile Tb6****Soil type:** Red Dermosol**Location:** Mount Boss, Upper Forbes road, map reference: 441627E 6547699N (GDA1994, MGA56)**Landform:** base of the hill**Slope:** 9°**Parent material:** fine lithic sandstone / siltstone**Elevation:** 902 m**Vegetation:** wet sclerophyll forest, 45 % ground cover**Land use:** old growth native forest**Other:** hard nodules of charcoal present down to 60 m in the profile, earthworms observed at site

Layer 1 – A1, 0-10 cm	moist and dry: very dark brown (7.5YR 2.5/2) silty loam; weak 5-10 mm polyhedral rough-faced peds; weak force; less than 10 % sub-angular shaped stones (60-200 mm); 10-50 % roots (2-5 mm); abrupt (5-20 mm) even boundary to...
Layer 2 – B2, 10-40 cm	moist: very dark brown (7.5YR 2.5/2), dry: dark reddish brown (5YR 3/2) silty loam; weak 5-10 mm polyhedral rough-faced peds; weak force; less than 10 % sub-angular shaped stones (60-200 mm); 10-50 % roots (2-5, >5 mm); clear (20-50 mm) even boundary to...
Layer 3 – BC, 40-62(90) cm	moist and dry: very dark brown (7.5YR 2.5/2) silty loam, mottles present, primary mottles: 15 % light grey (7.5YR7/1) pale distinct, secondary mottles: 15 % reddish yellow (7.5YR 6/8) pale distinct; moderate 5-10 mm sub-angular blocky peds; moderate force; 10-50 % sub-angular and angular stones (60-200 mm); 10-50 % roots (2-5, >5 mm); diffuse irregular boundary to the substrate (>100 mm) at 90 cm.

**Toposequence Plateau Beech (Te)*****Soil Profile Te38*****Soil type:** Brown Dermosol**Location:** Plateau Beech, North Plateau Road, map reference: 434707E 6550066N (GDA1994, MGA56)**Landform:** top of the hill**Slope:** 1°**Parent material:** fine lithic sandstone / siltstone**Elevation:** 1092 m**Vegetation:** cool temperate rainforest, 60 % ground cover**Land use:** old growth native forest**Other:** surface roots

Layer 1 – A1, 0-20 cm	moist: yellowish brown (10YR 5/6), dry: yellowish brown (10YR 5/8) silty clay; strong 20-50 mm polyhedral smooth-faced peds; moderate force; less than 10 % angular shaped stones (20-60 mm); 10-50 % roots (2-5 mm); clear (20-50 mm) even boundary to...
Layer 2 – B21, 20-40 cm	moist: strong brown (7.5YR 5/8), dry: strong brown (7.5YR 5/6) silty clay; strong 20-50 mm polyhedral smooth-faced peds; strong force; less than 10 % angular shaped stones (60-200 mm); 2-10 % roots (2-5 mm); gradual (50-100 mm) irregular boundary to...
Layer 3 – B22, 40-70 cm	moist and dry: yellowish red (5YR 5/6) silty clay, mottles present, primary mottles: 10 % red dark faint, secondary mottles: 5 % yellow (10YR 7/8) dark prominent; moderate 20-50 mm sub-angular blocky smooth-faced peds; strong force; less than 10 % angular shaped stones (20-60 mm); <2 % roots (1-2, >5 mm); clear (20-50 mm) irregular boundary to...
Layer 4 – B3, 70-88 cm	moist: yellowish red (5YR 5/8), dry: strong brown (7.5YR 5/8) silty clay loam, mottles present: 20 % yellow (10YR 7/8) dark prominent; moderate 20-50 mm sub-angular blocky peds; moderate force; 10-50 % angular stones (20-60 mm); <2 % roots (2-5 mm); diffuse irregular boundary to the substrate (>100 mm).

***Soil Profile TeM*****Soil type:** Brown Dermosol**Location:** Plateau Beech, North Plateau Road, map reference: 435155E 6550235N (GDA1994, MGA56)**Landform:** mid- hill**Slope:** 12°**Parent material:** fine lithic sandstone / siltstone**Elevation:** 1065 m**Vegetation:** cool temperate rainforest, 60 % ground cover**Land use:** old growth native forest**Other:** surface roots

Layer 1 – A1, 0-14 cm	moist and dry: dark brown (7.5YR 3/3) silty clay; moderate 10-20 mm polyhedral rough-faced peds; moderate force; less than 10 % angular shaped stones (20-60 mm); 10-50 % roots (2-5, >5 mm); clear (20-50 mm) even boundary to...
Layer 2 – B2, 14-38 cm	moist: strong brown (7.5YR 4/6), dry: strong brown (7.5YR 5/6) silty clay; strong 20-50 mm sub-angular blocky smooth-faced peds; strong force; less than 10 % angular shaped stones (20-60 mm); 2-10 % roots (1-2, 2-5 mm); gradual (50-100 mm) irregular boundary to...
Layer 3 – B3, 38-68 cm	moist and dry: yellowish red (5YR 5/6) silty clay, mottles present, primary mottles: 5 % yellow dark distinct, secondary mottles: 5 % grey dark prominent; strong 20-50 mm sub-angular blocky smooth-faced peds; strong force; less than 10 % sub-angular shaped stones (20-60 mm); 2-10 % roots (1-2, >5 mm); clear (20-50 mm) irregular boundary to substrate.

**Soil Profile Te3****Soil type:** Red Dermosol**Location:** Plateau Beech, North Plateau Road, map reference: 435220E 6549999N (GDA1994, MGA56)**Landform:** base of the hill**Slope:** 2°**Parent material:** fine lithic sandstone / siltstone**Elevation:** 1008 m**Vegetation:** cool temperate rainforest, 60 % ground cover**Land use:** old growth native forest**Other:** surface roots, earthworms observed at site

Layer 1 – A1, 0-10 cm	moist: dark brown (7.5YR 3/3), dry: brown (7.5YR 4/4) silty clay; moderate 5-10 mm polyhedral rough-faced peds; moderate force; 10-50 % angular shaped stones (60-200 mm); 10-50 % roots (2-5, >5 mm); clear (20-50 mm) even boundary to...
Layer 2 – B21, 10-37 cm	moist: strong brown (7.5YR 4/6), dry: strong brown (7.5YR 5/6) silty clay, mottles present: 5 % dark reddish grey (5YR 4/2) pale distinct; strong 10-20 mm sub-angular blocky rough-faced peds; moderate force; 10-50 % angular shaped stones (60-200 mm); 10-50 % roots (1-2, 2-5, >5 mm); gradual (50-100 mm) wavy boundary to...
Layer 3 – B22, 37-78 cm	moist and dry: yellowish red (5YR 4/6) silty clay, mottles present, primary mottles: 5 % yellow (10YR 7/8) pale distinct, secondary mottles: 2 % pinkish white (5YR 8/2) pale distinct; strong 10-20 mm sub-angular blocky smooth-faced peds; strong force; less than 10 % sub-angular shaped stones (6-20 mm); 2-10 % roots (<1, >5 mm); gradual (50-100 mm) wavy boundary to...
Layer 4 – B23, 78-103 cm	moist and dry: yellowish red (5YR 4/6) silty clay, mottles present: 5 % yellow (10YR 7/8) pale distinct; strong 20-50 mm angular blocky smooth-faced peds; moderate force; less than 10 % sub-angular shaped stones (20-60 mm); <2 % roots (1-2, 2-5 mm); gradual (50-100 mm) irregular boundary to substrate.

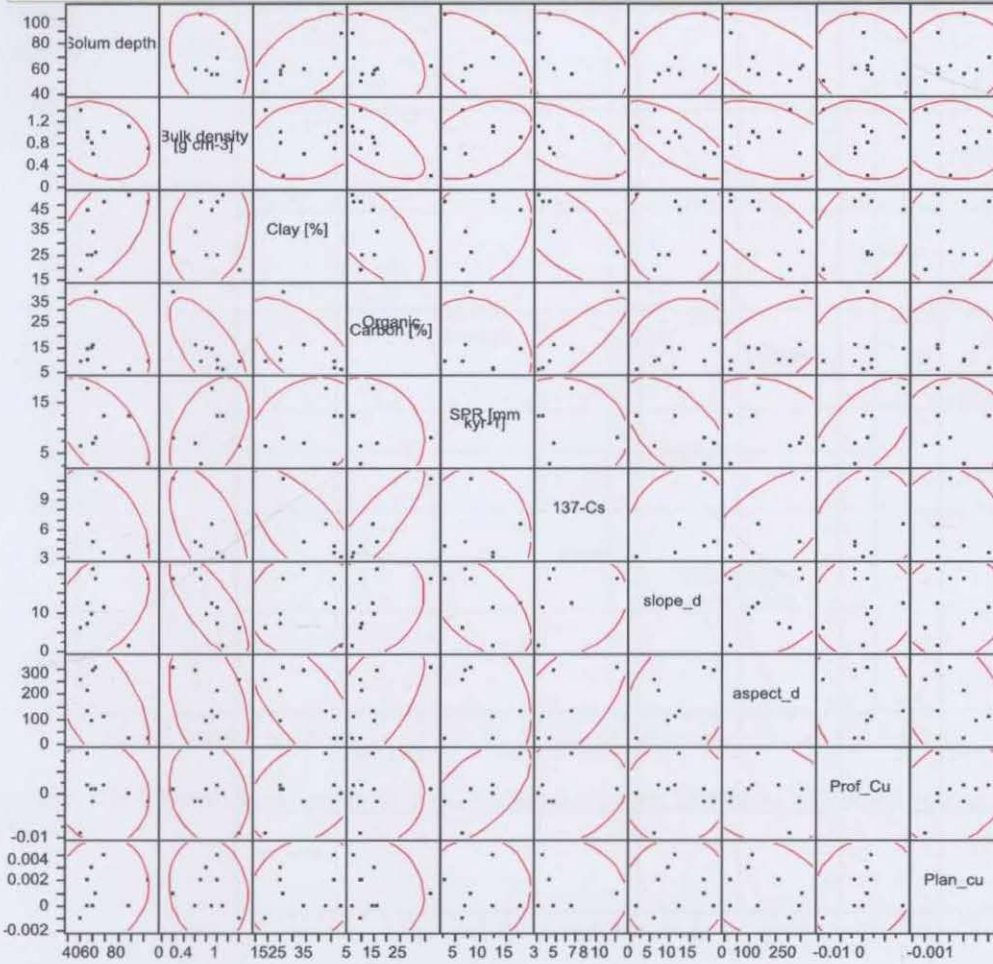


**Correlations**

	Solum depth	Bulk density [g cm-3]	Clay [%]	Organic Carbon [%]	SPR [mm kyr-1]	137-Cs	slope_d	aspect_d	Prof_Cu	Plan_cu
Solum depth	1.0000	-0.2619	0.5776	-0.2902	-0.5396	-0.3571	0.3587	-0.5327	-0.1045	0.1012
Bulk density [g cm-3]	-0.2619	1.0000	0.1906	-0.6902	0.4352	-0.5977	-0.7375	-0.3765	-0.2067	-0.1221
Clay [%]	0.5776	0.1906	1.0000	-0.6726	0.2624	-0.7128	0.0383	-0.6916	0.3259	0.1940
Organic Carbon [%]	-0.2902	-0.6902	-0.6726	1.0000	-0.1712	0.8789	0.2319	0.6290	-0.0268	-0.1029
SPR [mm kyr-1]	-0.5396	0.4352	0.2624	-0.1712	1.0000	-0.0805	-0.5846	-0.1980	0.6136	0.0304
137-Cs	-0.3571	-0.5977	-0.7128	0.8789	-0.0805	1.0000	0.1954	0.6441	0.2198	-0.1378
slope_d	0.3587	-0.7375	0.0383	0.2319	-0.5846	0.1954	1.0000	0.3013	0.0639	0.0573
aspect_d	-0.5327	-0.3765	-0.6916	0.6290	-0.1980	0.6441	0.3013	1.0000	-0.1941	-0.3390
Prof_Cu	-0.1045	-0.2067	0.3259	-0.0268	0.6136	0.2198	0.0639	-0.1941	1.0000	0.2075
Plan_cu	0.1012	-0.1221	0.1940	-0.1029	0.0304	-0.1378	0.0573	-0.3390	0.2075	1.0000

The correlations are estimated by REML method.

**Scatterplot Matrix**



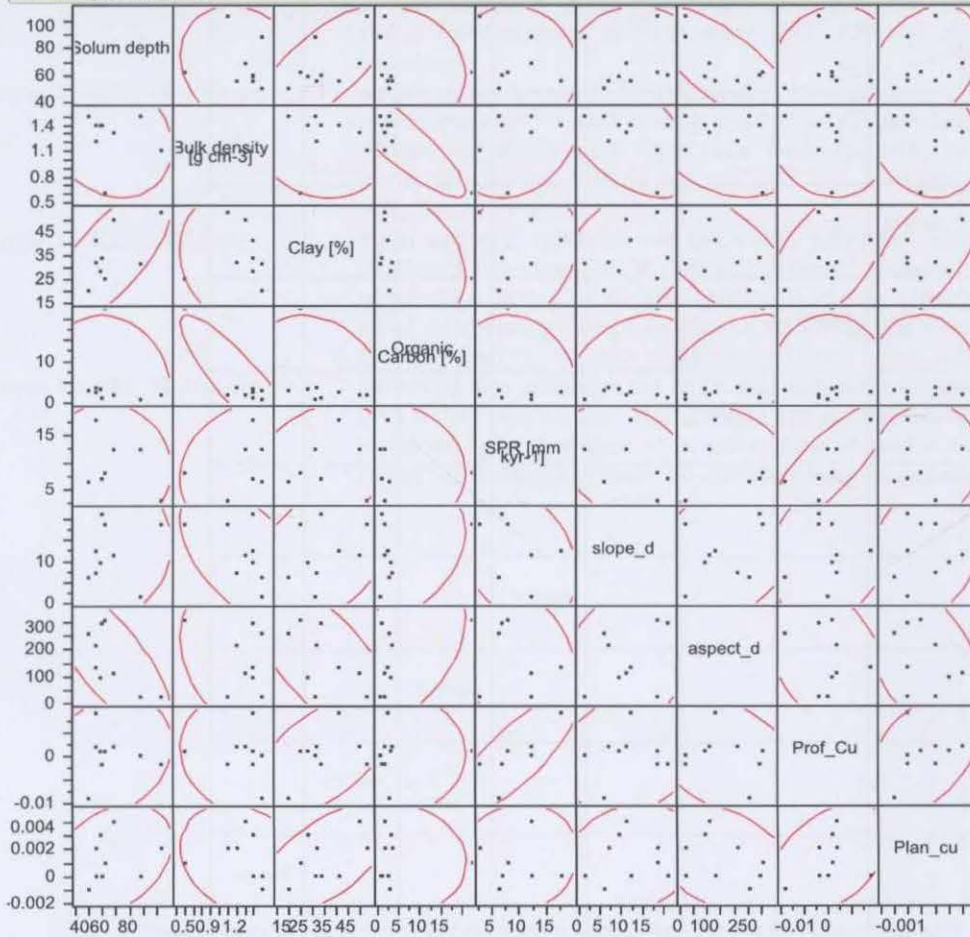
Appendix. Fig. 1. Correlation of topsoil properties and rates of soil production with terrain attributes (Chapter 6).

**Correlations**

	Solum depth	Bulk density [g cm-3]	Clay [%]	Organic Carbon [%]	SPR [mm kyr-1]	slope_d	aspect_d	Prof_Cu	Plan_cu
Solum depth	1.0000	-0.1798	0.7219	-0.1512	-0.0749	0.1600	-0.7507	0.1974	0.3440
Bulk density [g cm-3]	-0.1798	1.0000	-0.0742	-0.8865	0.2295	-0.5197	-0.3085	-0.1387	-0.2282
Clay [%]	0.7219	-0.0742	1.0000	-0.3198	0.2486	0.3647	-0.6400	0.5550	0.6273
Organic Carbon [%]	-0.1512	-0.8865	-0.3198	1.0000	-0.1411	-0.1411	0.3244	0.5262	-0.0502
SPR [mm kyr-1]	-0.0749	0.2295	0.2486	-0.1411	1.0000	-0.3209	-0.2859	0.8054	0.1371
slope_d	0.1600	-0.5197	0.3647	0.3244	-0.3209	1.0000	0.2784	0.1538	0.2220
aspect_d	-0.7507	-0.3085	-0.6400	0.5262	-0.2859	0.2784	1.0000	-0.3649	-0.3910
Prof_Cu	0.1974	-0.1387	0.5550	0.0218	0.8054	0.1538	-0.3649	1.0000	0.4387
Plan_cu	0.3440	-0.2282	0.6273	-0.0502	0.1371	0.2220	-0.3910	0.4387	1.0000

The correlations are estimated by REML method.

**Scatterplot Matrix**



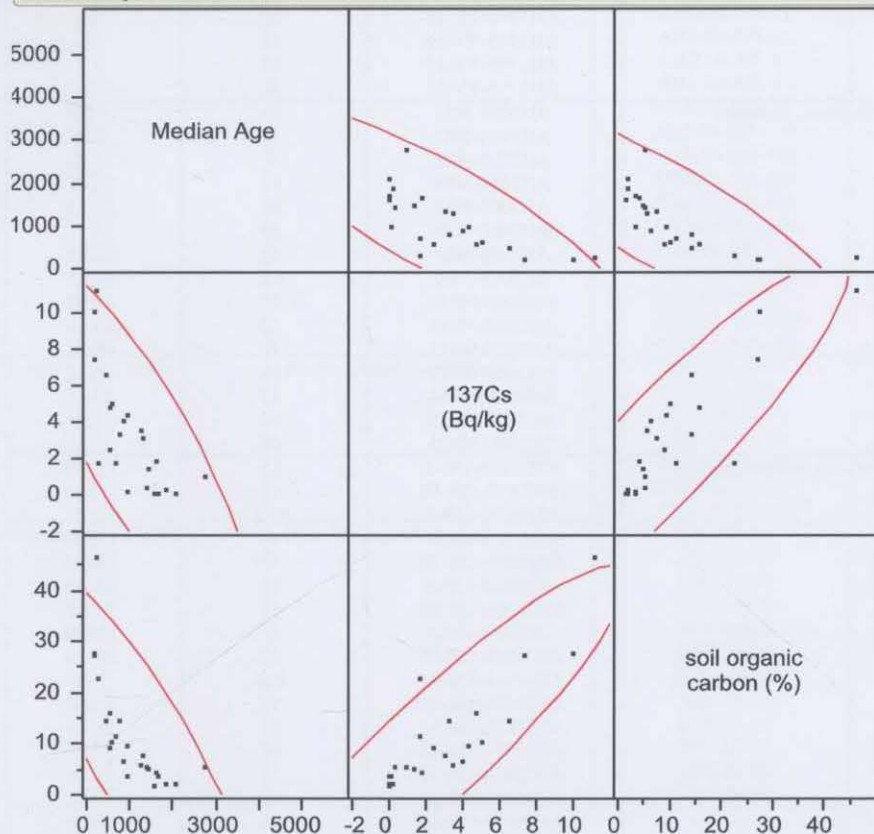
Appendix. Fig. 2. Correlation of subsoil properties and rates of soil production with terrain attributes (Chapter 6).

**Correlations**

	Median Age	<sup>137</sup> Cs (Bq/kg)	soil organic carbon (%)
Median Age	1.0000	-0.8476	-0.8575
<sup>137</sup> Cs (Bq/kg)	-0.8476	1.0000	0.9212
soil organic carbon (%)	-0.8575	0.9212	1.0000

The correlations are estimated by REML method.

**Scatterplot Matrix**



**Appendix. Fig. 3.** Correlation of median age (OSL single grain analysis), amounts of <sup>137</sup>Cs and contents of soil organic matter (Chapter 6).

Appendix. Tab. 1. TCN-derived soil production rates (Chapter 4).

Reference	Location	ID	Soil depth (cm)	SPR (mm kyr <sup>-1</sup> )		
Heimsath et al., 1997; 1999	Tennessee Valley, North America	AH1999-TV-2	0	39		
		AH1999-TV-3	16	47		
		AH1999-TV-4	0	20		
		AH1999-TV-5	0	15		
		AH1999-TV-6	35	26		
		AH1999-TV-7	58	21		
		AH1999-TV-10	51	25		
		AH1999-TV-11	0	107		
		AH1999-TV-12	30	60		
		AH1999-TV-13	49	26		
		AH1999-TV-15	20	48		
		AH1999-TV-16	35	33		
		AH1999-TV-17	60	27		
		AH1999-TV-23	0	91		
Heimsath et al., 2000	Nunnock River, Australia	AH2000-NR1	90	9.25		
		AH2000-NR2	10	45.6		
		AH2000-NR3	12	47.87		
		AH2000-NR4	60	20.61		
		AH2000-NR5	42	28.24		
		AH2000-NR6	30	34.51		
		AH2000-NR7	28	26.08		
		AH2000-NR9	40	20.82		
		AH2000-NR10	47	18.97		
		AH2000-NR11	22	56.53		
		AH2000-NR12	0	68.04		
		AH2000-NR13	52	15.26		
		AH2000-NR14	15	29.45		
		AH2000-NR15	66	21.83		
AH2000-NR23	40	25.62				
Heimsath et al., 2001a	Oregon Coast, North America	AH2001b-OR-5	15	130.09		
		AH2001b-OR-5R	15	174.15		
		AH2001b-OR-6	87.5	14.7		
		AH2001b-OR-7	0	135.19		
		AH2001b-OR-7R	0	169.01		
		AH2001b-OR-8	42	68.56		
		AH2001b-OR-8R	42	91.07		
		AH2001b-OR-9	0	138.73		
		AH2001b-OR-10	25	203.51		
		AH2001b-OR-11	100	14.8		
		AH2001b-OR-12	95	44.06		
		AH2001b-OR-15	92	26.59		
		AH2001b-OR-18	95	33.82		
		AH2001b-OR-19	75	44.75		
		AH2001b-OR-21	82	37.61		
		AH2001b-OR-22	60	56.88		
		AH2001b-OR-23	60	64.13		
		AH2001b-OR-24	35	113.23		
		AH2001b-OR-25	25	177.92		
		AH2001b-OR-26	58	34.39		
		AH2001b-OR-27	43	106.16		
		AH2001b-OR-29	0	146.67		
		AH2001b-OR-30	10	154.87		
		AH2001b-OR-31	12	169.3		
		AH2001b-OR-31R	12	239.2		
		AH2001b-OR-32	25	321.05		
		AH2001b-OR-32R	25	359.04		
		AH2001b-OR-33	30	187.26		
		AH2001b-OR-33R	30	216.08		
		AH2001b-OR-34	35	69.15		
		AH2001b-OR-34R	35	68.82		
		Heimsath et al., 2001b	Frogs Hollow, Australia	AH2001a-FH-3	0	18.69
				AH2001a-FH-10	0	26.42
				AH2001a-FH-5	25	49.08
AH2001a-FH-6	37			49.42		
AH2001a-FH-9	40			25.99		
AH2001a-FH-11	50			11.79		
AH2001a-FH-12	65			11.05		
Heimsath et al., 2005	Point Reyes, North America	AH2005-PR-1	80	28		
		AH2005-PR-2	0	80		
		AH2005-PR-3	0	102		
		AH2005-PR-4	25	49		
		AH2005-PR-5	20	54		
		AH2005-PR-6	57	36		

Reference	Location	ID	Soil depth (cm)	SPR (mm kyr <sup>-1</sup> )
		AH2005-PR-7	75	18
		AH2005-PR-8	47	50
		AH2005-PR-9	108	11
		AH2005-PR-10	93	22
		AH2005-PR-11	10	59
		AH2005-PR-12	27	58
		AH2005-PR-13	0	110
Heimsath et al., 2006	Snug, Brown Mountain, Australia	AH2006-NR-34	60	18.08
		AH2006-NR-36	0	22.21
		AH2006-NR-37	25	31.65
		AH2006-NR-39	55	16.7
		AH2006-NR-41	50	26.59
		AH2006-NR-42	100	6.23
		AH2006-NR-43	70	16.05
		AH2006-NR-45	73	6.79
		AH2006-NR-101	85	11.13
		AH2006-NR-102	27	24.51
		AH2006-NR-103	70	9.75
		AH2006-NR-104	90	9.48
		AH2006-NR-105	70	4.19
		AH2006-NR-106	45	11.43
		AH2006-NR-107	38	17.27
		AH2006-NR-108	60	11.3
		AH2006-NR-109	50	57.38
		AH2006-NR-110	70	7.01
		AH2006-NR-111	0	8.72
Heimsath et al., 2009	Arnhem Land, Australia	AH2009-TC-9	40	20.4
		AH2009-TC-10	45	20.3
		AH2009-TC-11	70	10.2
		AH2009-TC-12	55	11
		AH2009-TC-13	50	12.7
		AH2009-TC-14	38	25.8
		AH2009-TC-15	35	22.8
Wilkinson et al., 2005a	Blue Mountains, Australia	MW-JC-14	5	18.10
		MW-JC-15	40	16.30
		MW-BM-7	0	9.80
		MW-BM-9	0	9.90
		MW-BM-8	25	10.50
		MW-BM-6	55	9.10
		MW-BM-10	50	12.10
		MW-JC-18	55	9.60
		MW-JC-17	60	8.50
		MW-JC-16	87	9.50
		MW-JC-19	30	11.30
		MW-BM-11	0	12.60

**Appendix. Tab. 2.** Other soil formation rates derived from elemental fluxes (loss gain) in watersheds and products of the parent materials and weathering products studied, and derived from studies on 'physical weathering' (i. e. MCN, TCN), revised version from Montgomery (2007) (Chapter 4).

Reference	ID	Rate (mm kyr <sup>-1</sup> )	Rate (mm yr <sup>-1</sup> )	Elevation (m)	Climate	Geology
Alexander, 1985	Maryland	5.81	0.00581		N.A.	
	California	10.79	0.01079		N.A.	
	California	4.98	0.00498		N.A.	
	Maryland	19.92	0.01992		N.A.	
	Wales	40.67	0.04067		N.A.	
	Wales	13.28	0.01328		N.A.	
	British Columbia	54.78	0.05478		N.A.	
	Luxembourg	19.92	0.01992		N.A.	
	Hong Kong	6.64	0.00664		N.A.	
	Hong Kong	5.81	0.00581		N.A.	
	Hong Kong	9.96	0.00996		N.A.	
	England	11.62	0.01162		N.A.	
	England	14.94	0.01494		N.A.	
	Virginia	18.26	0.01826		N.A.	
	Viginia	83	0.083		N.A.	
	Java	116.2	0.1162		N.A.	
	England	38.18	0.03818		N.A.	
	Idaho	64.74	0.06474		N.A.	
	Wyoming	91.3	0.0913		N.A.	
	Wyoming	166	0.166		N.A.	
	New Mexico	24.9	0.0249		N.A.	
	New Mexico	49.8	0.0498		N.A.	
	New Mexico	240.7	0.2407		N.A.	
	Hawaii	83	0.083		N.A.	
	Mexico	91.3	0.0913		N.A.	
	Mexico	298.8	0.2988		N.A.	
	Papua	282.2	0.2822		N.A.	
	Wyoming	132.8	0.1328		N.A.	
	Colorado	58.1	0.0581		N.A.	
Alexander, 1988	CA	11	0.011	220	N.A.	Adamellite

Reference	ID	Rate (mm kyr <sup>-1</sup> )	Rate (mm yr <sup>-1</sup> )	Elevation (m)	Climate	Geology
	CH, BC, Can.	60	0.06	185	N.A.	Till/quartz diorite
	CS, BC, Can.	78	0.078	945	N.A.	Till/quartz diorite
	England	55	0.055	232	N.A.	Granite
	France	106	0.106	152	N.A.	Gneiss
	Idaho	65	0.065	478	N.A.	Adamellite
	Luxemburg	46	0.046	90	N.A.	Metashale
	Maryland	37	0.037	280	N.A.	Greenstone (metabas.)
	Minnesota	20	0.02	98	N.A.	Till/gabbro
	Maryland	5.8	0.0058	67	N.A.	Schist
	Maryland	20	0.02	70	N.A.	Serpentinite
	N. Hamp.	29	0.029	300	N.A.	Till/gneiss
	Scotland	160	0.16	542	N.A.	Till/granite
	V1, Victoria	33	0.033	144	N.A.	Dacite
	V2, Victoria	57	0.057	203	N.A.	Dacite
	Wash.	85	0.085	1150	N.A.	Till/quartz diorite
	WF, Wales	26	0.026	105	N.A.	Till/wacke
	WP, Wales	19	0.019	90	N.A.	Till/wacke
	ZJ, Zimbabwe	18	0.018	160	N.A.	Adamellite
	ZR, Zimbabwe	1.7	0.0017	60	N.A.	Adamellite
André, 2002	Pallenjakka, Norway	0.4	0.0004	500	Polar	Amphibolite
	Pallenjakka, Norway	0.3	0.0003	500	Polar	Amphibolite
	Pallenjakka, Norway	0.3	0.0003	500	Polar	Amphibolite
	Vassijaure, Norway	0.2	0.0002	500	Polar	Quartzophyllite and quartzite
	Vassijaure, Norway	0.2	0.0002	500	Polar	Quartzophyllite and quartzite
	Vassijaure, Norway	0.2	0.0002	500	Polar	Quartzophyllite and quartzite
	Bjoernfjell, Norway	0.3	0.0003	500	Polar	Acid granite and syenite
	Bjoernfjell, Norway	0.2	0.0002	500	Polar	Acid granite and syenite
	Bjoernfjell, Norway	0.1	0.0001	500	Polar	Acid granite and syenite
	Bjoernfjell, Norway	0.2	0.0002	500	Polar	Acid granite and syenite
	Bjoernfjell, Norway	0.2	0.0002	500	Polar	Acid granite and syenite
	Laktatjakka, Norway	0.2	0.0002	500	Polar	Acid granite and syenite
	Vassijaure, Norway	0.1	0.0001	500	Polar	Acid granite and syenite

Reference	ID	Rate (mm kyr <sup>-1</sup> )	Rate (mm yr <sup>-1</sup> )	Elevation (m)	Climate	Geology
	Bjoernfjell, Norway	2.6	0.0026	500	Polar	Biotite-rich granite and syenite
	Bjoernfjell, Norway	1	0.001	500	Polar	Biotite-rich granite and syenite
	Bjoernfjell, Norway	0.8	0.0008	500	Polar	Biotite-rich granite and syenite
	Bjoernfjell, Norway	1.2	0.0012	500	Polar	Biotite-rich granite and syenite
	Bjoernfjell, Norway	1.1	0.0011	500	Polar	Biotite-rich granite and syenite
	Laktatjakka, Norway	0.8	0.0008	500	Polar	Biotite-rich granite and syenite
	Vassijaure, Norway	1	0.001	500	Polar	Biotite-rich granite and syenite
	Vassijaure, Norway	1.4	0.0014	500	Polar	Biotite-rich granite and syenite
	Vassijaure, Norway	0.5	0.0005	500	Polar	Phyllite
	Vassijaure, Norway	0.8	0.0008	500	Polar	Phyllite
	Vassijaure, Norway	0.9	0.0009	500	Polar	Phyllite
	Kaerkevagge, Norway	5.5	0.0055	500	Polar	Dolomite
	Vassijaure, Norway	5.2	0.0052	500	Polar	Dolomite
Beach, 1998	Tikal, soil on ruins	70	0.07		Tropical	
Boulangé, 1984	Ivory Coast	14	0.014		Tropical	Granitic rock
Brown et al., 1995	Rio Icosos, Puerto Rico	37.5	0.0375		Humid tropical	Quartz diorite
Cleaves, 1993	Baltimore, Maryland	9.1	0.0091		Warm temperate	Plagioclase-muscovite-quartz
Dethier, 1986	Pacific Northwest	3	0.003		Cold temperate	Sedimentary and metamorphic
Dunne et al., 1978	Kenya	10	0.01		N.A.	Granite
Edmond et al., 1995	Guayana Shield, SA	10	0.01			
Fritz and Tardy, 1974	Senegal	3	0.003		Tropical	Granitic rock
Gac, 1979	Chad	13.5	0.0135		Tropical	Gneiss
Jahn, 1976	Spitsbergen	300	0.3		Polar	Overconsolidated Eocene marine shale
McKean et al., 1993	Black Diamond, CA	2.6	0.0026	130	Warm temperate	Granite
Owens and Watson, 1979	Rhodesia-Juliasdale	4.4	0.0044	1900	Tropical	Granite
Paces, 1986	Rhodesia-Rusape	0.17	0.00017	1600	Tropical	Biotitic gneiss with muscovite, sillimanite, quartzite
	Bohemian Maffif, X-0	8.9	0.0089	724	Warm temperate	Biotitic gneiss with muscovite, sillimanite, quartzite
	X-8	14	0.014	744	Warm temperate	Biotitic gneiss with muscovite, sillimanite, quartzite
Pavich, 1989	X-7	32	0.032	635	Warm temperate	Occoquan Granite
	Virginia Piedmont	4	0.004	250	Cool temperate	Metamorphic rocks
Pillans, 1997	Appalachian Piedmont	20	0.02		N.A.	Metamorphic rocks
Small et al., 1999	North Queensland	4	0.004		N.A.	Basalt



Reference	ID	Rate (mm kyr <sup>-1</sup> )	Rate (mm yr <sup>-1</sup> )	Elevation (m)	Climate	Geology
	Profile 0, b	14.4	0.0144		Alpine	
	Profile 0, c	14.8	0.0148		Alpine	
	Profile 2	13.3	0.0133		Alpine	
	Profile 4, a	12.6	0.0126		Alpine	
	Profile 4, b	12.5	0.0125		Alpine	
	Profile 4, c	15.5	0.0155		Alpine	
	Profile 4, d	15.9	0.0159		Alpine	
	Profile 4, f	17.5	0.0175		Alpine	
	WR-c1, a	10	0.01		Alpine	
	WR-c1, b	20	0.02		Alpine	
	WR-c2, a	7	0.007		Alpine	
	WR-c2, b	20	0.02		Alpine	
Trendall, 1962	Uganda	9	0.009		Tropical	
Trescases, 1973	New Caledonia	29	0.029		Tropical	Ultrabasic rock
Troeh et al., 1999	New Caledonia	47	0.047		Tropical	Ultrabasic rock
Velbel, 1986	Global soil production	83	0.083		N.A.	Garnet, plagioclase
Wakasa et al., 2006	Watershed 27, Coweeta	37	0.037		Warm temperate	Gneiss
	Southern Blue Ridge	37	0.037		Cold temperate	Granite dome
		55	0.055	650	Warm temperate	Granite dome
Wakatsuki and Rasyidin, 1992		42	0.042	650	Warm temperate	Granite dome
		150	0.15	650	Warm temperate	Granite dome
White et al., 1998	Global soil production	100	0.1	650	Warm temperate	

## References:

- André, M.-F. (2002). Rates of postglacial rock weathering on glacially scoured outcrops (Abisko-Riksgransen Area, 68°N). *Geografiska Annaler. Series A, Physical Geography* **84**, 139-150.
- Beach, T. (1998). Soil catenas, tropical deforestation, and ancient and contemporary soil erosion in the Peten, Guatemala. *Physical Geography* **19**, 378-405.
- Boulangé, B. (1984). Les formations bauxitiques latéritiques de Côte d'Ivoire. Les faciès, leur transformation, leur distribution et l'évolution du modèle. University of Paris.
- Brown, E. T., R. F. Stallard, M. C. Larsen, G. M. Raisbeck, and F. Yiu (1995). Denudation rates determined from the accumulation of *in situ* produced <sup>10</sup>Be in the Luquillo experimental forest, Puerto-Rico. *Earth and Planetary Science Letters* **129**, 193-202.
- Dunne, T., W. E. Dietrich, and M. J. Brunengo (1978). Recent and past erosion rates in semi-arid Kenya. *Zeitschrift für Geomorphologie, Supplement Band 29*, 130-140.
- Fritz, B., and Y. Tardy (1974). Étude thermodynamique du système gibbsite, quartz, kaolinite, gaz carbonique. Application à la genèse des podzols et des bauxites. *Science Géologiques Bulletin* **26**, 339-367.
- Gac, J. Y. (1979). Géochimie du bassin du lac Tchad. University of Strasbourg.
- Jahn, A. (1976). Geomorphological modelling and nature protection in arctic and subarctic environments. *Geoforum* **7**, 121-137.
- McKean, J. A., W. E. Dietrich, R. C. Finkel, J. R. Southon, and M. W. Caffee (1993). Quantification of soil production and downslope creep rates from cosmogenic <sup>10</sup>Be accumulations on a hillslope profile. *Geology* **21**, 343-346.
- Pillans, B. (1997). Soil development at snail's pace: evidence from a 6 Ma soil chronosequence on basalt in north Queensland, Australia. *Geoderma* **80**, 117-128.
- Small, E. E., R. S. Anderson, and G. S. Hancock (1999). Estimates of the rate of regolith production using <sup>10</sup>Be and <sup>26</sup>Al from an alpine hillslope. *Geomorphology* **27**, 131-150.
- Trendall, A. F. (1962). The formation of 'apparent peneplains' by a process of combined laterisation and surface wash. *Zeitschrift fuer Geomorphologie NF6*, 183-197.
- Trescases, J. J. (1973). Weathering and geochemical behaviour of the elements of ultramafic rocks in New Caledonia. *Bureau of Mineral Resources. Geology and Geophysics Bulletin Canberra* **141**, 149-161.
- Troeh, F. R., J. A. Hobbs, and R. L. Donahue (1999). "Soil and Water Conservation", 2nd ed., Englewood Cliffs, N.J., Prentice Hall.
- Wakasa, S., H. Matsuzaki, Y. Tanaka, and Y. Matsukura (2006). Estimation of episodic exfoliation rates of rock sheets on a granite dome in Korea from cosmogenic nuclide analysis. *Earth Surface Processes and Landforms* **31**, 1246-1256.
- White, A. F., A. E. Blum, M. S. Schulz, D. V. Vivit, D. A. Stonestrom, M. Larsen, S. F. Murphy, and D. Eberl (1998). Chemical Weathering in a Tropical Watershed, Luquillo Mountains, Puerto Rico: I. Long-Term Versus Short-Term Weathering Fluxes. *Geochimica et Cosmochimica Acta* **62**, 209-226.

**Appendix. Tab. 3.** Erosion rates from conventional agricultural practises (from Montgomery (2007)) (Chapter 6).

Reference	Location	Rate (in units reported)	Conventional erosion rate (mm yr <sup>-1</sup> )
Meade (1982) citing Trimble 1974	Piedmont uplands/ VA to AL	18 cm / 200 yr	0.9
Toy (1982) citing Gottschalk and Brune	western Iowa	444.5 t/ha/yr	36.9
Starkel (1972) citing Govt. of Madras	Bombay	20 cm / 15 yr	13
Hatch, 1981	Malaysia	107 t/ha/yr 62.71 t/ha/yr	8.9 5.2
Dunne, 1977	Kenya Athi-Kapiti plain  Northern Kenya	0.1 cm/yr 0.5 cm/yr 0.4 cm/yr 1.2 cm/yr	1 5 4 12
Rapp, 1975	Tanzania/ Ikowa Matumbulu Msalatu Imagi Kisongo Morogor Mgeta-Mzinga	0.2 mm/yr (*1.2) 0.73 mm/yr (*1.2) 0.41 mm/yr (*1.2) 0.6 mm/yr (*1.2) 0.48 mm/yr (*1.2) 0.26 mm/yr (*1.2) 14 mm/yr (*1.2)	0.24 0.876 0.492 0.72 0.576 0.312 16.8
Mieth and Bork, 2005	Easter Island/ AD1400-1900 1930s gullies	8.6 Mg/ha/yr 190 Mg/ha/yr	0.7138 15.8
Collins et al., 2001	Zambia, commercial cult. bush grazing communal cultivation	4.3 t/ha/yr 2.9 t/ha/yr 2.5 t/ha/yr	0.357 0.247 0.2075
Zhang et al., 2004	SE China	53 t/ha/yr 256 t/ha/yr	4.4 21
Happ, 1945	South Carolina	6 inches/150 yrs	1.016
Dunne at al., 1978	Kenya cracking clay Amboseli low Amboseli high Kilimanjaro lavas Kilimanjaro lavas	3 mm/yr 5.3 mm/yr 10.5 mm/yr 11.6 mm/yr 17.8mm/yr	3 5.3 10.5 11.6 17.8
Mäckel and Walther, 1984	Northern Kenya	20 cm /30 yr	6.6
Brown and Barber, 1985	Ripple Brook, Bronze Age Ag post 2350 BP ag	126.3 t/km <sup>2</sup> /yr 137.5 t/km <sup>2</sup> /yr	0.1048 0.114125
Beach, 1985	Guatemala, Milpa erosion, low Milpa erosion, high	2 cm/ 10yr 10 cm/ 10 yr	2 10
Battany and Grismer, 2000 (cited in)	Napa vineyard erosion, low Napa vineyard erosion, high	5 t/ha/yr 50 t/ha/yr	0.415 4.15
Sutherland, 1992	Bulldozing, low Bulldozing, high	40 t/ha/yr 90 t/ha/yr	3.32 7.47
Blakely et al., 1957	Ohio farm	1 in/ 9 yr	2.8
Dearing et al., 1987	Sweden 3050BC - 650 BC, 20th century	25 t/ha/yr	2.075
Saxton et al., 1971	Iowa Farms, corn field contoured Corn, field contoured	38.1 t/acre/yr 30.3 t/acre/yr	7.9 6.3
Gupta, 1996	SE Asia, cultivated, densely populated cultivated, Java	4051.2 t/km <sup>2</sup> /yr 1590 t/km <sup>2</sup> /yr	3.36 1.3197
Brown et al., 1981	Willamette Valley, E4F2 Willamette Valley, E4F2 Willamette Valley, WCS7 Willamette Valley, WCS7 Willamette Valley, E4F2, grav.	3 t/ha/yr 9 t/ha/yr 4 t/ha/yr 14 t/ha/yr 6 t/ha/yr	0.249 0.747 0.332 1.162 0.498
Bennett and Lowdermilk, 1938	Bethany, MO Tyler, TX Guthrie, OK Clarinda, Iowa Statesville, NC	7 in/ 16 yr 7 in/ 49 yr 7 in/ 50 yr 7 in/ 48 yr 7 in/ 51 yr	11.1 3.62 3.556 3.704 3.486
Dhruva Narayana, 1987	Dehradun, India, bare fallow bare and ploughed fallow maize contour cultivation	42.4 t/ha/yr 155.9 t/ha/yr 28.5 t/ha/yr 19.3 t/ha/yr	3.519 12.939 2.365 1.602

Reference	Location	Rate (in units reported)	Conventional erosion rate (mm yr <sup>-1</sup> )
Kaiser, 1961	Palouse, Alfalfa and grass/grain	1.8 t/acre/yr	0.375
	Alfalfa and grass/ grain and peas	4.4 t/acre/yr	0.91696
	alfalfa and grass/grain and peas	4.9 t/acre/yr	1.02116
	clover and peas, manure, grain	5 t/acre/yr	1.042
	recropping with grain	5 t/acre/yr	1.042
	clover and peas/manure, grain	6 t/acre/yr	1.2504
	grain/peas	7.5 t/acre/yr	1.563
	grain/fallow	12 t/acre/yr	2.5008
Chaplot et al., 2005	Northern Laos	18 Mg/ha/yr	1.49
		9.5 Mg/ha/yr	0.7885
De Santisteban, 2006	Spain, cereals	0.2 km/m <sup>2</sup> /yr	0.166
		11.5 km/m <sup>2</sup> /yr	9.5
	vinyards	0.33 km/m <sup>2</sup> /yr	0.274
	abandoned fields	16.19 km/m <sup>2</sup> /yr	13.4
		16.19 km/m <sup>2</sup> /yr	13.4
Langdale et al., 1992	Georgia, conventional tillage	11.3 tons/acre/yr	2.355
Harrold and Edwards, 1972	Ohio, corn, contour plowed	7.2 Mg/ha/yr	0.5976
		corn, not contour plowed	50.7 Mg/ha/yr
Edwards and Owens, 1991	Coshocton, Ohio, 1942-1969, 110	160.1 Mg/ha/yr	13.28
	106	187.4 Mg/ha/yr	15.55
	115	102 Mg/ha/yr	8.466
	118	13.1 Mg/ha/yr	1.087
	contour plowed, 1942-1969, 103	37.7 Mg/ha/yr	3.129
	121	72.9 Mg/ha/yr	6.051
	109	25.6 Mg/ha/yr	2.1248
	123	29.4 Mg/ha/yr	2.4402
	113	7.8 Mg/ha/yr	0.6474
Yoder et al., 2005	Tennessee, 1996 tillage tobacco Etowah	200 kg/ha/yr	0.0166
	1996 tillage tomatoes Etoway	8.3 kg/ha/yr	0.000689
	1996 tillage tomatoes Jefferson	3450 kg/ha/yr	0.28635
Lal, 1981	SW, Nigeria manual clearing - conventional till	4.64 t/ha/yr	0.38512
	tractor clearing - conventional till	19.57 t/ha/yr	1.62431
Deqi et al., 1981	Farmland, low	15800 t/km <sup>2</sup> /yr	13.114
	Farmland, high	19900 t/km <sup>2</sup> /yr	16.517
	Tuanshan gully	19600 t/km <sup>2</sup> /yr	16.268
	Shejia gully	18500 t/km <sup>2</sup> /yr	15.355
Yang et al., 2006	An'sai, Shaanxi, China; interfluves	20.95 Mg/ha/yr	1.73885
	top of ridge	46.40 Mg/ha/yr	3.8512
	ridge slopes	78.56 Mg/ha/yr	6.52048
	gully slopes	118.74 Mg/ha/yr	9.85542
	gully bottoms	188.75 Mg/ha/yr	15.6625
Fulajtar, 2003	Slovakia	24.1 t/ha/yr	2
Bujan et al., 2003	Argentina, Plateau	13.5 t/ha/yr	1.12
	High transect	16.5 t/ha/yr	1.3695
	High medium transect	36.0 t/ha/yr	2.988
	Low medium transect	28.7 t/ha/yr	2.3821
	Low transect	18.7 t/ha/yr	1.5521
Zhang et al., 2003	Tainshui City	4598 t/km <sup>2</sup> /yr	3.816
		5310 t/km <sup>2</sup> /yr	4.4073
		2864 t/km <sup>2</sup> /yr	2.37712
		8216 t/km <sup>2</sup> /yr	6.81928
	Zhenba County	7467 t/km <sup>2</sup> /yr	6.1976
		985 t/km <sup>2</sup> /yr	0.81755
		4200 t/km <sup>2</sup> /yr	3.486
	Nanchong City	4663 t/km <sup>2</sup> /yr	3.87029
		758 t/km <sup>2</sup> /yr	0.62914
	Kaixian County	6780 t/km <sup>2</sup> /yr	5.7021
		9452 t/km <sup>2</sup> /yr	7.84516
		7481 t/km <sup>2</sup> /yr	6.20923

Reference	Location	Rate (in units reported)	Conventional erosion rate (mm yr <sup>-1</sup> )
	Zigui County	9854 t/km <sup>2</sup> /yr	8.17882
	Muding County	2059 t/km <sup>2</sup> /yr	1.70897
	Yiliang County	6271 t/km <sup>2</sup> /yr	5.20493
		8543 t/km <sup>2</sup> /yr	7.09069
		2740 t/km <sup>2</sup> /yr	2.2742
	Yuanmou County	1405 t/km <sup>2</sup> /yr	1.16615
Schuller et al., 2003	Chile, A I, cropland	0.75 km/m <sup>2</sup> /yr	0.6225
	A II, cropland	0.72 km/m <sup>2</sup> /yr	0.5976
Theocharopoulos et al., 2003	Greece	18.34 t/ha/yr	1.52222
		22.12 t/ha/yr	1.83596
Basic et al., 2004	standard bare fallow	87 t/ha/yr	7.221
	plowed up and down slope	17 t/ha/yr	1.411
	standard bare fallow	0.55 cm/yr	5.5
	plowed up and down slope	0.11 cm/yr	1.1
Bennett et al., 2000	Alabama	1.34 kg/m <sup>2</sup> /yr	1.1122
	Alabama	2.9 kg/m <sup>2</sup> /yr	2.407
	Georgia	10.73 kg/m <sup>2</sup> /yr	8.9059
	Iowa	8.9 kg/m <sup>2</sup> /yr	7.387
	Iowa	0.62 kg/m <sup>2</sup> /yr	0.5146
	Iowa	0.97 kg/m <sup>2</sup> /yr	0.8051
	Iowa	3.75 kg/m <sup>2</sup> /yr	3.1125
	Mississippi	2.45 kg/m <sup>2</sup> /yr	2.0335
	Mississippi	6.04 kg/m <sup>2</sup> /yr	5.0132
	Belgium	0.56 kg/m <sup>2</sup> /yr	0.4648
	Belgium	0.82 kg/m <sup>2</sup> /yr	0.6806
	Belgium	0.85 kg/m <sup>2</sup> /yr	0.7055
	Belgium	0.52 kg/m <sup>2</sup> /yr	0.4316
	Belgium	1.90 kg/m <sup>2</sup> /yr	1.577
	France	0.29 kg/m <sup>2</sup> /yr	0.2407
	Spain	1.52 kg/m <sup>2</sup> /yr	1.2616
Vandaele and Poesen, 1995	Belgium	5.4m <sup>3</sup> /ha/yr	0.54
		8.2m <sup>3</sup> /ha/yr	0.82
Spomer and Hjelmfelt, 1986	Iowa, conventional 1	17 Mg/ha/yr	1.411
	Conventional 2	13 Mg/ha/yr	1.079
Osuji et al., 1980	Nigeria, manual, 1976	4.61 t/ha/yr	0.38263
	plough	7.76 t/ha/yr	0.64408
	conventional	8.46 t/ha/yr	0.70218
	bare fallow	17.63 t/ha/yr	1.46329
	Nigeria, manual, 1977	6.60 t/ha/yr	0.5478
	plough	8.85 t/ha/yr	0.73455
	conventional	9.80 t/ha/yr	0.8134
	bare fallow	19.52 t/ha/yr	1.62016
Van der Linden, 1983	Java, maize/cassava	0.6 mm/yr	0.6
		1244.4 t/km <sup>2</sup> /yr	1.03
Larson et al., 1983	Minnesota, Root River	7 t/ha/yr	0.581
	Zumbro River	12 t/ha/yr	0.996
	Straight River	7 t/ha/yr	0.581
	Redwood River	4 t/ha/yr	0.332
	Pelican River	2 t/ha/yr	0.166
Brink et al., 1977	Wisconsin, Maunsha River	13.3 t/ha/yr	1.1039
	Door Creek	19.3 t/ha/yr	1.6019
	Sixmile Creek	16.9 t/ha/yr	1.4027
	Pheasant Branch Creek	14.6 t/ha/yr	1.2118
	Mount Vernon Creek	11.7 t/ha/yr	0.9711
Pimentel et al., 1976	Corn - Missouri	19.7 t/acre/yr	4.1
	Corn - Wisconsin	89 t/acre/yr	18.5
	Corn - Mississippi	21.8 t/acre/yr	4.54
	Corn - Iowa	28.3 t/acre/yr	5.8977
	Corn - Indiana	20.9 t/acre/yr	4.355
	Corn - Ohio	12.2 t/acre/yr	2.542

Reference	Location	Rate (in units reported)	Conventional erosion rate (mm yr <sup>-1</sup> )
	Corn - Ohio	2.8 t/acre/yr	0.5835
	Corn - South Dakota	2.7 t/acre/yr	0.56268
	Corn - Missouri	21 t/acre/yr	4.376
	Corn - Iowa	21.4 t/acre/yr	4.4597
	Corn- Iowa	24 t/acre/yr	5
	Corn - Missouri	24 t/acre/yr	5
	Cotton	19.1 t/acre/yr	3.9804
	Cotton - Georgia	20.4 t/acre/yr	4.2514
	Wheat - Missouri	10.1 t/acre/yr	2.1048
	Wheat - Nebraska	6.3 t/acre/yr	1.3129
	Wheat - Pacific Northwest	7.5 t/acre/yr	1.563
	Wheat - Pacific Northwest	5.6 t/acre/yr	1.167
	Wheat - Washington	8.25 t/acre/yr	1.719
Van Oost et al., 2006	Greece - tillage erosion	23 Mg/ha/yr	1.909
	Greece	4 Mg/ha/yr	0.332
	Greece	18 Mg/ha/yr	1.494
	Belgium	10 Mg/ha/yr	0.83
	Canada	54 Mg/ha/yr	4.482
	Spain	40 Mg/ha/yr	3.32
	Spain	60 Mg/ha/yr	4.98
	New Zealand	19 Mg/ha/yr	1.577
	Belgium	8.7 Mg/ha/yr	0.7221
	USA	81 Mg/ha/yr	6.723
	Philippines	106 Mg/ha/yr	8.798
	Philippines	601 Mg/ha/yr	49.883
	Lesotho	19 Mg/ha/yr	1.577
	Zimbabwe	2.9 Mg/ha/yr	0.2407
	Rwanda	68 Mg/ha/yr	5.644
	China	16.9 Mg/ha/yr	1.4027
	China	14 Mg/ha/yr	1.162
	China	55 Mg/ha/yr	4.565
	China	18 Mg/ha/yr	1.494
	Thailand	8 Mg/ha/yr	0.664
	Thailand	18 Mg/ha/yr	1.494
	China	8.8 Mg/ha/yr	0.7304
Basher and Ross, 2002	New Zealand	7 t/ha/yr	0.581
		11 t/ha/yr	0.913
		30 t/ha/yr	2.49
Hewawasam et al., 2003	Sri Lanka - cultivated	359 t/km <sup>2</sup> /yr	0.29797
		134 t/km <sup>2</sup> /yr	0.11122
		224 t/km <sup>2</sup> /yr	0.18592
		395 t/km <sup>2</sup> /yr	0.32785
		553 t/km <sup>2</sup> /yr	0.45899
		2120 t/km <sup>2</sup> /yr	1.7596
		1612 t/km <sup>2</sup> /yr	1.33796
		447 t/km <sup>2</sup> /yr	0.37101
		510 t/km <sup>2</sup> /yr	0.4233
Lewis et al., 1988	Rwanda - average	10.1 t/ha/yr	0.8383
	Rwanda - cultivated corn	13.6 t/ha/yr	1.1288
	taro	10.0 t/ha/yr	0.83
	potato	9.8 t/ha/yr	0.8134
	manioc	9.4 t/ha/yr	0.7802
	sorghum	6.5 t/ha/yr	0.5395
	sweet potato	6.1 t/ha/yr	0.5063
	peas	6.0 t/ha/yr	0.498
	beans	5.1 t/ha/yr	0.4233
	fallow	3.3 t/ha/yr	0.2739
	peanut	1.9 t/ha/yr	0.1577
	banana	1.5 t/ha/yr	
	coffee	0.3 t/ha/yr	

Reference	Location	Rate (in units reported)	Conventional erosion rate (mm yr <sup>-1</sup> )
	corn	12.9 t/ha/yr	1.0707
	manioc	8.8 t/ha/yr	0.7304
	taro	8.1 t/ha/yr	0.6723
	sorghum	7.4 t/ha/yr	0.6142
	potato	7.0 t/ha/yr	0.581
	sweet potato	6.3 t/ha/yr	0.5229
	peas	5.9 t/ha/yr	0.4897
	beans	4.7 t/ha/yr	0.3901
	peanuts	4.1 t/ha/yr	0.3403
	fallow	3.6 t/ha/yr	0.2988
	banana	1.4 t/ha/yr	
	coffee	0.3 t/ha/yr	
Alegre et al., 1990	Peru-Santa Ana	4.1 t/ha/yr	0.3403
		11.8 t/ha/yr	0.9794
		5.7 t/ha/yr	0.4731
		10.7 t/ha/yr	0.8881
		3.2 t/ha/yr	0.2656
	Peru-Tupac Amaru	148 t/ha/yr	12.28
		119 t/ha/yr	9.877
		46 t/ha/yr	3.818
		72 t/ha/yr	5.976
	José Santos Atahualpa	98.7 t/ha/yr	8.192
		97.8 t/ha/yr	8.117
		104.1 t/ha/yr	8.64
		15.9 t/ha/yr	1.3197
Paskett and Philoctete, 1990	Haiti, maize	179 t/acre/yr	37.3
	Haiti, maize	215 t/acre/yr	44.8
	maize, beans	116 t/acre/yr	24.174
	maize, beans	75 t/acre/yr	15.63
	maize, beans	197 t/acre/yr	41.0548
	maize, beans	33 t/acre/yr	6.8772
	maize, beans	82 t/acre/yr	17.0888
	maize	165 t/acre/yr	34.386
	sorghum	123 t/acre/yr	25.6332
	sorghum	171 t/acre/yr	35.6364
Tagwira, 1992	Zimbabwe, average	50 t/ha/yr	4.15
		127 t/ha/yr	10.54
Whitmore et al., 1994	China, Yunnan, Er Hai	0.44 t/ha/yr	0.03652
	Qilu Hu	1.42 t/ha/yr	0.11786
	Xingyun Hu	2.07 t/ha/yr	0.17181
	Er Hai	5.57 t/ha/yr	0.46231
Boardman, 1998	Central Belgium (Govers 1991)	3.6 t/ha/yr	0.36
	NE Scotland (Watson & Evans 1991)	6.7 m <sup>3</sup> /ha/yr	0.67
	UK (Evans 1995)	2.3 m <sup>3</sup> /ha/yr	0.23
	UK South Downs (Boardman & 1993)	0.5 m <sup>3</sup> /ha/yr	0.05
	UK South Downs (Boardman & 1993)	5.0 m <sup>3</sup> /ha/yr	0.5
	S. Sweden (Alstrom & 1992)	0.8 t/ha/yr	0.08
	N France (Ludwig et al. 1995)	11.7 m <sup>3</sup> /ha/yr	1.17
Zhang et al., 2003	Sichuan Province, SW China	48 Mg/ha/yr	3.984
	SW China	151 Mg/ha/yr	12.533
Zhang et al., 1998	Shaanxi, China A	3.65 kg/m <sup>2</sup> /yr	3.0295
	B 1	4.74 kg/m <sup>2</sup> /yr	3.9342
	B 2	7.32 kg/m <sup>2</sup> /yr	6.0756
	B 3	10.66 kg/m <sup>2</sup> /yr	8.8487
	A lower	7.18 kg/m <sup>2</sup> /yr	5.9594
	C 1	10.44 kg/m <sup>2</sup> /yr	8.6652
	C 2	8.45 kg/m <sup>2</sup> /yr	7.0135
	C 3	9.70 kg/m <sup>2</sup> /yr	8.051
	A total	6.41 kg/m <sup>2</sup> /yr	5.3203
	1	8.41 kg/m <sup>2</sup> /yr	6.9803

Reference	Location	Rate (in units reported)	Conventional erosion rate (mm yr <sup>-1</sup> )
	2	8.07 kg/m <sup>2</sup> /yr	6.6981
	3	9.74 kg/m <sup>2</sup> /yr	8.0842
Lal, 1988	Ivory Coast	28 t/acre/yr	5.21
	Ivory Coast	254 t/acre/yr	52.9336
	Nigeria	6 t/acre/yr	1.2504
	Nigeria	103 t/acre/yr	21.465
	Madagascar	22 t/acre/yr	4.5848
	Madagascar	112 t/acre/yr	23.3408
	Benin	8 t/acre/yr	1.6672
	Benin	13 t/acre/yr	2.7092
	Kenya	2 t/acre/yr	0.4168
	Kenya	21 t/acre/yr	4.3764
	Ethiopia	9 t/acre/yr	1.8756
	Ethiopia	15 t/acre/yr	3.126
	Guinea	8 t/acre/yr	1.6672
	Guinea	11 t/acre/yr	2.2924
	Lesotho	18 t/acre/yr	3.7512
	Niger	16 t/acre/yr	3.3344
	Niger	31 t/acre/yr	6.4604
	Senegal	7 t/acre/yr	1.4588
	Senegal	25 t/acre/yr	5.21
	Tanzania	4 t/acre/yr	0.8336
	Tanzania	42 t/acre/yr	8.7528
	Zimbabwe	22 t/acre/yr	4.5848
Siebert and Belsky, 1990	Sumatra, control	3.81 t/ha/yr	0.31623
	control w/fertilizer	1.59 t/ha/yr	0.13197
Gantzer et al., 1990	1918-1931, uncropped, cult. corn	93 t/ha/yr	7.719
	corn-wheat rotation	44 t/ha/yr	3.652
	corn	6 t/ha/yr	0.498
	16.8 cm/100 yrs		1.68
	22 cm/60 yr		3.667
Wood and Worsham, 1986	North Carolina, tobacco	33 t/ha/yr	2.739
	North Carolina, tobacco	40 t/ha/yr	3.32
	Upper Tar River, NC	25.5 t/ha/yr	2.1165
	Piedmont Bright Leaf	40 t/ha/yr	3.32
	1982 total	2457 kg/ha/yr	0.203931
	1983 total	9004 kg/ha/yr	0.747332
McGregor et al., 1975	Mississippi, conventional soy	17.5 t/ha/yr	1.4525
Harrold et al., 1970	Ohio, Conventional	1740 kg/ha/yr	0.14442
Lal, 1975	W. Nigeria	3-4 mm/yr	3.5
Bernard and Laverdière, 2001	Québec, Canada	13 t/ha/yr	1.079
Nearing et al., 1999		0.241973	0.200838
		16.155407	13.408988
		0.900487	0.747404
		4.143965	3.439491
		4.143965	3.439491
		4.135558	3.432513
		3.350621	2.781015
		3.350621	2.781015
		2.722335	2.259538
		6.385280	5.299783
		6.385280	5.299783
		5.966050	4.951821
		5.243045	4.351727
		5.243045	4.351727
		3.124192	2.593079
		0.209690	0.174043
		17.069868	14.167990
		1.338774	1.111182
		3.978627	3.302260

Reference	Location	Rate (in units reported)	Conventional erosion rate (mm yr <sup>-1</sup> )
		4.135558	3.432513
		3.978627	3.302260
		3.461314	2.872890
		2.722335	2.259538
		3.461314	2.872890
		5.838263	4.845758
		5.966050	4.951821
		5.838263	4.845758
		3.624690	3.008493
		3.124192	2.593079
Lowrance et al., 1988	Little River Exp. Watershed, Georgia	63 Mg/ha/yr	5.230000
Zuzel et al., 1993	Pendelton, OR winter wheat fall plow continuous fallow (bare earth)	42 t/ha 22 t/ha 460 t/ha	3.486000 1.826 38.180000
Norton, 1986	Indiana	>26 Mg/ha/yr	2.158000
Jackson, 2006	North Carolina, Daughtery O.C. Jackson Williford Jackson Godwin McLanb Williams Jones Baseline Site Dudley	3 mm/yr 3 mm/yr 2.6 mm/yr 2.1 mm/yr 1.8 mm/yr 1.8 mm/yr 1.8 mm/yr 1.5 mm/yr 1.5 mm/yr 1.1 mm/yr	3.00 3.00 2.60 2.10 1.80 1.80 1.80 1.50 1.50 1.10
Lowrance et al., 1986	uplands, Little River Georgia	15 Mg/ha/yr	1.25
Phillips, 1993	North Carolina	>9.5 t/ha/yr	0.79
Phillips et al., 1993	North Carolina	> 0.55 mm/yr	0.55
Nagle et al., 2000	Dominican Republic, FM-1 FM-5 BI-1 FM-4 FM-7 PC-1 FM-2a FM-3 FM-6 LC-1 LM-1 PC-2 PC-3 SC-1	6.0 t/ha/yr 28.9 t/ha/yr 14.8 t/ha/yr 15.2 t/ha/yr 6.8 t/ha/yr 26.5 t/ha/yr 33.0 t/ha/yr 17.9 t/ha/yr 27.1 t/ha/yr 14.3 t/ha/yr 34.3 t/ha/yr 53.0 t/ha/yr 61.6 t/ha/yr 26.5 t/ha/yr	0.498 2.3987 1.2284 1.2616 0.5644 2.1995 2.739 1.4857 2.2493 1.1869 2.8469 4.399 5.1128 2.1995
Busacca et al., 1993	Palouse	11.6 t/ha/yr	0.9628
Phillips, 1997	Croatan N.F. North Carolina, T6 PI1 FL1 FL2 CP1 CP2 CP4 CP5 CP6 CP7 CP8 IC1 IC2 IC8 T1 T2	24.7 cm/285 yr 35.7 cm/285 yr 9.7 cm/285 yr 10.9 cm/285 yr 16 cm/285 yr 12.9 cm/285 yr 26.1 cm/285 yr 9.9 cm/285 yr 34.9 cm/285 yr 27.8 cm/285 yr 16.7 cm/285 yr 15.5 cm/285 yr 14.5 cm/285 yr 21.0 cm/285 yr 12.5 cm/285 yr 17.0 cm/285 yr	0.86666 1.25263 0.34035 0.382456 0.5614 0.45263 0.91578 0.34737 1.22456 0.97544 0.58596 0.543859 0.50877 0.73684 0.43589 0.59649



Reference	Location	Rate (in units reported)	Conventional erosion rate (mm yr <sup>-1</sup> )
	T4	2.5 cm/285 yr	0.08772
	T5	16.5 cm/285 yr	0.5789
	OP1	17.0 cm/285 yr	0.59649
	OP2	4.5 cm/285 yr	0.15789
	EP1	1.0 cm/285 yr	0.03509
Nagle and Ritchie, 2004	Pasture since 1971	7.5 t/ha/yr	0.6225
	Cultivated with residue manag	3.0 t/ha/yr	0.249
	No-till for some years	6.6 t/ha/yr	0.5478
Walling et al., 2002	Smisby 103	5.05 t/ha/yr	0.4191
	38	7.99 t/ha/yr	0.66317
	7	5.97 t/ha/yr	0.4955
	67	4.53 t/ha/yr	0.37599
	89	2.14 t/ha/yr	0.17762
	8	1.20 t/ha/yr	0.0996
	115a	3.60 t/ha/yr	0.2988
	115b	0.20 t/ha/yr	0.0166
	65a	3.36 t/ha/yr	0.27888
	65b	4.04 t/ha/yr	0.33532
	39	5.52 t/ha/yr	0.45816
	45	4.46 t/ha/yr	0.37018
	Rosemaund, Stoney a	4.61 t/ha/yr	0.38263
	Stoney b	8.48 t/ha/yr	0.70384
	Stoney c	3.14 t/ha/yr	0.26062
	Stoney d	3.26 t/ha/yr	0.27058
	Stoney e	3.45 t/ha/yr	0.28635
	Longlands a	3.62 t/ha/yr	0.30046
	Longlands b	5.44 t/ha/yr	0.45152
	Pear tree	4.03 t/ha/yr	0.33449
	Rickyard	5.32 t/ha/yr	0.44156
	Moorfield	7.67 t/ha/yr	0.6366
	Five Acres	4.82 t/ha/yr	0.40006
	Comonation	6.54 t/ha/yr	0.54282
	Stone	3.68 t/ha/yr	0.30544
Uri and Lewis, 1999	U.S. average cropland, 1982	8.0 t/acre/yr	1.67
	1997	5.2 t/acre/yr	1.08

Appendix. Tab. 4. Erosion rates from conservation agricultural practises (from Montgomery (2007)) (Chapter 6).

Reference	Location	Rate (in units reported)	Conservation erosion rate (mm yr <sup>-1</sup> )
Hatch, 1981	Malaysia, terraced	1.44 t/ha/yr	0.119
Saxton et al., 1971	Iowa farms ,rotation grazed	0.8 t/acre/yr	0.16672
	Level Terraced	0.9 t/acre/yr	0.18756
Dhruva Narayana, 1987	Dehradun, India grass cover	2.1 t/ha/yr	0.1743
	pueraria hirsuta	0.1 t/ha/yr	0.0083
	Dichanthium annulatum	0.2 t/ha/yr	0.0166
	Chrsopogon fulvus	0.3 t/ha/yr	0.0249
	Eulaliopsis binata	0.3 t/ha/yr	0.0249
Langdale et al., 1992	Georgia, conservation tillage	0.05 tons/acre/yr	0.01042
Harrold and Edwards, 1972	Ohio, Corn, no-till	0.07 Mg/ha/yr	0.00581
Yoder et al., 2005	Tennessee 1996 no-till tobacco Etowah	10 kg/ha/yr	0.00083
	1996 no-till tomatoes Etoway	0.35 kg/ha/yr	0.000029
	1996 no-till tomatoes Jefferson	986 kg/ha/yr	0.08183
Lal, 1981	SW Nigeria, no-till (traditional)	0.01 t/ha/yr	0.00083
	manual clearing	0.37 t/ha/yr	0.03071
Schuller et al., 2003	Chile, B I, cropland, conservation	0.13 km/m <sup>2</sup> /yr	0.1079
	B II, cropland, conservation	0.03 km/m <sup>2</sup> /yr	0.0249
Basic et al., 2004	no till	7.4 t/ha/yr	0.6142
	disked and harrowed	3.5 t/ha/yr	0.2905
	disked and harrowed	5.4 t/ha/yr	0.4482
	disked and harrowed	1.2 t/ha/yr	0.0996
	no till	0.04cm/yr	0.4
	disked and harrowed	0.02 cm/yr	0.2
	disked and harrowed	0.04 cm/yr	0.4
	disked and harrowed	0.01 cm/yr	0.1

Reference	Location	Rate (in units reported)	Conservation erosion rate (mm yr <sup>-1</sup> )
Spomer and Hjelmfelt, 1986	Iowa, conservation tilled 3	2 Mg/ha/yr	0.166
Osuji et al., 1980	Nigeria, no till 1976	0.05 t/ha/yr	0.00415
	Nigeria, no till 1977	0.08 t/ha/yr	0.00664
Pimentel et al., 1976	Bermuda Grass - Texas	0.03 t/acre/yr	0.00625
Alegre et al., 1990	Peru-Tupac Amaru	1.3 t/ha/yr	0.1079
Tagwira, 1992	Zimbabwe, average	0.5 t/ha/yr	0.0415
Siebert and Belsky, 1990	Sumatra, bench terraces	1.13 t/ha/yr	0.09379
	grass bunds	0.81 t/ha/yr	0.06723
	grass & mulch	0.53 t/ha/yr	0.04399
Gantzer et al., 1990	grass	0.8 t/ha/yr	0.0664
Wood and Worsham, 1986	North Carolina, 1982 total, no till	121 kg/ha/yr	0.01
	1983 total, no till	101 kg/ha/yr	0.008383
McGregor et al., 1975	Mississippi, no till soy/wheat	1.8 t/ha/yr	0.1494
	no till corn after soy	5.2 t/ha/yr	0.4316
	no till soy after corn	1.3 t/ha/yr	0.1079
	no till soy	2.5 t/ha/yr	0.2075
Harrold et al., 1970	Ohio, no-till	27 kg/ha/yr	0.00224

Appendix. Tab. 5. Erosion rates under native vegetation (from Montgomery (2007)) (Chapter 6).

Reference	Location	Rate (in units reported)	Native vegetation erosion rate (mm yr <sup>-1</sup> )
Smith and Stamey, 1965	Columbia, MO	0.34 t/acre/yr	0.070856
	Bethany, MO	0.16 t/acre/yr	0.033344
	Bethany, MO	0.15 t/acre/yr	0.03126
	Bethany, MO	0.06 t/acre/yr	0.0125
	Blacksburg, VA	0.04 t/acre/yr	0.008336
	Blacksburg, VA	0.07 t/acre/yr	0.014588
	Blacksburg, VA	0.01 t/acre/yr	0.002084
	Blacksburg, VA	0.02 t/acre/yr	0.004168
	Blacksburg, VA	0.01 t/acre/yr	0.002084
	Clarinda, IA	0.1 t/acre/yr	0.02084
	Clarinda, IA	0.03 t/acre/yr	0.006252
	Guthrie, OK	0.02 t/acre/yr	0.004168
	Guthrie, OK	0.01 t/acre/yr	0.002084
	Guthrie, OK	0.11 t/acre/yr	0.022924
	La Crosse, WI	0.09 t/acre/yr	0.018756
	La Crosse, WI	0.02 t/acre/yr	0.004168
	Mayaguez, Puerto Rico	1.2 t/acre/yr	0.25008
	Mayaguez, Puerto Rico	0.18 t/acre/yr	0.037512
	Mayaguez, Puerto Rico	0.73 t/acre/yr	0.152132
	Pullman, WA	0.08 t/acre/yr	0.016672
	Pullman, WA	0.01 t/acre/yr	0.002084
	Statesville, NC	0.31 t/acre/yr	0.064604
	Statesville, NC	0.002 t/acre/yr	0.0004168
	Statesville, NC	3.08 t/acre/yr	0.641872
	Temple, TX	0.1 t/acre/yr	0.02084
	Temple, TX	0.02 t/acre/yr	0.004168
	Tyler, TX	0.08 t/acre/yr	0.016672
Tyler, TX	0.005 t/acre/yr	0.001042	
Tyler, TX	0.05 t/acre/yr	0.01042	
Tyler, TX	0.36 t/acre/yr	0.075024	
Zanesville, OH	0.03 t/acre/yr	0.006252	
Zanesville, OH	0.02 t/acre/yr	0.004168	
Zanesville, OH	0.1 t/acre/yr	0.02084	
Zanesville, OH	0.01 t/acre/yr	0.002084	
Brown and Barber, 1985	Ripple Brook, 12,000-2,950 BP	16.4 t/km <sup>2</sup> /yr	0.013612
	10,000 - 2,950 BP	21.1 t/km <sup>2</sup> /yr	0.017513
	8,000 - 2,950 BP	29.4 t/km <sup>2</sup> /yr	0.024402
Blakely et al., 1957	Ohio pasture	1 in / 1500 yr	0.01693
	Ohio forest	< 1 in / 1500 yr	0.01
Dearing et al., 1987	Sweden 3050BC - 650 BC	0.25 t/ha/yr	0.2075
Gupta, 1996	Java, native	30 t/km <sup>2</sup> /yr	0.0249
Bennett and Lowdermilk, 1938	Bethany, MO	7 in / 3,900 yr	0.045589
	Tyler, TX	7 in / 11,100 yr	0.016018
	Guthrie, OK	7 in / 38,200 yr	0.004654
	Clarinda, Iowa	7 in / 15,200 yr	0.011697
	Statesville, NC	7 in / 95,800 yr	0.001856
Dhruva Narayana, 1987	Dehradun, India natural grass	1 t/ha/yr	0.083
Fowler and Heady, 1981	Undisturbed forest, US, low	0.001 t/acre/yr	0.0002084
	Undisturbed forest, US, low	0.009 t/acre/yr	0.0018756

Reference	Location	Rate (in units reported)	Native vegetation erosion rate (mm yr <sup>-1</sup> )
	Undisturbed forest, US, high	3.3 t/acre/yr	0.68772
Pimentel et al., 1976	Native Grass - Kansas	0.03 t/acre/yr	0.00625
	Forest - North Carolina	0.002 t/acre/yr	0.0004168
	Forest - New Hampshire	0.01 t/acre/yr	0.002084
Hewawasam et al., 2003	Sri Lanka - native forest	8.0±0.7 mm/ka	0.008
		4.7±0.3 mm/ka	0.0047
		5.1±0.4 mm/ka	0.0051
		10.8±0.7 mm/ka	0.0108
		11.4±0.8 mm/ka	0.0114
		10.9±0.7 mm/ka	0.0109
Whitmore et al., 1994	China, Er Hai	0.35 t/ha/yr	0.02905
	Qilu Hu	0.20 t/ha/yr	0.0166
	Xingyun Hu	0.28 t/ha/yr	0.023

RARE BOOKS LIB.

- 8 APR 2011

UNIVERSITY OF SYDNEY LIBRARY



000000614714867